# JOURNAL OF APPLIED PHYSICS

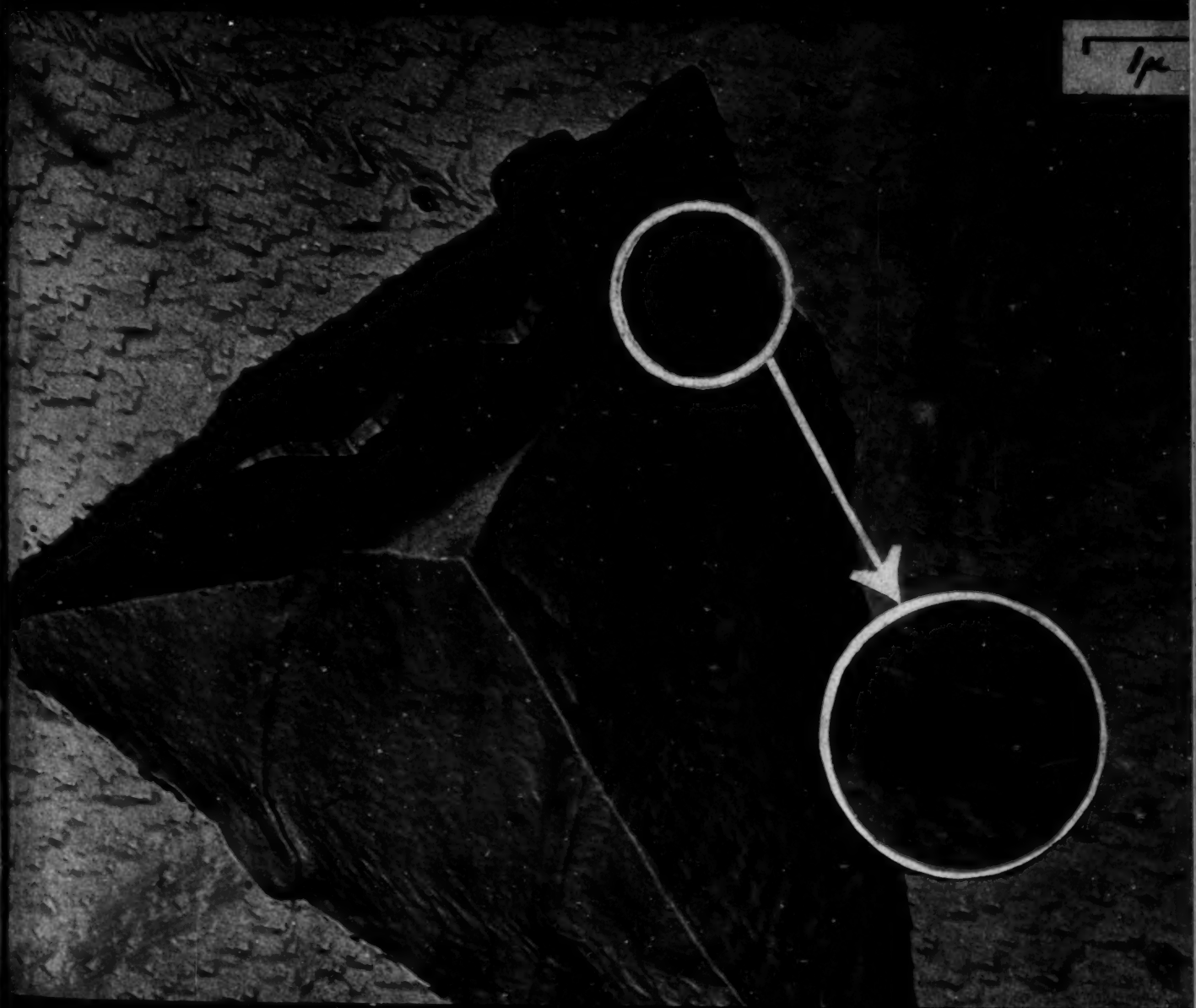

# JOURNAL OF APPLIED PHYSICS

Vol. 18, No. 11 NOVEMBER, 1947


## *In This Issue*


| | | Page |
|---|---|---|
| **Initial Oscillation on a Rotational Viscometer** | RUTH N. WELTMANN | 933 |
| **Stability and High Frequency** | AUREL WINTNER | 941 |
| **Mechanism of Fracture of Glass and Similar Brittle Solids** | NELSON W. TAYLOR | 943 |
| **Acceleration of Electrons by a Resonant Cavity** | FRANK L. HEREFORD, JR. | 956 |
| **Infra-Red Spectra of Hydrocarbons** | W. H. AVERY AND J. R. MORRISON | 961 |
| **Magnetic Field Configurations Due to Air Core Coils** | JOHN P. BLEWETT | 968 |
| **Design of an Air Core Synchrotron** | JOHN P. BLEWETT | 976 |
| **Sound Velocity Method for Determining the Compressibility of Finely Divided Substances** | R. J. URICK | 983 |
| **End-Effect in Rotational Viscometers** | CHARLES H. LINDSLEY AND EARL K. FISCHER | 988 |
| **Theory of Disk-Loaded Wave Guides** | E. L. CHU AND W. W. HANSEN | 996 |
| **Equations for the Inductances of Three-Phase Coaxial Busses Comprised of Square Tubular Conductors** | THOMAS J. HIGGINS AND HENRY P. MESSINGER | 1009 |
| **Mechanical Behavior of High Damping Metals** | CLARENCE ZENER | 1022 |
| **Field of a Microwave Dipole Antenna in the Vicinity of the Horizon. II** | C. L. PEKERIS | 1025 |
| **Letters to the Editor:** | | |
| **Grain Growth in Alpha-Brass** | J. E. BURKE | 1028 |
| **Comments on "Grain Growth in Alpha-Brass"** | PAUL A. BECK | 1028 |
| **Electron Microscope and Electron Diffraction Study of Slip in Metal Crystals** | R. D. HEIDENREICH AND W. SHOCKLEY | 1029 |


*In Every Issue*


| | |
|---|---|
| **Calendar of Meetings** | 1021 |
| **New Books** | 1031 |
| **New Booklets** | 1033 |
| **Here and There** | 1033 |
| **Index to Advertisers** | xxxiv |



**BOARD OF EDITORS**

ELMER HUTCHISSON, *Editor*

*Associate Editors*

R. BOWLING BARNES
OTTO BEECK
W. F. BUSSE
W. JAMES LYONS
PHILIP MORRISON
PAUL E. SABINE
FREDERICK SEITZ
J. R. TOWNSEND
JOHN VON NEUMANN

**Publication of the American Institute of Physics**

**ADMINISTRATIVE STAFF**

HENRY A. BARTON, *Director*

CLEVELAND NORCROSS, *Assistant Director*

RUTH F. BRYANS, *Publication Manager*

THEODORE VORBURGER, *Business Manager*

JOHN T. TATE, *Adviser on Publications*

**GOVERNING BOARD**

GEORGE R. HARRISON, *Chairman*

WALLACE WATERFALL, *Secretary*

GEORGE B. PEGRAM, *Treasurer*

E. U. CONDON
A. J. DEMPSTER
W. F. FAIR, JR.
FLOYD A. FIRESTONE
HARVEY FLETCHER
R. C. GIBBS
K. S. GIBSON
PAUL E. KLOPSTEG
A. H. PFUND
JOHN T. TATE
M. W. WHITE
A. G. WORTHING



The JOURNAL OF APPLIED PHYSICS, published monthly at Prince and Lemon Sts., Lancaster, Pa., is devoted to physics in its role as the science basic to other natural sciences and to the arts and industries. Previous to 1937 this publication was known as PHYSICS. The JOURNAL OF APPLIED PHYSICS publishes editorials, news of physicists, and reviews, as well as technical papers of applied physics.

**Manuscripts** should be submitted to Elmer Hutchisson, Editor, Case Institute of Technology, Cleveland 6, Ohio.

**Subscriptions** and orders for back numbers should be addressed to Prince and Lemon Streets, Lancaster, Pa. or to the American Institute of Physics, 57 East 55 Street, New York 22, N. Y.

**Subscription Price**

| | U.S. AND CANADA | ELSEWHERE |
|---|---|---|
| To members and associate members of the American Institute of Physics | $6.00 | $7.00 |
| To all others | 8.00 | 9.00 |

**Back Number Prices**

Complete set: Vol. 1, July, 1931–Vol. 17, 1946—$124.00
Yearly back number rate: $10.00
Single copies: $1.00 each.

**Changes of address** and proofs should be addressed to the Publications Manager.

**Advertising rates** supplied on request. Orders, advertising copy, and cuts should be sent to the American Institute of Physics.

Entered as second class matter January 22, 1937, at the Post Office at Lancaster, Pennsylvania, under the Act of March 3, 1879.
Accepted for mailing at the special rate of postage provided for in the Act of February 28, 1925, authorized May 2, 1932.



Copyright 1947, by the American Institute of Physics.

Journal
of
Applied Physics

Volume 18, Number 11 November, 1947

# Initial Oscillation on a Rotational Viscometer

RUTH N. WELTMANN
*Interchemical Corporation, New York, New York*
(Received May 7, 1947)

The oscillatory system of a rotational viscometer has been investigated. The oscillation equations were checked with experimental bob deflection-time curves obtained for Newtonian liquids.

To be able to rapidly obtain correct values when taking flow curves the oscillatory system should be critically damped. Since this condition cannot be easily obtained in practice, the system should be slightly overdamped, meaning that the inertia ($I$) should be equal or smaller than $\pi\mu^2/720KS^2$. It is shown that due to the higher viscosity of thixotropic materials at lower rates of shear, the flow curves at these rates of shear give an indication of rather too low than too high shearing stresses.

THE flow characteristics of thixotropic substances are known to change as a function of time, when these materials are subjected to shearing forces. However, there is little information available about the change in structure of the material during the initial period of agitation, since no instantaneous readings can be made with most systems of measurement. For studying the structural changes in the initial period, the use of recording equipment is most desirable since it provides a continuous graph of the position of the indicating means of the viscometer, thus seemingly allowing an interpretation of the flow behavior of the material from the start of motion.

This paper deals with the problems encountered with a rotational viscometer when changing the cup speed from one to another angular velocity. Details of the viscometer have been described by Green.[1] The recorder which has been used in conjunction with this viscometer has also been previously discussed.[2]

However, even the recorded values are not always true representations of the flow characteristics of the investigated material, since the indicating means which control the recording mechanism do not instantaneously adjust themselves to the proper position but require time to perform the necessary motion.

In a rotational viscometer the shearing force at any rate of shear is obtained from the angular deflection of a bob, but only after the bob has come to an equilibrium position. In Green's design of a viscometer the bob is suspended on a helical spring. The stiffness of the spring and the inertia of the bob structure form an oscillatory system in which damping is provided by the viscosity of the test material which is located between the cup and the bob. When the cup of the rotational viscometer is set into motion for the purpose of performing a viscometric measurement the bob starts to move from its zero position until it reaches its final deflection. The time which is required to complete the bob motion depends upon the three elements of the oscilla-

[1] H. Green, Ind. Eng. Chem. Anal. Ed. **14**, 576 (1942).
[2] R. N. Weltmann, Rev. Sci. Inst. **16**, 7, 184 (July, 1945).

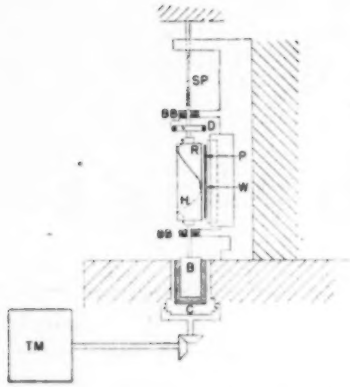


FIG. 1. Schematic viscometer and recorder assembly.

tory system, the stiffness of the spring, the inertia of the bob parts and the viscosity of the material. Though reference has been made to a condition which exists only when starting a viscometric measurement, the same reasoning also applies when the cup speed is changed step by step from one speed to another to obtain a rate of shear—shearing stress diagram.

It is of greatest importance to design properly the spring-bob combination so that the bob will come to its equilibrium condition in the shortest period of time. An analysis is being made of the most suitable physical dimensions of the elements of the oscillatory system for various test materials.

## INSTRUMENTATION

Figure 1 is a schematic sketch of the measuring and recording means of a rotational viscometer. The test material is contained between cup ($C$) and bob ($B$). The cup which is placed in a 30°C constant temperature bath is driven at various speeds to obtain different shearing forces in the material. The bob, supported between two ball nearings ($BB$), deflects until the torsional force of the spring ($SP$) equals the resistance force in the test material. This deflection is a measure of the applied shearing stress. The bob carries the deflection indicating disk ($D$) for visual measurements and the movable registering elements of the recorder ($R$). The recorder consists of two electrodes between which a high frequency spark is generated. The one electrode is a straight wedge ($W$), while the other electrode is a helical wire ($H$) wound around a cylinder concentric to the bob shaft, so that each position of the wire with respect to the straight wedge coincides with a unique deflection reading. The recording paper ($P$) travels between these electrodes at a constant speed, being moved by a slow constant speed motor (2.9 cm/sec.), and holes are pierced in the paper whenever a spark jumps over the gap. Thus the continuation of pierced points on the paper represents a bob deflection-time curve. On recording a flow curve the paper is coupled to the drive mechanism, the transmission motor combination ($TM$), in such a manner that the paper position becomes a function of the cup speed.

## CUP INERTIA

The cup as part of the drive mechanism is expected to obtain a constant angular rotation which is being impressed on it by the synchronous motor and transmission combination as soon as the initial acceleration period is over. This has been checked experimentally by rigidly connecting the cup with the bob from which temporarily the spring was removed. Wax was poured in the clearance between cup and bob and left to solidify before the test. The deflection of the bob as a function of time was recorded. Small curvatures are obtained at the beginning of the straight lines characteristic for each applied speed, as shown in Fig. 2. This is evidence that the cup needs a certain time before it attains its given speed. This time lag of the cup was determined by extending the straight line to zero deflection. From numerous experiments performed at various speeds this time intercept was found to average about 0.14 second. For further reference it will be designated as $t_c$.

## OSCILLATORY SYSTEM

The force equilibrium of the oscillatory system in such a rotational viscometer is given by the basic differential equation,

$$I\frac{d\alpha^2}{dt^2}+\frac{\mu}{S}\frac{d\alpha}{dt}+K\frac{360}{2\pi}\alpha=\frac{\mu}{S}\omega, \qquad (1)$$

$I$—the inertia of the bob, bob shaft, and deflection indicating dial in gram cm²,
$\alpha$—the deflection in radians,
$\mu$—the viscosity in poises,

$t$—the time of motion in seconds,
$S$—an end effect corrected instrumental constant $S=[(1/R_b^2-1/R_c^2)/4\pi(h+h_e)]$,
$R_c$—radius of cup in cm,
$R_b$—radius of bob in cm,
$h$—immersed height of bob in cm,
$h_e$—hypothetical height added to bob to correct for end effect,
$K$—torsion constant of spring in dynes cm determined per degree deflection,
$\omega$—applied angular velocity in radians per second.

The end effect is the shear produced between the bottom of the cup and the bob. It can be experimentally obtained by measuring shearing stresses for various bob heights under otherwise constant conditions. Upon extrapolation of the shearing stress—bob height curve, which is a straight line, it is found that for zero shearing stress a negative bob height is required. This is the hypothetical bob height $h_e$—contributing a shear equal to the shear effect between the bottom of the cup and bob—which has to be added to the immersed bob height in the equation for the end effect corrected instrumental constant $S$. In the cup and bob assembly employed, the end effect amounts to about 2 percent and the corrected $S$ equals $2.24\times10^{-3}$.

Equation (1) is only strictly correct for materials whose viscosity is independent of time and rate of shear. It has three solutions:

(1) The overdamped or aperiodic oscillation, where the bob deflection increases slowly until the bob reaches its final position. If the bob creeps very slowly towards its maximum deflection there is some danger that the cup speed is increased to the next step before the bob has reached its final position and thus incorrect results will be obtained. Case 1 is realized when:

$$\frac{\mu^2}{4I^2S^2}>\frac{360K}{2\pi I} \quad \text{or} \quad I<\frac{\pi\mu^2}{720KS^2}. \tag{2}$$

Then the solution of Eq. (1), if $D$, the deflection in degrees, is substituted for $(360/2\pi)\alpha$, is:

$$D=\frac{\mu\omega}{2KS\Gamma}e^{-(\mu/2IS)t}[(-\mu/2IS-\Gamma)e^{\Gamma+} -(-\mu/2IS+\Gamma)e^{-\Gamma t}]+\frac{\mu\omega}{KS},$$

where

$$\Gamma=(\mu^2/4I^2S^2-360K/2\pi I)^{\frac{1}{2}}. \tag{3}$$

(2) The underdamped or periodic oscillation, where the bob deflection increases rather fast but exceeds its final position and oscillates around this position before it ultimately reaches it. In this case the most erroneous values can be obtained giving either too low or too high readings depending on the time after which they are taken. Case 2 is realized when:

$$\frac{\mu^2}{4I^2S^2}<\frac{360K}{2\pi I} \quad \text{or} \quad I>\frac{\pi\mu^2}{720KS^2}. \tag{4}$$

With this condition and again substituting $D$ for $(360/2\pi)\alpha$, Eqs. (1) and (2) become:

$$D=-\frac{\mu\omega}{KS}e^{-(\mu/2IS)t}\left[\cos\Gamma t+\frac{\mu}{2IS\Gamma}\sin\Gamma t\right]+\frac{\mu\omega}{KS}$$

where

$$\Gamma=(360K/2\pi I-\mu^2/4I^2S^2)^{\frac{1}{2}}. \tag{5}$$

(3) The oscillation with critical damping where the bob reaches its final position fastest. This most desired case 3 is realized when:

$$\frac{\mu^2}{4I^2S^2}=\frac{360K}{2\pi I} \quad \text{or} \quad I=\frac{\pi\mu^2}{720KS^2}. \tag{6}$$

Then

$$D=-\frac{\mu\omega}{KS}e^{-(\mu/2IS)t}\left(1+\frac{\mu t}{2IS}\right)+\frac{\mu\omega}{KS}. \tag{7}$$

It is also interesting to investigate the case in which the inertia is negligibly small. Under these conditions when $I=0$, the first term of Eq. (1) is omitted and then the equation becomes:

$$\frac{\mu}{S}\frac{d\alpha}{dt}+K\frac{360}{2\pi}\alpha=\frac{\mu}{S}\omega. \tag{8}$$

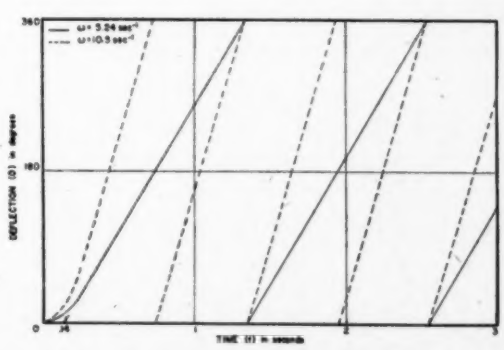

FIG. 2. Recorded cup deflections versus time of rotation for two different cup speeds to indicate cup inertia.

The solution of Eq. (8), if $D$ is again substituted for $(360/2\pi)\alpha$ is:

$$D=-\frac{\mu\omega}{KS}e^{-(360KS/2\pi\mu)t}+\frac{\mu\omega}{KS}. \tag{9}$$

Equation (7) represents the case in which the inertia in the oscillatory system has the highest permissible value without allowing the system to fall into a periodic oscillatory motion. Equation (9) on the other hand represents due to the removal of inertia the extreme case of aperiodic damping provided that everything else is maintained equal (same stiffness and same damping).

Equations (3), (5), (7), and (9) give the deflection ($D$) at any instant only if the angular velocity prevailing in the system before a change took place was zero. Otherwise $D$ is the deflection which has to be added to the prevailing deflection to obtain the new deflection value. The prevailing deflection is equal to $\mu\Omega/KS$, where $\Omega$ is the prevailing angular velocity.

## EXPERIMENTS

Experimental bob deflection-time curves for various rates of shear, test oils and bob inertias, were obtained with the recorder. As mentioned before, Eq. (1) is only correct when dealing with materials whose viscosity is independent of rate of shear and time of application at a constant rate of shear. Therefore, only true Newtonian materials can be used to check experimentally the solutions of Eq. (1). Oils, as shown in the literature,[3] are only true liquids up to their limiting rates of shear. Hence for these experiments they were tested at various rates of shear but only below the limiting rate of shear, where they are definitely known to behave like true liquids.

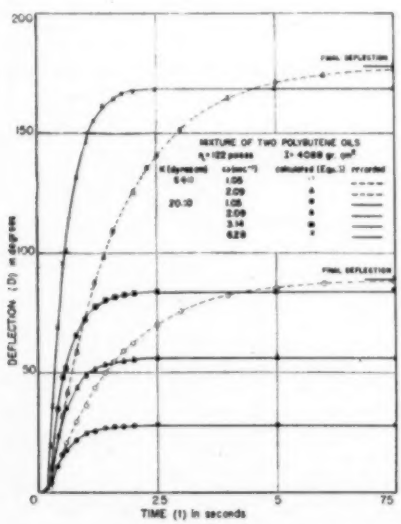


FIG. 3. Aperiodic oscillation curves for an oil in the Newtonian region, showing calculated points superimposed on experimentally recorded curves.

By using materials which varied in viscosity the damping of the oscillatory system was changed. In most cases for materials of different viscosity a change in the stiffness of the spring was required, since otherwise the deflection readings would have become either too small, thus lacking in accuracy, or too large so that the spring would have been overstrained.

In Fig. 3, bob deflection-time curves following Eq. (3), representing the case of over damped or aperiodic oscillation, are shown, for different applied rates of shear. Two bob springs of different stiffness were used. The same is shown in Fig. 4, but for an oil which gives underdamped bob deflection-time curves representing the case of periodic oscillation. In each case the cup started motion at zero time. Thus the prevailing angular velocity ($\Omega$) in both cases was zero. It was found that the equations check the experimental curves only when the time lag ($t_c$) of the cup is taken into consideration. This was done by deducting $t_c$ in each case from the measured time $t$. In Figs. 3 and 4 points obtained from Eqs. (3) and (5), have been super-imposed on the respective experimental curves with very good agreement.

In all cases so far described the inertia of the bob system was kept constant, ($I=4088$ g cm$^2$). In Fig. 5 curves are shown, representing conditions in which the inertia of the bob parts was varied in order to demonstrate that an increase in inertia can change the oscillatory system in such a manner that aperiodic oscillations will become periodic ones even though the same material and the same spring are used. Experimentally the inertia of the bob system was changed by operating without and with the deflection-indicating dial and by substituting the

[3] Weltmann, R. N., Ind. Eng. Chem. Anal. Ed. **15**, 424 (July, 1943).

deflection-indicating dial with various lead disks. The weight of the lead disks was limited only by the carrying capacity of the spring. Thus the inertia was changed in various steps from 452 to 29308 grams cm². The bob deflection-time curves in Fig. 5 have been taken with one oil and at one applied rate of shear but with bob systems of different inertia. As can be seen two of these curves follow Eq. (3), while the other three follow Eq. (5). Again experimentally obtained and calculated bob deflection values are plotted.

### INERTIA OF THE TEST MATERIAL

Since the test material has to be accelerated when changing the cup speed, it was thought that the inertia of the test material in the viscometer might have to be taken into consideration in deciding whether under critical conditions periodic or aperiodic oscillation will result. To obtain experimental evidence about the inertia effect of the material the time-deflection curves of two substances of almost the same viscosity but of quite different specific gravity were recorded at various rates of shear. To exclude the stiffness element from the measurement the bob was decoupled from the spring. The time-deflection curves which were thus obtained were identical for the two test materials used which had a viscosity of about 5.5 poises. One of the two substances was a mineral oil with a specific gravity of 0.93 and the other one was a mercury potassium iodide solution in glycerine with a specific gravity of 2.84. The results are not surprising since the inertia of the test material even with the high specific gravity does not exceed 15 percent of that of the lightest bob system. The specific gravity of the mercury salt solution has been chosen to be high enough so that it will hardly be exceeded by any other material to be tested in the viscometer.

### PRACTICAL CONSIDERATIONS FOR NEWTONIAN LIQUIDS

In the measurement of flow curves of materials of which the flow characteristics had not been previously determined, it is important that the rate of shear can be increased and decreased at a very fast pace. On the other hand precautions must be taken that the rate of increase and decrease is not so high that the bob is prevented

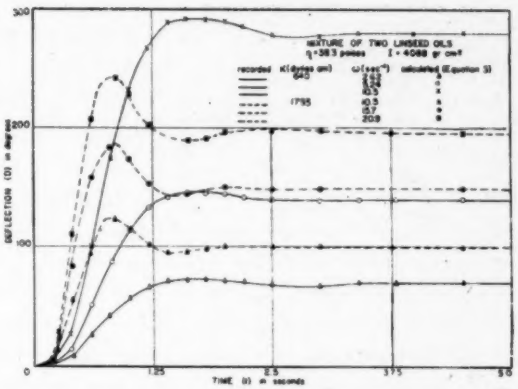


FIG. 4. Periodic oscillation curves for an oil in the Newtonian region, showing calculated points superimposed on experimentally recorded curves.

from attaining its final deflection value for each rate of shear step. The fastest adjustment of the the bob takes place when the oscillatory system is critically damped and it is thus this condition which is most desirable to maintain while performing a flow curve measurement. If the system is underdamped, a condition which will produce periodic oscillations whenever the rate of shear is changed, flow curves could be recorded which would provide shearing stress values for the different rates of shear which are either lower or higher than the correct values. For this reason an overdamped oscillatory system should be used in preference to an underdamped one. In order to accomplish this for materials of low viscosity an extremely low bob inertia is required.

The bob reaches its final position after an infinite time has elapsed. This end value of the deflection is realized in all cases when,

$$D=\frac{\mu\omega}{KS} \quad \text{for} \quad \Omega=0 \tag{10}$$

and

$$D=\frac{\mu(\Omega+\omega)}{KS} \quad \text{for} \quad \Omega\neq 0. \tag{11}$$

Equation (10) represents not only the final deflection when the prevailing angular velocity was zero, but also equals the final deflection value which has to be added to any previously prevailing deflection.

Both Eqs. (10) and (11) will be recognized as the general viscosity equations for a rotational viscometer,[4] and are obtained from Eqs. (3),

[4] M. Reine and R. Riwlin, Kolloid Zeits. **43**, 1 (1927).

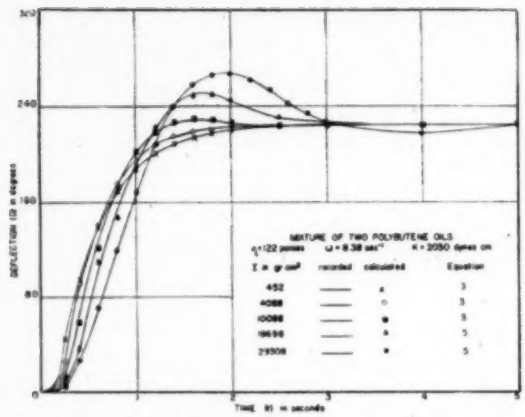

FIG. 5. Oscillation curves of an oil in the Newtonian region obtained with different bob inertias under otherwise constant conditions, showing calculated points superimposed on experimentally recorded curves.

(5), (7), and (9) for an infinite time. When $t$ is infinite the whole first term of all four equations becomes zero. However, for all practical purposes the end position can be assumed to have been reached when the deflection is about 1 percent less than the ultimate value. To obtain a value of 1 percent less than the deflection value $D$ of Eq. (10), the whole first term of Eqs. (3), (5), (7), and (9) has to be equal to the one percent which in turn means that the multiplicant of $\mu\omega/KS$ in the first term has to equal 0.01.

Since periodic oscillations are undesirable because of the possibility of obtaining not only too low, but also too high deflection readings and since the case of critical damping is difficult to achieve in practical tests, the damped oscillation curves will occur most frequently and therefore have been investigated further. It might be recalled that the two limiting conditions for the damped oscillation curves are the critical damping with the highest inertia before periodicity is obtained and the case where no inertia is present.

For the case of critical damping, which gives the fastest deflection movement, the equation which contains the time $t_F$ necessary to reach the final deflection value within 1 percent is,

$$e^{-(\mu/2IS)t_F}\left(1+\frac{\mu}{2IS}t_F\right)=0.01. \tag{12}$$

By employing the graphical method,

$$t_F(\text{critical})\cong\frac{2IS\,6.64}{\mu} \tag{13}$$

and since in this case Eq. (6) is valid,

$$t_F(\text{critical})\cong\frac{6.64\pi\mu}{360KS}. \tag{14}$$

In the case that there is no inertia present the time for a deflection which is 1 percent short of its final position becomes from Eq. (9)

$$t_F(\text{inertialess})=-\frac{2\pi\mu\ \ln 0.01}{360KS}. \tag{15}$$

Thus Eqs. (14) and (15) differ by a factor of about 1.4 That means, that everything else being equal, the fastest swing of the bob takes a little less than $\frac{3}{4}$ of the time which would be required for a swing with an inertialess system. Equation (15) can be written:

$$t_F=0.08\mu/KS=0.08D/\omega. \tag{16}$$

In prior experimental work the author has taken most flow curves in one of the following manners. In the majority of cases the speed of the cup was raised in about 10 distinct steps during a period of about 26 seconds to cover a change of angular cup velocity of about 10 reciprocal seconds. For special runs the change of angular cup velocity of about 10 reciprocal seconds was attained in 13 seconds by taking only 5 steps. Under both these measuring conditions the time available for adjustment of the bob to its final position was 2.6 seconds. Thus $t_F$ in Eq. (16) should not exceed 2.6 seconds. Therefore in the case of flow curve measurements with an inertialess bob system $\mu/KS$ or $D/\omega$ should not exceed 32.5. It is relatively easy to review the validity of previous flow curve measurements by considering the ratio $D/\omega$. In most cases the viscometer constants were so adjusted that for a top angular velocity of about 42 reciprocal seconds (400 r.p.m. of the cup) the bob would rotate for a maximum of 360 degrees. Under these conditions $D/\omega=8.6$, which corresponds to a value of 0.69 second for $t_F$. This certainly means that flow curve measurements have been made with a substantial margin of safety as far as final adjustment time of the bob was concerned. This, of course, is only correct under the assumption that the oscillatory system was overdamped. Therefore, prior to a flow curve

measurement it has to be determined whether the inertia of the oscillatory system is of the correct order (Eq. (2)) to assure overdamped conditions. For low viscosity materials the inertia of the bob and its associated parts were found of the correct order for the overdamped condition only after removing the deflection indicating dial.

## PRACTICAL CONSIDERATIONS FOR NON-NEWTONIAN MATERIALS

Though Eq. (1) as mentioned before is only correct for Newtonian materials, its interpretation can be used to determine whether the decrease in deflection obtained with a thixotropic material is derived from the thixotropic breakdown of that substance or from an undesirable overshooting effect of an underdamped system. The following reasoning might be applied. If the thixotropic material has a sufficiently high viscosity at the top rate of shear at which the shearing stress is measured to overdamp the oscillatory system then it must be assumed from the nature of the thixotropic substance that it would have even a higher damping effect at lower rates of shear since its viscosity must be higher. However, because of the relatively high viscosity at the low rates of shear the time $t_F$ which is required to get the bob within 1 percent of the final position could conceivably be longer than the time interval which is used in performing the step by step flow curve measurement, even if $D/\omega$ is adjusted to be less than 32.5. When that happens the measured shearing stress for a given shearing force is lower than it should be. To illustrate the condition which might exist when measuring a flow curve of a thixotropic material the assumption can be made that the ratio $D/\omega$ for the top rate of shear is again equal to 8.6 which means that the time $t_F$ equals 0.69 second. If a further assumption is made that the viscosity for the first measuring step of the flow curve is four or five times higher than for the top rate of shear, then at this point 2.76 and 3.45 seconds, respectively, would have been required to make the bob come up to within 1 percent of its final deflection. From Eq. (15) it can be calculated that if only 2.6 seconds are allowed to perform a measurement the bob was about 1.4 and 3.2 percent, respectively, off its final value at the instant of recording. In such a case the hysteresis loop of the flow curve would be recorded smaller than the material warrants, especially at the low rate of shear.

It is unfortunate that two contradictory conditions have to be met, when running flow and time-deflection curves of thixotropic materials. Because of the thixotropic nature of the material the measurement should be made speedily to obtain the flow characteristics of the materials before breakdown takes place. On the other hand due to the high viscosity in the beginning of motion the damping is so great that breakdown will start before the final deflection is reached. From Eq. (16) it can be seen that the swing in time ($t_F$) is proportional to the viscosity ($\mu$) and inversely proportional to the torsion constant ($K$). Therefore, to determine the viscosity values of thixotropic materials at low rates of shear with a higher degree of accuracy it is suggested to use a stiffer bob spring than would be otherwise employed. Though the bob deflection when using a stiffer spring will be smaller, the indicated shearing stress allowing the same limited time for taking the measurement will be greater, since the final deflection will be approached faster with the stiffer spring. Unfortunately one is restricted in increasing the spring constant since finally the motion of the bob becomes too small for accurate reacings even when a recorder is used.

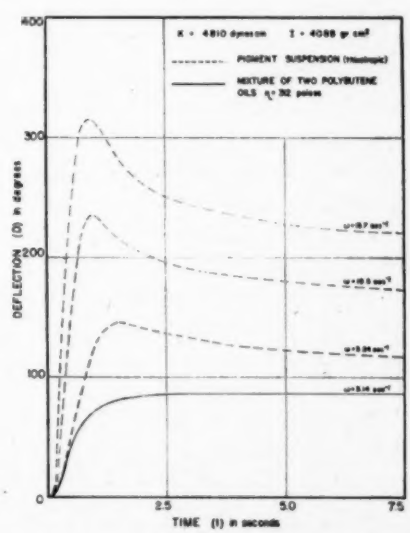


FIG. 6 Aperiodic oscillation curves of a thixotropic pigment suspension compared to that of an oil in the Newtonian region.

For the study of the initial conditions of thixotropic materials a special recorder might have to be designed which could provide some means of amplification of the purposely low deflection readings obtained with a too stiff spring. Such a recorder, for example, might make use of a long light beam which is thrown on a photographic recording paper. Another possibility might be to use a bob arrangement in which the bob is essentially motionless and the shearing force is measured with a strain gage. A high speed electrical recorder should be used to draw the flow curve from the indication of the strain gage.

## COMPARISON BETWEEN NEWTONIAN AND NON-NEWTONIAN BOB DEFLECTION-TIME CURVES

Since bob deflection-time curves can be calculated for true liquids, a deviation from the expected curve will show up any material which is non-Newtonian. Pryce-Jones[5] used a method which was based on this consideration. In accordance with this procedure the bob was in a deflected position before the measurement was started and the bob deflection-time curve was recorded while the bob returned to its zero position. Recently Clark and Hodsman[6] employed a method similar to the one of Pryce-Jones for measuring viscosities.

In distinction to Pryce-Jones and Clark and Hodsman the author is presently engaged in studying at different rates of shear bob deflection-time curves which result from changes of the cup speed for Newtonian and non-Newtonian materials.

In Fig. 6 overdamped bob deflection-time curves are shown at three rates of shear for a thixotropic pigment suspension. In each case the curves were measured starting from a zero rate of shear. The breakdown in thixotropic structure is apparent from the decrease in bob deflection with time. As can be calculated by substituting the maximum deflection in Eq. (16), thixotropic breakdown occurred long before the bob would have reached its final deflection. For comparison one overdamped oil curve was added, which was taken at a rate of shear below its limiting rate of shear and which has a Newtonian viscosity of 312 poises. Attempts are being made to find some means of correlating the bob deflection values for Newtonian and non-Newtonian materials at any instant and rate of shear. No definite data are as yet available. But there are indications that this approach might make it possible to evaluate the consistency of thixotropic materials at very low rates of shear.


## ACKNOWLEDGMENT

The author is grateful to the Interchemical Corporation for permission to publish this paper and expresses thanks to Evelyn Berezin, Marjorie McElligott and Vera Osman for assistance in preparing it.


[5] J. Pryce-Jones, J. Oil and Col. Chem. Assn. **17**, 171 (September, 1934).
[6] A. A. Clark and H. J. Hodsman, J. Soc. Chem. Ind. **56** (February, 1937).

# Stability and High Frequency

AUREL WINTNER
*The Johns Hopkins University, Baltimore 18, Maryland*
(Received April 21, 1947)

In a linear oscillator which is not conservative, let the frequency vary so as to tend to infinity when time increases indefinitely. It seems to be evident that the oscillations must then be of stable type. Actually, this is not true. The paradox results from the circumstance that the relevant criterion of stability depends on the monotone decrease, rather than on the indefinite decrease, of the instantaneous period.

## I

IF a continuous $\omega=\omega(t)$, given for large positive $t$, varies so as to satisfy

$$\omega(t)\to\infty \quad \text{as} \quad t\to\infty, \tag{1}$$

it is usually assumed to be quite evident that the corresponding non-conservative oscillator

$$x''+\omega^2x=0 \tag{2}$$

must be of stable type (in the sense that

$$|x(t)|<\text{const. as } t\to\infty, \tag{3}$$

if $x=x(t)$ is any solution). A closer reflection on the energy balance shows, however, that the stipulation of (1) in (2) as a sufficient criterion for (3) is just a superstition. In fact, it turns out that the variability of $\omega(t)$ can be subject to (1) and be still so much in phase with the loss and gain in energy, that the local amplitudes of a solution of (2) fail to remain under any preassigned bound.

What *is* always true is that (2) must be of stable type if

$$d\omega(t)\geqq 0 \quad \text{when} \quad t_0<t<\infty. \tag{4}$$

But (1) does not imply that (4) is satisfied (nor is, of course, the converse inference true). In fact, if $\omega(t)$ is asymptotically proportional to $t$, say $\omega(t)=t+\theta(t)$, where $\theta(t)$ is of a lower order than $t$ as $t\to\infty$, then (1) is satisfied but (4) need not hold. For, even if the remainder term, $\omega(t)-t$, is of so small an order as to satisfy an inequality $|\theta(t)|<C$ (for some $C=$const.), possible fluctuations of $\theta(t)$ can lead to a situation violating (4). The construction of a $\omega(t)$, by means of which the actual insufficiency of the alleged stability criterion will now be proved, turns out to be precisely of this fluctuating type.

## II

The proof will consist in calculating a pair of functions, $\omega=\omega(t)$ and $r=r(t)$, which satisfy (1) and

$$r(t)\to\infty \quad \text{as} \quad t\to\infty, \tag{5}$$

respectively, and are such that

$$x(t)=r(t)\cos(t^2) \tag{6}$$

becomes a solution of (1). Clearly, (5) and (6) will imply the failure of (3); they will imply even more. In fact, (5) and (6) show that the local maxima (that is, the successive amplitudes) of the elongation $|x(t)|$, instead of being just unbounded, *tend* to $\infty$ as $t\to\infty$.

Substitution of (6) into (2) gives

$$\tfrac{1}{2}\omega^2=\{(2tr'+r)\tan(t^2)+2t^2r-\tfrac{1}{2}r''\}/r. \tag{7}$$

Hence, it is sufficient to show that it is possible to choose some function $r=r(t)$ in such a way that, on the one hand, (5) is fulfilled and, on the other hand, (7) defines, in terms of this $r=r(t)$, a *continuous* function $\omega=\omega(t)$ satisfying (1).

It is understood that $r(t)$ should have continuous derivatives. But this of itself does not take care of the proviso just italicized, since the $\tan(t^2)$, occurring in the definition of $\omega(t)$, has a sequence of infinities. These infinities can, however, be eliminated from (7), by choosing $r=r(t)$ so as to satisfy, for instance, the relation

$$(2tr'+r)r=t\cos^2(t^2). \tag{8}$$

In fact, (7) is reduced by (8) to

$$\tfrac{1}{2}\omega^2=\{t\sin(t^2)\cos(t^2)\}/r^2+2t^2-\tfrac{1}{2}r''/r; \tag{9}$$

so that the infinities of the tangent are compensated by the choice (8) of $r=r(t)$.

## III

Since the product on the left of (8) is identical with the derivative of $tr^2$, the differential equation (8) for $r=r(t)$ is satisfied by

$$r=\left\{\int_0^t s\cos^2(s^2)ds\right\}^{\frac{1}{2}}/t^{\frac{1}{2}}. \tag{10}$$

Clearly, the function (10) is asymptotically proportional to $\{t^2\}^{\frac{1}{2}}/t^{\frac{1}{2}}=t^{\frac{1}{2}}$, that is, there exists a numerical constant, say $c$, satisfying

$$r\sim ct^{\frac{1}{2}} \text{ as } t\to\infty, \text{ where } c>0. \tag{11}$$

But (11) implies (5). Consequently, the proof will be complete if it is verified that, when $r$ is given by (10), the (positive) function $\omega$ which is then defined by (9) is such as to satisfy (1).

According to (11), the first of the three terms on the right of (9) is asymptotically proportional to $\sin(2t^2)$ and remains, therefore, in absolute value less than a constant, as $t\to\infty$. Since the second term on the right of (9) is $t^2$, it follows that the sum of the three terms, which is $\frac{1}{2}\omega^2$, will be asymptotically equal to $t^2$ if the third term is of a lower order than $t^2$. Finally, the third term is the function $r''/r$ which, in view of (11), is of the order of $r''/t^{\frac{1}{2}}$.

Consequently, (1) will be assured if it is ascertained that $r''/t^{\frac{1}{2}}$ is of a lower order than $t^2$. This (and more) will be proved by showing that

$$r''=O(t^{\frac{1}{2}}). \tag{12}$$

In (12), use is made of the familiar notation, $f=O(t^\alpha)$, for any function $f=f(t)$ which is of the order of $t^\alpha$, *at most*. In other words, $f(t)=O(t^\alpha)$ means that the quotient $f(t)/t^\alpha$ stays between finite bounds, as $t\to\infty$. In particular, $f(t)=O(1)$, where $\alpha=0$ means that $|f|<\text{const.}$ as $t\to\infty$. In the following proof of (12), the obvious rules

$$O(t^\alpha)O(t^\beta)=O(t^{\alpha+\beta}), \quad O(1)+O(1)=O(1) \tag{13}$$

will repeatedly be applied.

According to (8),

$$2tr'+r=O(t)/r=O(t^{\frac{1}{2}})$$

by (11). Since this means that $r'=O(t^{\frac{1}{2}})/t-rO(t^{-1})$, it follows that

$$r'=O(t^{-\frac{1}{2}}), \tag{14}$$

again by (11). On the other hand, differentiation of (8) gives

$$(2tr''+3r')r+(2tr'+r)r'=O(t^2).$$

Hence, from (14),

$$tr''r+O(t^{-\frac{1}{2}})r+tO(t^{-\frac{1}{2}})^2+rO(t^{-\frac{1}{2}})=O(t^2).$$

In view of (11), this can be simplified to

$$tr''r+O(1)=O(t^2).$$

Consequently, $rr''=O(t)$, and so (12) follows from (11).

## IV

This proves that condition (1), without (4), does not insure the stability of (2). On the other hand, condition (4), without (1), does insure stability (if $\omega=\omega(t)$ is positive), even though (4) is not a *necessary* condition. That it is *sufficient* for stability, is known to follow by an argument familiar from the theory of Bessel's functions. It proceeds as follows:

Whether (4) is satisfied or not, it is seen (by differentiation) that

$$d(x^2+x'^2/\omega^2)=x'^2d(\omega^{-2}) \tag{15}$$

is an identity in $t$ along any solution $x=x(t)$ of (2), where $\omega=\omega(t)$. If (4) is assumed, then, since $\omega(t)$ is supposed to be positive, the increment on the right of (15) cannot be positive. Hence, the same is true of the increment on the left of (15). This means that the function

$$x^2(t)+x'^2(t)/\omega^2(t) \tag{16}$$

does not increase when $t$ increases. In particular, if $t_1<t_2<\cdots$ is a sequence of $t$-values at which $x'(t)$ vanishes, then, since (16) reduces to $x^2(t)$ when $t=t_1, t_2, \cdots$,

$$|x(t_1)|\geqq|x(t_2)|\geqq\cdots.$$

In other words, the successive amplitudes $|x(t_1)|$, $|x(t_2)|$, $\cdots$, representing the relative maxima of $|x(t)|$, do not increase. This proves more than what is claimed by (3), that is, by mere stability.

# Mechanism of Fracture of Glass and Similar Brittle Solids*

NELSON W. TAYLOR
*Research Department, Minnesota Mining and Manufacturing Company, St. Paul, Minnesota*
(Received May 15, 1947)

A theory is proposed which connects the stress, $f$, required to break a brittle material in simple tension, with its duration of application, $t$. The slow process preceding fracture is shown to be the orientation of the atomic network contained in an elementary prism of length $r=\lambda_0 E/f$, where $E$ is Young's modulus and $\lambda_0$ is the critical elongation required for fracture. The rate-controlling factor is the activation energy, $E\alpha/f$, for the orientation or rearrangement of the atomic network under the stress, $f$. Moisture on glass, and moisture plus oxygen on certain metals, are important catalytic or fatigue-promoting factors because they reduce the unit activation energy, $\alpha$. The theory leads to the equations

$$t=(1/k_0)e^{E\alpha/fkT}$$

and

$$\log t=-\log k_0+(E\alpha/2.3kT)/f,$$

where $t$ is the time for fracture (duration of the stress), $k$ is the Boltzmann constant, $T$ the absolute temperature, and $\alpha$ and $k_0$ are experimentally determined constants. The logarithmic expression has the same form as the Glathart-Preston [J. App. Phys. **17**, 189 (1946)] empirical relation $\log t=-a/m+1/fm$, which, in the case of glass, appears to be valid over a time factor of $10^7$.

The theory shows why a solid object does not have a single characteristic breaking strength, and how it adjusts its fracture mechanism to whatever stress is applied. Quantitative tests of the theory are made, using fracture data on various glasses and on one glass at various temperatures. Applicability of the theory to certain aspects of fatigue of metals under stress-corrosion conditions, as well as to failure by fracture of the more rigid organic plastics, is indicated.

An equation, $E\lambda_0=2\gamma$, is proposed which connects Young's modulus and the critical fracture distance with the surface tension, $\gamma$, of the solid. Some examples are given.

## INTRODUCTION

IN a discussion of the strength of "brittle" materials, it is desirable to define such terms as brittle, ductile, elastic, etc. We speak of glass as a brittle material "par excellence," and yet glass when hot is quite ductile or plastic. Under some conditions, for example under impact, tar is a brittle material, whereas if a more gentle pressure is applied over a period of time the tar will undergo some deformation, part of which is permanent and part slowly recoverable. Rubber, quite typically elastic at room temperature, is brittle at liquid-air temperatures. Thus, we see that time and temperature are important factors.

Webster's new International Dictionary, Second Edition, defines *brittle* as "breaking with very slight deformation;" *ductile* as "capable of being permanently drawn out or hammered thin; capable of being molded or worked;" *elastic* as "capable of recovering size and shape after deformation."

In view of the fact that a substance like glass is quite fluid at very high temperatures, ductile in the temperature range where it is worked into useful shapes, simultaneously ductile and elastic in the annealing range of temperature, brittle at ordinary temperatures and below, and that a substance like tar is brittle or ductile depending on the time element, it is to be seen that there is no sharp dividing line where a substance can pass exclusively from one property to another. It is not surprising, therefore, to find that a brittle material shows elastic properties including not only the instantaneous response but also lesser known reactions called elastic after-working, delayed elastic effect, primary creep, etc. Likewise, normally ductile materials, under impact or brief intense stresses show essentially brittle properties.

As soon as we recognize that "time is a necessary dimension of strength," that it is vital to any consideration of the mechanical properties, we look for the reason. The problem takes on some of the aspects of a chemical reaction running at a characteristic rate, and the concepts and methods of physical chemistry should be applicable.

The strength of brittle materials depends on many factors, not only on the time, but also on the chemical environment, on pre-stressing or residual stresses resulting from the preparation of the test piece, on the method of testing, and on

* Presented at the Annual Meeting, Society of Rheology, New York, New York, November 2, 1946, as part of the Bingham Memorial Symposium.

size and shape. This latter factor is very significant in thin fibers, wires, and foils. Surface cracks may also act as centers of dangerous local stresses. The common belief that every material has a characteristic breaking strength is very far from the truth.

Probably most materials are brittle at the time of actual rupture or fracture. The various molecular or atomic mechanisms which can adjust to the applied stress are exhausted just prior to the instant of fracture. "Primary creep," "slip," "delayed elastic adjustment" appear to be a necessary prelude, determining by their slowness how long the stress can be sustained.

The theory developed in this paper emphasizes this atomic rearrangement as the essential factor determining the time for fracture, and advocates a method of plotting which has both practical and theoretical value.

## I. THE EMPIRICAL LINEAR RELATION: RECIPROCAL STRESS *VS.* LOG TIME

J. L. Glathart and F. W. Preston[1] have presented a linear equation showing the strength of glass as a function of time under constant load. This equation is $1/f=a+m\log t$, where $f$ is the breaking stress, $t$ the time, and $a$ and $m$ are constants. Each line is thus defined by its slope $m=d(1/f)/d(\log t)$ and by the point $(t_0)$, where the line intersects the time axis. This equation is based on the experiments by T. C. Baker[2] in Preston's laboratory, covering the exceptionally large time range of $10^7$.

The above equation may be written

$$\log t=-a/m+1/fm.$$

The numerical values of the slope $m$ range from $0.72\times10^{-5}$ to $2.93\times10^{-5}$ in.$^2$/lb. for disannealed Pyrex, dry, and for plate glass, dry, respectively. However, much smaller values of the slope are indicated in the case of glass which had been especially dried by baking at 350°C in high vacuum. From the data on experiment VII of the Baker and Preston paper the value of $m$ for soda-lime glass is calculated to be only $0.04\times10^{-5}$. In fact, some data are shown in which there appears, within the limits of experimental error, to be no decline of strength in glass which had been very thoroughly vacuum-dried by baking at 0.1-micron mercury pressure for 10 minutes at 350°C. The value of $m$ in this case would be smaller than $0.04\times10^{-5}$. This shows that moisture plays a very important role in bringing about fatigue or decline in strength of glass under load, with the passage of time. Removal of moisture also raises the absolute strength in experiments conducted at constant time. As stated by Baker and Preston, in certain tests the ratio of the vacuum strength to the wet strength is 2.5 for Pyrex, 2.0 for soda-lime glass, 1.7 for silica glass, and 1.5 for porcelain.

If we regard the empirical relation of Glathart and Preston as measuring the speed of a molecular process, we can consider that this speed is controlled by an activation energy, just as we find the speed of an ordinary chemical reaction controlled by such an energy. This activation energy is a minimum energy which a molecular complex must acquire before it is in a position to undergo reaction. Certain bonds must be broken or weakened before new bonds can form. It would appear that moisture has the effect of greatly lowering the activation energy for fracture of glass. In other words, the presence of moisture somehow provides a mechanism of molecular rearrangement which requires lower energy than if moisture is absent. This seems reasonable since $H_2O$ can convert the strong Si−O−Si bond into weak Si−OH bonds. A theoretical derivation of an equation taking account of this activation energy will now be set forth.

## II. THEORY OF THE FRACTURE PROCESS

We shall imagine that the elementary process in fracture consists in the slow elongation of the strongest bonds in an elementary or unit rectangular prism having length, $r$, cross-sectional area, $A$, and volume $V=rA$. Under tension $f$ parallel to the length, there will be, according to Hooke's law, an extension of the prism in the amount $\lambda_0$ where $\lambda_0/r=f/E$, $E$ being Young's modulus. This establishes the length $r$ in terms of a characteristic unit of length, $\lambda_0$. The prism may be regarded as made up of $E/f$ layers, each $\lambda_0$ in

[1] J. L. Glathart and F. W. Preston, "The fatigue modulus of Glass," J. App. Phys. **17**, 189 (1946). See also F. W. Preston, "Strength of glass and duration of stressing," Nature **156**, 55 (July 14, 1945).

[2] T. C. Baker and F. W. Preston, "Fatigue of glass under static loads; effect of water on the strength of glass," J. App. Phys. **17**, 170 (1946).

thickness and $A$ in area. Let the extension $\lambda_0$ of the prism be just sufficient for fracture. The activation energy for fracture is then equal to $\alpha E/f$, where $\alpha$ is the activation energy required for orientation and associated stretching of each layer of thickness $\lambda_0$ and area $A$. (See Fig. 1.) The product $\alpha E/f$ represents the whole activation energy for orientation and consequent stretching of all of the network of atoms contained in the volume $V$. Since $\lambda_0/r=f/E$ and since $\lambda_0$ is a characteristic constant length, $r$ becomes less as $f$ increases, so that for constant cross-sectional area the volume $V$ diminishes as $f$ increases. It thus appears that the activation energy for orientation and stretching of the material contained in volume $V$ will diminish as $f$ increases. The rate of the fracture process is, therefore, the rate at which the material in $V$ acquires its critical activation energy $\alpha E/f$, and this can be written:

$$\text{rate of fracture}^{**}=k_0e^{-E\alpha/fkT}.$$

The corresponding time for fracture then becomes:

$$t=(1/k_0)e^{E\alpha/fkT}$$

and

$$\log t=-\log k_0+(E\alpha/2.3kT)/f.$$

This equation is of exactly the same form as that of the empirical Glathart-Preston relation: $\log t=-a/m+1/fm$. We see that $m=2.3kT/E\alpha$. It is to be emphasized that the assumption of a characteristic or critical energy which must be supplied per unit of length $\lambda_0$ (or more exactly, per unit of volume $\lambda_0A$) leads to a theoretical equation exactly identical in form with the empirical linear relation, namely that the logarithm of time for fracture is inversely proportional to the stress.

The equation $m=2.3kT/E\alpha$ is dimensionally correct because $m$ has the dimensions of reciprocal stress, $E$ has the dimensions of stress, and $\alpha$ and $kT$ have the dimensions of energy. It is probably impossible to predict the value of $\alpha$ from fundamental considerations, since it is the experience in chemical kinetics that the activation energy can be calculated from fundamental constants only in the case of very simple gas reactions. However, $\alpha$ can be derived from the experimental data by the use of the equation given here.

The basic assumptions may be re-stated as follows: The strongest atomic bond in the system must be stretched a distance $\lambda_0$ in order to effect fracture. This elongation $\lambda_0$ is constant, regardless of the stress. The length of the chain of atoms which cooperates to produce this elongation $\lambda_0$ is $r=\lambda_0E/f$ and, therefore, is inversely proportional to $f$. The elongation of this chain, or more properly speaking, the elongation of a prism of length $r$ and area $A$, is a slow process because of the many bond angles which must be changed and the many atoms which have to be squeezed and rearranged in order to permit elongation of the strongest bond in the amount $\lambda_0$. When this elongation has occurred, it can be imagined as being distributed in a statistical way among all the bonds whose total length is $r$, but because of extremely rapid thermal vibration, the whole $\lambda_0$ soon concentrates on some one bond and then fracture occurs. This redistribution is a very rapid process. The rate-controlling process is a relatively slow orientation of the whole network of atoms whose total length is $r$. The activation energy necessary for the orientation process has a characteristic value per unit of length, so that if for convenience $\lambda_0$ be regarded as that unit, we define $\alpha$ as the activation energy required per unit of length $\lambda_0$, with cross-sectional area $A$. The whole activation energy, then, for the elementary process of fracture, is $\alpha E/f$. One can see that when the stress is small, the time for fracture is

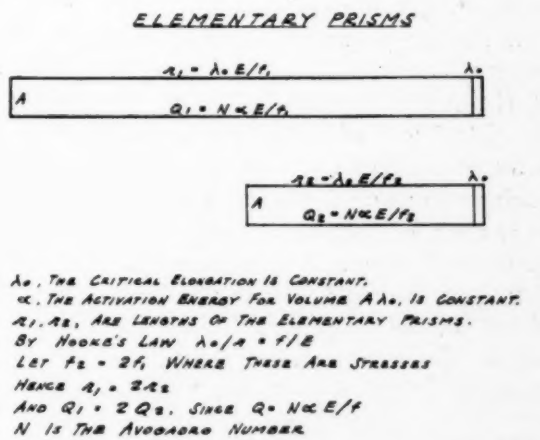


FIG. 1. Elementary prisms functioning as units in the fracture process.

** For details as to the connection between rate of elongation and rate of fracture, see the next section.

very long because the elementary cell or prism which has to acquire the critical activation energy $\alpha E/f$ is large. When the breaking stress is high, the elementary cell is smaller, $\alpha E/f$ is smaller, and fracture occurs sooner. The solid responds automatically to any tension which is imposed, and will break under that stress if it is applied for the right length of time. *Thus we cannot speak of a definite characteristic breaking stress of the specimen.* However, for practical purposes the times for fracture under mild stresses may be so extremely long that they can be regarded as unlimited. This is why the concept of an "endurance limit" has been found useful in the fatigue testing of metals.

### A. Phenomena Preceding Fracture

A series of researches by Taylor[3] and coworkers have shown that in the annealing range of temperature the elastic deformation of a glass fiber or rod under tension may be represented by one or more terms, each of which follows the law $dl/dt=-kl$, where $l$ is the unstretched length or the distance from equilibrium. The elongation is rapid at first but falls off with time because the fraction of the molecular network available for orientation is rapidly decreased. In this respect the phenomenon is much like radioactive decay.

The same law is found to hold at room temperature, for example, in the change of readings of a fixed point such as the ice-point of a thermometer. (See Taylor and Noyes.[4]) In one case, measured at room temperature, the "half-life" for the process was 6.75 months.

In fracture phenomena, our tests are usually of much shorter duration, and we find that the rate of elongation appears to follow the law $dl/dt=-k_0'e^{-Ea/fkT}$, which is to say, that for a given value of the stress, $f$, the rate $dl/dt$ is constant. Such a result would follow if the magnitude of the elongation $\lambda_0$ which is necessary for fracture is quite small compared with the original length, so that $l$ on the right side of the expression $dl/dt=-kl$ (or the apparent value of $r$ in the expression $dr/dt=-kr$) changed very little. Now the ratio $f/E$ in the glass fracture studies of Baker and Preston never exceeded 1/300, so this represents the maximum ratio of $\lambda_0/r$ for these experiments. This ratio is also small in most fatigue tests on metals, since $E$ is about $10^7$ p.s.i., and $f$ rarely exceeds $5\times10^4$, yielding a maximum $f/E$ of 1/200. Hence, we appear to be justified in converting the differential rate, $dl/dt$, to the integral form $\Delta l/\Delta t=\lambda_0/t$, where $\lambda_0$ is the characteristic critical elongation required for fracture, and $t$ is the duration of the stress.

Hence if the rate of elongation of the unit cell or prism of length, $r$, under stress, $f$, is $dr/dt=-frk_0''e^{-Ea/fkT}$, then $\lambda_0/t=-frk_0''e^{-Ea/fkT}$. But the apparent value of $r$ does not change appreciably, and $fr=E\lambda_0$, so that

$$\lambda_0/t=-E\lambda_0k_0''e^{-Ea/fkT},$$

$$1/t=-Ek_0''e^{-Ea/fkT},$$

$$t=-\frac{e^{Ea/fkT}}{k_0},\quad\text{where}\quad Ek_0''=k_0,$$

and

$$\log t=-\log k_0+(E\alpha/2.3kT)/f.$$

(in converting to logarithms we discard the negative sign in the preceding equation since this came originally from the equation $dr/dt=-kr$, and has no effect on the *numerical* value of $t$ or $\log t$). Negative values of $t$, the duration of stress, are meaningless.

The proper value of $E$ to use in the calculation is the mean value of the modulus over the whole range of strain from $dr/r=0$ to $dr/r=\lambda_0/r$. Since $\lambda_0/r$ is 1/200 or less we are justified in using the ordinarily measured value of $E$ which is obtained for lower values of $dr/r$ (or of $dl/l$).

If fracture tests are conducted at relatively high ratios of $f/E$, e.g., as high as 10 percent, the ratio $\lambda_0/r$ would be as high as 10 percent when fracture occurs. Some very strong short glass fibers, having a diameter $5\times10^{-4}$ inch, which were studied by F. O. Anderegg[5] showed 6 percent elongation at fracture. The percentage elongation was less for longer fibers, following a systematic trend. Anderegg estimated that a fiber of zero length would elongate 14.5 percent before fracturing. For these relatively large elongations

[3] N. W. Taylor, "Elastic after-effects and dielectric absorption in glass," J. App. Phys. **12**, 753 (1941).

[4] N. W. Taylor and B. Noyes, "Aging thermometers," J. Am. Ceram. Soc. **27**, 57 (1944).

[5] F. O. Anderegg, "Strength of glass fiber," Ind. Eng. Chem. **31**, 290 (1939).

we must express the rate of elongation

$$dr/dt = -frk_0''e^{-E\alpha/fkT},$$

in the form

$$d\ \ln r/dt = -fk_0''e^{-E\alpha/fkT},$$

$$[-\ln r/(r+\lambda_0)]/t = fk_0''e^{-E\alpha/fkT}.$$

Again we discard the negative sign, so that

$$t = \frac{\ln r/(r+\lambda_0)}{fk_0''} \cdot e^{E\alpha/fkT}.$$

Actually these very strong fibers broke immediately, as soon as the full stress was reached, and it is practically impossible to determine the time effect. The reason for the extremely rapid fracture is that the ratio $E/f$ in Anderegg's case is only about 10 instead of about 300–1000 of Preston *et al*, so that the activation energy, $E\alpha/f$ is reduced by the factor 10/300 or 10/1000. This change occurs in the exponent so that it (profoundly) reduces the time for fracture, $t$, to a time which is inaccessible by our ordinary methods of measurement. The following excerpts are from Anderegg: "It seems unlikely that variation in the rate of loading is of any importance in these results. The stress-strain curves were all perfectly straight, as far as the methods would indicate." This latter statement indicates that the ordinary modulus $E$ is applicable right up to fracture.

We are therefore justified in writing our theoretical equation connecting breaking stress, $f$, with its duration, $t$ as follows:

$$\log t = -\log k_0 + (E\alpha/2.3kT)/f.$$

Some very careful experiments have been made which have failed to reveal evidence of creep. For example, F. W. Preston[6] quotes some experiments by J. T. Littleton on strong rods of borosilicate glass where very high stresses were used and where delicate optical tests failed to show creep. Preston also mentions experiments by a French worker, Grenet, in 1899, which had been carried to the point of fracture, but no displacement of optical interference fringes were observed during the last two or three minutes before fracture took place.

[6] F. W. Preston, "The time factor in the testing of glassware," J. Am. Ceram. Soc. **18**, 220 (1935).

One possible interpretation of the negative results of Littleton and of Grenet would be that there is an internal molecular rearrangement taking place in the glass at constant total strain. In other words, the effect of the load is to produce deformation of a certain magnitude, and then with the passage of time molecular rearrangement occurs, resulting in fracture. There is direct evidence for such molecular rearrangement in glass at room temperature. Some of the early work by F. Kohlrausch[7] in 1863 demonstrated this. Kohlrausch twisted a glass filament through a given angle and measured the torque necessary to hold the filament at that constant angle of twist over a period of 24 hours. The torque gradually fell approximately proportionally to the logarithm of the time. There is much subsequent work demonstrating this relaxation phenomenon under constant deformation, and it has been shown that this is an elastic phenomenon rather than a viscous flow or permanent set, because the phenomenon is reversible. It therefore appears that we are justified in our belief that slow internal molecular rearrangements do, in fact, precede the actual fracture. Not very much detail can be given as to the actual molecular process, but it seems likely that the weaker parts of the network take up the initial strain and that this strain is transferred slowly to the stronger bonds, so as to effect a more equitable distribution of the strain energy between all the kinds of bonds in the system. However, when these stronger bonds become stretched sufficiently, fracture results.

Similar ideas regarding the transfer of strain energy by molecular rearrangement have been expressed by S. A. Shorter.[8] The following is quoted from Shorter: "If a given force be applied rapidly and maintained for a lengthy period of time, we get a rapid extension followed by a slow one. The process of extension proceeds for a very lengthy period—days or even weeks. The explanation of this is not as might be supposed that the elastic elements are showing a plastic yield, but

[7] F. Kohlrausch, "Ueber die Elastische Nachwirkung bei der Torsion," Pogg. Ann. Physik [4] **29**, 337 (1863).

[8] S. A. Shorter, "Investigation of the nature of elasticity of fibers," J. Textile Inst. **15**, T207 (1924); "The physical properties of textile fibers in relation to technical processes and to general colloid theory," Trans. Faraday Soc. **20**, 228 (1924).

that the fiber contains elastic elements with very different degrees of damping so that on the first application of an external force, the more lightly damped elements extend, and as time goes on, the extension of the more highly damped elements begins to show itself, We get a similar effect on removing the external force, and it is undoubtedly the extreme slowness of the recovery of the more highly damped elements that has given rise to the erroneous ideas of plasticity and permanent strains. Similar considerations apply to the case where a fiber is held stretched to a definite length. We get an apparent elastic relaxation which, however, is very different from the effect contemplated in Maxwell's theory of viscosity."

A familiar example of decrease in tension in a fiber held at constant length is the decline in pitch of a violin string.

"It is not the disappearance of a state of strain owing to molecular readjustment, it is merely a transference of a state of strain from lightly damped to highly damped elements."

### B. Role of the Chemical Environment

One can only guess at the details of the atomic rearrangements which occur during the instantaneous and the delayed elastic elongation. The instantaneous part probably corresponds to elongation of the network as a whole, that is, each atom or ion is displaced or deformed slightly without disrupting the framework. This establishes a higher potential energy for the system, and *sets the stage* for the slow rearrangement which follows. This slow step is of a much more profound nature than the first since it calls for the expenditure of a substantial activation energy, which may be as high as 100,000 to 200,000 calories.[9] On the other hand, it may be quite small if "catalytic" agents such as moisture or other chemically active gases are present. In soda-lime glass which has been vacuum-baked to remove moisture, the atomic rearrangement probably involves first breaking of Na−O bonds, these being the weakest bonds in the structure. The stress is then transferred to stronger bonds such as Ca−O, and ultimately to Si−O which is the strongest of all. Finally, when the Si−O bonds are stretched to a sufficient extent, fracture occurs. In silicate crystals cleavage usually takes place in such a way as to avoid breaking the strong Si−O bonds, but in quartz and in glasses this cannot be avoided. All of this rearrangement (prior to fracture) could take place without any elongation beyond the original instantaneous stretch, since the stretch due to bond breaking might be compensated by a contraction due to the deformed atoms returning in part to their normal shape. We have a good deal of experimental evidence of such compensation in the behavior of electric condensers made of glass,[3] and also in the elastic response of glass, rubber, etc. as a result of a complex history.

Corrosive or chemically active gases or liquids definitely accelerate the rearrangement of the atoms of the solid and shorten the time for fracture. They do this by providing a mechanism of low activation energy, as shown by the steep $E/f$ *vs.* $\log t$ curves, the slope being $2.3kT/\alpha$. There are various possible mechanisms for this acceleration. One is that strong primary bonds such as Si−O−Ca or Si−O−Si are disrupted by reaction (e.g., with $H_2O$) and that the heat of this reaction supplies part of the requirements of the activation energy for the delayed elastic process. Likewise in metals, the heat of oxidation would supply energy to aid in the dissociation of the bonds which join the metal atoms.

The linear relation, $\log t = -a/m + 1/fm$ implies constancy of the slope $m$ over the whole duration of the test. This means that the "catalyst" has a constant influence over the whole period, and that the activation energy for molecular rearrangement is constant over this period. One would expect this to happen in glass if the moisture content remained constant. However, the situation might arise in long time tests where the sample gradually dried out. In this case, the activation energy would gradually rise and the later points of the curve would fall below the projected straight line which represented the results of the early part of the experiment. Likewise, an increase in moisture content, due to a higher humidity in the atmosphere, might cause an upward trend in the $1/f$ values. This sensitivity to the environment must be a general phenomenon in the fatigue testing of materials of

[9] N. W. Taylor, E. McNamara, and J. Sherman, "A study of the elastico-viscous properties of a soda-lime-silica glass at temperatures near the transformation point," J. Soc. Glass. Tech. **21**, 61 (1937).

TABLE I. Percentage elongation at rupture (or fracture).

| $f$ (p.s.i.) | $E$ (p.s.i.) | calculated $(f/E)100$ | observed $(dl/l)100$ |
|---|---|---|---|
| $0.204\times10^6$ | $2.8\times10^6$ | 7.3 | $6.1\pm1.7$ |
| 0.219 | 4.9 | 4.5 | $4.5\pm0.8$ |
| 0.182 | 5.2 | 3.5 | $4.1\pm0.2$ |
| 0.160 | 6.3 | 2.5 | $2.6\pm0.5$ |
| 0.112 | 4.7 | 2.4 | $2.3\pm0.4$ |
| 0.107 | 6.3 | 1.7 | $1.7\pm0.2$ |

all kinds. The test piece should be seasoned before the fatigue tests are begun in order that it may come into "equilibrium" with the environment.

Solids under tension are at a higher potential energy and are therefore more susceptible to chemical attack than when stress-free, so that even the mildest agents may shorten the time for fracture. For this reason, investigations pointing toward more chemically-resistant materials, toward stable protective coatings, and toward reduction of tension by pre-stressing, are very much worth while. In high temperature service, corrosion may be very rapid and the danger of fracture very greatly enhanced. The problem is a critical one for the development of gas turbines, jet engines, etc.

In view of the intimate relation which appears to exist between the slow atomic rearrangement and the time required for fracture, it would be of great interest to determine quantitatively the rate constants for the delayed elastic effects in solids as affected by different chemical environments, comparing these with corresponding data from fatigue tests under stress-corrosion conditions. These studies could take the form of measurement of the decrease in Young's Modulus as a function of the time, for example by measuring the force needed to maintain a given displacement. Another procedure would be to measure the residual displacement (and its rate of relaxation) after holding a sample under a given tension for various lengths of time. Recent developments in strain gauges should make these latter measurements quite easy.

### C. Percentage Elongation at Fracture as a Test of the Theory

The present theory assumes that $\lambda_0$ is constant. The percentage elongation at fracture, $(\lambda_0/r)100$, should therefore not be constant for different stresses, but should be equal to the corresponding percentage of the breaking stress in terms of the modulus of elasticity, $(f/E)100$. Now $\lambda_0/r$ cannot be measured directly but $\lambda_0/r=dl/l$, if the tension is the same along the whole length, $l$, of the specimen. Fortunately, all the necessary data are available from the work of Anderegg,[5] who broke his very strong glass fibers by straight pulling. Table I shows Anderegg's directly observed percentage elongations and also those calculated as the ratio of his observed $f$'s and $E$'s. The data are from Table II of Anderegg's paper.

It is to be noted that the agreement is quite good. The lack of constancy in the percentage elongation forces us to discard the old idea that fracture occurs when a certain percentage elongation of the specimen is reached. On the other hand, the results are consistent with the concept that the elongation $\lambda_0$, necessary for fracture, is constant. Unfortunately, we are not in a position as yet to calculate $\lambda_0$ with certainty. Anderegg estimated by extrapolation that a fiber of zero length should elongate 14.5 percent before fracture. We might regard this as 14.5 percent of the normal length of the strongest bond in a glass, which is the silicon-oxygen bond, known from x-ray data to be 1.62 Ångstrom units. In this case, $\lambda_0$ would be $1.62\times0.145=0.23$A. Hence, for example, when $E/f=r/\lambda_0=1000$, we find $r=230$A.

### D. Possibility of Viscous Flow?

The term "primary creep" is used in this paper in the sense of a reversible delayed elastic process. The question arises as to whether true viscous flow accompanies the elastic deformation preceding fracture of brittle materials, as it does, for example, in glasses in their annealing range of temperature. Anderegg's observations that the percentage elongation at fracture of his glass fibers were equal to the calculated elastic distortion $f/E$, would seem to eliminate the presence of viscous flow, or at least make it negligible. Under "weaker" stresses, where $f/E$ is 1/200 or less, it seems even less probable. Viscous flow is not the essential process in fracture, although it is barely possible that it goes on in parallel with the elastic deformation that does lead to fracture. Possibly one reason why a material is brittle is that it may have lost that capacity for

viscous flow which it possessed at higher temperatures.

### E. Surface Tension of the Solid

The product $E\lambda_0$ measures the energy per unit area which is released when fracture occurs. If this all goes into new surface we may write $E\lambda_0 = 2\gamma$, where $\gamma$ is the surface tension, or specific surface energy. Taking $E = 5.0\times10^6$ p.s.i., which is the mean value of Anderegg's moduli in his Table II, and using $\lambda_0 = 0.23\times10^{-8}$ cm, gives $\gamma = 400$ ergs/cm². Since this result depends very much on the values assigned to $E$ and to $\lambda_0$, it must be taken with caution. It is, however, of the right order of magnitude. Parmelee, Lyon, and Harmon[10] give $\gamma = 336 - 0.0671t$, where $t$ = °C, for a glass containing 10 percent $Na_2O$, 20 percent $B_2O_3$, 70 percent $SiO_2$, the measurements being made at 1150–1350°C. Extrapolation to 24°C yields $\gamma = 335$ ergs/cm².

In cases where $E$ and $\gamma$ are known, $\lambda_0$ can be calculated, $\lambda_0 = 2\gamma/E$. Let us assume that the ratio $\gamma/E$ for ice is the same as that for water. From the velocity of sound in water, $v = 1.45\times10^5$ cm/sec., we calculate $E$ from the relation $v = (E/\rho)^{\frac{1}{2}}$ where $\rho$ is the density. Thus $E = 2.10\times10^{10}$ dynes/cm². Taking $\gamma = 73$ dynes/cm we find $\lambda_0 = 0.7$A. This is about one-half the length of the H−O bond in water or ice, 1.275A. We shall make similar calculations for lead and zinc in order to get some idea of the critical bond elongation in these metals. The calculations are only approximate, since the pertinent data are not all available for one and the same temperature. For *lead*, $\gamma_{liq} = 445$ dynes/cm, $E$ (calc. from the velocity of sound and density of the solid Pb) $= 1.60\times10^{11}$ dynes/cm². Then $\lambda_0 = 0.56$A. The Pb-Pb distance from x-ray data is 3.5A, so that $\lambda_0$ is 16 percent of this bond length. For *zinc*, $\gamma_{liq} = 750$ dynes/cm, $E_{solid} = 9.8\times10^{11}$ dynes/cm². Therefore, $\lambda_0 = 0.15$A. The Zn-Zn distance is 2.65A, so that $\lambda_0$ is 6 percent of this bond length. The percentages are substantially less than that for $H_2O$, and more like that for the glass. Probably each substance has its characteristic percentage determined by its valences, type of binding, etc.

TABLE II. (Temperature 75°F, 297°A). Unit activation energies, $\alpha$.

| Material | $m$(in.²/lb.) | $E$(lb./in.²) | $\alpha$ |
|---|---|---|---|
| Disannealed Pyrex, dry | $0.72\times10^{-5}$ | $8.86\times10^6$ | $10.7k$ |
| Scratched Pyrex, wet | 1.74 | $8.86\times10^6$ | $4.44k$ |
| Annealed soda-lime glass, wet | 1.51 | $(1\times10^7)$ | $4.53k$ |
| Annealed lead glass, wet | 1.34 | $8.7\times10^6$ | $6.10k$ |
| Fused silica, wet | 0.70 | $1.01\times10^7$ | $9.67k$ |
| Porcelain, type $A$, dry | 0.88 | $1.28\times10^7$ | $6.07k$ |
| Porcelain, type $B$, dry | 0.90 | $1.28\times10^7$ | $5.94k$ |
| Porcelain, type $C$, dry | 1.35 | $1.28\times10^7$ | $3.96k$ |
| Plate glass, dry | 2.93 | $1.00\times10^7$ | $2.33k$ |

### F. Testing Procedure

Some tests on breaking strength or on fatigue are conducted with a steadily increasing load. Such tests are difficult to interpret because of the difficulty of integrating the effects of the load over a period of time. Some tests, for example, on organic plastics, are conducted under such a condition that the cross section of the sample decreases markedly during the test. These tests are also difficult, if not impossible, to interpret. Some tests apply a periodic or cyclic stress, the mean value of which may or may not be calculable. The simplest method of testing which will give results useful from a theoretical point of view are those conducted at constant stress.

The condition of the surface of the material, of course, plays an important role in determining its strength characteristics. Presence of scratches or notches act as stress concentrators and, therefore, make it difficult to calculate the actual stress existing prior to failure. Probably one of the main factors in causing scatter of test results is just this inability to be able to determine actually the stress which exists at the point where fracture starts. Precompression of the surface by special heat treatments or, in the case of metals, by peening, tends to raise the strength. However, if the amount of pre-stressing is not accurately known, the net tensional stress existing will not be truly known.

In view of the well-known influence on strength of the size and shape of the specimen, it is necessary that this be recognized in any series of tests. James Bailey[11] has given a statistical treatment

[10] C. W. Parmelee, K. C. Lyon, and C. G. Harmon, "The surface tensions of molten glasses," Univ. of Ill. Eng. Exp. Sta. Bull. Ser. No. 311 (1939).

[11] J. Bailey, "An attempt to correlate some tensile strength measurements on glass," Glass Ind. **20**, 21, 59, 95, 143 (1939).

which shows that if surface defects (flaws) are distributed randomly, the probability of obtaining a flaw in the highly stressed region of the specimen becomes a function of the stressed area. His idea explains the fact that the mean strength of a number of rods or laths is higher when tested in cross-bending by the single knife-edge method than by the double knife-edge method. In some A.S.T.M. experiments made at Corning, these mean values were 15,000 and 10,000 p.s.i., respectively. The latter method establishes a high uniform stress over a large area, whereas the single knife edge produces a high stress gradient.

Bailey saw that his theory was not sufficient to account for the very high strength of glass fibers, and he postulated that possibly there was a very good orientation of the "flaws" in these fibers, parallel to the fiber axis. Later, Powell and Preston[12] showed that equally high strengths could be obtained on large pieces of glass under certain conditions of loading. These authors concluded that the assumption of oriented flaws was of no help in explaining the high strengths. The writer makes an alternate proposal in this regard: exceptionally high strengths always appear to be associated with tests which place some part of the specimen in compression. Thus, for example, fine wires or fibers are compressed radially while being stretched axially, and the strength goes up as the diameter diminishes. Likewise, in the Hertz ball method[12] the area directly beneath the ball is under compression, surrounded by a cone in radial tension. The smaller the ball the higher is the measured breaking strength of the glass. Careful analysis of the stress distribution in these two cases should lead to a relation between strength and area which should be valid if the duration of the stress to produce fracture, i.e., the breaking time, is kept constant.

Bailey recognized that time is a factor in determining the breaking strength of glass, and in fact he conducted a series of tests "wherein strips of window glass were loaded by bending to a stress corresponding to approximately 12,000 p.s.i. in about 0.2 sec., then released and reloaded at a rate of about 1 cycle per sec. The samples were eventually broken by this repeated loading.

[12] H. E. Powell and F. W. Preston, "Microstrength of glass," J. Am. Ceram. Soc. 28, 145 (1945).

TABLE III. Molal activation energies, $Q$, for fracture.

| Material | Time ($t$) (sec.) | $f$ (p.s.i.) | $E/f$ | $Q$ (cal.) |
|---|---|---|---|---|
| Disannealed Pyrex, dry | 0.01 | 24,600 | 360 | 7,704 |
| | 1.00 | 17,100 | 518 | 11,085 |
| | 1000.00 | 12,800 | 692 | 14,809 |
| Scratched Pyrex, wet | 0.01 | 12,900 | 687 | 6,100 |
| | 1.00 | 9,000 | 984 | 8,738 |
| | 1000.00 | 5,750 | 1540 | 13,675 |
| Porcelain, type *B*, dry | 0.01 | 15,400 | 830 | 9,800 |
| | 1.00 | 11,900 | 1076 | 12,783 |
| | 1000.00 | 9,100 | 1407 | 16,715 |
| Vacuum-baked soda-lime glass | 10.00 | 25,330 | 395 | 135,090 |
| Soda-lime glass, wet | 10.00 | 10,500 | 952 | 8,625 |

The usual spread of results was found but the evidence was definite that the effect of repeated loading was, at least to some degree, cumulative. Fatigue effects could, no doubt, be entirely removed by annealing or heating the glass to a sufficient temperature to permit molecular rearrangements."

### G. Importance of the $E/f$ *vs.* log$t$ Relation

The present theory indicates the desirability of plotting $1/f$ or $E/f$ *versus* log$t$. Objection may be raised to the use of reciprocal stress, $1/f$, on the ground that it is a difficult concept to understand. On the other hand, $E$ can usually be determined, and it is preferable to use $E/f$, which is the ratio of Young's modulus to the stress, and is a pure number. A plot of $E/f$ as ordinate *vs.* log$t$ as abscissa, should yield a straight line having the slope $2.3kT/\alpha$. A steep slope thus denotes a small value of $\alpha$, while a nearly horizontal line denotes that $\alpha$, the unit activation energy, is quite large. Increase of $T$ will increase the slope, if $\alpha$ remains constant.

When the object has been pre-stressed to a surface compression, $x$, parallel to the applied tension, the net tension is $f-x$. In this case a plot of $E/(f-x)$ *vs.* log$t$ should be linear, and a plot of $E/f$ *vs.* log$t$ should be concave downward. The magnitude of the original compression, $x$, can be determined by trial, until the plot of $E/(f-x)$ *vs.* log$t$ becomes linear. It may also be determined analytically by simultaneous solution of three equations, since the only unknowns are log$k_0$, $\alpha$, and $x$. In order to insure constancy of $\alpha$, the sample should be allowed to come to equilibrium with the chemical environment, before stress is applied. The existence of a substantial precom-

pression, $x$, may be responsible for the extremely long life of specimens when tested under low tensions, $f$, since $f-x$ may actually be quite small.

If a systematic study is made of the variation of $\alpha$ resulting from different chemical environments, e.g., moisture, oxygen, moisture plus oxygen, vacuum, etc. a pattern will undoubtedly develop which will lead to a more detailed understanding of the chemistry of the stress-corrosion process in any particular case, and of the means of protection. Some examples will now be presented.

### III. CALCULATION OF $\alpha$ FOR SEVERAL GLASSES

Data summarized by Glathart and Preston in their Table I "Average breaking stress in pounds per square inch (and its reciprocal) for various durations of load" permit calculation of the slopes $m$. These are shown in Table II. Additional columns show $E$ (from the International Critical Tables) and $\alpha$ calculated from the equation $m=2.3kT/E\alpha$. The value of the Boltzmann constant $k=1.38\times10^{-16}$ ergs per degree, but for convenience $\alpha$ will be expressed as a certain number of $k$'s, rather than in absolute units.

The molal activation energies, $Q$ (Table III), may be calculated for each value of the breaking stress at corresponding durations of load, by the equation $Q=N\alpha E/f$, where $N=$ Avogadro's number and where $Nk=R=2$ cal./mole. Typical calculations will be made for breaking times of 0.01 sec., 1 sec., and 1000 sec. We shall also calculate the results for a vacuum-baked (350°C) soda-lime glass where $m=0.04\times10^{-5}$ in.$^2$/lb., assuming $E$ to be $1.0\times10^7$ p.s.i. In this case $\alpha=171k$. (See Fig. 2.)

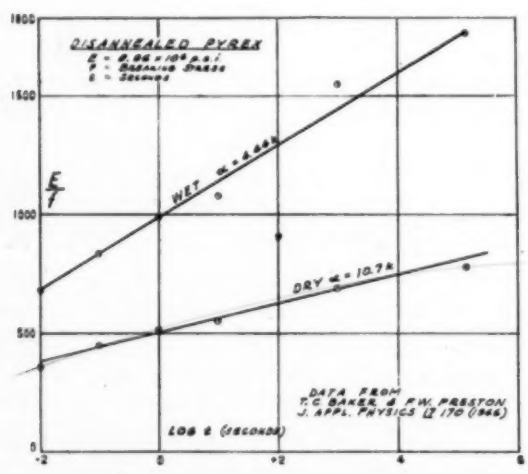


FIG. 2. $E/f$ *vs.* log$t$ for wet and dry Pyrex under static load.

It is to be noted that the molal activation energies are not large under wet conditions or "ordinary" conditions of dryness. They are of the order of 8000–16,000 cal. This can be compared with the activation energy for electrolytic or ionic conduction in soda-silica glasses (25,000 to 30,000 calories per mole.), as found by Seddon, Tippett, and Turner.[13] On the other hand, when special pains are taken to produce very dry glass, as by baking in vacuo, the molal activation energy for fracture is 135,000 cal., roughly 15 times as large as that for glass in its "ordinary" condition. The "catalytic" role of water is obvious. It provides a mechanism of low activation energy. The 135,000-calorie value is very nearly identical with 140,000 cal. for the delayed elastic process in soda-lime glass in the annealing range of temperature as found by Taylor, McNamara, and Sherman.[9] The close agreement indicates that the rate controlling process for fracture is in reality a delayed elastic phenomenon.

#### A. Constancy of Young's Modulus, $E$

In the preceding calculations, it was necessary to assume that $E$ is constant for a given glass regardless of its water content. This assumption is of doubtful validity because it would seem that the replacement of strong bonds by weaker ones should lower the modulus. The writer has been unable to find the report of any scientific study of the role of water on the elastic modulus of glass. However, there is a small variation in moduli of various samples which could be attributed to varying water content. Some erratic data on vitreous silica, shown by Sosman,[14] show about twofold variation in modulus.

A reduction of $E$ would result in a corresponding increase of the calculated $\alpha$, since $\alpha=2.3kT/Em$, but, on the other hand, would

[13] E. Seddon, J. Tippett, and W. E. S. Turner, "Electrical conductivity of sodium metasilicate-silica glasses," J. Soc. Glass. Tech. **16**, 450 (1932).

[14] R. B. Sosman, *Properties of Silica* (Chemical Catalog Company, New York, 1927), p. 450.

have no effect on the computed molal activation energies, $Q$, for fracture, since

$$Q=(E/f)N\alpha=(EN/f)(2.3kT/Em)$$
$$=(2.3RT/m)/f.$$

In fact, the molal activation energies are given directly by multiplying by $2.3RT$ the last term of the Glathart-Preston equation

$$\log t=-a/m+1/fm.$$

### B. Effect of Temperature

The effect of temperature on the strength and fatigue of soda-lime glass rods has been measured by B. Vonnegut.[15] Table IV shows values of $m$ which I have computed from that data. The last column shows $\alpha$, based on the equation $\alpha=2.3kT/Em$. $E$ is assumed to be $1\times10^7$ p.s.i. at all temperatures, for lack of better information. The value of $\alpha$ at 20°C based on Baker's work (see Table I) is $4.53k$. Vonnegut and Glathart state that they believe their "fatigue" to be too large at 24°C which leads to too small a value for $\alpha$. Similarly, $\alpha$ at 110°C is probably a little too large. There appears to be a minimum value for $\alpha$ at about 200°C. The rise in $\alpha$, that is, in activation energy, at higher temperatures is undoubtedly due to loss of moisture from the glass. At the very low temperatures the moisture is less active, possibly because of a very slow rate of diffusion into the glass at such temperature. It is to be noted that in no case, even at 520°C, does $\alpha$ rise as high as when the glass is vacuum-baked at 350°C ($\alpha=171k$). This shows how strongly moisture is retained by silicate glasses. Vonnegut and Glathart drew the conclusion that variation in the activity of adsorbed moisture on the surface of the glass is the primary cause of strength variation, and suggest that experiments should be made "over the same temperature range in high vacuum, in the absence of adsorbed films."

### C. Evaluation of Log$k_0$

The general equation

$$\log t=-\log k_0+(E\alpha/2.3kT)/f$$

permits evaluation of $\log k_0$ by determining the value of $1/f$ when $\log t=0$. In such a case $(E\alpha/2.3kT)/f=\log k_0$. The corresponding empirical equation is $1/fm=a/m$. Table V lists $1/f$, $m$, and $a/m=\log k_0$, for soda-lime glass at several temperatures, based on Vonnegut's data. No simple interpretation of the numerical values of $\log k_0$ can be given because of the variation in moisture content following the different heat treatments. The size of the rod specimens, and their surface condition as to scratches, etc., also affect $\log k_0$. A study of the breaking strength at various times and temperatures of thoroughly dry glass would be very desirable. Such measurements should be paralleled by determinations of the modulus $E$. It is also of importance to find the systematic relationship between $E$ and moisture content at various temperatures.

## IV. FRACTURE OF METALS: STRESS-CORROSION PHENOMENA

The subject of fatigue failure of metals has received a great deal of attention. References 16–27 inclusive contain data which are of interest in connection with any theory of the mechanism of fracture.[16–27] In general this work supports the

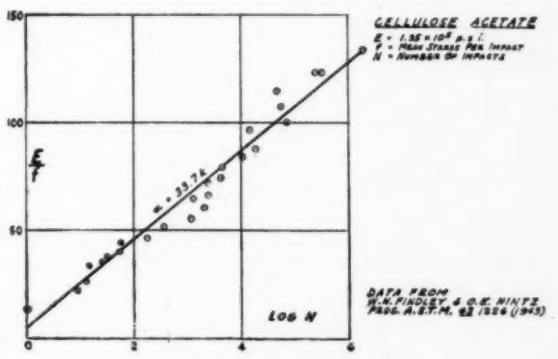


FIG. 3. $E/f$ *vs.* $\log N$ for cellulose acetate fractured under $N$ impacts.

[15] B. Vonnegut and J. L. Glathart, "The effect of temperature on the strength and fatigue of glass rods," J. App. Phys. **17**, 1082 (1946).

[16] P. W. Bridgman, "Shearing phenomena at high pressures, particularly in inorganic compounds," Proc. Am. Acad. Arts and Sci. **71**, 387 (1937).

[17] S. Glasstone, K. J. Laidler, and H. Eyring, *The Theory of Rate Processes* (McGraw-Hill Book Company, Inc., New York, 1941).

[18] E. H. Dix, Jr., "Introduction, Symposium on stress-corrosion cracking of metals," Trans. A.S.T.M. and A.I.M.E. (1946).

[19] B. P. Haigh and B. Jones, "Atmospheric action in relation to fatigue in lead," Engineering **129**, 423 (1930). Also in J. Inst. Metals, preprint No. 521.

[20] B. P. Haigh, "Chemical action in relation to fatigue in metals," Inst. Chem. Eng. (March 20, 1929).

TABLE IV. $m$ and $\alpha$ at various temperatures.

| Temperature | | $m$(in.²/lb.) | $\alpha$ |
|---|---|---|---|
| −190°C | 83°A | $0.23\times10^{-5}$ | $8.31k$ |
| −80°C | 193°A | 0.33 | $13.48k$ |
| 20°C | 293°A | 2.70 | $2.50k$ |
| 110°C | 383°A | 2.89 | $3.05k$ |
| 200°C | 473°A | 4.20 | $2.59k$ |
| 300°C | 573°A | 3.10 | $4.26k$ |
| 420°C | 693°A | 1.42 | $11.2k$ |
| 520°C | 793°A | 0.94 | $19.4k$ |

idea that deformation or atomic rearrangement is a prelude to fracture and that even quite mild corrosive agents accelerate the process. However, I have not found fatigue data covering a time range which in any way approaches the $10^7$ factor which Baker was able to investigate in his glass work. The metallurgical data are particularly deficient in the short-time high stress region.

## V. FRACTURE OF ORGANIC "RESINS"

W. N. Findley and O. E. Hintz, Jr.[28] have published a paper entitled, "The relation between results of repeated blow impact tests and of fatigue tests." Their Fig. 5 is an $(S-N)$ diagram, stress *versus* log cycles, for repeated impact and fatigue-bending tests of cellulose acetate containing 26 percent plasticizer. Mr. Findley has very kindly furnished me with his actual data on number of blows at various stresses. His data can be represented by the equation: $\log N=-2.68+1/(0.523\times10^{-4}f)$, over the range from 10 cycles to $1.87\times10^6$ cycles. The deviation of the actual points from the straight line is no greater than the variation between comparable points at the same (or nearly the same) $\log N$. We shall take $m=0.523\times10^{-4}$ in.²/lb. Since the stress is not steady but periodic, we shall consider the mean stress over a cycle to be one-half of the recorded stress. On this basis $m=1.05\times10^{-4}$ in.²/lb. (See Fig. 3.) The unit activation energy $\alpha=2.3kT/Em$. Findley and Hintz found $E=1.95\times10^5$ p.s.i., and $t=77$°F, which is 298°A. We shall use $T=300$°A in the calculations. Thus $\alpha=33.7k$. This is quite large compared to normal (wet) glasses where $\alpha$ ranged from $2k$ to $10k$. However, $Q$, the molal activation energy ranges from 1735 cal. (for failure in 10 impacts) to 8622 cal. (for failure in $10^6$ impacts). The corresponding values of $E/f$ are 25.7 and 128, respectively. It would be of interest to examine the relation between $\alpha$ and the kind and amount of plasticizer present.

A rough idea of $\lambda_0$ for the cellulose acetate can be obtained from the relation $\lambda_0=2\gamma/E$. We estimate that $\gamma$ is about 50 dynes/cm. Hence, $\lambda_0=0.7$Å (approx.), which is about one-half of the typical C−O distance 1.42Å. The typical C−C distance is about 1.54Å.

This work on the fracture failure of cellulose acetate appears to demonstrate the validity of the theory when applied to a brittle organic plastic, having a modulus $E$ as low as $1.95\times10^5$ p.s.i. Since some glasses have $E$ values as high as $10^7$, a wide range of applicability is indicated.

At temperatures below zero Centrigrade, many of the common synthetic and natural organic polymers show brittle behavior. Strong threads of silk, cotton, hemp, etc., are brittle at ordinary temperatures. It would be of interest to study these materials in a quantitative way with the aid of the principles set forth in this paper.

## VI. DESIGNING STRONG PRODUCTS TO LAST

The modulus of elasticity is a fundamental constant of matter. On the other hand, it is wrong to assign one definite tensile strength to a material or even to an object, because its atoms can move and let it be broken at any stress, if the latter is applied long enough. Further, if the atmosphere or the medium has any chemical action on the material, its "strength" may decline rapidly.

[21] M. Fink and U. Hofmann, "Wear of metallic materials by rubbing oxidation and the question of the origin of fatigue fractures," Metallwirtschaft **13**, 623 (1934).

[22] J. N. Kenyon, "The rotating wire arc fatigue machine for testing small diameter wire," Proc. A.S.T.M. **35**, part II 156 (1935); "The fatigue properties of some cold-drawn nickel alloy wires," *ibid.* **43**, 765 (1943).

[23] F. W. Preston, "Mechanical properties of glass," J. App. Phys. **13**, 623 (1942).

[24] A. Morris, "Stress-corrosion cracking of annealed brasses," Trans. A.I.M.E. **89**, 256 (1930).

[25] W. A. Wood, "X-ray studies of grain-size in steels of different hardness values," Phil. Mag. **10**, (1930).

[26] H. J. Gough, "Crystalline structure in relation to failure of metals, especially by fatigue," Proc. A.S.T.M. **33**, 3 (1933).

[27] J. O. Almen, "The useful data to be derived from fatigue tests," Metal. Prog. 254 (1943); "Endurance of machines under a few heavy loads," *ibid.* 435 (1943); "Improving fatigue-strength of machine parts," Mech. Eng. **65**, 553 (1943).

[28] W. N. Findley and O. E. Hintz, Jr., "The relation between results of repeated blow impact tests and of fatigue tests," Proc. A.S.T.M. **43**, 1226 (1943).

The highest apparent tensile strengths are always observed where the procedure of the test places some part of the object (e.g., the surface layer) under compression. This can occur in the testing of wires, fibers, and foils, and also of more massive objects loaded on a minute area by the Hertz ball[12] (or other) method. For practical purposes the greatest progress toward highest usable strengths per unit of weight will come by paying attention to the shape factor—the use of wires, fibers, thin sheets, laminations, etc. These shapes possess a large specific surface area, which renders them more sensitive to corrosive agents. Hence, the pertinent chemistry must be well understood, and proper steps taken to make the material inert to its future environment, if this is known. The manufacturing procedures should be directed toward introducing compression into the surface region, and the product so designed and fabricated that tension stresses in service are kept to a minimum. Thus chemistry, physics, and engineering unite to form a stable tripod which carries the promise of better things for the needs of man.

TABLE V. Log$k_0$ at various temperatures.

| Temp. | $1/f$(in.²/lb.) | $m$(in.²/lb.) | $a/m = \log k_0$ |
|---|---|---|---|
| −190°C | $7.10\times10^{-5}$ | $0.23\times10^{-5}$ | 30.9 |
| −80°C | 8.65 | 0.33 | 26.2 |
| 20°C | 12.65 | 2.70 | 4.68 |
| 110°C | 15.40 | 2.89 | 5.33 |
| 200°C | 16.0 | 4.20 | 3.81 |
| 300°C | 14.37 | 3.10 | 4.64 |
| 420°C | 11.20 | 1.42 | 7.89 |
| 520°C | 9.27 | 0.94 | 9.86 |

## VII. ACKNOWLEDGMENTS

I wish to express my thanks to several of my colleagues in the Research Department of the Minnesota Mining and Manufacturing Company, in particular to: C. A. Dahlquist, J. O. Hendricks, G. R. Pole, A. F. Schmelzle, H. M. Scholberg, H. N. Stephens, and W. W. Wetzel, for fruitful discussions.

I am indebted also to my friends, J. O. Almen, F. O. Anderegg, H. Eyring, J. L. Glathart, F. H. MacDougall, A. Nadai, E. L. Piret, E. F. Poncelet, F. W. Preston, and H. C. Urey, for suggestions and criticism and for the stimulus arising from their genuine interest in "how things break."

# Acceleration of Electrons by a Resonant Cavity*

FRANK L. HEREFORD, JR.**
*Physics Laboratory, University of Virginia, Charlottesville, Virginia*
(Received June 16, 1947)

Electrons were accelerated by means of a single resonant cavity operating at 75-cms wavelength. Energies as high as 0.75 Mev were attained by single-stage acceleration, the electrons entering the cavity at virtually zero velocity. By turning the emergent beam about, and reinjecting it into the cavity in the opposite direction two stage acceleration was achieved and 1.25-Mev electrons were produced. Possibilities of a "shuttle accelerator" are discussed.

AMONG the various schemes currently being applied to the acceleration of charged particles is a linear accelerator[1,2] comprising a series of cavity resonators so arranged that the stream of particles passes successively through each cavity gaining energy from the high electric field in each resonator. In most of these methods, present plans specify a finite injection energy at the first cavity which in cases where this injection energy is as high as 1 to 2 Mev will require considerable apparatus.

This paper describes a single cavity electron accelerator similar to that employed by Bowen, Pulley, and Gooden[3] in which no injection apparatus is utilized, but rather the electrons enter the acceleration region at virtually zero velocity and by means of a single trip through the cavity are accelerated to relativistic energies of the order of 0.75 Mev. Such a scheme provides a simple and compact device for the production of intense pulsed beams of high energy electrons in the relativistic energy range.

A new multiple-stage acceleration method has also been successively worked out in which the beam emerging from the cavity is turned sharply through 180 degrees by an appropriate magnetic-field configuration and caused to traverse the acceleration region in the opposite direction a half cycle after the first traversal. This method offers possibilities of a "shuttle" accelerator whereby a single cavity might yield energies in the 10-Mev range.

* This work was supported in part by a Navy Bureau of Ordnance, Contract NOrd-7873.
** National Research Predoctoral Fellow. Now at Bartol Research Foundation, Swarthmore, Pa.
[1] J. C. Slater, Phys. Rev. **70**, 799A (1946).
[2] L. W. Alvarez, Phys. Rev. **70**, 799A (1946).
[3] Bowen, Pulley, Gooden, Nature **157**, 840 (1946).

## EXPERIMENTAL APPARATUS

The cavity employed was of the reentrant type as shown in Fig. 1. It was operated at a wave-length of approximately 75 cm, the source of high frequency power being a Western Electric 7C22 pulse operated twin triode. This tube is tunable over a 390–425-megacycle range and has a maximum peak power rating of 500 kilowatts. It was operated in this case on a four-microsecond pulse, the repetition rate being 60 cycles per second, yielding a duty cycle of 0.00024. The pulse was formed by means of a conventional spark-gap modulator with an artificial transmission line forming the square wave.

The details of the cavity construction are shown in Fig. 2. It was made from brass and later copper plated to increase the $Q$. Tuning was accomplished by adjusting the gap distance between the inner conductors, the sylphon bellows shown in Fig. 2 making this adjustment possible during operation. The radio frequency power was fed into the cavity from the concentric line output of the 7C22 oscillator by means of a magnetic coupling loop. Another sylphon-bellows arrangement made possible adjustment of this loop during operation thus facilitating proper matching of the load to the oscillator. The loop itself is indicated in Fig. 1. It was made by slipping a section of sylphon tubing inside a length of ordinary wire shielding.

## PUMPING SYSTEM

The cavity was evacuated by a Distillation Product MC275 oil-diffusion pump backed by a Megavac. The pumping lead to the cavity was rather large, being 4″ in diameter and was covered at the cavity wall by a perforated $\frac{1}{32}$″ copper plate. This plate was made to fit the

inner wall contour of the cavity and the perforations were drilled along lines parallel to the cavity axis in order to minimize impedance to the wall currents.

By means of this system it was possible to evacuate the cavity to a pressure of $3\times10^{-6}$ mm Hg before the R.F. power was turned on. If the system had been exposed to air for an appreciable period before evacuation the pressure rose to about $4\times10^{-5}$ mm Hg in operation at resonance due to glow discharge. After several minutes of operation, however, the system cleaned up and the pressure dropped back to approximately $5\times10^{-6}$ mm Hg, where optimum acceleration conditions existed. The large 4″ diameter pumping lead to the cavity was definitely necessary in order that this condition be achieved.

## SINGLE-STAGE ACCELERATION

The source of electrons for single-stage acceleration was a 2″ length of tungsten wire wound in a helix and mounted just inside the cathode inner conductor as shown in Fig. 3(a). The filament was supported by a brass tube which slipped inside the cathode inner conductor and was adjusted by means of a sylphon bellows. Each side of the filament was coupled to the cathode inner conductor by circular mica condensers. This was necessary in order that the filament be electrically a short distance from the end of the cathode.

The essentials of the system insofar as electron optics is concerned are shown in this figure also. The gap distance of approximately $1\frac{1}{2}$″ was of such length that an electron emerging at 0.75 Mev would traverse the gap in about one tenth of the 400-mc oscillator period or about $3\times10^{-10}$ second. No baffle was used over the end of the cathode inner conductor. The anode inner conductor was covered by a 0.030″ copper baffle with a $\frac{1}{4}$″ hole in the center. After traversing the acceleration region, *A*, the beam was collimated to a diameter of 0.060″, and the energy was measured by magnetic deflection, the radius of curvature being computed from the displacement on the willemite screen, *C*. The magnetic-field strength was measured by a flip coil and ballistic galvanometer and a gauss meter.

With the 7C22 operating at maximum plate voltage and the cavity properly tuned, electrons were accelerated to energies as high as 0.75 Mev. In general the extent of the spectrum was as follows:

| | |
|---|---|
| Lower limit | 0.30±10 percent Mev |
| Maximum intensity | 0.65±10 percent Mev |
| Upper limit | 0.75±10 percent Mev |

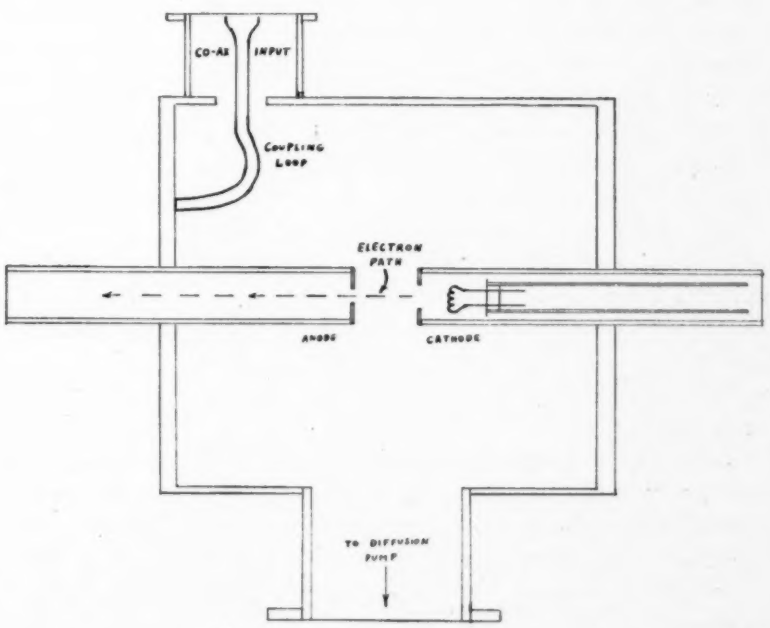


FIG. 1. A schematic drawing of the cavity as applied to single-stage acceleration.

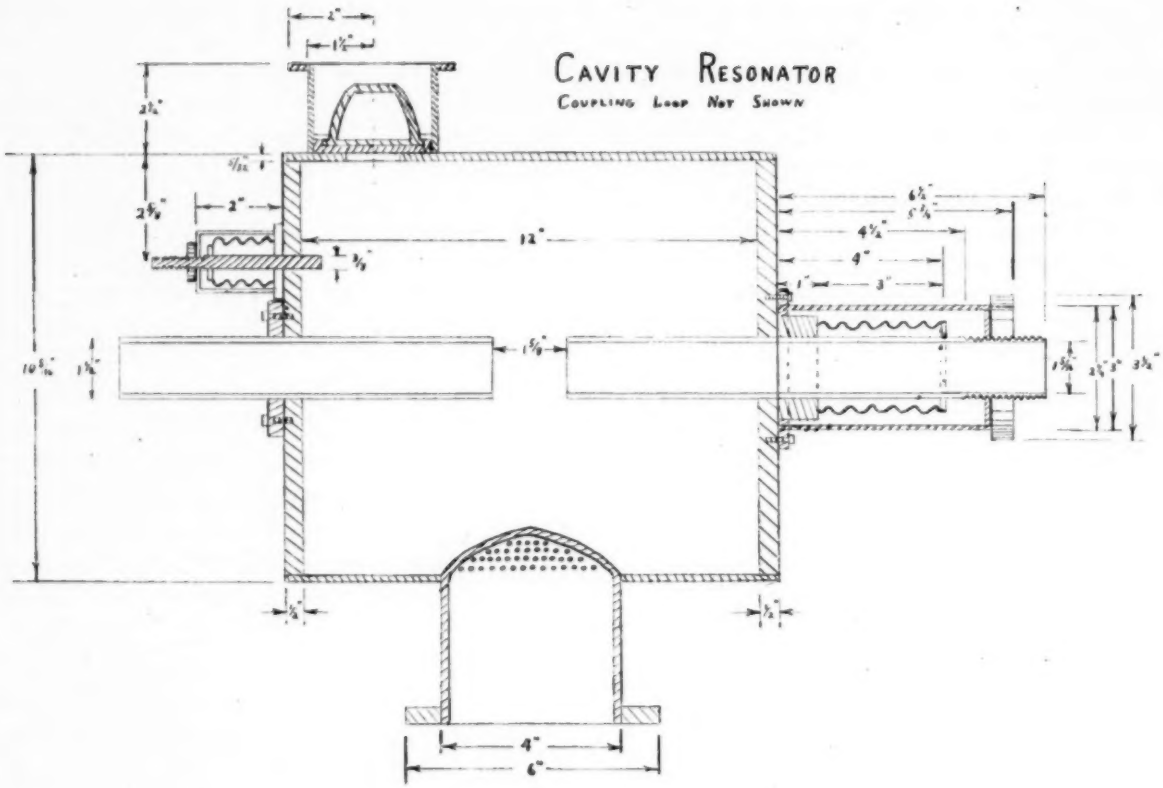


FIG. 2. Details of the cavity construction.

On several occasions an extremely narrow spectrum width was observed of the order of 50 to 100 Kev. Bowen, Pulley and Gooden[3] have reported a similar "energy bunching" effect. There seems no immediately obvious explanation of this phenomenon. A solution of the non-relativistic equations of motion of an electron in a spatially uniform electric field with a sinusoidal time variation predicts such an effect. In particular, if the energy imparted to the electron is plotted against the entrance phase angle, the curve is found to be approximately flat over a fairly large variation in phase angle. This characteristic of the curve, however, did not seem sufficiently pronounced to account for the extreme effect.

Various experiments were carried out to ascertain whether the effect was due to the focussing of only a given electron energy on the first 0.060" aperture in the collimator, but in general changes in the electron-optics system did not effect the beam energy.

## BEAM CURRENT

By means of the scheme shown in Fig. 3(b) the current in the electron beam was measured. The beam was collimated by two $\frac{1}{4}$" diameter apertures and electrons were collected in a Faraday cage mounted just behind the second aperture. This cage was made 7" in length to reduce losses due to secondary electron emission from the walls.

It was possible to maintain a steady electron current to the cage of 17 microamperes. In view of the duty cycle of 0.00024 this indicated a mean beam current during the pulse of 70 milliamperes. Since the average energy was approximately 0.65 Mev, this rather high current represents a peak power loss in the $\frac{1}{4}$" beam of 45 kilowatts. In addition to this beam there is a return beam in the opposite direction caused by the liberation of secondary electrons at the anode, some of which are emitted from the anode surface when the field is in such a direction to accelerate them. With the cavity set up for double stage

acceleration as described below this return beam of secondaries was actually observed. If we assume the current in this beam to be approximately equal to that in the primary beam, we see that approximately 90-kilowatts peak power is absorbed in the electron beam alone.

The power dissipated in the cavity walls was determined by measuring the temperature rise in the walls with the R.F. power on and the cavity tuned and comparing it to the temperature rise with a heater of known dissipation in the cavity. This dissipation was found to be $220\pm20$ kilowatts. Thus the total peak power absorbed by the cavity and the electron beam was approximately 300 kilowatts.

## DOUBLE-STAGE ACCELERATION

Using the same cavity employed in the single-stage system, double-stage acceleration was achieved by turning the beam sharply through 180 degrees as it emerged from the cavity and re-injecting it in the opposite direction. In order to carry out this scheme it was necessary to redesign the filament assembly to allow the return beam of electrons to pass through the cathode inner conductor. Furthermore, the cavity geometry was altered as indicated in Fig. 4. It was, of course, necessary that the total distance that an electron travel in emerging from the cavity, being turned about and re-injected be approximately that distance travelled in one half cycle by a 0.65-Mev electron, that being the mean energy of the beam after a single acceleration.

The double-stage system is shown in Fig. 4. The beam was not collimated after the first traversal of the gap. The two magnets used to reverse the beam direction had $\frac{3}{4}''\times1''$ pole faces spaced at $\frac{3}{8}''$. Magnet $A$ was an electromagnet of field strength about 500 gauss, while magnet $B$ was a permanent Alnico magnet of field strength about 7000 gauss. The value of $H\rho$ for 0.65-Mev electrons is 3400 gauss cms; thus the magnet $B$ should turn the beam in a radius of $\frac{1}{2}$ cm.

The energy of the return beam of electrons was measured by an improved magnetic-deflection method. A wide spectrum was observed with limits as follows:

| | |
|---|---|
| Lower limit | $0.30\pm10$ percent Mev |
| Upper limit | $1.25\pm10$ percent Mev |

This width, however, was not due entirely to the return beam of doubly accelerated electrons. When the beam reversal magnets were removed the upper limit of the spectrum dropped to about 0.7 Mev, this beam arising from secondary emission at the anode as previously stated. Thus the lower limit of the doubly accelerated beam was approximately 0.7 Mev. The current in the return beam was considerably smaller than in the primary beam, but with improved focussing it should be possible to increase it appreciably.

There seems to be no obvious reason why such a "shuttle" acceleration method could not be applied to the production of higher energy electrons, perhaps in the 10-Mev range. With an extremely high magnetic field to reverse the beam direction the electron path in this field would be a negligible portion of the total path

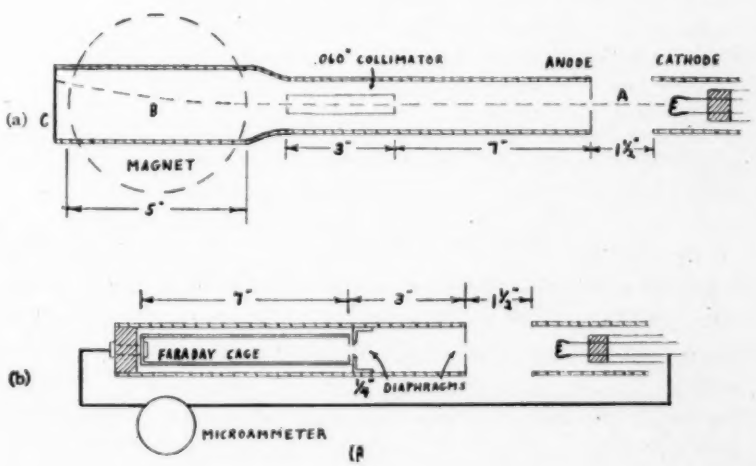


FIG. 3. (a) Schematic drawing of the single-stage system. (b) Arrangement for measurement of beam current.

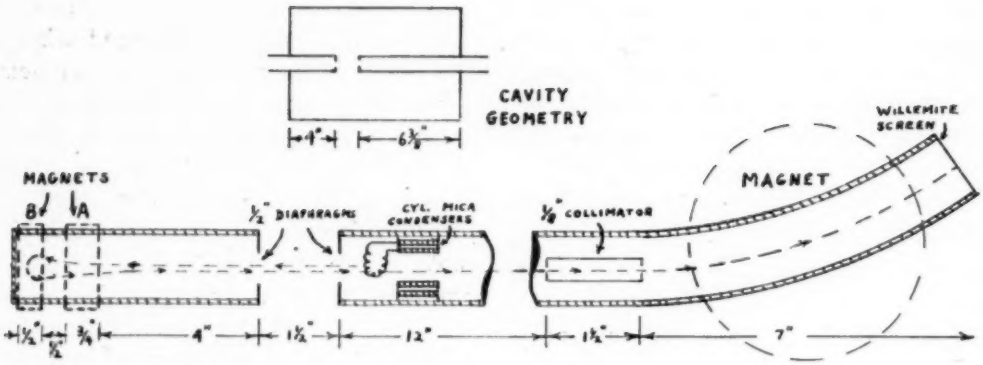


FIG. 4. The double-stage acceleration system.

per stage and consequently the increase in path due to the relativistic mass increase of the electron would not cause dephasing difficulties. Radiation losses in the reversal of the beam are of negligible value. According to an expression given by Schwinger,[4] the energy radiated in turning a 10-Mev electron about in a field of 25,000 gauss is less than 1-electron volt.

[4] J. Schwinger, Phys. Rev. **70**, 798A (1946).

The author wishes to express his indebtedness to Professors J. W. Beams and L. B. Snoddy for the frequent and helpful advice which they gave in consultation. Their constant interest and willingness to help was sincerely appreciated. The work of Messrs. Fritz Linke and Phillip Sommer who constructed the cavity and parts also contributed much to the completion of the project.

# Infra-Red Spectra of Hydrocarbons

## II. Analysis of Octane Mixtures by the Use of Infra-Red Spectra Obtained at Low Temperatures*

W. H. AVERY** AND J. R. MORRISON

(Received June 17, 1947)

Infra-red spectra in the region 2 to 22 microns were obtained for the four trimethylpentanes, at temperatures of 0°C and −195°C. In agreement with theory, the band "widths" at −195°C are roughly half as great as at 0°C. The spectra were observed experimentally by condensation of a film of the hydrocarbon on the reflecting bottom surface of a cell mounted vertically, with its lower end immersed in ice or liquid nitrogen. A method of forming films of reproducible dimensions and thickness is described.

To provide a quantitative estimate of the advantage for analytical purposes of the use of spactra obtained at low temperatures, an expression is derived which gives the probability (for random distribution of the band positions) that at least one band can be found for each component of a mixture, which does not "overlap" bands of the other components. Application of the formula, with some simplifying assumptions, to a mixture of the 18 octane isomers, indicates that reduction of the band "width" from 40 $cm^{-1}$ to 20 $cm^{-1}$ (corresponding to the temperature change from 0°C to −195°C) increases the calculated probability of the existence of a "non-overlapped" band for at least 17 of the isomers from 0.003 to 0.999. The importance of this result in infra-red analyses is pointed out.

The use of spectra obtained at liquid helium temperatures is suggested as offering attractive possibilities for the analysis of complex mixtures.

### INTRODUCTION

THE theoretical background leading to the utilization of the low temperature technique for infra-red absorption measurements and its obvious advantages in the analytical field have been outlined previously.[1] The present paper deals with the applicability of the tech-

* The work reported here was completed early in 1942. Publication was delayed by the pressure of other work during the war.

** Present address is Applied Physics Laboratory, Johns Hopkins University, Silver Spring, Maryland.

[1] W. H. Avery and C. F. Ellis, J. Chem. Phys. **10**, 10 (1942).

nique to the analysis of multi-component mixtures of paraffin hydrocarbons of eight carbon atoms, a complex problem of commercial as well as scientific interest since the available analytical method of precision distillation is arduous and time-consuming. Comparative absorption spectra of the trimethyl pentanes of 0°C and −195°C are presented to substantiate a theoretical discussion of the effect of band width in the problem of analyzing a complex mixture by spectroscopic methods.

## EXPERIMENTAL

The spectrometer has been described,[2] but the optical arrangement and the absorption cell mounting for low temperature measurements[1] have been revised considerably.

The present optical arrangement (Fig. 1) has the advantage of allowing the entrance of the light beam nearly normal to the cross section of the absorption cell, permitting the use of a smaller diameter cell without interception of a part of the beam. A Nernst glower, $N$, is located a few millimeters on one side of the focus of a 60° off-axis paraboloidal mirror, $P$.*** Radiation from the glower is reflected in a parallel beam from the mirror, $P$, and strikes the bottom of the cell, a plane reflecting (gold or aluminum) surface, $M_5$, at a nearly perpendicular incidence. After reflection from $M_5$ the radiation returns to the mirror, $P$, which focuses it on the plane mirror, $M_6$. $M_6$ and $N$ are situated symmetrically on opposite sides of the focal point of the mirror, $P$. $M_6$, which is also at the focal point of the off-axis paraboloidal mirror $C_1$, directs the deflected beam to $C_1$. From $C_1$ the collimated beam is focused upon the entrance slit of the spectrometer by means of plane mirror $M_3$ and the condensing mirror $C_2$.

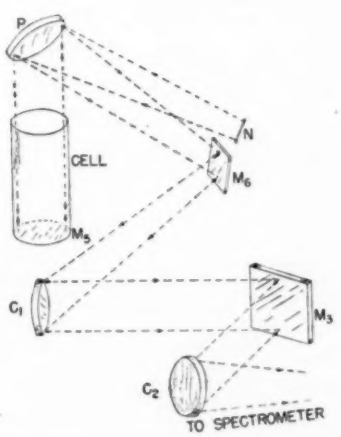


FIG. 1. Optical arrangement for low temperature spectra.

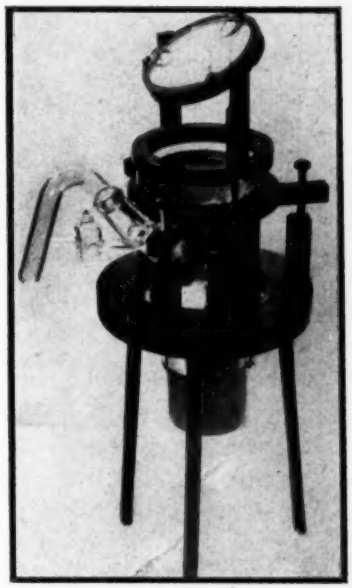

FIG. 2. Absorption cell for low temperature spectra.

The absorption cell,† 7 cm in diameter, 15 cm in depth, and fitted with a side arm for convenient sample retention during blank energy determinations, is mounted in the holder shown in Fig. 2. Both the cell holder and its supporting tripod are set into V-ways to facilitate the accurate reproduction of the cell position after filling. A similar kinematically designed arrangement permits the removal and replacement of mirror $P$ without disturbing its focus. Leveling of the cell and mirror is accomplished through convenient adjustment screws.

In the original procedure a measured quantity of the sample to be examined was retained in the side arm of the absorption cell during the recording of the energy of the source in a desired spectral region. The sample was then evaporated

[2] W. H. Avery, J. Opt. Soc. Am. **31**, 633 (1941).

*** The mirror was prepared by the Bausch and Lomb Optical Company by cutting a section from the edge of one of their large paraboloidal searchlight mirrors.

† Obtained from the American Instrument Company.

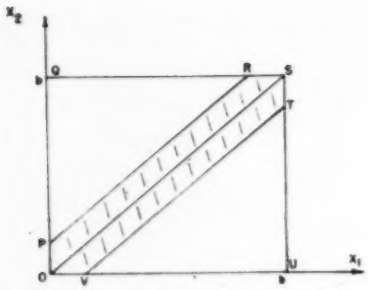


FIG. 3.

from the side arm, condensed upon the cooled cell bottom, and the same spectral region again recorded. Percentage transmissions were computed from sample to blank ratios or recorded directly by the method previously described. (A suitable factor was applied in plotting absorption curves to correct for the scattering of incident radiation from the polycrystalline film.)

The cooling of the cell bottom to −195°C was accomplished through immersion in a Dewar flask containing liquid nitrogen. By this method, however, reproducible thicknesses of deposited films were difficult to obtain since a small, variable amount of sample condensed on the cell wall adjacent to the bottom. To overcome this difficulty, a copper cylinder of a slightly smaller diameter than the cell (shown in Fig. 2) was clamped concentrically to the bottom of the cell, the cylinder rather than the cell being immersed in the liquid nitrogen. Intimate thermal contact was maintained through a thin oil film interposed between the cylinder and cell. With this arrangement the sample condensed as an accurately defined disk which did not extend to the side walls and the films were repeatedly of the same thickness to a high degree of precision. A similar technique, with the copper cylinder being immersed in an ice bath, may be used for liquid films, since films of thicknesses useful in infra-red investigations do not spread after deposition.

An absorption cell of this type presents many advantages over the conventional shim-type cell. There is no danger of contamination or evaporation of the sample; the temperature may be varied at will without condensation of water vapor or loss of sample; the sample may be recovered after examination; films of any useful thickness may be employed; the thickness may be easily varied; and, finally, the spectrum of the blank may be easily obtained.

## THE ANALYSIS OF OCTANE MIXTURES

Simplicity, accuracy, and rapidity in an infra-red analysis of a multi-component mixture depend primarily upon the location of strong absorption bands unique for each compound of interest in a spectral region relatively free from absorption by the remaining components. (An additional method has been developed[3] involving the solution, for an $n$-component system, of $n$ simultaneous equations wherein the augumentation of principal absorption by secondary absorbers caused by overlapping of bands is considered, but in this method the complexity of solution becomes increasingly great with increased values of $n$.)

Since the band widths are roughly one-half as great at −195°C as at room temperature, it is immediately obvious that the probability of locating interference-free, "characteristic" bands is increased by the utilization of the low temperature technique. A quantitative estimate of the increase is deduced in the theoretical treatment given below of the probability that an infra-red analysis can be made, taking as a criterion of possibility that at least one band of all but one of the components does not overlap a band of any other component. (It would not be necessary to find a characteristic band for each component since if all but one could be determined by the infra-red technique the last could be found by difference.) An expression is obtained applicable to any number of compounds, having any number of bands apiece and having bands of variable width from compound to compound. The position of any band is assumed to be given purely by chance.

Given $M$ compounds, designated $A$, $B$, $C$, $\cdots M$, having $n_A$, $n_B$, $n_C$, $\cdots n_M$ bands of width $w_A$, $w_B$, $w_C$, $\cdots w_M$ cm$^{-1}$ distributed at random within a spectral region $b$ cm$^{-1}$ wide, we wish to find the probability that at least one band of each $M-1$ of the compounds will occur in a region unoccupied by any bands of the other compounds.

[3] R. R. Brattain, R. S. Rasmussen, and A. M. Cravath, J. App. Phys. **14**, 418 (1943).

Consider first the case where $M=2$, $n_A=1$, $n_B=1$. Let $x_1$ represent the position of the center of the first band ($0<x_1<b$), $x_2$ represent the position of the band center of the second compound, $0<x_2<b$. $x_1$ and $x_2$ may be plotted as rectangular coordinates (Fig. 3); then the coordinates of every point in the square $OQSU$ will correspond to a possible disposition of the centers of the two bands. Band $A$ will overlap band $B$ whenever

$$0<x_1-x_2<\frac{w_A+w_B}{2}$$

or when

$$0<x_2-x_1<\frac{w_A+w_B}{2}.$$

$$\left(\text{Let } OP=\frac{w_A+w_B}{2}=OV=RS=ST.\right)$$

All possible values of $x_1$ and $x_2$ that satisfy the first condition lie within the shaded area of $OVTS$, while all values of $x_1$ and $x_2$ that satisfy the second condition will be found in the area $OPRS$. Let

$$\frac{w_A+w_B}{2}=w_{AB}.$$

The probability, $P_{AB}$, that two bands chosen at random will overlap is, then, the ratio of the area $OPRSTV$ to the area $OQSU$, i.e.,

$$P_{AB}=\frac{b^2-\frac{2(b-w_{AB})^2}{2}}{b^2}=1-\frac{(b-w_{AB})^2}{b^2}. \quad (1)$$

The probability that the bands do ***not*** overlap is

$$Q_{AB}''=1-P_{AB}=\frac{(b-w_{AB})^2}{b^2}=\left(1-\frac{w_{AB}}{b}\right)^2. \quad (2)$$

Suppose now that $A$ and $B$ have each three bands labelled $A_1$, $A_2$, $A_3$, and $B_1$, $B_2$, $B_3$' the probability that $A_1$ does not overlap $B_1$, $B_2$, or $B_3$ is

$$\left(1-\frac{w_{AB}}{b}\right)^2\left(1-\frac{w_{AB}}{b}\right)^2\left(1-\frac{w_{AB}}{b}\right)^2$$

$$=\left(1-\frac{w_{AB}}{b}\right)^6=Q_{AB}'. \quad (3)$$

TABLE I. 2,2,3-trimethylpentane wave-lengths and frequencies of significant bands.

| 0°C | | −195°C | |
|---|---|---|---|
| Wave-lengths in microns | Frequencies in cm$^{-1}$ | Wave-lengths in microns | Frequencies in cm$^{-1}$ |
| 19.02 | 526 | 19.12 | 523 |
| 13.95 | 717 | 13.95 | 717 |
| 12.82 | 780 | 12.89 | 776 |
| 12.07 | 829 | 12.08 | 828 |
| 11.20 | 893 | 11.23 | 890 |
| 10.77 | 929 | 10.78 | 928 |
| | | 10.37 | 964 |
| 10.30 | 971 | 10.24 | 977 |
| 9.98 | 1002 | 9.98 | 1002 |
| | | 9.81 | 1020 |
| 9.74 | 1027 | 9.72 | 1029 |
| 9.27 | 1079 | 9.26 | 1080 |
| 8.95 | 1117 | 8.93 | 1120 |
| 8.65 | 1156 | 8.65 | 1156 |
| 8.30 | 1205 | 8.30 | 1205 |
| 8.19 | 1221 | 8.19 | 1221 |
| 8.05 | 1242 | 8.02 | 1247 |
| | | 7.86 | 1274 |
| 7.65 | 1307 | 7.67 | 1304 |
| 7.30 | 1370 | 7.26 | 1377 |
| 6.77 | 1477 | 6.84 | 1462 |
| 3.83 | 2611 | 3.72 | 2688 |
| 3.50 | 2857 | 3.49 | 2865 |
| 3.26 | 3067 | 3.26 | 3067 |
| 2.34 | 4274 | 2.43 | 4115 |

TABLE II. 2,2,4-trimethylpentane wave-lengths and frequencies of significant bands.

| 0°C | | −195°C | |
|---|---|---|---|
| Wave-lengths in microns | Frequencies in cm$^{-1}$ | Wave-lengths in microns | Frequencies in cm$^{-1}$ |
| 13.45 | 743 | 13.44 | 744 |
| 12.04 | 830 | 12.03 | 831 |
| 11.59 | 863 | 11.59 | 863 |
| | | 11.09 | 902 |
| | | 10.89 | 918 |
| 10.80 | 926 | 10.77 | 929 |
| 10.19 | 981 | 10.18 | 982 |
| 9.80 | 1020 | 9.81 | 1019 |
| 9.06 | 1104 | 9.11 | 1097 |
| | | 8.97 | 1115 |
| 8.54 | 1170 | 8.55 | 1170 |
| 8.30 | 1205 | 8.28 | 1208 |
| 8.01 | 1248 | 7.99 | 1252 |
| 7.79 | 1284 | 7.80 | 1282 |
| 7.30 | 1370 | 7.35 | 1361 |
| | | 7.21 | 1387 |
| 6.78 | 1475 | 6.82 | 1466 |
| | | 4.05 | 2469 |
| 3.70 | 2703 | 3.70 | 2703 |
| 3.47 | 2882 | 3.50 | 2857 |
| 3.25 | 3077 | 3.16 | 3165 |
| 2.39 | 4184 | 3.06 | 3268 |

If $B$ has $n_B$ bands of width $w_B$,

$$Q_{AB}' = \left(1 - \frac{w_{AB}}{b}\right)^{2n_B}.$$

Similar expressions are obtained for the probability that $A_2$ and $A_3$ (taken separately) do not overlap any $B$ bands.

The probability that at least one of the three $A$ bands does not overlap any of the $B$ bands will be the sum:

the probability that $A_1$ does not overlap any $B$ bands but $A_2$ and $A_3$ do
+ the probability that $A_2$ does not overlap but $A_1$ and $A_3$ do
+ the probability that $A_3$ does not overlap but $A_1$ and $A_2$ do
+ the probability that neither $A_1$ nor $A_2$ overlaps any $B$ bands but $A_3$ does
+ a similar term for $A_1$, $A_3$
+ a similar term for $A_2$, $A_3$
+, finally, the probability that neither $A_1$ nor $A_2$ nor $A_3$ overlaps any $B$ bands.

Substituting, the probability that at least one $A$ band does not overlap a $B$ band is:

$$\begin{aligned} Q_{AB} &= 3Q_{AB}'(1-Q_{AB}')^2 + 3Q_{AB}'^2(1-Q_{AB}) + Q_{AB}'^3 \\ &= [Q_{AB}' + (1-Q_{AB}')]^3 - (1-Q_{AB}')^3 \\ &= 1-(1-Q_{AB}')^3. \end{aligned} \tag{4}$$

If $A$ has $n_A$ bands

$$Q_{AB} = 1-(1-Q_{AB}')^{n_A}. \tag{5}$$

If there are three compounds $A$, $B$, and $C$, the probability that at least one band of $A$ does not overlap any band in $C$ is

$$Q_{AC} = 1-(1-Q_{AC}')^{n_A}. \tag{6}$$

The probability that at least one $A$ band does not overlap any bands in either $B$ or $C$ is

$$\begin{aligned} Q_{AB} \cdot Q_{AC} &= Q_{A,B,C} \\ &= [1-(1-Q_{AB}')^{n_A}][1-(1-Q_{AC}')^{n_A}]. \end{aligned} \tag{7}$$

Given $M$ compounds (where $M$ is any number), the probability that at least one $A$ band does not overlap any bands in any of the compounds is

$$Q_{A,B\cdots M} = \prod_{i=B}^{i=M} Q_{Ai}. \tag{8}$$

Similarly, the probability that at least one $B$ band will be characteristic (i.e., not overlap) is

$$Q_{B,AC\cdots M} = \prod_{i=A}^{i=M\ (B\text{ omitted})} Q_{Bi}. \tag{9}$$

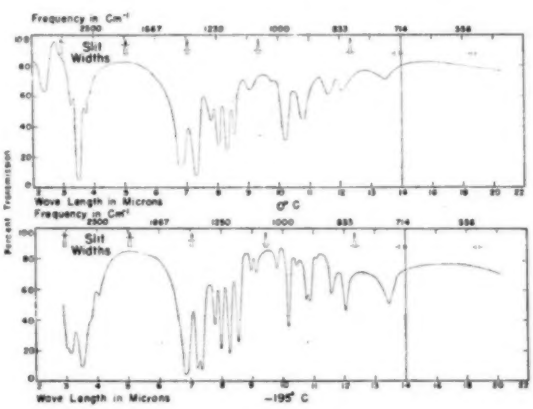


FIG. 5. Spectra of 2,2,4-trimethylpentane at 0 and −195°C.

The probability that $M-1$ compounds will have characteristic bands is††

$$P_{M-1} = \sum_{i=A}^{i=M} (1-Q_{i,A\cdots M}) \prod_{j=A}^{j=M-1\ (j\neq 1)} Q_{j,A\cdots M} + \prod_{j,A\cdots M}^{M} Q_{j,A\cdots M}. \tag{10}$$

If the bands are all of equal width, $w$, and each

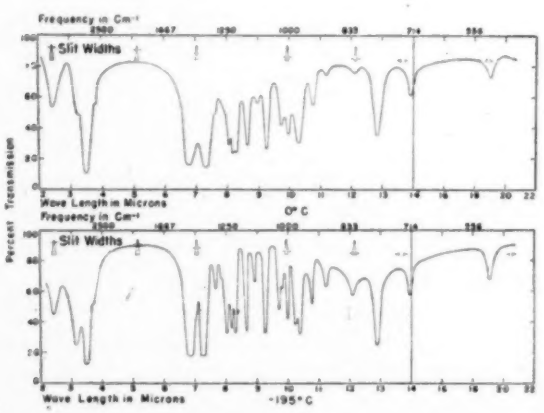


FIG. 4. Spectra of 2,2,3-trimethylpentane at 0 and −195°C.

†† The symbol $Q_{i,A\cdots M}$ signifies that when $j$ is replaced by a given letter, that letter is to be omitted from the sequence of letters following the comma in subscript. Thus if $j=A$ we have $Q_{A,BC\cdots M}$. If $j=C$ we have $Q_{C,ABDE\cdots M}$, etc.

compound has the same number of bands, $n$, expression (10) may be simplified to

$$P_{M-1}=MQ_{A,B\cdots M}^{(M-1)}-(M-1)Q_{A,B\cdots M}^{M}. \quad (11)$$

$$P_{M-1}=MQ_{A,B\cdots M}{}^{(M-1)}-(M-1)Q_{A,B\cdots M}{}^{M}. \quad (11)$$

With these conditions,

$$Q_{AB'}=Q'=\left(1-\frac{w}{b}\right)^{2n},$$

$$Q_{AB}=1-(1-Q')^{n}=\left\{1-\left[1-\left(1-\frac{w}{b}\right)^{2n}\right]^{n}\right\},$$

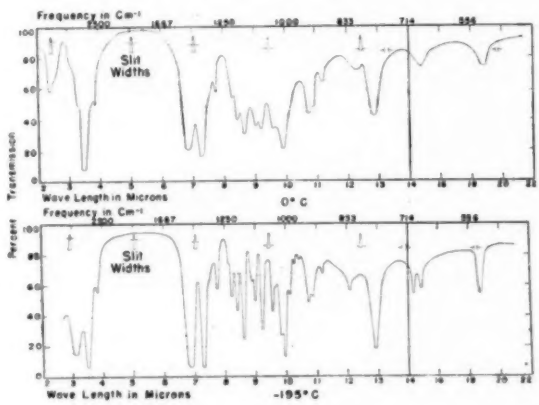


FIG. 6. Spectra of 2,3,3-trimethylpentane at 0 and −195°C.

$$Q_{A,B\cdots M}=\left\{1-\left[1-\left(1-\frac{w}{b}\right)^{2n}\right]^{n}\right\}^{M-1},$$

$$P_{M-1}=M\left\{1-\left[1-\left(1-\frac{w}{b}\right)^{2n}\right]^{n}\right\}^{(M-1)(M-1)}$$

$$-(M-1)\left\{1-\left[1-\left(1-\frac{w}{b}\right)^{2n}\right]^{n}\right\}^{M(M-1)}.$$

If $w=0$, $P_{M-1}=M-(M-1)=1$.
If $w=b$, $P_{M-1}=0-0=0$.

If we make the assumptions, which are in approximate agreement with the facts, that all of the octane isomers have the same number of bands (15) in the region 500 to 1300 cm$^{-1}$ and that the band width at room temperature is 40 cm$^{-1}$, then: $w=40$ cm$^{-1}$; $b=800$ cm$^{-1}$; $n=15$

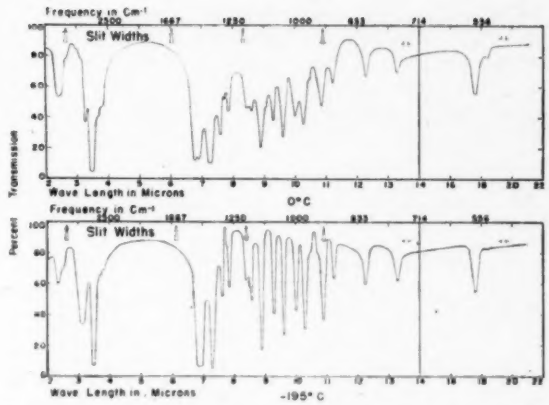


FIG. 7. Spectra of 2,3,4-trimethylpentane at 0 and −195°C.

bands; and $M=18$ compounds

$$Q_{A,B\cdots M}=\left\{1-\left[1-\left(1-\frac{40}{800}\right)^{30}\right]^{15}\right\}^{17}$$

$$=0.628,$$

$$P_{M-1}=18(0.628)^{17}-17(0.628)^{18}$$

$$=0.00268.$$

When the temperature is −195°C

$$w=40\left(\frac{78}{300}\right)^{\frac{1}{3}}=20.4=20 \text{ cm}^{-1},$$

$b=800$ cm$^{-1}$, $r=15$ bands, $M=18$ compounds

$$Q_{A,B\cdots M}=\left\{1-\left[1-\left(1-\frac{20}{800}\right)^{30}\right]^{15}\right\}^{17}$$

$$=1-0.00132=0.99867,$$

$$P_{M-1}=18(0.99867)^{17}-17(0.99867)^{18}$$

$$=0.999.$$

Thus halving the band width enormously increases the probability that there will be a characteristic band for each compound.

This rather striking result has been reached through the use of the simplifying assumptions that (1) the band widths are all the same, (2) the band intensities are the same, (3) the octanes all have the same number of bands (15), and (4), that the bands are distributed at random within the interval 500–1300 cm$^{-1}$. None of the assumptions is strictly valid. However, an in-

TABLE III. 2,3,3-trimethylpentane wave-lengths and frequencies of significant bands.

| 0°C | | −195°C | |
|---|---|---|---|
| Wave-lengths in microns | Frequencies in $cm^{-1}$ | Wave-lengths in microns | Frequencies in $cm^{-1}$ |
| 18.82 | 531 | 18.85 | 531 |
| 14.74 | 678 | 14.90 | 671 |
| | | 14.36 | 696 |
| 12.87 | 777 | 12.91 | 775 |
| 12.30 | 813 | 12.08 | 828 |
| 11.18 | 894 | 11.19 | 894 |
| 10.87 | 920 | 10.88 | 919 |
| 10.74 | 931 | 10.74 | 931 |
| | | 10.44 | 958 |
| | | 10.28 | 973 |
| | | 10.13 | 987 |
| 9.92 | 1008 | 9.98 | 1004 |
| | | 9.83 | 1017 |
| 9.66 | 1035 | 9.66 | 1035 |
| | | 9.56 | 1046 |
| 9.19 | 1088 | 9.22 | 1085 |
| 9.02 | 1109 | 9.00 | 1111 |
| | | 8.89 | 1125 |
| 8.64 | 1157 | 8.61 | 1161 |
| 8.42 | 1188 | 8.40 | 1190 |
| 8.26 | 1210 | 8.23 | 1215 |
| | | 8.12 | 1232 |
| 7.73 | 1293 | 7.75 | 1290 |
| | | 7.28 | 1374 |
| 6.83 | 1464 | 6.88 | 1454 |
| 3.84 | 2604 | 3.82 | 2618 |
| 3.46 | 2890 | 3.50 | 2857 |
| | | 3.10 | 3226 |
| 2.36 | 4237 | | |

TABLE IV. 2,3,4-trimethylpentane wave-lengths and frequencies of significant bands.

| Wave-lengths in microns | Frequencies in $cm^{-1}$ | Wave-lengths in microns | Frequencies in $cm^{-1}$ |
|---|---|---|---|
| 18.40 | 544 | 18.36 | 545 |
| 17.64 | 567 | 17.59 | 569 |
| 13.28 | 753 | 13.29 | 752 |
| 12.28 | 814 | 12.26 | 816 |
| 11.22 | 891 | 11.22 | 891 |
| 10.85 | 922 | 10.89 | 918 |
| | | 10.70 | 935 |
| 10.45 | 957 | 10.47 | 955 |
| 10.28 | 973 | 10.29 | 972 |
| 10.01 | 999 | 10.01 | 999 |
| 9.61 | 1041 | 9.61 | 1041 |
| 9.30 | 1075 | 9.30 | 1075 |
| 9.07 | 1103 | | |
| 8.90 | 1124 | 8.89 | 1125 |
| 8.60 | 1163 | 8.58 | 1166 |
| | | 8.50 | 1176 |
| 8.43 | 1186 | 8.40 | 1190 |
| 7.86 | 1272 | 7.87 | 1271 |
| 7.72 | 1295 | 7.79 | 1284 |
| 7.59 | 1318 | 7.62 | 1312 |
| 7.26 | 1377 | 7.29 | 1372 |
| 6.90 | 1449 | 6.90 | 1449 |
| 6.78 | 1475 | | |
| 3.83 | 2611 | 3.83 | 2611 |
| 3.70 | 2703 | 3.70 | 2703 |
| 3.47 | 2882 | 3.49 | 2865 |
| 3.27 | 3058 | | |
| 3.10 | 3226 | 3.12 | 3205 |
| 2.98 | 3356 | | |
| 2.68 | 3731 | 2.61 | 3831 |
| 2.41 | 4150 | 2.34 | 4274 |

spection of the spectra of the trimethylpentanes presented in this paper shows that (1), (3), and (4) are approximately correct. Consideration of differences in intensities instead of (2) would seriously complicate the problem. But it would appear that the general conclusion would be unchanged, i.e., that analysis would be greatly simplified by the low temperature technique. It would appear, therefore, that use of spectra obtained at −195°C would facilitate greatly the analysis of mixtures containing all of the octanes. Analyses of mixtures of greater complexity should be possible by use of spectra obtained at the temperatures of liquid hydrogen or helium.

## SPECTRA OF TRISUBSTITUTED OCTANES

Two previously published works have contained infra-red absorption measurements over extensive regions between 2 to 20 mu for compounds of this type. In 1933, Kettering and Sleator[4] obtained the spectrum of 2,2,4-trimethylpentane in the vapor phase between 1 and 16 mu, and in 1938 Lambert and Lecomte[5] obtained the liquid spectra of all of the octanes between 7 and 15 mu. However, these measurements were made with rather low resolution and consequently are unsuitable for analytical work.

The spectra obtained in the work reported here are shown in Figs. 4 to 7 while wave-lengths and frequencies of the significant bands are listed in Tables I to IV.

The film thickness employed in each experiment was 0.071 mm, representing an absorption path of 0.142 mm (since the light traversed the film twice) and each spectrum is the result of at least four determinations for the entire region 2–22 mu. Experimental difficulties attributable to interference of absorption bands of water and carbon dioxide in the air of the laboratory prevented accurate identification of the positions and intensities of the weak hydrocarbon bands

[4] C. F. Kettering and W. W. Sleator, Physics **4**, 47 (1933).

[5] P. Lambert and J. Lecomte, Ann. d. Physik **10**, 503 (1938).

in the 4–6-micron region, but this region is unimportant in paraffinic surveys since the strong bands suitable for analysis occur in the region 500–1500 $cm^{-1}$.††† As a result, the curves serve only to illustrate the relative transmissions in this region.

A comparison of the positions and relative intensities of the bands at the two temperatures shows that only minor changes are produced by the change in state, with the exception of the 3-micron region. In the absence of more detailed examination of this region no explanation can be made of the pronounced bands at about 3 microns.

A comparison of the band widths in the liquid and low temperature spectra indicates close agreement between experimental and theoretical values. In nearly every case the band width at low temperature is equal (or less than) the value predicted by theory. The anticipated marked increase in resolution is also evident.

All of the pure hydrocarbons were prepared in this laboratory by the precision distillation of petroleum fractions in glass columns packed with helices. The efficiencies of the columns ranged from 60 to 100 theoretical plates. The physical properties of the samples, listed in Table V, indicate a purity of 99+ percent in every case.

††† In this region C−C stretching frequencies, $CH_2$, and $CH_3$ rocking and twisting, C−C−C bending frequencies, and torsional oscillations about the single bond occur. This interval is therefore most suitable for distinguishing structural differences between molecules.

TABLE V.

| Compound | *BP*, °F | $n_{20}^D$ | $d_4^{20}$ |
|---|---|---|---|
| 2,2,3-trimethylpentane | 229.6 | 1.40293 | 0.7160 |
| 2,2,4-trimethylpentane | 210.6 | 1.39157 | 0.6919 |
| 2,3,3-trimethylpentane | 238.6 | 1.40732 | 0.7253 |
| 2,3,4-trimethylpentane | 236.1 | 1.4045 | 0.7191 |

## CONCLUSIONS

Since a complete system of infra-red analysis cannot be developed without the spectra of all of the components for reference in locating characteristic bands, elaboration on an analytical method is reserved until the entire group of isomers has been studied. However, it is evident that such an analysis can be evolved, and through the use of diminished temperatures the method can be of a simple nature.

There exists the interesting possibility that the analyses could be further simplified by the use of liquid hydrogen or helium as cooling materials. If so, the bands would be roughly one-third to one-seventh as wide as at room temperature, assuming that the band width remains proportional to the square root of the absolute temperature.

## ACKNOWLEDGMENT

We wish to acknowledge our indebtedness to Mr. C. C. Templeton and Mr. C. F. Ellis who ably assisted in the experimental work, to Dr. H. T. Bollman, under whose direction the distillation of the samples was carried out, and to Dr. Harold Gershinowitz for his interest and advice.

# Magnetic Field Configurations Due to Air Core Coils*

JOHN P. BLEWETT**
*East Patchogue, Long Island, New York*
(Received June 17, 1947)

The field configurations around a circular loop of wire bearing current are discussed, and a tabulation is presented for the field component parallel to the axis of the loop. Formulae are derived for the current distribution which must obtain in cylindrical and ellipsoidal coils in order that the field inside be uniform. Several special cases are noted. The energy storage in the return flux is evaluated in each case.

## I. INTRODUCTION

THE designer of magnetic field coils who wishes to produce a field of a particular configuration is almost invariably hampered by the complexity of the associated mathematical analysis. If he is successful in this task, his formulae are usually so complicated that substitution in them is extremely tedious. In this paper an attempt has been made to simplify this problem, first by a partial tabulation of the fields due to a circular loop, the fundamental component of most air core coils, and, second by the calculation of several coil configurations for production of uniform fields. These basic coils can serve as components for synthesis of more complicated coil forms.

The present investigation was undertaken in connection with the design of electron accelerators having air core field coils. Since such accelerators may be operated intermittently and energy storage may be an important consideration, particular attention has been paid to the determination of energy stored in leakage fluxes.

## II. MAGNETIC FIELDS DUE TO CURRENT IN A CIRCULAR LOOP

The magnetic field configurations due to current flowing in a circular loop can be described in cylindrical coordinates using complete elliptic integrals, or in spherical polar coordinates using infinite series of spherical harmonics.[1] The latter expression converges very slowly and does not give directly the paraxial component which is usually the component of interest. We shall therefore use the former representation. The cylindrical coordinates $\rho$ and $z$ will be employed, and all quantities will be expressed in unrationalized M.K.S. units.

The radial and axial field components are as follows:

$$B_\rho=\frac{2\mu Iz}{\rho\{(a+\rho)^2+z^2\}^{\frac{1}{2}}}\left[-K+\frac{a^2+\rho^2+z^2}{(a-\rho)^2+z^2}E\right] \text{ webers per sq.m,} \quad (1)$$

$$B_z=\frac{2\mu I}{\{(a+\rho)^2+z^2\}^{\frac{1}{2}}}\left[K+\frac{a^2-\rho^2-z^2}{(a-\rho)^2+z^2}E\right] \text{ webers per sq.m,} \quad (2)$$

where

$\mu$ = permeability = $10^{-7}$ henry per meter for free space
$I$ = current in the loop in amperes
$a$ = radius of the loop in meters
$\rho$ and $z$ are expressed in meters and are measured from an origin at the center of the loop. The loop axis is the $z$ axis of the coordinate system
$K$ and $E$ are the complete elliptic integrals of the modulus

$$k^2=\frac{4a\rho}{(a+\rho)^2+z^2}. \quad (3)$$

In the regions close to the axis of the loop, or very far from the loop, $k^2$ is small, and the elliptic integrals can be expressed in the form:

$$K=\frac{\pi}{2}\left\{1+\left(\frac{1}{2}\right)^2k^2+\left(\frac{1\cdot3}{2\cdot4}\right)^2k^4+\left(\frac{1\cdot3\cdot5}{2\cdot4\cdot6}\right)^2k^6+\cdots\right\}, \quad (4)$$

* Most of the work described in this paper was supported by the Office of Naval Research under Contract N5-ORI-178.
** Formerly Research Laboratory, General Electric Company. Now at Brookhaven National Laboratory, Brookhaven, Long Island.
[1] Compare W. R. Smythe *Static and Dynamic Electricity* (McGraw-Hill Book Company, Inc., New York, 1939), pp. 267 and 270.

TABLE I. $B_z a/\mu I$.

| $\rho/a$ ↓ $z/a$ → | 0 | 0.02 | 0.04 | 0.06 | 0.08 | 0.10 |
|---|---|---|---|---|---|---|
| 0.0 | 6.2832 | 6.2793 | 6.2682 | 6.2494 | 6.2235 | 6.1900 |
| .1 | 6.3309 | 6.3267 | 6.3153 | 6.2961 | 6.2687 | 6.2341 |
| .2 | 6.4792 | 6.4744 | 6.4612 | 6.4396 | 6.4092 | 6.3705 |
| .3 | 6.7465 | 6.7408 | 6.7254 | 6.6988 | 6.6621 | 6.6159 |
| .4 | 7.1713 | 7.1642 | 7.1429 | 7.1075 | 7.0593 | 6.9976 |
| .5 | 7.8264 | 7.8160 | 7.7847 | 7.7323 | 7.6613 | 7.5715 |
| .52 | 7.9962 | 7.9847 | 7.9501 | 7.8930 | 7.8150 | 7.7164 |
| .54 | 8.1825 | 8.1699 | 8.1316 | 8.0684 | 7.9820 | 7.8744 |
| .56 | 8.3873 | 8.3733 | 8.3303 | 8.2602 | 8.1652 | 8.0454 |
| .58 | 8.6132 | 8.5971 | 8.5492 | 8.4712 | 8.3646 | 8.2312 |
| .60 | 8.8631 | 8.8453 | 8.7913 | 8.7031 | 8.5829 | 8.4344 |
| .62 | 9.1409 | 9.1201 | 9.0588 | 8.9586 | 8.8228 | 8.6549 |
| .64 | 9.4500 | 9.4267 | 9.3557 | 9.2412 | 9.0866 | 8.8960 |
| .66 | 9.7966 | 9.7695 | 9.6884 | 9.5560 | 9.3775 | 9.1595 |
| .68 | 10.1886 | 10.1568 | 10.0609 | 9.9060 | 9.6989 | 9.4467 |
| .70 | 10.6329 | 10.5944 | 10.4808 | 10.2987 | 10.0551 | 9.7622 |
| .72 | 11.1401 | 11.0944 | 10.9583 | 10.7404 | 10.4515 | 10.1060 |
| .74 | 11.7272 | 11.6696 | 11.5051 | 11.2404 | 10.8932 | 10.4834 |
| .76 | 12.4097 | 12.3398 | 12.1334 | 11.8090 | 11.3864 | 10.8916 |
| .78 | 13.2160 | 13.1269 | 12.8661 | 12.4582 | 11.9347 | 11.3350 |
| .80 | 14.1831 | 14.0644 | 13.7293 | 13.2076 | 12.5481 | 11.8081 |
| .82 | 15.3580 | 15.2025 | 14.7516 | 14.0670 | 13.2269 | 12.3028 |
| .84 | 16.8247 | 16.6169 | 15.9888 | 15.0683 | 13.9694 | 12.8011 |
| .86 | 18.7023 | 18.3841 | 17.4982 | 16.2175 | 14.7505 | 13.2647 |
| .88 | 21.1950 | 20.7008 | 19.3663 | 17.5167 | 15.5219 | 13.6181 |
| .90 | 24.6635 | 23.8317 | 21.6833 | 18.9180 | 16.1756 | 13.7500 |
| .92 | 29.8546 | 28.2885 | 24.5048 | 20.2236 | 16.4402 | 13.4517 |
| .94 | 38.3974 | 34.9057 | 27.6377 | 20.8636 | 15.8663 | 12.4406 |
| .96 | 44.6382 | 45.1306 | 29.5790 | 19.4803 | 13.7732 | 10.4189 |
| .98 | 93.9679 | 43.8104 | 24.4478 | 13.9945 | 9.5639 | 7.2928 |
| 1.00 | ∞ | 4.9912 | 4.2969 | 3.8899 | 3.6004 | 3.3734 |
| 1.02 | −94.0877 | −44.9238 | −15.6759 | −6.1192 | −2.3052 | −.4881 |
| 1.04 | −44.8502 | −35.1530 | −20.6741 | −11.4415 | −6.3880 | −3.5412 |
| 1.06 | −28.5817 | −25.4049 | −18.8187 | −12.7635 | −8.3979 | −5.4477 |
| 1.08 | −20.6171 | −19.2334 | −15.8890 | −12.1590 | −8.9202 | −6.3894 |
| 1.10 | −15.8750 | −15.1625 | −13.3003 | −10.9663 | −8.6526 | −6.6536 |
| 1.12 | −12.7434 | −12.3320 | −11.2241 | −9.7017 | −8.0675 | −6.5359 |
| 1.14 | −10.5495 | −10.3852 | −9.5686 | −8.5542 | −7.3872 | −6.2133 |
| 1.16 | −8.9219 | −9.1774 | −8.2640 | −7.5549 | −6.6980 | −5.8115 |
| 1.18 | −7.6723 | −7.5554 | −7.2182 | −6.7013 | −6.0718 | −5.3767 |
| 1.20 | −6.6928 | −6.6012 | −6.3570 | −5.9751 | −5.4984 | −4.9640 |
| 1.22 | −5.8949 | −5.8330 | −5.6448 | −5.3561 | −4.9903 | −4.5691 |
| 1.24 | −5.2448 | −5.1971 | −5.0540 | −4.8309 | −4.5406 | −4.2059 |
| 1.26 | −4.6983 | −4.6613 | −4.5497 | −4.3749 | −4.1481 | −3.8789 |
| 1.28 | −4.2409 | −4.2123 | −4.1231 | −3.9839 | −3.7978 | −3.5792 |
| 1.30 | −3.8473 | −3.8239 | −3.7522 | −3.6398 | −3.4885 | −3.3091 |
| 1.32 | −3.5081 | −3.4892 | −3.4315 | −3.3389 | −3.2147 | −3.0630 |
| 1.34 | −3.2139 | −3.1985 | −3.1503 | −3.0746 | −2.9715 | −2.8447 |
| 1.36 | −2.9564 | −2.9413 | −2.9019 | −2.8384 | −2.7521 | −2.6455 |
| 1.38 | −2.7287 | −2.7180 | −2.6846 | −2.6290 | −2.5558 | −2.4660 |
| 1.40 | −2.5266 | −2.5156 | −2.4879 | −2.4429 | −2.3807 | −2.3034 |
| 1.42 | −2.3460 | −2.3384 | −2.3143 | −2.2742 | −2.2210 | −2.1548 |
| 1.44 | −2.1842 | −2.1782 | −2.1576 | −2.1231 | −2.0773 | −2.0188 |
| 1.46 | −2.0400 | −2.0329 | −2.0150 | −1.9853 | −1.9463 | −1.8964 |
| 1.48 | −1.9086 | −1.9023 | −1.8869 | −1.8612 | −1.8273 | −1.7825 |
| 1.5 | −1.7891 | −1.7850 | −1.7703 | −1.7490 | −1.7178 | −1.6785 |
| 1.6 | −1.3321 | −1.3290 | −1.3220 | −1.3095 | −1.2917 | −1.2713 |
| 1.7 | −1.0267 | −1.0256 | −1.0207 | −1.0139 | −1.0030 | −.9906 |
| 1.8 | −.8131 | −.8125 | −.8096 | −.8054 | −.7986 | −.7903 |
| 1.9 | −.6580 | −.6577 | −.6557 | −.6526 | −.6482 | −.6427 |
| 2.0 | −.5416 | −.5414 | −.5401 | −.5381 | −.5346 | −.5308 |

TABLE I.—*Continued.*

| $\rho/a$ ↓ $z/a$ → | 0.12 | 0.14 | 0.16 | 0.18 | 0.20 | 0.22 | 0.24 |
|---|---|---|---|---|---|---|---|
| 0.0 | 6.1497 | 6.1028 | 6.0496 | 5.9896 | 5.9243 | 5.8533 | 5.7769 |
| .1 | 6.1925 | 6.1436 | 6.0882 | 6.0271 | 5.9590 | 5.8854 | 5.8069 |
| .2 | 6.3242 | 6.2703 | 6.2087 | 6.1403 | 6.0651 | 5.9844 | 5.8977 |
| .3 | 6.5596 | 6.4942 | 6.4210 | 6.3389 | 6.2503 | 6.1547 | 6.0533 |
| .4 | 6.9242 | 6.8389 | 6.7439 | 6.6389 | 6.5255 | 6.4046 | 6.2777 |
| .5 | 7.4644 | 7.3430 | 7.2077 | 7.0606 | 6.9044 | 6.7400 | 6.5693 |
| .52 | 7.6004 | 7.4670 | 7.3206 | 7.1620 | 6.9933 | 6.8166 | 6.6344 |
| .54 | 7.7469 | 7.6013 | 7.4417 | 7.2690 | 7.0870 | 6.8968 | 6.7006 |
| .56 | 7.9055 | 7.7453 | 7.5701 | 7.3819 | 7.1841 | 6.9788 | 6.7680 |
| .58 | 8.0756 | 7.8991 | 7.7064 | 7.5011 | 7.2856 | 7.0631 | 6.8362 |
| .60 | 8.2594 | 8.0646 | 7.8512 | 7.6256 | 7.3896 | 7.1478 | 6.9034 |
| .62 | 8.4596 | 8.2412 | 8.0048 | 7.7557 | 7.4970 | 7.2337 | 6.9686 |
| .64 | 8.6748 | 8.4295 | 8.1662 | 7.8902 | 7.6055 | 7.3178 | 7.0307 |
| .66 | 8.9080 | 8.6311 | 8.3350 | 8.0281 | 7.7138 | 7.3992 | 7.0870 |
| .68 | 9.1587 | 8.8448 | 8.5117 | 8.1679 | 7.8208 | 7.4755 | 7.1357 |
| .70 | 9.4302 | 9.0686 | 8.6925 | 8.3068 | 7.9217 | 7.5424 | 7.1734 |
| .72 | 9.7189 | 9.3046 | 8.8747 | 8.4426 | 8.0140 | 7.5970 | 7.1963 |
| .74 | 10.0273 | 9.5475 | 9.0572 | 8.5682 | 8.0916 | 7.6346 | 7.2001 |
| .76 | 10.3541 | 9.7926 | 9.2300 | 8.6778 | 8.1493 | 7.6480 | 7.1787 |
| .78 | 10.6923 | 10.0349 | 9.3864 | 8.7646 | 8.1760 | 7.6298 | 7.1240 |
| .80 | 11.0666 | 10.2594 | 9.5131 | 8.8123 | 8.1626 | 7.5689 | 7.0305 |
| .82 | 11.3620 | 10.4499 | 9.5922 | 8.8052 | 8.0936 | 7.4572 | 6.8871 |
| .84 | 11.6525 | 10.5762 | 9.5984 | 8.7236 | 7.9548 | 7.2784 | 6.6850 |
| .86 | 11.8621 | 10.6012 | 9.4967 | 8.5425 | 7.7238 | 7.0195 | 6.4173 |
| .88 | 11.9247 | 10.4696 | 9.2515 | 8.2321 | 7.3826 | 6.6715 | 6.0720 |
| .90 | 11.7385 | 10.1080 | 8.8074 | 7.7622 | 6.9122 | 6.2176 | 5.6459 |
| .92 | 11.1689 | 9.4404 | 8.1253 | 7.1064 | 6.3008 | 5.6585 | 5.1361 |
| .94 | 10.0596 | 8.3880 | 7.1668 | 6.2523 | 5.5488 | 4.9978 | 4.5503 |
| .96 | 8.3201 | 6.9152 | 5.9358 | 5.2146 | 4.6709 | 4.2407 | 3.8981 |
| .98 | 5.9421 | 5.0775 | 4.4776 | 4.0349 | 3.6944 | 3.4235 | 3.2008 |
| 1.00 | 3.1949 | 3.0343 | 2.8979 | 2.7816 | 2.6715 | 2.5713 | 2.4834 |
| 1.02 | .4743 | 1.0118 | 1.3422 | 1.5358 | 1.6599 | 1.7334 | 1.7737 |
| 1.04 | −1.8235 | −.7692 | −.0727 | .3931 | .7134 | .9375 | 1.0986 |
| 1.06 | −3.4863 | −2.1580 | −1.2398 | −.5903 | −.1230 | .2237 | .4804 |
| 1.08 | −4.5162 | −3.1463 | −2.1366 | −1.3837 | −.8190 | −.3916 | −.0649 |
| 1.10 | −5.0309 | −3.6799 | −2.7532 | −1.9764 | −1.3729 | −.9010 | −.5259 |
| 1.12 | −5.1963 | −4.0669 | −3.1426 | −2.3944 | −1.7915 | −1.3007 | −.9046 |
| 1.14 | −5.1358 | −4.1771 | −3.3567 | −2.6653 | −2.0851 | −1.6037 | −1.2022 |
| 1.16 | −4.9444 | −4.1465 | −3.4364 | −2.8117 | −2.2772 | −1.8198 | −1.4297 |
| 1.18 | −4.6927 | −4.0341 | −3.4227 | −2.8735 | −2.3891 | −1.9626 | −1.5937 |
| 1.20 | −4.4116 | −3.8727 | −3.3544 | −2.8742 | −2.4384 | −2.0507 | −1.7054 |
| 1.22 | −4.1250 | −3.6734 | −3.2371 | −2.8249 | −2.4417 | −2.0925 | −1.7757 |
| 1.24 | −3.8454 | −3.4726 | −3.1035 | −2.7470 | −2.4108 | −2.0969 | −1.8100 |
| 1.26 | −3.5811 | −3.2711 | −2.9594 | −2.6525 | −2.3566 | −2.0777 | −1.8174 |
| 1.28 | −3.3340 | −3.0752 | −2.8089 | −2.5449 | −2.2863 | −2.0405 | −1.8069 |
| 1.30 | −3.1051 | −2.8854 | −2.6592 | −2.4324 | −2.2071 | −1.9880 | −1.7793 |
| 1.32 | −2.8927 | −2.7097 | −2.5167 | −2.3189 | −2.1222 | −1.9239 | −1.7413 |
| 1.34 | −2.7013 | −2.5434 | −2.3783 | −2.2069 | −2.0338 | −1.8629 | −1.6960 |
| 1.36 | −2.5242 | −2.3894 | −2.2451 | −2.0964 | −1.9451 | −1.7945 | −1.6456 |
| 1.38 | −2.3627 | −2.2466 | −2.1223 | −1.9909 | −1.8580 | −1.7233 | −1.5909 |
| 1.40 | −2.2132 | −2.1131 | −2.0052 | −1.8908 | −1.7739 | −1.6549 | −1.5351 |
| 1.42 | −2.0764 | −1.9905 | −1.8948 | −1.7959 | −1.6915 | −1.5858 | −1.4792 |
| 1.44 | −1.9525 | −1.8758 | −1.7936 | −1.7053 | −1.6132 | −1.5179 | −1.4225 |
| 1.46 | −1.8374 | −1.7703 | −1.6970 | −1.6192 | −1.5373 | −1.4534 | −1.3676 |
| 1.48 | −1.7310 | −1.6720 | −1.6088 | −1.5390 | −1.4663 | −1.3907 | −1.3131 |
| 1.5 | −1.6332 | −1.5819 | −1.5245 | −1.4638 | −1.3979 | −1.3300 | −1.2606 |
| 1.6 | −1.2489 | −1.2158 | −1.1828 | −1.1472 | −1.1084 | −1.0679 | −1.0255 |
| 1.7 | −.9751 | −.9572 | −.9371 | −.9143 | −.8905 | −.8651 | −.8373 |
| 1.8 | −.7803 | −.7687 | −.7556 | −.7412 | −.7253 | −.7086 | −.6901 |
| 1.9 | −.6363 | −.6283 | −.6196 | −.6098 | −.5990 | −.5874 | −.5750 |
| 2.0 | −.5262 | −.5208 | −.5147 | −.5080 | −.5002 | −.4923 | −.4835 |

$$E=\frac{\pi}{2}\left\{1-\left(\frac{1}{2}\right)k^2-\left(\frac{1\cdot 3}{2\cdot 4}\right)^2\frac{k^4}{3}-\left(\frac{1\cdot 3\cdot 5}{2\cdot 4\cdot 6}\right)^2\frac{k^6}{5}-\cdots\right\}. \quad (5)$$

If, as is usually the case, the region of particular interest is that close to the wire, it will be found that $k^2$ approaches unity. Within a distance of almost $0.5a$ of the wire, $k^2$ will be greater than 0.9. For $k^2$ greater than 0.9, the approximate expressions:

$$K=\ln 4-0.5\ln(1-k^2)$$
$$=1.39-1.15\log_{10}(1-k^2), \quad (6)$$

$$E=1/k^2 \quad (7)$$

give values correct to within about 3 percent.

Unfortunately, no approximate expressions seem to make any very material simplification in the relations (1) and (2). If the procedures of coil designing are to be expedited, it seems that there is no alternative to a tabulation. Since the axial component $B_z$ has been of primary interest as far as air core field coils are concerned, the tabulation has been completed only for $B_z$. The

TABLE I.—*Continued.*

| ρ/a ↓ \ z/a → | 0.26 | 0.28 | 0.30 | 0.32 | 0.34 | 0.36 |
|---|---|---|---|---|---|---|
| 0.0 | 5.6963 | 5.6104 | 5.5216 | 5.4280 | 5.3325 | 5.2335 |
| .1 | 5.7234 | 5.6355 | 5.5434 | 5.4480 | 5.3500 | 5.2483 |
| .2 | 5.8066 | 5.7108 | 5.6103 | 5.5070 | 5.4003 | 5.2912 |
| .3 | 5.9470 | 5.8358 | 5.7201 | 5.6014 | 5.4810 | 5.3574 |
| .4 | 6.1452 | 6.0083 | 5.8681 | 5.7252 | 5.5805 | 5.4354 |
| .5 | 6.3940 | 6.2157 | 6.0358 | 5.8555 | 5.6761 | 5.4982 |
| .52 | 6.4477 | 6.2582 | 6.0685 | 5.8788 | 5.6904 | 5.5051 |
| .54 | 6.5012 | 6.3007 | 6.0998 | 5.8998 | 5.7020 | 5.5081 |
| .56 | 6.5555 | 6.3412 | 6.1282 | 5.9176 | 5.7101 | 5.5072 |
| .58 | 6.6077 | 6.3797 | 6.1537 | 5.9310 | 5.7133 | 5.5014 |
| .60 | 6.6580 | 6.4143 | 6.1747 | 5.9420 | 5.7113 | 5.4893 |
| .62 | 6.7047 | 6.4448 | 6.1897 | 5.9421 | 5.7022 | 5.4708 |
| .64 | 6.7471 | 6.4688 | 6.1981 | 5.9363 | 5.6846 | 5.4438 |
| .66 | 6.7813 | 6.4839 | 6.1966 | 5.9207 | 5.6577 | 5.4062 |
| .68 | 6.8066 | 6.4886 | 6.1840 | 5.8943 | 5.6188 | 5.3582 |
| .70 | 6.8188 | 6.4800 | 6.1579 | 5.8535 | 5.5667 | 5.2972 |
| .72 | 6.8152 | 6.4547 | 6.1151 | 5.7962 | 5.4991 | 5.2211 |
| .74 | 6.7913 | 6.4084 | 6.0513 | 5.7207 | 5.4133 | 5.1286 |
| .76 | 6.7415 | 6.3385 | 5.9656 | 5.6228 | 5.3080 | 5.0185 |
| .78 | 6.6618 | 6.2375 | 5.8520 | 5.5007 | 5.1802 | 4.8874 |
| .80 | 6.5435 | 6.1035 | 5.7081 | 5.3505 | 5.0274 | 4.7359 |
| .82 | 6.3804 | 5.9298 | 5.5280 | 5.1695 | 4.8484 | 4.5597 |
| .84 | 6.1668 | 5.7123 | 5.3105 | 4.9567 | 4.6423 | 4.3607 |
| .86 | 5.8967 | 5.4454 | 5.0529 | 4.7091 | 4.4068 | 4.1401 |
| .88 | 5.5623 | 5.1281 | 4.7534 | 4.4281 | 4.1431 | 3.8915 |
| .90 | 5.1649 | 4.7583 | 4.4127 | 4.1124 | 3.8522 | 3.6232 |
| .92 | 4.7037 | 4.3409 | 4.0325 | 3.7670 | 3.5361 | 3.3348 |
| .94 | 4.1830 | 3.8781 | 3.6171 | 3.3946 | 3.2003 | 3.0294 |
| .96 | 3.6156 | 3.3785 | 3.1760 | 3.0002 | 2.8478 | 2.7076 |
| .98 | 3.0136 | 2.8558 | 2.7180 | 2.5937 | 2.4859 | 2.3865 |
| 1.00 | 2.4012 | 2.3240 | 2.2513 | 2.1828 | 2.1195 | 2.0592 |
| 1.02 | 1.7924 | 1.7965 | 1.7898 | 1.7765 | 1.7590 | 1.7354 |
| 1.04 | 1.2094 | 1.2893 | 1.3469 | 1.3831 | 1.4073 | 1.4203 |
| 1.06 | .6723 | .8162 | .9271 | 1.0100 | 1.0739 | 1.1190 |
| 1.08 | .1906 | .3856 | .5429 | .6638 | .7600 | .8369 |
| 1.10 | −.2289 | .0069 | .1975 | .3504 | .4734 | .5763 |
| 1.12 | −.5841 | −.3211 | −.1066 | .0710 | .2158 | .3120 |
| 1.14 | −.8729 | −.5948 | −.3661 | −.1742 | −.0126 | .1218 |
| 1.16 | −1.1002 | −.8198 | −.5833 | −.3814 | −.2099 | −.0673 |
| 1.18 | −1.2734 | −.9988 | −.7625 | −.5583 | −.3822 | −.2312 |
| 1.20 | −1.4022 | −1.1379 | −.9052 | −.7019 | −.5258 | −.3714 |
| 1.22 | −1.4911 | −1.2388 | −1.0164 | −.8191 | −.6437 | −.4906 |
| 1.24 | −1.5476 | −1.3121 | −1.0996 | −.9086 | −.7394 | −.5898 |
| 1.26 | −1.5800 | −1.3602 | −1.1595 | −.9788 | −.8167 | −.6702 |
| 1.28 | −1.5877 | −1.3857 | −1.1994 | −1.0299 | −.8748 | −.7336 |
| 1.30 | −1.5814 | −1.3972 | −1.2248 | −1.0652 | −.9178 | −.7826 |
| 1.32 | −1.5628 | −1.3937 | −1.2355 | −1.0861 | −.9498 | −.8220 |
| 1.34 | −1.5340 | −1.3803 | −1.2342 | −1.0978 | −.9695 | −.8488 |
| 1.36 | −1.5001 | −1.3595 | −1.2263 | −1.0992 | −.9795 | −.8678 |
| 1.38 | −1.4604 | −1.3334 | −1.2104 | −1.0942 | −.9834 | −.8780 |
| 1.40 | −1.4181 | −1.3016 | −1.1902 | −1.0836 | −.9799 | −.8826 |
| 1.42 | −1.3726 | −1.2679 | −1.1663 | −1.0671 | −.9722 | −.8808 |
| 1.44 | −1.3272 | −1.2322 | −1.1384 | −1.0483 | −.9597 | −.8756 |
| 1.46 | −1.2805 | −1.1943 | −1.1094 | −1.0258 | −.9457 | −.8669 |
| 1.48 | −1.2344 | −1.1567 | −1.0783 | −1.0023 | −.9276 | −.8551 |
| 1.5 | −1.1898 | −1.1184 | −1.0473 | −.9776 | −.9082 | −.8411 |
| 1.6 | −.9809 | −.9361 | −.8902 | −.8443 | −.7984 | −.7527 |
| 1.7 | −.8093 | −.7793 | −.7494 | −.7188 | −.6873 | −.6553 |
| 1.8 | −.6715 | −.6513 | −.6309 | −.6096 | −.5879 | −.5659 |
| 1.9 | −.5614 | −.5479 | −.5338 | −.5184 | −.5030 | −.4870 |
| 2.0 | −.4740 | −.4642 | −.4538 | −.4428 | −.4318 | −.4200 |

computations involved the use of a computing machine and an interpolation table of $K$ and $E$ drawn up from Dwight's tables.[2] The results are collected in Table I in which the values of $aB_z/\mu I$ are given for $\rho/a$ between 0.0 and 2.0, and for $z/a$ between 0.0 and 0.36.

In Fig. 1, $aB_z/\mu I$ has been plotted as a function of $\rho/a$ for three values of $z/a$. The curves have a common characteristic form. For the values of $z/a$ which have been calculated, $B_z$ increases with distance from the axis to pass through a maximum at a radius less than that of the loop. It then decreases, goes through zero at a radius greater than that of the loop, and has a minimum at a point roughly as far outside the loop radius as was the maximum inside the loop radius. From the minimum, the field increases with increasing radius and tends asymptotically to zero. In Fig. 2 the radial coordinates and heights of the maxima and minima are plotted as functions of $z/a$.

If values of $B_\rho$ are desired, fairly good accuracy can be attained from a numerical integration using the table of $B_z$ and the relation

$$(\text{curl } B)_\phi = \frac{\partial B_\rho}{\partial z} - \frac{\partial B_z}{\partial \rho} = 0. \tag{8}$$

The integration proceeds from $z=0$, where $B_\rho$ is zero for all values of $\rho$. In several cases this method of determining $B_\rho$ has been found to be materially faster than substitution in Eq. (1).

## III. PRODUCTION OF A UNIFORM TRANSVERSE FIELD INSIDE AN INFINITE CYLINDER

In a cylinder of radius $R$ and infinite length, whose axis is the $x$ axis in a right-handed rectangular coordinate system, a uniform field $B_0$ in the $z$ direction will be produced by a current $I_x$ in the cylinder wall having current density[3]

$$I_x = -\frac{B_0}{2\pi\mu}\frac{y}{R}. \tag{9}$$

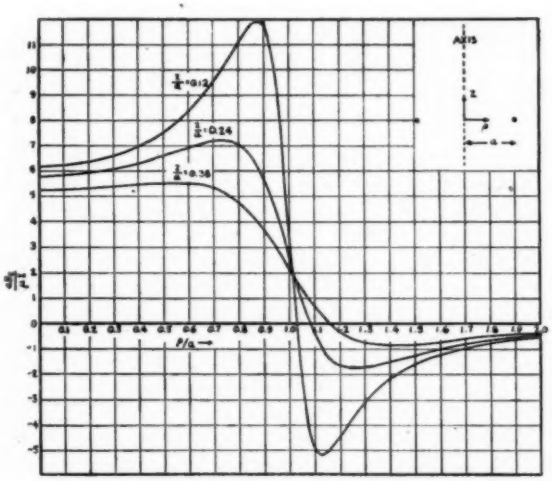

FIG. 1. Axial magnetic fields around a circular loop carrying current $I$.

[2] H. B. Dwight, *Mathematical Tables* (McGraw-Hill Book Company, New York, 1941), pp. 199 *et. seq.*

[3] Compare I. I. Rabi, Rev. Sci. Inst. **5**, 78 (1934).

Outside the cylinder the field components will be

$$\left.\begin{aligned} B_x &= 0 \\ B_y &= 2B_0R^2\frac{yz}{(y^2+z^2)^2} \\ B_z &= B_0R^2\frac{z^2-y^2}{(y^2+z^2)^2} \end{aligned}\right\}. \tag{10}$$

The field pattern outside the cylinder is the same as that which would be produced by currents $+B_0/\delta$ and $-B_0/\delta$ parallel to the axis of the cylinder and displaced $-\delta$ and $+\delta$ from the axis in the $xy$ plane, $\delta$ being an infinitesimal.

The energy stored inside and outside the cylinder is given as usual by integrating $B^2/(8\pi\mu)$ over the appropriate volume. The energy stored per unit length in the field external to the cylinder is

$$E_0=\int_R^\infty \frac{B_0^2R^4\pi d(y^2+z^2)}{8\pi\mu(y^2+z^2)^2}=\frac{B_0^2R^2}{8\mu}. \tag{11}$$

The energy stored per unit length inside the cylinder is simply

$$E_i=\frac{B_0^2}{8\pi\mu}\cdot\pi R^2.$$

So in this case, $E_0=E_i$.

## IV. ELLIPSOIDAL COILS FOR PRODUCTION OF UNIFORM FIELDS

The mathematical techniques necessary for dealing with ellipsoidal coils for production of uniform magnetic fields are similar to those applying to dielectric ellipsoids in uniform electric fields.[4] We shall consider only ellipsoids of revolution in which it is desired to establish a uniform field in the direction of the axis of symmetry. In cylindrical coordinates, the equation of such an ellipsoid is

$$\frac{\rho^2}{a^2}+\frac{z^2}{b^2}=1. \tag{12}$$

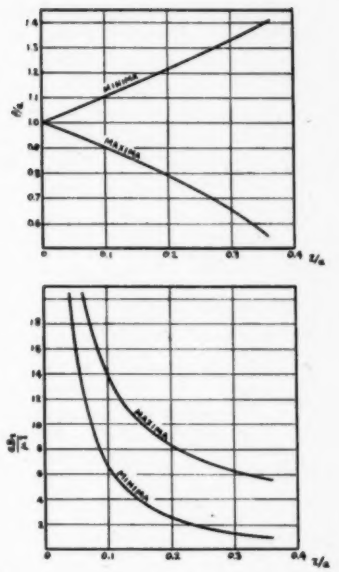


FIG. 2. Positions and heights of maxima and minima in fields of circular loop.

It is convenient to describe the external fields in terms of the parameter $s$ which describes the ellipsoids confocal with the ellipsoid of Eq. (12) through the relation

$$\frac{\rho^2}{a^2+s}+\frac{z^2}{b^2+s}=1. \tag{13}$$

The solution for $s$ of (13) is

$$s=\tfrac{1}{2}\{\rho^2+z^2-a^2-b^2\pm[(a^2+b^2-\rho^2-z^2)^2+4(\rho^2b^2+z^2a^2-a^2b^2)]^{\frac{1}{2}}\}. \tag{14}$$

The choice of sign in (14) must be such that on the surface of the ellipsoid $s=0$ and outside of the ellipsoid $s$ is always positive. (If $s$ does not satisfy this criterion, Eq. (13) describes a family of confocal hyperboloids rather than ellipsoids.) For the most part, the criterion is satisfied by a plus sign in Eq. (14).

The external fields are derivable from a scalar potential function which, if $a$ is greater than $b$, has the form

$$V=B_0Z\left\{\frac{\dfrac{1}{(s+b^2)^{\frac{1}{2}}}-\dfrac{1}{(a^2-b^2)^{\frac{1}{2}}}\tan^{-1}\left(\dfrac{a^2-b^2}{s+b^2}\right)^{\frac{1}{2}}}{-\dfrac{b}{a^2}+\dfrac{1}{(a^2-b^2)^{\frac{1}{2}}}\tan^{-1}\dfrac{(a^2-b^2)^{\frac{1}{2}}}{b}}\right\}. \tag{15a}$$

[4] J. A. Stratton, *Electromagnetic Theory* (McGraw-Hill Book Company, New York, 1941), Sections 3.25 to 3.27.

If $a$ is less than $b$

$$V=B_0z\left\{\frac{\dfrac{1}{(s+b^2)^{\frac{1}{2}}}-\dfrac{1}{(b^2-a^2)^{\frac{1}{2}}}\tanh^{-1}\left(\dfrac{b^2-a^2}{s+b^2}\right)^{\frac{1}{2}}}{-\dfrac{b}{a^2}+\dfrac{1}{(b^2-a^2)^{\frac{1}{2}}}\tanh^{-1}\dfrac{(b^2-a^2)^{\frac{1}{2}}}{b}}\right\}, \tag{15b}$$

where $B_0$ is the value of the uniform field inside the ellipsoid. These functions were derived by methods similar to those used by Stratton in dealing with the dielectric ellipsoid. The fields derived from this function for the case $a$ greater than $b$, are:

$$B_\rho=-\frac{\partial V}{\partial\rho}=\frac{B_0z\rho(a^2-b^2)}{(2s-\rho^2-z^2+a^2+b^2)(s+a^2)(s+b^2)^{\frac{1}{2}}\left[-\dfrac{b}{a^2}+\dfrac{1}{(a^2-b^2)^{\frac{1}{2}}}\tan^{-1}\dfrac{(a^2-b^2)^{\frac{1}{2}}}{b}\right]}, \tag{16}$$

$$B_z=-\frac{\partial V}{\partial z}=\frac{B_0\left\{\dfrac{z^2(a^2-b^2)}{(2s-\rho^2-z^2+a^2+b^2)(s+b^2)}-1+\left(\dfrac{s+b^2}{a^2-b^2}\right)^{\frac{1}{2}}\tan^{-1}\left(\dfrac{a^2-b^2}{s+b^2}\right)^{\frac{1}{2}}\right\}}{(s+b^2)^{\frac{1}{2}}\left[-\dfrac{b}{a^2}+\dfrac{1}{(a^2-b^2)^{\frac{1}{2}}}\tan^{-1}\dfrac{(a^2-b^2)^{\frac{1}{2}}}{b}\right]}. \tag{17}$$

If $a$ is less than $b$, the changes necessary in (16) and (17) are obvious from a comparison of (15a) and (15b).

From the potential function of (15a) or (15b) we can deduce also the field components $B_n$ and $B_t$ normal and tangent to the surface of the ellipsoid:

$$B_n=\frac{B_0za^2}{(\rho^2b^4+z^2a^4)^{\frac{1}{2}}} \tag{18}$$

$$B_t=\frac{B_0\rho b^2}{(\rho^2b^4+z^2a^4)^{\frac{1}{2}}}\left\{\frac{\dfrac{1}{b}-\dfrac{1}{(a^2-b^2)^{\frac{1}{2}}}\tan^{-1}\dfrac{(a^2-b^2)^{\frac{1}{2}}}{b}}{\dfrac{b}{a^2}-\dfrac{1}{(a^2-b^2)^{\frac{1}{2}}}\tan^{-1}\dfrac{(a^2-b^2)^{\frac{1}{2}}}{b}}\right\}. \tag{19}$$

Inside the ellipsoid, the normal field component is the same as that outside given by (18). The tangential field component $B_t'$ at the inside surface of the ellipsoid is

$$B_t'=\frac{B_0\rho b^2}{(\rho^2b^4+z^2a^4)^{\frac{1}{2}}}. \tag{20}$$

From Maxwell's equations, the azimuthal current density

$$I_\phi=\frac{B_t-B_t'}{4\pi\mu}=\frac{B_0}{4\pi\mu}\frac{\rho b^2}{(\rho^2b^4+z^2a^4)^{\frac{1}{2}}}\left\{\frac{a^2-b^2}{b^2-\dfrac{ba^2}{(a^2-b^2)^{\frac{1}{2}}}\tan^{-1}\dfrac{(a^2-b^2)^{\frac{1}{2}}}{b}}\right\}. \tag{21}$$

This is the current per unit distance measured tangent to the surface of the ellipsoid. Between $\rho$

and $\rho+d\rho$ the current will be

$$I(\rho)d\rho = I_\phi d\rho[1+(dz/d\rho)^2]^{\frac{1}{2}} = \frac{B_0 d\rho}{4\pi\mu}\frac{\rho b}{a(a^2-\rho^2)^{\frac{1}{2}}}\left\{\frac{a^2-b^2}{b^2-\dfrac{ba^2}{(a^2-b^2)^{\frac{1}{2}}}\tan^{-1}\dfrac{(a^2-b^2)^{\frac{1}{2}}}{b}}\right\}. \tag{22}$$

Similarly, between $z$ and $z+dz$ the current will be

$$I(z)dz = \frac{B_0 dz}{4\pi\mu}\left\{\frac{a^2-b^2}{b^2-\dfrac{ba^2}{(a^2-b^2)^{\frac{1}{2}}}\tan^{-1}\dfrac{(a^2-b^2)^{\frac{1}{2}}}{b}}\right\}, \tag{23}$$

which is a constant independent of $z$. From this fact we may conclude that if the current distribution is achieved by varying the thickness of the ellipsoid wall, keeping constant current density within the wall, the wall thickness in the radial direction will be a constant. It is assumed that the wall thickness remains infinitesimal compared with the ellipsoid dimensions; for thick walls the above theory is no longer correct.

## V. ENERGY STORAGE IN FIELDS OF ELLIPSOIDAL COILS

The energy stored in the field outside the ellipsoid is evaluated most easily by an application of Green's theorem. The energy is given by

$$E_0 = \int \frac{B\cdot B}{8\pi\mu}d\tau = -\int \frac{V_s B_n}{8\pi\mu}dS, \tag{24}$$

where $V_s$ is the value of $V$ (from 15a or 15b) on the surface of the ellipsoid, and $B_n$, the normal field just outside the surface, is given by (18). The integral is taken over the surface of the ellipsoid. When the appropriate substitutions have been made in (24), the integral is easily evaluated. The result is

$$E_0 = -\frac{a^2 b B_0^2}{6\mu}\left\{\frac{\dfrac{1}{b}-\dfrac{1}{(a^2-b^2)^{\frac{1}{2}}}\tan^{-1}\dfrac{(a^2-b^2)^{\frac{1}{2}}}{b}}{\dfrac{b}{a^2}-\dfrac{1}{(a^2-b^2)^{\frac{1}{2}}}\tan^{-1}\dfrac{(a^2-b^2)^{\frac{1}{2}}}{b}}\right\}. \tag{25}$$

The energy inside the ellipsoid where the field is uniform is

$$E_i = \frac{4}{3}\pi a^2 b\frac{B_0^2}{8\pi\mu} = \frac{a^2 b B_0^2}{6\mu}. \tag{26}$$

The ratio of the energy stored outside to the energy stored inside is

$$\frac{E_0}{E_i} = -\frac{\dfrac{1}{b}-\dfrac{1}{(a^2-b^2)^{\frac{1}{2}}}\tan^{-1}\dfrac{(a^2-b^2)^{\frac{1}{2}}}{b}}{\dfrac{b}{a^2}-\dfrac{1}{(a^2-b^2)^{\frac{1}{2}}}\tan^{-1}\dfrac{(a^2-b^2)^{\frac{1}{2}}}{b}}. \tag{27}$$

This ratio is one measure of efficiency of a coil for intermittent operation since it indicates the relative values of useless to useful stored energy. In Fig. 3 $E_0/E_i$ is plotted as a function of the ratio $b/a$. Figure 4 shows the variation of $E_0$ as the ellipsoid parameters vary. In this figure, $6\mu E_0/(a^3B_0^2)$ is plotted as a function of $b/a$.

## VI. SPECIAL CASES OF THE ELLIPSOID

### a. The Infinite Solenoid

This familiar configuration appears when the semi-axis $b$ of the ellipsoid is allowed to become infinite. The potential $V$ outside, the external fields, and the ratio of external to internal stored energy all tend to zero. From (23) the current per unit length in the wall becomes $B_0/4\pi\mu$.

### b. The Sphere

When $b=a$, the ellipsoid becomes a sphere. From (15), (16), and (17) the external potential

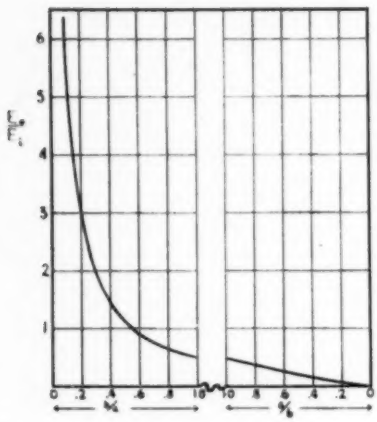

FIG. 3. Ratio of external to internal energy storage for ellipsoidal coils.

and fields are

$$V=\frac{B_0za^3}{2(\rho^2+z^2)^{3/2}}, \tag{28}$$

$$B_\rho=\frac{3B_0z\rho a^3}{2(\rho^2+z^2)^{5/2}}, \tag{29}$$

$$B_z=\frac{B_0a^3(2z^2-\rho^2)}{2(\rho^2+z^2)^{5/2}}. \tag{30}$$

The uniform field in the sphere is produced by a current whose density, from (21), is

$$I_\phi=\frac{3B_0\rho}{8\pi\mu a}. \tag{31}$$

From (25) the external stored energy is

$$E_0=\frac{a^3B_0^2}{12\mu} \tag{32}$$

and the ratio $E_0/E_i$ is given by (27)

$$\frac{E_0}{E_i}=\tfrac{1}{2}. \tag{33}$$

Spherical coils of this type have been discussed and applied to mass spectrometer design by Hipple.[5]

### c. The Plane Coil

If $b$ is reduced to zero the ellipsoidal coil becomes a flat pancake. The external potential becomes from (15):

$$V=\frac{2aB_0z}{\pi}\left(\frac{1}{\sqrt{s}}-\frac{1}{a}\tan^{-1}\frac{a}{\sqrt{s}}\right). \tag{34}$$

From (16) and (17) the external fields are

$$B_\rho=\frac{2B_0z\rho a^3}{\pi(2s-\rho^2-z^2+a^2)(s+a^2)\sqrt{s}}. \tag{35}$$

$$B_z=\frac{2aB_0}{\pi\sqrt{s}}\left(\frac{z^2a^2}{s(2s-\rho^2-z^2+a^2)}-1+\frac{\sqrt{s}}{a}\tan^{-1}\frac{a}{\sqrt{s}}\right). \tag{36}$$

In the neighborhood of this coil where $\rho$ is materially less than $a$, and $z$ is small,

$$B_\rho=\pm\frac{2B_0\rho}{\pi(a^2-\rho^2)^{\frac{1}{2}}}\ \text{approx.} \tag{37}$$

the sign depending on whether $z$ is positive or negative, and

$$B_z=B_0\ \text{approx.} \tag{38}$$

From (21) the current density is

$$I_\phi=\frac{B_0\rho}{\pi^2\mu(a^2-\rho^2)^{\frac{1}{2}}}. \tag{39}$$

(The value deduced from Eq. (21) by letting $b$ tend to zero must be multiplied by a factor of two to obtain (39) since when $b=0$ the upper and lower surfaces of the ellipsoid become coincident.) From (25) the external stored energy is

$$E_0=\frac{a^3B_0^2}{3\pi\mu}, \tag{40}$$

and the internal energy is, of course, zero.

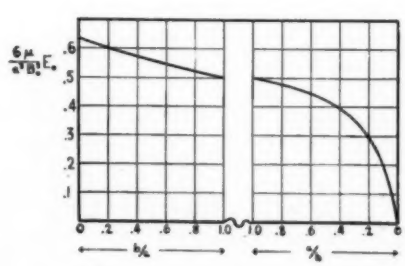

FIG. 4. External stored energy for ellipsoidal coils.

[5] J. A. Hipple, Phys. Rev. **55**, 597 (1939).

## VII. COMPARISON OF IRON CORE AND AIR CORE FIELD COILS

As a basis on which to compare iron core and air core coils for practical applications, we shall evaluate the number of ampere turns required in the two cases to provide a uniform field $B_0$ within a given region.

We assume the ellipsoidal coil to be made up of $N$ turns, each turn carrying a current $I_0$ amperes. If the number of turns between $\rho$ and $\rho+d\rho$ is $n(\rho)d\rho$ then

$$I_0\int_{-a}^{+a} n(\rho)d\rho=\int_{-a}^{+a} I(\rho)d\rho=NI_0. \quad (41)$$

We substitute for $I(\rho)$ from Eq. (22) and perform the integration to obtain for the total number of ampere turns:

$$NI_0=\frac{B_0 b}{2\pi\mu}\left\{\frac{a^2-b^2}{b^2-\dfrac{ba^2}{(a^2-b^2)^{\frac{1}{2}}}\tan^{-1}\dfrac{(a^2-b^2)^{\frac{1}{2}}}{b}}\right\}. \quad (42)$$

The number of ampere turns $N'I'$ required in an iron core coil for generation of a field $B_0$ webers per sq.m in an air gap of length $l$ meters is

$$N'I'=\frac{B_0 l}{4\pi\mu}=8.0\times10^5 B_0 l \quad (43)$$

provided the air gap is short compared with the other dimensions of the region in which the field is to be maintained. If the air gap becomes comparable with the other dimensions the number of ampere turns will be materially higher than the value given by (43), since the fields begin to suffer in strength and uniformity as edge effects become more important.

A comparison between Eqs. (42) and (43) shows that for small air gaps the iron core has marked advantages. For an air gap one-tenth of the pole-piece diameter, the iron core magnet requires only about one-eighth of the ampere turns needed by the corresponding ellipsoidal air core coil for which $b/a=0.1$. When the air gap becomes about half the pole-piece diameter, the magnets become comparable in ampere turn requirements, and for larger air gaps the ampere turn requirements remain comparable. Evidently the mechanical simplicity and compactness of the air core coil merit consideration in any case where the air gap in the corresponding iron core magnet would be greater than half the pole-piece diameter.

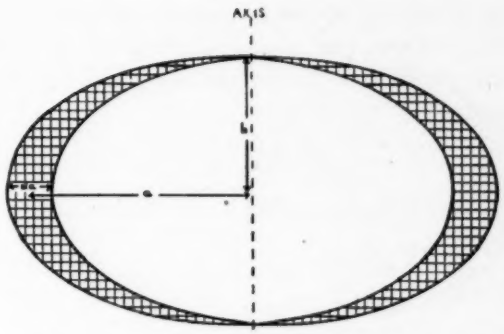


FIG. 5. Cross section through ellipsoidal coil for production of uniform field.

## VIII. POWER CONSUMPTION IN ELLIPSOIDAL D.C. FIELD COILS

The distribution of turns in the wall of the ellipsoid can be expressed rather simply using Eqs. (22), (41), and (42). The number of turns between $\rho$ and $\rho+d\rho$ is

$$n(\rho)d\rho=\frac{N\rho d\rho}{2a(a^2-\rho^2)^{\frac{1}{2}}}. \quad (44)$$

Similarly, the number of turns between $z$ and $z+dz$ is

$$n(z)dz=\frac{Ndz}{2b}. \quad (45)$$

The total length of wire used in the winding will be

$$\int_{-a}^{+a} 2\pi\rho n(\rho)d\rho=\frac{\pi^2 aN}{2}\text{ meters}. \quad (46)$$

If the coil is wound with copper wire having a cross-sectional area of $s$ sq.m. the total resistance of the winding will be

$$R_0=1.7\times10^{-8}\frac{\pi^2 aN}{2s}\text{ ohms}. \quad (47)$$

From (42) and (47) the power consumption in the coil will be

$$I_0^2R_0=\frac{1.9\times10^5 ab^2B_0^2}{Ns}\times\left\{\frac{a^2-b^2}{b^2-\dfrac{ba^2}{(a^2-b^2)^{\frac{1}{2}}}\tan^{-1}\dfrac{(a^2-b^2)^{\frac{1}{2}}}{b}}\right\}^2\text{ watts}. \quad (48)$$

If the thickness of the coil in the $z=0$ plane is $\alpha a$ (from (23) or (45) $\alpha a$ will also be the thickness in any plane parallel to the $z=0$ plane) then from (45)

$$Ns=2\alpha ab \tag{49}$$

and the power consumption may be written

$$I_0^2R_0=\frac{9.5\times10^4bB_0^2}{\alpha}\times\left\{\frac{a^2-b^2}{b^2-\dfrac{ba^2}{(a^2-b^2)^{\frac{1}{2}}}\tan^{-1}\dfrac{(a^2-b^2)^{\frac{1}{2}}}{b}}\right\}^2 \text{watts.} \tag{50}$$

For $b/a=0.6$, 1.0, and infinity, the quantity in the bracket will have the values 1.9, 1.5, and 1.0, respectively.

Figure 5 is a sketch of the cross section through an ellipsoidal coil for which $b/a=0.6$ and $\alpha=0.2$.

### VIII. ACKNOWLEDGMENTS

The author is indebted to Professor F. W. Grover for a considerable amount of information on techniques for dealing with the circular loop problem and with elliptic integrals. Professor Grover's study of the fields around a circular loop will appear in a forthcoming paper in the *Proceedings of the Institute of Radio Engineers*. The tables of magnetic fields around a circular loop represent a long period of patient and painstaking calculation on the part of Miss M. Kay.

---

## Design of an Air Core Synchrotron*

JOHN P. BLEWETT**
*East Patchogue, Long Island, New York*
(Received June 17, 1947)

The analysis of the preceding paper is applied to the problem of designing a synchrotron in which the magnetic fields are produced by air core coils. The air core synchrotron is shown to be practical and to present certain advantages.

### I. INTRODUCTION

IN the preceding paper an analysis has been presented of the problems, first, of the magnetic fields caused by current flowing in a circular loop, and second, of the coil configurations necessary to produce uniform fields in regions of various geometries. The magnetic field requirements of the betatron and the synchrotron will now be considered in the light of this analysis.

Air core magnets present three major advantages. First, they free the magnet designer from the upper limit of 1.8 webers per square meter (18,000 gausses) or so associated with iron cores because of the saturation characteristics of iron. Second, they do not introduce the random local inhomogeneities in field which are found in the fields of iron core magnets as a result of defects in fabrication or spottiness in previous treatment. This drawback of iron cores may be a serious one in the betatron or the synchrotron in which injection takes place just after the field has passed through zero. If all parts of the field do not pass through zero simultaneously it may be difficult to initiate a beam, particularly in the higher energy machines. The third advantage of air core coils is the obvious one that a large and costly iron structure is avoided. This is particularly important in betatrons and synchrotrons where the iron must be laminated, and the core construction is an extremely tedious and expensive proposition.

The problems which arise when a switch is made from iron to air core are mainly associated with the choice of the correct geometry for the

* Most of the work described in this paper was supported by the Office of Naval Research under Contract N5-ORI-178.
** Formerly Research Laboratory, General Electric Company. Now at Brookhaven National Laboratory, Brookhaven, Long Island.

current carrying conductors. Possible solutions to these problems are discussed in Sections II, III, IVa, and IVb. Other problems associated with air core coils such as cooling, auxiliary circuits, mechanical support, and so forth do not seem unduly serious. Typical solutions of several such problems are presented in Sections IVc, IVd, and IVe.

## II. AIR CORE GUIDE FIELDS FOR BETATRONS OR SYNCHROTRONS

The primary economic factor in the design of a betatron or synchrotron, aside from the magnet itself, is the capacitor bank in which the energy to appear in the magnetic field must be stored during the inactive periods. It is therefore important that as much of the field generated as possible shall be actually useful. An iron core magnet designed to produce a field of a particular type generally stores two or three times as much energy as is required for fields which actually deflect particles. This is simply because the shape of the pole piece which produces the desired field is generally not the same as the shape of the vacuum envelope in which the field is utilized. In addition wasted energy is always stored in leakage fluxes. The air core magnet can be designed to fit the vacuum envelope. It must, however, have a finite thickness to permit it to dissipate power. And it must store unused energy in return fluxes.

For toroidal regions such as those enclosed by the vacuum envelopes of betatrons and synchrotrons, air cores and iron cores are about equally economical in stored energy. The problem of generation of uniform fields in a toroidal region has not yet been solved analytically so far as the author is aware. An approximate attack is suggested, however, by the infinite cylinder case treated in Section III of the preceding paper. If the cylinder is bent in the $x, y$ plane on a radius of curvature materially greater than its own radius, the external distribution of energy will not be too violently disturbed. It follows from Eq. (11) of the preceding paper that three-quarters of the energy in the external field of the cylinder lies between the cylinder wall (radius $R$) and a cylinder of radius $2R$. This will probably still be approximately true when the cylinder has been bent into a torus. It is therefore a reasonable assumption that the energy stored in the external fields of the torus is approximately the same as the energy stored within the torus wall, just as was true in the case of the infinite cylinder. In other words, in setting up a uniform paraxial field within a toroidal region we shall store approximately twice the energy we use because of the energy stored in the external return flux. If now we arbitrarily increase the factor of two to a factor of three to take care of the excess energy stored because of the necessarily finite thickness of the coil, we shall have a design factor not far from that actually realizable.

If a roughly uniform field $B_0$ webers per sq. m is set up within a toroidal region whose cross-sectional area is $\pi r^2$ sq. m and whose mean radius is $R$ m, the energy stored in this region will be

$$E_i=\frac{\pi R r^2 B_0^2}{4\mu} \text{ joules,} \tag{1}$$

where $\mu$, the permeability, $=10^{-7}$ henry per meter for free space. To obtain the total energy stored in all fields we multiply this quantity by our factor of three to obtain

$$E=\frac{3\pi R r^2 B_0^2}{4\mu}=2.4\times 10^7 R r^2 B_0^2 \text{ joules.} \tag{2}$$

This equation can be rewritten in terms of the energy $W$ ($=mc^2/e$ electron volts) of a particle bent in a circle of radius $R$ in a field $B_0$ through the relation

$$W=B_0 c^2 R/v \text{ electron volts,} \tag{3}$$

where $v$ is the particle velocity in meters per sec., $c$, the velocity of light, $=3\times 10^8$ m per sec. From (2) and (3)

$$E=2.7\times 10^{-10}\frac{r^2 W^2}{R}\frac{v^2}{c^2}. \tag{4}$$

If, for example, $R$ is one meter, the vacuum envelope is a torus of three-inch tubing so $r=0.038$ m and $W$ is 100 Mev, $v$ will be approximately equal to $c$ if the particles are electrons, and $E$ will be about 4000 joules. This much energy could be stored at 5000 volts in sixteen 20-microfarad capacitors.

If this device is to be operated continuously

TABLE I.

| $W$(Mev) | $R$(m) | Number of capacitors for 5-Mev betatron | Number of capacitors for guide field |
|---|---|---|---|
| 100 | 0.5 | 7 | 30 |
| 500 | 2.5 | 35 | 150 |
| 1000 | 5.0 | 70 | 300 |

at a frequency $\omega/(2\pi)$ the power required may be deduced if an estimate can be made of the $Q$ of the coil. From the definition of $Q$,

$$\text{power required} = \omega E/Q \text{ watts.} \tag{5}$$

At 60 cycles, $Q$'s higher than 5 or 6 are hard to achieve in air core coils. For a $Q$ of 5 and the coil discussed above the power required would be about 300 kilowatts. This is rather high and might justify reconsideration of the higher $Q$'s obtainable in iron core coils. But if, for example, the machine is to be used for cloud-chamber investigations, it need be fired only once or twice a minute. In this case the power consumption drops to the negligible range below 200 watts.

The actual design of guide-field coils will be treated in more detail in Section IV.

## III. AIR CORE FLUX COILS FOR BETATRON ACCELERATION

In iron core machines the energy stored in fluxes used for betatron acceleration can be negligible if air gaps are kept out of the flux paths. This is because the energy stored for a given flux density is inversely proportional to the permeability of the medium. The air core betatron is therefore at a disadvantage so far as flux coils are concerned. To obtain order of magnitude figures for air core flux coil energy requirements we shall now consider an idealized case.

Efficient energy storage will be achieved if we keep the flux density uniform within the orbit. This could be done with a pancake coil of the sort discussed in Section VIc of the preceding paper. The flux through such a coil of radius $R$ will be

$$\phi = \pi R^2 B_0 \text{ webers.} \tag{6}$$

But from the betatron condition

$$\phi = 2\pi R^2 B_1 \text{ where } B_1 \text{ is the guide field at the orbit}$$
$$= \frac{2\pi R}{c}\frac{v}{c} W \text{ webers} \tag{7}$$

(compare Eq. (3) above). But from Eq. (38) of the preceding paper the energy stored by the flux coil is

$$E_f = \frac{R^3 B_0^2}{3\pi\mu} \text{ joules.} \tag{8}$$

From (6), (7), and (8)

$$E_f = \frac{4R}{3\pi\mu}\frac{v^2}{c^2} W^2 = 4.7\times 10^{-11} R W^2 \frac{v^2}{c^2} \text{ joules.} \tag{9}$$

If $W = 10$ Mev, $R = 0.5$ m, and $v$ is approximately equal to $c$, then $E_f = 2400$ joules. If $W = 100$ Mev, $R = 1$ m, and $v$ is approximately equal to $c$, $E_f$ will be 470,000 joules. In the former case the energy could be stored in ten 5000 volt, 20 microfarad capacitors, while in the latter case 2000 such capacitors would be required. Which, if either, of these quantities is reasonable depends, of course, on the designer's purse and viewpoint. It is evident in any case that air core betatrons for higher energies than 20 Mev will begin to be expensive.

In view of the idealized geometry considered, the figures derived from Eq. (9) are merely lower limits. It would be impractical to extend the flux coil all the way to the orbit and it would, moreover, be impractical to use a pancake coil since its external fields which would exist at the orbit are strongly radially dependent and would interfere with the guide field. A more practical design will be presented in the next section. For the practical flux coil, the factor of 4.7 in Eq. (9) should be replaced by a factor of about 14 to give

$$E_f = 1.4\times 10^{-10} R W^2 \frac{v^2}{c^2} \text{ joules.} \tag{10}$$

## IV. DESIGN OF AN AIR CORE SYNCHROTRON

In the introduction we have pointed out the advantages of air core machines. In Section II air core guide fields were shown to be economically comparable with iron core guide fields, particularly for intermittent operation, and in Section III it was shown that betatron acceleration up to 10 Mev with air core flux coils involves not unreasonable figures for energy storage. Since betatron acceleration up to four or five Mev is quite sufficient to initiate the usual sequence of events in the synchrotron, the betatron coils of an air core

synchrotron could just as well be air core. Introduction of an iron core for the betatron flux would result in rather a tricky problem of synchronization between air core fields and iron core fluxes. It would therefore appear from what has gone before that a high energy air core synchrotron is quite practical. If we speak in terms of 5000-volt 20-microfarad capacitors and of a three-inch diameter vacuum envelope, the results of Eqs. (4) and (10) are as given in Table I for a few typical cases.

We now proceed to a more detailed consideration of design.

### a. Guide-Field Coils

The guide field must decrease with radius at a rate not faster than $1/\rho$ in order that the electron motion shall be stable both in $\rho$ and in $z$. For most designs this means a variation across the vacuum envelope of not more than about ten percent, and the guide-field coils will not differ much from those required to produce a uniform field. As was mentioned in Section II, this problem has not been solved analytically, but a measure of similarity exists between the torus and the infinite cylinder. We should, therefore, begin with a coil system suggested by the cylinder case, such as that shown in cross section in Fig. 1, and, by numerical work based on the tables in the preceding paper or by measurements on models, make the small changes which will result in the desired variation of field with radius.

### b. Flux coils

The flux coils will be required to build up a flux at a rate governed by the rate of rise of the guide field to the point at which the electron energy is about 5 Mev. Now the radiofrequency signal should be turned on and synchrotron acceleration initiated. The guide field should continue to rise, but the betatron flux should cease rising since further increases will result merely in useless storages of energy. In iron core machines this object is accomplished by saturation of the flux core. In an air core machine different methods must be used. One possible method is described in Section c below.

Since the time variations of field and flux are to be different, it follows that no appreciable

FIG. 1. Cross section through air core synchrotron.

field from the flux coil can be permitted to exist in the neighborhood of the orbit. On the other hand, in order that we do not store large amounts of energy needlessly in the flux, it is desirable that the flux coils couple as closely as possible with the orbit. These apparently mutually exclusive requirements can be met by the compromise to be described below.

In the case of the infinite cylinder discussed in Section III of the preceding paper, had we set up currents $I_x$ in the walls proportional to the absolute value of $y$ instead of $y$, the internal field would have been zero. If, now, a wire parallel to the cylinder axis were located somewhere within the cylinder unity coupling would exist between it and the currents in the cylinder walls since no magnetic flux interposes between wire and wall. Presumably an analogous case exists for the toroid. The exact distribution of azimuthal current in a toroid wall, which would give zero internal field, has not yet been worked out. A fairly good approximation can easily be set up, however, using only four wires appropriately located in the torus wall. The four wires $A$, $B$, $C$, and $D$ of Fig. 1 lie in one possible configuration. The choice of positions for these four wires is made after a consideration of the field distributions around a circular loop discussed in Section II of the preceding paper and shown graphically in Figs. 1 and 2 of that paper. Wire $A$ is located so that the maximum in its field pattern lies at the orbit. The position of wire $B$ is such that the minimum in its field pattern lies at the orbit, and the relative currents in the two wires are so adjusted that the minimum and maximum are equal in height. In this way the axial field at the orbit and its first derivative with respect to radius are reduced to zero. The selection of parameters may be expedited by using the graph in Fig. 2 of the preceding paper. In applying this method it will become evident that the

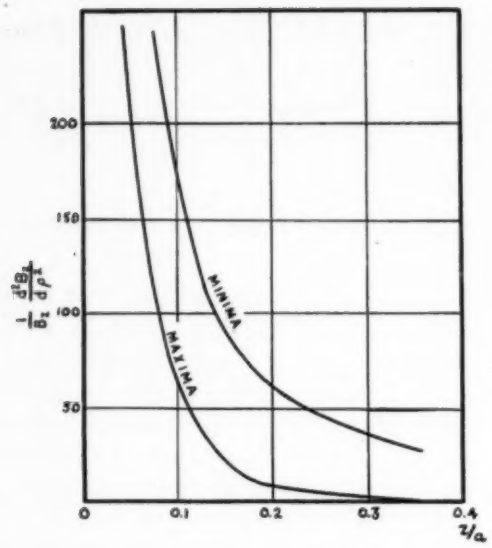


FIG. 2. Second derivatives at maxima and minima in fields of circular loop such that these extrema lie at $\rho=1$.

choice of location and size of the coils is not unique. For each coil, loci of the form $z=f(\rho)$ exist along which cancellation can be achieved by appropriate choices of current ratios. This extra degree of freedom can be utilized to permit cancellation of second derivatives. To facilitate this procedure, the ratios of second derivatives of $B_z$ with respect to $\rho$, to the values of $B_z$, have been plotted in Fig. 2 for the cases where the extrema of the field distributions lie at $\rho=1$. When the value of $z/a$ for one coil has been chosen, the $z/a$ for the second coil will be that for which the ordinates of the curves of Fig. 2 have equal values. Given $z/a$ for each coil, the correct value of $\rho/a$ may be found from Fig. 2 of the preceding paper. The results of this rather complex procedure are summarized in the graphs of Fig. 3 which give complete design data for pairs of loops which give cancellation of the field, its first and second derivatives, at the orbit. For the case where the orbit is located at $\rho=1$ the radius $a_0$ and height $z_0$ of the outer coil and the radius $a_i$ of the inner coil are plotted as functions of the height $z_i$ of the inner coil. Also included in Fig. 3 is the ratio of currents in the two coils as a function of $z_i$. This graph indicates that for the geometry shown in Fig. 1 the ratio of ampere turns in the inner coil to ampere turns in the outer coil is about 4:1.

After cancellation of axial fields and derivatives thereof has been accomplished, addition of the two coils $C$ and $D$, symmetrically located below the plane of the orbit, will give cancellation of radial fields.

It is unnecessary to add further refinements to provide cancellation of fields adjacent above and below the orbit. If $B_z$, and its derivatives with respect to radius, and $B_\rho$ are zero in the plane of the orbit, the fact that the curl and divergence of the field are zero insures the disappearance of the fields at all points in the neighborhood of the orbit.

A further improvement in cancellation and a closer approximation to the ideal case would result from the use of six or more coils so adjusted that still higher derivatives of the field would disappear. This rather formidable problem has not yet been worked out.

Experimentally it has been found that the coupling coefficient between the orbit and a set of coils in about the configuration of Fig. 1 is between 0.8 and 0.9. In other words, the energy gained per revolution by an electron in this system will be between 80 and 90 percent of the voltage per turn applied to the flux coil. This result was obtained with coils about 20 cm in

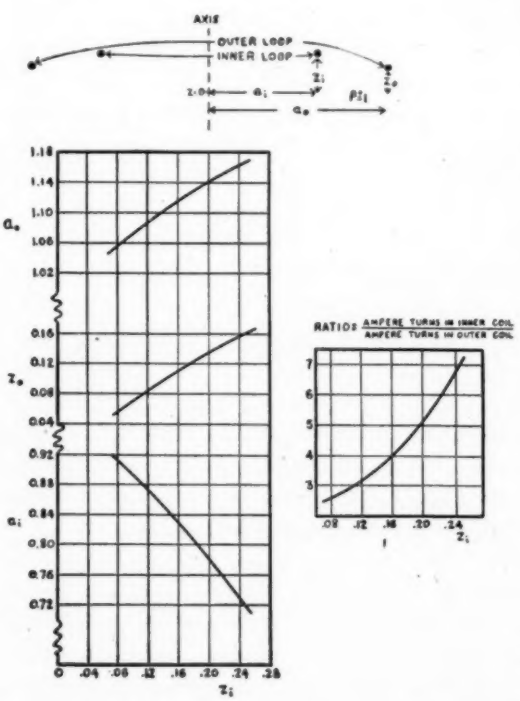


FIG. 3. Design parameters for matching second derivatives.

radius and having cross sections of about one sq. cm. The coupling coefficient might be materially lower for coils of smaller cross section.

### c. Construction of Field and Flux Coils

Two important problems must be kept in mind during the actual construction of the field and flux coils. The first is associated with the forces between conductors. In a high energy machine these forces may be of the order of several tons per meter of coil. The forces will be attractive between conductors passing currents in the same direction and repulsive between conductors passing currents in opposite directions. These forces, fortunately, are such that the coils will tend to be held in place, rather than explode, in a coil form of the convenient shape indicated by dotted lines in Fig. 1. During several months of model experiments on a small 100-Mev design for intermittent operation no difficulty was experienced with these forces.

The second problem lies in the discontinuities at points where leads enter or leave the coils. Theoretically, if entering and return leads lie very close together, no discontinuity will appear, but in practice some space must be left for insulation and detectable inhomogeneities in field do appear. This problem was solved in model experiments by making each coil several coils in parallel. The leads to the several coils were brought out at equally spaced points around the coil circumference. The entering and return leads to each coil were then carried close together and parallel to the coil axis a distance of about one coil radius. They were then bent inward and carried together to the coil axis. All connections were made on the coil axis. Measurements good to 0.1 percent on fields in the neighborhood of the orbit failed to show any measureable inhomogeneity when each coil had been made six coils in parallel. When coils are paralleled thus it is, of course, necessary to interweave the windings in such a way as to maintain uniform current density through the coil and avoid circulation of parasitic currents.

TABLE II.

| Phase of sine wave: | 5° | 10° | 15° | 20° | 25° |
|---|---|---|---|---|---|
| Deviation of sine from linear expression (%): | 0.13 | 0.51 | 1.14 | 2.03 | 3.18 |

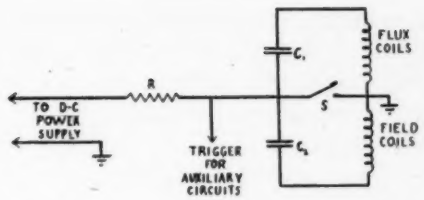


FIG. 4. Circuit for air core synchrotron.

### d. Auxiliary Circuits and Equipment

The requirement that the flux should cease rising after the electron velocity is approximately that of light (compare Section IVb above) can be met by making the flux coils part of a circuit whose resonant frequency is several times that of the circuit which includes the field coils. When a capacity $C$ charged to a voltage $V$ is discharged into an inductance $L$, the current is given by

$$i = V(C/L)^{\frac{1}{2}} \sin(t/(LC)^{\frac{1}{2}}). \qquad (11)$$

For $t$ small, $i = Vt/L$ approximately. As $t$ increases the expression (11) deviates from linearity with $t$ in accordance with Table II. If these figures relate to the higher frequency flux wave, the lower frequency field wave will be essentially linear, and the table gives the percentage error from the betatron condition. The equilibrium orbit will change to a new radius, and the ratio of the change in radius to the original radius can be shown to be essentially the same as the deviation given in the above table.

Since the vacuum envelope must certainly be large enough that a variation in orbit radius of two or three percent can be tolerated, betatron acceleration will be satisfactory up to 20° or 25° of the flux wave. At this point the radiofrequency acceleration must be initiated. We shall now store energy uselessly in the flux coils until 90° in the flux wave, an inelegant feature of this method which is partly counterbalanced by the method's simplicity in execution.

As the flux wave falls off past 90° we shall have a negative betatron effect, but the stability of the synchrotron orbit has often been shown to be sufficient to offset this provided the radiofrequency signal level is sufficiently high.

A circuit for generating the desired sequence of events is shown in Fig. 4. The field and flux capacitor banks, $C_2$ and $C_1$, are charged as indicated from the same power supply. They are then discharged simultaneously by the switch $S$ which can be a large circuit breaker or a bank of ignitrons. At the moment of closing, the potential of the left-hand contact of the switch drops discontinuously to zero. This sharp wave front provides a good trigger for timing injection and radiofrequency turn on and off.

Design data for timing and injection circuits, vacuum envelopes, cooling systems, electron guns, and radiofrequency systems are available in profusion and will not be discussed here.

### e. Summary of Test Results

A program of construction of a 100-Mev air core synchrotron was initiated by the author in the Research Laboratory of the General Electric Company, but his departure from that laboratory prevented him from carrying the program to completion. Numerous model measurements were made on field and flux coils and preliminary circuit tests were performed, but the construction of circuits and electron gun did not reach the point where electrons could be accelerated.

The machine had an orbit radius of 7 inches and was designed for once per minute operation. The structure was generally as indicated above except for the guide field coils which were simply coaxial 44 turn solenoids about 3 inches long. The outer solenoid was divided into two halves in a plane normal to its axis, and it was found that a paraxial separation of about an eighth of an inch of these two half-coils gave a field in the neighborhood of the orbit which fell off approximately as the inverse half-power of radius. This coil design was not as economical as the one indicated in Fig. 1 should be, since considerable amounts of energy were stored in regions above and below the vacuum envelope.

The coils were wound on Bakelite forms generally similar to those shown in Fig. 1.

The vacuum envelope was a toroid of one-inch glass tubing. The electron gun was brought in from the top; other associated equipment was conventional in design.

Once a minute operation solved all cooling problems. It did, however, introduce a difficulty which might well be eliminated in any future machines of this type. Experience with the 70-Mev iron core synchrotron in the General Electric Research Laboratory has indicated that the serious problems in synchrotron operation are all betatron problems; if successful betatron operation can be achieved, further acceleration by radiofrequency fields is very easy. It would seem, therefore, that even though a machine is to be used for intermittent high energy operation it should still be capable of continuous low energy betatron operation. This will speed up very materially the initial tests when a number of parameters are varied in attempts to find a beam. Given a beam, further adjustments to maximize beam intensity or to carry it to higher energy are relatively simple and can be carried on at a once per minute rate without reducing the operator to a state of impatient exasperation.

No special means were included for bringing out the beam. It was hoped eventually that the beam could be deflected into the space above the orbit. It seems on paper to be much easier to move or at least to tilt the beam axially, than it is to expand it in a controlled fashion. In iron core machines, of course, the pole pieces are in the way. In an air core machine a weak auxiliary field might be sufficient to bring a sharp beam into the clear region above the coils.

## V. ACKNOWLEDGMENTS

The author is indebted to Mr. L. Redmond for his invaluable assistance in the performance of the experiments discussed above. Mr. A. M. Gurewitsch, Dr. R. V. Langmuir, Dr. E. E. Charlton, Dr. G. Ragan, and Dr. J. L. Lawson and many others of the author's former associates in the General Electric Research Laboratory have contributed materially in assistance and suggestions. Finally, it is a pleasure to acknowledge the continued advice and support of Dr. A. W. Hull.

# A Sound Velocity Method for Determining the Compressibility of Finely Divided Substances

R. J. URICK
*Naval Research Laboratory, Washington, D. C.*
(Received June 23, 1947)

A method is presented whereby the adiabatic compressibility of a finely divided material can be found from sound velocity and density measurements of a suspension of the particles in a liquid. The method is based on the assumption that the velocity of sound in a suspension is the same as it would be in an ideal solution of the two substances. This is verified experimentally by measurements of sound velocity in kaolin-water suspensions and xylene-water emulsions, and the method is illustrated by the determination of compressibility of the oil droplets in an oil emulsion and of the blood corpuscles in horse blood. Considerable accuracy is attainable for materials which are not too incompressible compared to the suspending liquid.

## INTRODUCTION

THE ultrasonic interferometer has been employed for many years for the determination of the adiabatic compressibility of liquids. This instrument serves to measure the wavelength of sound waves in the liquid, and thereby the velocity of sound, and a simple calculation yields the compressibility once the density of the liquid is known. Extensive tables of compressibility of pure liquids are available.[1]

In 1930, K. H. Herzfeld[2] suggested that this method might be extended to the study of solid substances by grinding them, suspending the particles in a liquid, and measuring the velocity of sound in the suspension. He derived an expression for the adiabatic compressibility of the solid in terms of the velocity, density of solid and liquid, and the compressibility of the liquid. This was based on extensive theoretical considerations of the effect of scattering by numerous small rigid spherical particles in the sound field. The result was applied for this purpose by Randall[3] a short time later, but extremely small, or even negative, compressibilities were found.

The failure of Herzfeld's formula to find experimental verification seems to have been followed by a long period of neglect in the application of the ultrasonic interferometer to substances other than homogeneous liquids and gases.

In the present paper a simple expression will be derived for the velocity of sound in a suspension based on the assumption that the mixture behaves the same as would an ideal solution of the two substances. The result will be verified by some data on kaolin-in-water suspensions and on some emulsions of xylene and water. These considerations permit a determination of the adiabatic compressibility of the particles in a suspension from measurements of sound velocity and density, and this method will be illustrated by the computation of the compressibility of (1) the oil particles in some oil-in-water emulsions and (2) blood corpuscles in horse blood.

## SOUND VELOCITY IN IDEAL MIXTURES

In approaching the subject of the velocity of sound in a suspension or emulsion of one substance in another, it is simplest to consider what takes place in a homogeneous ideal mixture of the two materials. In so doing, we must make the assumption that the suspended particles are infinitesimally small compared to the wavelength of the sound, and that accordingly the effects of scattering on the sound velocity may be neglected. This is seen to be not too unreasonable an assumption when it is realized that at a frequency of one megacycle the size of the particles in a course dispersion is less than a hundredth of the wave-length of sound in water. Making this assumption, we may proceed to find the sound velocity in the same manner as for an ideal solution of one substance in the

[1] L. Bergman, *Der Ultraschall* (Edwards Bros., Ann Arbor, Michigan, 1942), pp. 175–181.
[2] K. H. Herzfeld, "The propagation of sound in suspensions," Phil. Mag. 9, 752–68 (1930).
[3] C. R. Randall, "Ultrasonic measurements of the compressibility of solutions and of solid particles in suspension," *Bur. Stand. J. Research* 8, 79–99 (1932).

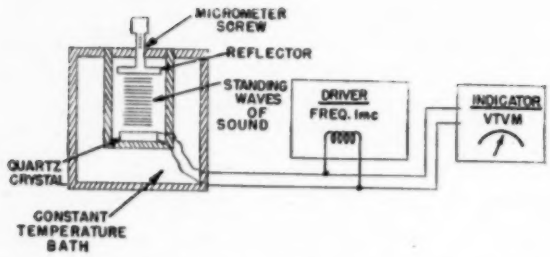


FIG. 1. Diagram of 1-megacycle acoustic interferometer.

other.[4] In this case both the density and the compressibility of the mixture are additive properties of the corresponding quantities for the two materials, depending upon the proportional amount of each substance in the mixture. Thus, $\rho_0=\rho_2\beta+\rho_1(1-\beta)$ and $\kappa_0=\kappa_2\beta+\kappa_1(1-\beta)$, where $\rho_0$, $\kappa_0$ are the density and compressibility of the suspension, $\rho_2$, $\kappa_2$ are the density and compressibility of the suspended particles, $\rho_1$, $\kappa_1$ are the density and compressibility of the suspending substance, $\beta$ is the volume percentage of particles. The subscripts 0, 1, and 2 refer to the suspension, suspending liquid, and the suspended particles, respectively. Hence, the velocity of sound in the mixture is

$$V_0=\frac{1}{(\rho_0\kappa_0)^{\frac{1}{2}}}=\left[\frac{1}{[\rho_2\beta+\rho_1(1-\beta)][\kappa_2\beta+\kappa_1(1-\beta)]}\right]^{\frac{1}{2}}.$$

After dividing by $V_1^2=1/\rho_1\kappa_1$, this expression may be simplified in form by writing, $\gamma=V_1/V_0$, the ratio of the velocity of the suspending liquid to that of the suspension, $a=(\rho_2-\rho_1)/\rho_1$, $b=(\kappa_2-\kappa_1)/\kappa_1$, and we may then obtain

$$\gamma^2=(1+a\beta)(1+b\beta). \qquad (1)$$

Thus the velocity ratio $\gamma$ is a parabolic function of the concentration $\beta$ and will therefore have a maximum or a minimum at some particular concentration $\beta_m$. This concentration,

$$\beta_m=-(a+b)/2ab$$

will be physically realizable, of course, only if it happens to lie between 0 and plus 1. It will be seen later that a minimum of velocity was found for mixtures of kaolin and water.

[4] A. B. Wood, *A Textbook of Sound* (G. Bell & Sons, London, 1941), pp. 361–362.

## THE INTERFEROMETER

The ultrasonic interferometer consists of a piezoelectric crystal mounted in an enclosed chamber. At the opposite end is a reflecting plate capable of being moved parallel to the direction of propagation of the sound by a micrometer screw. The crystal is driven through a loosely coupled coil by a source of constant frequency, and the voltage across the crystal is indicated by a meter. This system is shown schematically in Fig. 1. As the micrometer screw is moved outward or inward, the meter is found to exhibit regular deflections at intervals of a half wave-length, because of the reaction of the standing wave system upon the driving crystal. Thus, the micrometer serves to measure the half wave-length, and since the frequency is known, the velocity of sound in the chamber is readily found. The interferometer chamber is surrounded by a bath whose temperature can be kept constant to 0.01° or so. It is estimated that the interferometer enabled velocity measurements to be made with an average error of 1 part in 3000 or 0.03 percent.

The driving frequency was kept constant at 1 megacycle. At this frequency the wave-length of wound in water is 1.5 mm; the particle size of the suspensions to be described was in the range 1 to 10 microns.

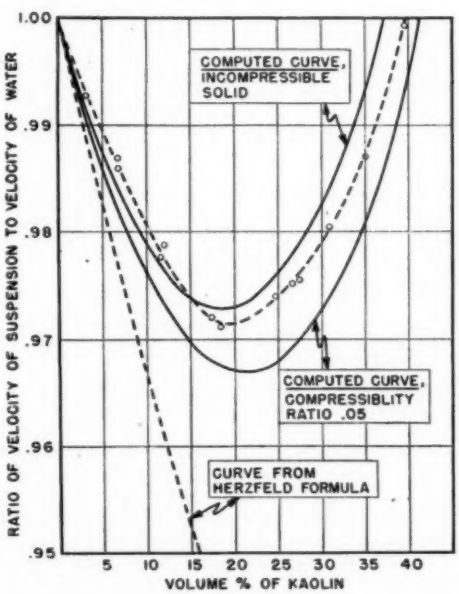


FIG. 2. Sound velocity ratio *vs.* concentration, kaolin suspensions.

## KAOLIN SUSPENSIONS

The validity of the additive formula for sound velocity may be demonstrated by some data on suspensions of kaolin in water. Kaolin is a complex aluminum silicate occurring in nature in a rather high degree of purity. It is a residual weathering product and a common constituent of natural clays and muds. It is an admirable material for providing solid aqueous suspensions since it disperses readily in water, does not gel, and needs no grinding to render the particles fine. By using a suitable deflocculant, such as sodium pyrophosphate, in an amount necessary to give a pH of 9–10, suspensions of kaolin with a volume concentration of 35–40 percent can be made rather readily with sufficient fluidity for use in the interferometer. Care was taken to remove the air mixed into the suspension by the dispersion process. A size analysis showed that 90 percent of the particles were between 0.4 and 5.0 microns in diameter, with a median size of 1.1 microns. The concentration of kaolin was determined by density measurements, using a density of 2.60 for kaolin.

Figure 2 shows a plot of sound velocity in such mixtures against percentage by volume of kaolin. The velocity is plotted as the ratio of velocity in the suspension to that of the liquid (water and deflocculant) in which the kaolin particles are suspended. The velocity at first falls as kaolin is added to the liquid, reaches a minimum at 20 percent kaolin by volume, then rises. The two solid curves are computed from Eq. (1) for a

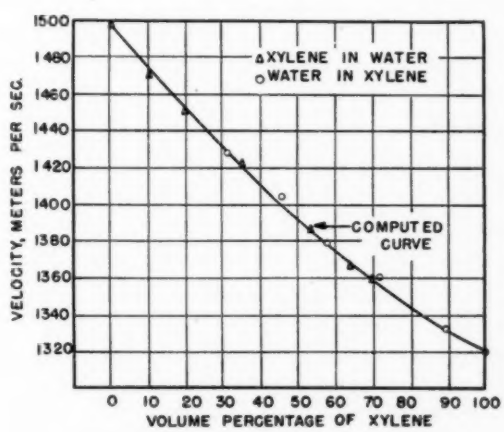


FIG. 3. Sound velocity *vs.* concentration for xylene-water emulsions.

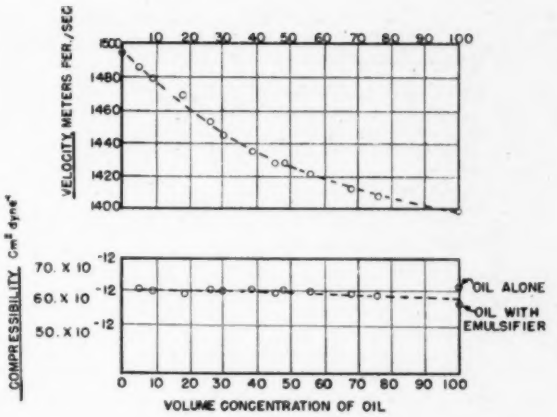


FIG. 4. Sound velocity *vs.* concentration for transformer oil-in-water emulsions.

compressibility ratio of 0.05 and zero times the compressibility of the suspending liquid. The zero compressibility-ratio curve refers, of course, to the limiting case of an incompressible solid. Also plotted in this figure is a curve computed from Herzfeld's formula mentioned above.

## EMULSIONS

The applicability of the additive formula can be further illustrated by some emulsions of xylene-in-water and its inversion, water-in-xylene. A xylene-in-water emulsion consists of small separate globules of xylene suspended in a continuous volume of water; such emulsions were made by using sodium oleate as emulsifier. On the other hand, in a water-in-xylene emulsion the globules are water and the continuous liquid is xylene; these were prepared with the aid of sorbitan monooleate as emulsifier. As is common in emulsion technology, phase reversal was avoided by adding a small part of the discontinuous medium (say xylene in the xylene-in-water emulsions) to all of the other medium plus all the emulsifier, then shaking to produce an emulsion, and repeating the process for more and more of the first medium, until all of it was emulsified. The type of emulsion finally obtained was checked by the simple method of observing the miscibility of the emulsion with water and with xylene. Measurement of particle size in these emulsions with a microscope indicated a median particle size of approximately 5 microns.

Velocity measurements made over a range of concentration for the two types of emulsions are

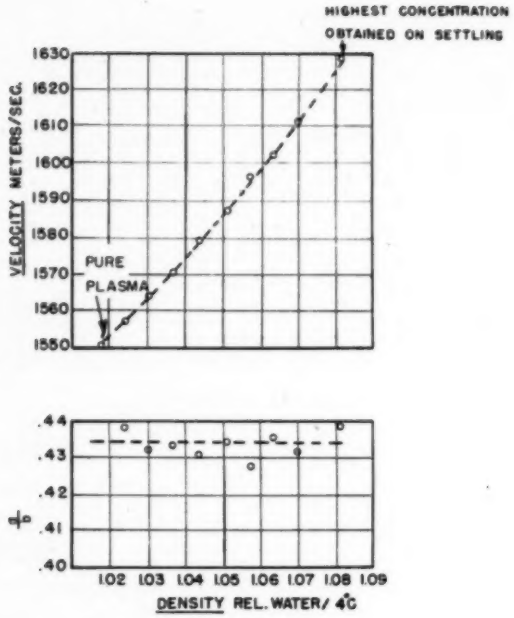


FIG. 5. Sound velocity and the ratio $a/b$ for various dilutions of horse blood with plasma.

shown in Fig. 3. It is interesting to observe that both types of emulsions have the same sound velocity at the same concentration of xylene, indicating that the sound velocity is determined by the composition of the emulsion. The measured sound velocity and density of the end members, xylene and water, enable their compressibility to be found, and Eq. (1) yields the velocity for different mixtures of the two. The velocity so computed is plotted as the solid line in this figure.

## DETERMINATION OF COMPRESSIBILITY

The additive formula provides a method for determining the compressibility of a material which occurs as, or can be rendered into, fine particles. Since the density of the particles is known, it is necessary only to suspend them in a liquid of known or measurable density and sound velocity, and measure the density and velocity of the suspension. For this purpose, we may write Eq. (1) as

$$b=\frac{\kappa_2-\kappa_1}{\kappa_1}=\frac{1}{\beta}\left(\frac{\gamma^2}{\rho}-1\right) \qquad (2)$$

where $\rho$ is the ratio of the density of the suspension to that of the suspending liquid.

The application of this formula may be illustrated by some data obtained on emulsions of transformer oil in water. These emulsions were made by adding 8 percent by weight of triethanolamine oleate to the oil as emulsifier, and agitating thoroughly with water to produce an emulsion. This particular emulsifier is very soluble in oil but only slightly soluble in water. An emulsion of high oil concentration was made in this manner, and those of lower concentration were obtained through successive dilutions with water. Occluded air was removed by placing the emulsion in a vacuum until no further air was seen to come off. Velocity and density measurements were made on eleven such emulsions of varying percentage of oil, and also on water alone and on the oil with and without emulsifier. Figure 4 shows sound velocity plotted against concentration, and in the lower part of the figure, the computed values of compressibility of the oil. These values are seen to be nearly, but not quite constant, and lie intermediate between the measured values for the oil with and without emulsifier. The slight change of compressibility with concentration in this case may represent the effect of partial leaching out of emulsifier from the oil by the successive dilutions with water.

In a similar manner there may be obtained an approximate value of compressibility of the kaolin particles in the suspensions of Fig. 2. Using the data for the three highest kaolin concentrations, $b$ may be found to be $-0.984$, $-0.972$, and $-0.977$ and thus the ratio of compressibilities of kaolin to water $(1+b)$ equal to 0.016, 0.028, and 0.023. Apparently no great percentage accuracy is attainable for substances of such low compressibility as kaolin, since the much larger compressibility of the suspending liquid all but masks the slight effect of the compressibility of the particles themselves.

An alternative method of computation is available in case the concentration $\beta$ is not immediately obtainable. If in Eq. (1) we substitute

$$\beta=\frac{\rho_0-\rho_1}{\rho_2-\rho_1}$$

we may obtain this equation in the form

$$\frac{\rho(\rho-1)}{\gamma^2-\rho}=\frac{a}{b}.$$

The ratio $a/b$, denoting the ratio of the difference of density to the difference of compressibility, is a property of a suspension independent of the concentration of suspended substance, and can be found from density and velocity measurements on any one suspension and the suspending liquid.

This may be exemplified by data on some fresh horse blood obtained from the Naval Medical Research Institute. Blood can be considered to be a suspension of several types of blood corpuscles in a clear pale yellow fluid called the plasma. The red blood cells, or erythrocytes, with a diameter of about 8 microns, outnumber the other types of corpuscles by about 800 to 1, and consist of the red substance, hemoglobin, surrounded by a thin flexible membrane.

By allowing a quantity of fresh blood to settle, samples of clear plasma and concentrated red cells were obtained. Velocity and density measurements were made on these two end members, and also on samples of intermediate red cell concentration obtained by mutual dilution. This data is plotted in Fig. 5, with density, representing concentration of red cells, as abscissa. The lower portion of the plot shows the values of the ratio $a/b$ found from the velocity and density measurements. It is seen to have a constant value, within 3 percent, of $-0.433$. In order to obtain the compressibility of the corpuscles, from this value, we must know their density. This was found by centrifuging a sample of previously measured density. The percentage volume of corpuscular material (or hematocrit reading) yields the density of the corpuscles. This value, 1.091, together with the average value of $a/b$, and the compressibility of the plasma, $40.9\times10^{-12}$ cm$^2$ dyne$^{-1}$ (found from its density and velocity) give as a result the value of $34.1\times10^{-12}$ cm$^2$ dyne$^{-1}$ as the compressibility of the blood corpuscles. Thus, the corpuscles are found to be 16.7 percent less compressible than the plasma in which they are immersed.

## SUMMARY

A method is described by which the adiabatic compressibility of small particles can be found. It requires the measurement of the velocity of sound and of the density on both a suspension of the particles, and on the suspending liquid. The limitations of the method in regard to particle size are undetermined, but a coarse suspension such as blood seems to yield velocities (at a frequency of 1 megacycle) predictable by the simple theory outlined. The requirement of having a sample of the suspending liquid available for measurement is easily met by allowing the mixture to settle, or by centrifuging. It is necessary to control the temperature of the sample to 0.1°C, since the velocity change between suspension and the pure liquid is often slight. The accuracy obtainable is rather small for relatively incompressible solids, such as kaolin, but is probably fairly great for particles having a compressibility not too much smaller than that of the suspending liquid.

# End-Effect in Rotational Viscometers

CHARLES H. LINDSLEY AND EARL K. FISCHER
*Institute of Textile Technology, Charlottesville, Virginia*
(Received July 7, 1947)

In the classical equations for the traction on concentric cylinders by a viscous substance, it is assumed that traction on the top and bottom of the inner cylinder (bob) is negligible in comparison with that on the curved surface. In viscometers of practical dimensions, however, it is necessary to compensate for the end-traction or end-effect by adopting one of several expedients in design or by determining the magnitude of the effect and accounting for it in terms of increased length of bob.

In the experiments reported in this paper, the method of multiple bobs has been used, and the variation of end-effect with the following factors studied: (1) radius of bob; (2) clearance between cylindrical surfaces; (3) separation between bottom of bob and cup; and (4) viscosity.

The magnitude of the end-effect increases with radius and with clearance. For separations at the bottom greater than 1 cm and for viscosities above 1 poise the end-effect is nearly constant, but must be determined for each cup and bob combination. At lower viscosities the correction must be determined either by calibration with a standard liquid of about the same viscosity as the unknown, or by the multiple-bob method.

It is shown that trapping a layer of air beneath the bob is not effective in making the traction on the bottom negligible. The end-effect is almost as large for a bob with an open bottom as for a closed one.

When the method of multiple bobs is used, data with an accuracy of ±2 percent can be obtained without calibration. When the instrument constant is determined with standard liquids or computed from a value for the end-effect previously found, data of somewhat lower accuracy result, but the uncertainty should be within ±5 percent.

## INTRODUCTION

THE co-axial-cylinder viscometer is generally considered the most versatile instrument for the measurement of viscosity. It may be used on suspensions that exhibit anomalous flow properties as well as on Newtonian liquids, and it is suitable for determinations over a wide range of viscosities at variable rates of shear. The literature on instruments of this type is extensive, but relatively few studies have been made on several factors, inherent in the design, which seriously affect the validity of the measurement.

One of the most important of these factors is the contribution of the ends of the inner cylinder or bob to the total retarding force between the bob and the liquid surrounding it. This end-effect has not received the consideration it needs. Accordingly, the present investigation was undertaken with the following objectives: (1) critical evaluation of various methods for eliminating or measuring the end-effect; (2) experimental measurement of the end-effect for cups and bobs of several sizes; and (3) determination of the variation of the end-effect with viscosity and with clearance between cup and bob. To carry out these objectives a commercial Stormer viscometer was used after modification, but the results can be applied to any rotational viscometer equipped with cylindrical cups and bobs.

The mathematical analysis for the determination of viscosities in rational units by the method of rotating co-axial cylinders leads to the expression:[1]

$$T=4\pi\left[\frac{R_c^2\times R_b^2}{R_c^2-R_b^2}\right]h\eta\omega \qquad (1)$$

where $T$ is the driving (or retarding) torque on the bob, $R_c$ the radius of the cup, $R_b$ the radius of the bob, $h$ the length of the bob, $\eta$ the viscosity of the liquid between cup and bob, and $\omega$ the speed of rotation at equilibrium. The radii and length being known, $T$ and $\omega$ are found experimentally, and hence $\eta$ may be calculated. For materials that exhibit plastic-flow properties the equation given by Reiner and Riwlin[2] is now considered to account fairly well for the results obtained.

[1] See, for example, H. Lamb, *Hydrodynamics* (Cambridge University Press, London, 1932), 6th edition, p. 587.

[2] M. Reiner and R. Riwlin, Kolloid Zeits. **43**, 1–5 (1927); M. Reiner, J. Rheology **1**, 5–10 (1929); H. Green, Ind. Eng. Chem. Anal. Ed. **14**, 576–585 (1942), has examined this equation critically and found experimental evidence to support it.

## METHODS FOR CORRECTING FOR TRACTION ON BOB ENDS

In the derivation of Eq. (1) it is assumed that the traction of the viscous liquid on the top and bottom of the inner cylinder is negligible in comparison with the traction on the curved surface. No adequate mathematical treatment has yet been given of the contribution of the ends to the total traction on the bob. It is necessary, therefore, to take it into account in one of the following ways: (1) use of a very long bob of small radius, with small clearance between cup and bob, to make the correction negligible; (2) calibration of the instrument with liquids of known viscosity, thus absorbing the end-effect in the instrument constant; (3) reduction of the relative motion of the liquid above and below the ends of the bob by mechanical expedients; and (4) measurement of the effect experimentally in order to include it in the calculations of viscosity and yield value.

The first method imposes many difficulties in the design of suitable apparatus. The second method is widely used, but one should be aware of the fact that the correction (and hence the instrument constant) changes with viscosity as will be shown in the experimental portion of this paper. Mooney and Ewart[3] devised an ingenious way of including the correction in the instrument constant: the bottom of their bob was a very flat cone (half angle 87.03°) with the apex resting on the center of the bottom of the cup. With this arrangement they showed that the rate of shear across the bottom was the same as that along the cylindrical surface; the constant obtained on calibration should therefore hold much better over a wide range of rotational speeds and viscosities than is the case with a bob of conventional type.

The third method was used in the instruments of Couette,[4] Drew,[5] and Hatschek.[6] Stationary guard rings of the same radius as the inner (suspended) bob were placed as closely as possible above and below the bob. These rings prevented the liquid at the ends from rotating as the cup turned without interfering with the traction on the cylindrical surface, and thus eliminated the end-effect. Such instruments require machining and alignment of high precision and are difficult to clean. They are, therefore, suitable for standardization and research but are hardly practical for routine control use.

A widely used method, purporting to eliminate or greatly reduce the end-effect is to make the bottom of the bob slightly concave so that air is trapped in the cavity when the bob is immersed in the liquid to be measured (Fig. 1C). The assumption is that since the bottom of the bob rotates against a layer of air, of very low viscosity, the traction will be negligible. We have not found any experimental evidence in the literature that validates this assumption. Mercier[7] provided a raised portion in the bottom of the cup that almost closed the recess in the bob in order to exclude the liquid. His experimental data do now show whether he succeeded, however.[8] Nevertheless, Mooney and Ewart[3] refer to Mercier's "ingenious design (which) practically eliminates shearing stresses over the bottom surface." Goodeve[9] describes an instrument in which the cylindrical cup and bob are replaced by co-axial truncated cones, the ends of which are dished out. In the first paper he states that this reduces the end-effects to negligible values, and calculates viscosities using the measured dimensions of the cones; yet he gives no evidence to show that valid results are so obtained. In the second paper he only claims that the drag on the lower end is reduced by the trapped air, adding that "the reduction is not as large as might be expected because surface tension draws the fluid up into the rim"; he therefore calibrates the instrument with liquids of known viscosity,

[3] M. Mooney and R. H. Ewart, Physics **5**, 350–354 (1934).
[4] M. M. Couette, Ann. de chimie **21**, 433–510 (1890).
[5] E. R. Drew, Phys. Rev. (First Series) **12**, 114–120 (1901).
[6] E. Hatschek, *Viscosity of Liquids* (Bell, London, 1928).
[7] P. Mercier, J. Rheology **3**, 391–412 (1932).
[8] There is a strange gap in Mercier's discussion of his experimental results (reference 7, p. 405). It would appear that a considerable portion of the discussion had been omitted from the printed paper. The graphical presentation of his data gives no indication of success or failure in eliminating the end-effect. Furthermore, the graph indicates that the instrument was used at speeds as high as 4000 r.p.m. It is remarkable, to say the least, that he was able to operate this type of instrument, with a clearance of only 1 mm between cup and bob, at such speeds without getting turbulence and centrifugal effects that would cause deviations from a linear relationship.
[9] C. F. Goodeve and G. W. Whitfield, Trans. Faraday Soc. **34**, 511–520 (1938), and C. F. Goodeve, J. Sci. Inst. **16**, 19–27 (1939).

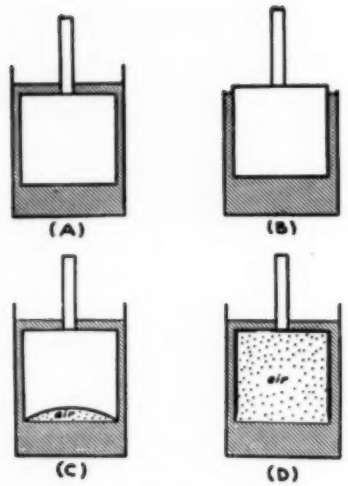


FIG. 1. Types of Cylindrical Bobs: A. Closed bob, completely immersed; B. Closed bob, immersed to different depths; C. Bob with concave bottom; D. Open bob.

including the end-effect in the empirically determined instrument constant.

In the absence of any sound experimental evidence of the effectiveness of this method in eliminating end-effect, we have studied the behavior of cylindrical bobs with open bottoms and find an effect almost as large as for a closed bob of the same dimensions. The effect as measured includes, of course, the drag on the top, which is the same for both bobs, but this can be shown to be smaller than the bottom effect. The method therefore does not accomplish the purpose for which it was designed and introduces a new uncertainty, namely, the extent to which the liquid does rise inside the bob.

The fourth method of evaluating the end-effect has been used by several investigators. In principle the traction on two bobs of the same radius but different lengths is measured, and by a difference calculation, the effect of the ends may be determined. Searle[10] designed an instrument with a long inner cylinder, the height of liquid about it being changed by raising or lowering the surrounding cup (cf. Fig. 1B). The time $T$ for one revolution was determined for several values of a falling weight $W$ used to turn the inner bob. For any given depth of immersion $h$, the product $WT$ was constant, and when $WT$ was plotted against $h$ for several depths, a straight line was obtained with a negative intercept $h_0$ on the $h$-axis. This intercept may be interpreted as an increment in bob length; that is, a bob having no end-effect, when immersed to a depth $h+h_0$, would exert the same traction as the actual bob immersed to depth $h$.

Lillie[11] made a careful study of the end-effect with an instrument designed primarily to measure viscosities of molten glass. He used two sets of five bobs each, those within each set having a constant radius but differing in length. Substitution in Eq. (1) for the dimensions of cup and bob and for the experimental quantities $T$ and $\omega$ gave a value for the "apparent viscosity" for each bob used with a given liquid. When these values were plotted against the reciprocals of the corresponding bob lengths ($h$), a straight line was obtained; its intercept on the axis $1/h=0$ (i.e. for a bob of infinite length) gave what Lillie termed the "true viscosity." Substitution of this value for $\eta$ in Eq. (1), $h$ being considered unknown, gave a value $h^*$ that might be called the effective length of each bob. The difference between this value and the actual length, $h^*-h=h_0$, was a measure of the end-effect quite analogous to $h_0$ as found by Searle.

## EXPERIMENTAL PROCEDURES

A commercial model Stormer viscometer was used after some important modifications had been made. The water jacket supplied with the

TABLE I. Dimensions of cups and bobs.

| | No. | Radius, cm | Height, cm |
|---|---|---|---|
| Cup | 1 | 1.746 (inside) | 5.2 (inside) |
| | 2 | 2.342 (inside) | 4.9 (inside) |
| | 4 | 2.181 (inside) | 5.0 (inside) |
| | 5 | 2.539 (inside) | 5.3 (inside) |
| | 6 | 2.800 (inside) | 5.3 (inside) |
| Bob | 1 | 1.565 | 3.53 |
| | 5 | 1.566 | 2.00 |
| | 6 | 1.565 | 1.00 |
| | 7 | 1.566 | 0.08 |
| | 14 (open) | 1.590 | 3.49 |
| | 3 | 1.269 | 3.51 |
| Bob | 4 | 2.104 | 3.49 |
| | 10 | 2.100 | 1.99 |
| | 11 | 2.100 | 1.00 |
| | 12 | 2.100 | 0.08 |
| | 15 (open) | 2.103 | 3.46 |

[10] G. F. C. Searle, Proc. Camb. Phil. Soc. **16**, 600–606 (1912). For an earlier application of the method, see L. E. Gurney, Phys. Rev. (First Series) **26**, 98–120 (1908).

[11] H. R. Lillie, J. Am. Cer. Soc. **12**, 505–515 (1929); Phys. Rev. **36**, 347–362 (1930).

instrument was wound with resistance wire (18 ft. of 22-gauge Nichrome) and then with several layers of asbestos paper. Current for this heating coil was supplied through a Variac and controlled by a fixed-contact mercury thermoregulator and a suitable relay. At 30°C the temperature could be held to within ±0.1°. Other thermoregulators were available to give temperatures up to 90°C. At high temperatures, however, enough heat may be lost through the shaft of the bob to lower the temperature of the bob and of the liquid in contact with it and thus introduce appreciable error. A plastic bob with brass shaft was made for use at high temperatures; the heat transfer at the surface of such a bob is far less than with an all-metal bob.

The construction of the cup and bob supplied with the instrument makes them unsuited for determination of viscosity in absolute units. Several cylindrical cups and bobs were machined from brass of such sizes that a variety of rates of shear for any given rate of rotation was possible. The dimensions are shown in Table I. The larger bobs were hollow to reduce inertia and weight on the bearing. Duplicates of two bobs were made with the lower ends left open to permit a study of the end-effect for concave bobs (Fig. 1D).

In order to evaluate the results obtained by the several procedures followed, four viscosity

TABLE II. Calculation of viscosity and end-effect for sample N-13 at 30°C. (Bobs 1, 5, 6, 7 in cup 1.) $K/r^2 = 99.0/12.46 = 7.95$.

| | Bob 1 | Bob 5 | Bob 6 | Bob 7 |
|---|---|---|---|---|
| Bob length, $h$ | 3.53 | 2.00 | 1.00 | 0.08 |
| Load/r.p.m., $P$ | 3.18 | 1.00 | 1.17 | 0.42 |
| $\Delta P$ | — | 1.18 | 2.01 | 2.76 |
| $\Delta h$ | — | 1.53 | 2.53 | 3.45 |
| $\eta$, poises | — | 6.14 | 6.31 | 6.35 |
| Average value of $\eta$ | | 6.27 | | |
| Effective length, $h^*$ (cm) | 4.13 | 2.60 | 1.52 | 0.56 |
| End-effect, $h_0 = h^* - h$ (cm) | 0.60 | 0.60 | 0.52 | 0.48 |

TABLE III. Experimentally determined viscosities of certified samples at 30°C.

| Sample | Experimental viscosity (poises) Bob combination 1-5 | 1-6 | 1-7 | Av. of first two | Certified viscosity | Deviation (%) |
|---|---|---|---|---|---|---|
| K-5 | 0.255 | 0.276 | 0.261 | 0.265 | 0.2648 | 0.0 |
| M-11 | 1.12 | 1.17 | 1.19 | 1.15 | 1.166 | −1.4 |
| N-13 | 6.14 | 6.31 | 6.35 | 6.22 | 6.124 | 1.5 |
| OB-1 | 156. | 158. | 154. | 157. | 153.9 | 2.0 |

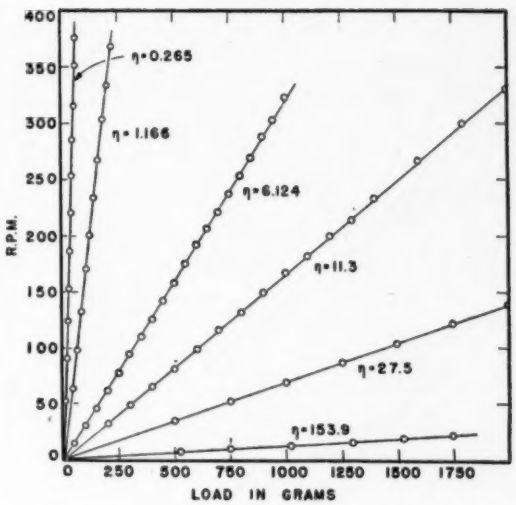


FIG. 2. Experimental values for load and r.p.m. for oils showing Newtonian flow.

samples, certified at 30°C, were obtained from the National Bureau of Standards, the viscosity ranging from 0.2648 to 153.9 poises. A description of these standards has been given recently by Swindells.[12] In addition, a series of four bodied linseed oils (litho-varnishes) were obtained to give better coverage of the range.

The procedure in using the viscometer follows. The cup and bob were carefully aligned, the bob being raised about 1.3 cm above the bottom of the cup. The cup was then filled to the top with the sample to be measured. After the sample had reached 30°C (the temperature at which all measurements here reported were made), at least ten measurements of the time of rotation with different loads were taken. The ratio of load to r.p.m. was calculated and found to be nearly constant for each sample so long as the rotation was held below 400 r.p.m. (Fig. 2). This constancy indicated that the oils were Newtonian in their flow properties.

## THE SINGLE-BOB METHOD

Some preliminary measurements were made with one of the standard samples (N-13) following the method of Searle, that is, by immersion of one bob to varying depths. The intercept was found to be 0.29 cm with bob 1 and cup 1. With this value for the end-effect added to the actual

[12] J. F. Swindells, J. Colloid Sci. 2, 177–84 (1947).

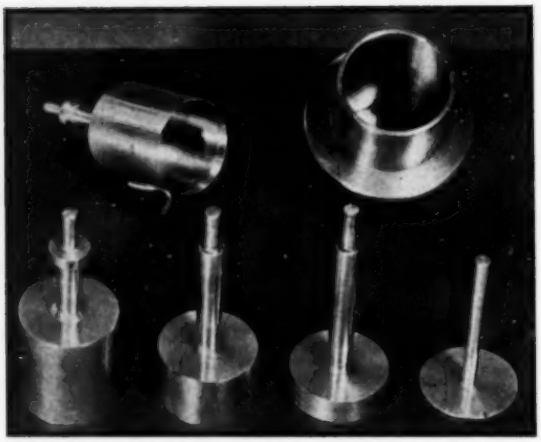

FIG. 3. Four bobs of equal radius but different height; open bob; cup.

length of the bob, the viscosity of the sample was found by Eq. (1) to be 6.36 poises, in approximate agreement with the certified value of 6.12 poises. The principal source of error in the method lies in the inaccuracy with which depth of immersion of the bob is measured. In spite of this drawback, the method affords a rapid and easy means of obtaining viscosities in cgs units with an accuracy of about 5 percent, and only one machined cup and bob are needed.

### THE MULTIPLE-BOB METHOD

For more accurate results a method similar to that used by Lillie is preferred: the end-effect may be first eliminated and afterwards evaluated (if desired) by using a set of bobs equal in radius but different in length (Fig. 3). For each bob the ratio of load to r.p.m. is determined in the usual way. From the ratios for any pair the viscosity is calculated by the following modification of Eq. (1). Let $L$ be the torque exerted by the liquid against the ends of the bob, and $T$ the total torque exerted against the ends and cylindrical surface. Equation (1) may then be written for two bobs of length $h_1$ and $h_2$:

$$T_1=4\pi r^2 h_1\eta\omega_1+L$$

and

$$T_2=4\pi r^2 h_2\eta\omega_2+L$$

where

$$r^2=R_c^2\times R_b^2/(R_c^2-R_b^2).$$

If $T_1$ and $T_2$ are chosen so that $\omega_1=\omega_2$, these equations may be solved for $\eta$:

$$\eta=\frac{T_1/\omega_1-T_2/\omega_2}{4\pi r^2(h_1-h_2)}. \tag{2}$$

Since $T/\omega$ is constant for all values of $\omega$ for a Newtonian liquid, the average values of $T_1/\omega_1$ and $T_2/\omega_2$ may be used, and not just those for which $\omega_1=\omega_2$. With the Stormer viscometer the weight or load may be substituted for torque thus:

$$T=Wgl$$

where $g$ is the acceleration of gravity and $l$ the effective length of the arm on which the weight acts. It is also more convenient to express angular velocity in r.p.m. than in radians per second:

$$\omega=\frac{2\pi}{60}\cdot\text{r.p.m.}$$

If we designate by $P$ the experimentally determined ratio $W$/r.p.m., Eq. (2) becomes:

$$\eta=\frac{K}{r^2}\times\frac{\Delta P}{\Delta h} \tag{3}$$

where

$$K=\frac{60gl}{8\pi^2}.$$

For the Stormer viscometer $l$ is the radius of the drum on which the cord is wound plus the cord radius, divided by the gear ratio. In our instrument $l=1.456/11$, and the constant $K$ has the value 99.0.

To illustrate the use of this equation, data obtained with bobs 1, 5, 6, and 7 in cup 1 are shown in Table II. For $\Delta P$ and $\Delta h$ the differences between the $P$ and $h$ values for bob 1 and each of the other bobs are taken. (Three other combinations are possible but are not so useful.) The average of the three calculated viscosities is 6.27 poises, in fair agreement with the certified value of 6.124. Since the relative effect of the ends is less for bobs 1 and 5 than for bobs 6 and 7, the first two should yield a more accurate value for $\eta$. This expectation is borne out by the agreement with the certified value.

In Table III are given the viscosities of four of the certified samples determined by the method just illustrated in detail. Although the

viscosities calculated using bob 7 were not included in the averages, to have done so would not have changed the results significantly. The figures indicate that viscosities over a wide range may be determined in absolute units with an accuracy of about 2 percent.

With the value of $\eta$ so determined the same experimental values of $P$ are used to calculate the effective length of the bob $h^*$, and from it the end-effect $h_0$ expressed as increment in length, by means of the equation:

$$h^* = \frac{K}{r^2} \times \frac{P}{\eta} = h + h_0. \qquad (4)$$

Such calculations are illustrated in the last two lines of Table II. It is interesting that even for a very thin bob (No. 7) for which the traction on the end is nearly 90 percent of the total, the end-effect is nearly the same as for a bob more than 40 times longer.

One would expect the end-effect to increase as the bottom of the bob is brought closer to that of the cup; moving in the other direction, one would expect that above a certain point there would be no significant change with increasing separation. This behavior was demonstrated by determining the end-effect with a short bob (No. 5) at varying depths of immersion. The results are shown graphically in Fig. 4. Above 1 cm the variation of end-effect with depth is insignificant. The height of liquid above the top of the bob is not critical, so long as it is at least 2 mm.

A different approach to the measurement of end-effect was attempted by use of bobs open at the bottom as noted above. At the same time a check on the effect of the top of the bob was made by carrying out runs with the top just level with the top of the cup filled with liquid and with it submerged 5 mm below the surface of the liquid. The results are shown in Table IV. The second column shows the combined effect of top and bottom; the third column the effect of the bottom, while the difference (fourth column) shows the effect of the top. The uncertainty in the values for end-effect in this series of measurements is estimated as about 1 mm. The apparent inversion for the data of bob 1, cup 1 may be ascribed to this factor.

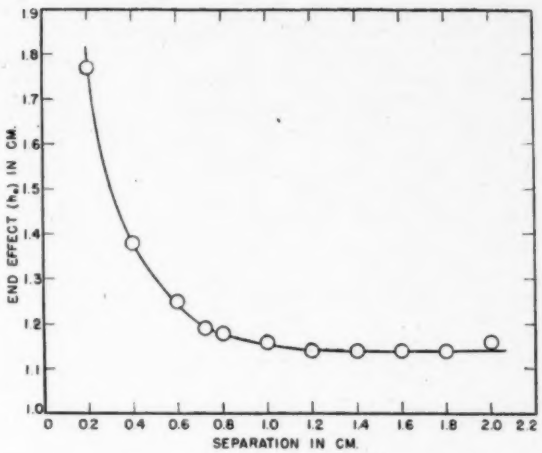


FIG. 4. Variation in end-effect with separation between bottom of bob and cup.

With the limitations on precision in such measurements in mind, the following observations may be made: (1) virtually the same traction is exerted at the bottom of the bob whether it is open or closed; (2) in general the bottom exerts a greater traction than the top, due probably to the greater freedom of the liquid above the bob to rotate with it. The first result was quite unexpected, and is contrary to much that is stated or implied in the literature and in the design of several viscometers. It was therefore checked by repeating the comparison of closed and open bobs in liquids differing markedly in viscosity. The results are shown in Table V. Since a number of variables are involved, the most valid comparisons are made for each pair of figures for open and closed bobs. In the last column in which end-effect is expressed as percent of effective bob length, it will be seen that although the results with the open bob are less

TABLE IV. End-effect for bobs closed and open at the bottom, with tops immersed or exposed.

| Cup and bob combination | | End-effect, cm: Top immersed 0.5 cm | Top exposed | Difference |
|---|---|---|---|---|
| Cup 1 | Bob 1—closed | 0.6 | 0.4 | 0.2 |
| | Bob 14—open | 0.7 | 0.5 | 0.2 |
| Cup 2 | Bob 1—closed | 1.1 | 0.7 | 0.4 |
| | Bob 14—open | 1.0 | 0.5 | 0.5 |
| Cup 2 | Bob 4—closed | 0.7 | 0.3 | 0.4 |
| | Bob 15—open | 0.6 | 0.3 | 0.3 |

TABLE V. Comparison of end-effects for closed and open bobs.

| Cup no. | Clearance (cm) | Approx. viscosity (poises) | Effective bob length, $h^*$ Bob 1 (closed) $h$=3.53 cm | Bob 14 (open) $h$=3.48 cm | End-effect, $h_0$ Bob 1 (closed) cm | Bob 14 (open) cm | $100h_0/h^*$ Bob 1 (closed) (%) | Bob 14 (open) (%) |
|---|---|---|---|---|---|---|---|---|
| 1 | 0.18 | 1.17 | 4.10 | 4.04 | 0.57 | 0.56 | 16 | 16 |
| | | 6.12 | 4.07 | 3.95 | 0.54 | 0.47 | 15 | 14 |
| 4 | 0.60 | 1.17 | 4.46 | 4.17 | 0.93 | 0.69 | 26 | 20 |
| | | 6.12 | 4.25 | 4.06 | 0.72 | 0.58 | 20 | 17 |
| | | 27.5 | 4.48 | 4.18 | 0.95 | 0.70 | 27 | 20 |
| | | 154. | 3.97 | 3.67 | 0.44 | 0.19 | 13 | 5 |
| | | | Bob 4 (closed) $h$=3.49 cm | Bob 15 (open) $h$=3.46 cm | Bob 4 (closed) cm | Bob 15 (open) cm | Bob 4 (closed) (%) | Bob 15 (open) (%) |
| 2 | 0.24 | 1.17 | 4.04 | 3.91 | 0.55 | 0.45 | 16 | 13 |
| | | 6.12 | 3.92 | 3.81 | 0.43 | 0.35 | 12 | 10 |
| | | 27.5 | 4.31 | 4.20 | 0.80 | 0.74 | 23 | 21 |
| | | 154. | 4.12 | 4.04 | 0.63 | 0.58 | 18 | 17 |
| 3 | 0.17 | 1.17 | 4.00 | 3.84 | 0.51 | 0.38 | 15 | 11 |

than those with the closed bob, the reduction is not nearly so high as one would expect.

Since the end-effect as normally measured varied with separation between bottom of bob and cup, it was of interest to see if a similar change would be observed with an open bob. The results obtained are shown in Fig. 5: the end-effect is slightly less when the bob has no bottom, but otherwise is quite similar.

## VARIATION OF END-EFFECT WITH CLEARANCE AND VISCOSITY

The influence on the end-effect of the following factors was studied: radius of the bob, clearance between bob and cup, and viscosity of the liquid being measured. Table VI summarizes many determinations with different cup and bob combinations; most of the values given are averages of several measurements made with bobs of the same radius but different lengths (as illustrated by the data for $h_0$ in Table II) and with oils of viscosities between 1 and 154 poises. The precision of the measurements as shown by variation in $h_0$ for different oils appears low, amounting to as much as 25–30 percent, but this is because errors are magnified since $h_0$ is obtained by difference. For example, if the effective length of a bob 3.5 cm long is found to be 4.5 cm, the end-effect is 1.0 cm; then an error of 5 percent in $h^*$ makes an error of 22 percent in $h_0$. It is clear, however, that the effect increases with clearance and that, for a given clearance, the effect may be somewhat larger the larger the radius of the bob. In explanation, perhaps more disturbance is created in the liquid by the end of the bob with relatively large clearances than when these surfaces are close together. The same explanation may account for the lower precision attained at the larger clearances.

TABLE VI. Variation of end-effect with clearance between cup and bob for several bob radii.

| Bob radius, cm | Clearance, cm | End-effect, cm |
|---|---|---|
| 1.27 | 0.48 | 0.8 |
| | 1.08 | 1.2 |
| 1.57 | 0.18 | 0.6 |
| | 0.78 | 1.0 |
| | 0.97 | 1.4 |
| | 1.24 | 1.4 |
| 2.10 | 0.08 | 0.6 |
| | 0.24 | 0.8 |
| | 0.44 | 1.2 |
| | 0.70 | 1.4 |

TABLE VII. Variation of end-effect with viscosity (clearance 0.18 cm).

| Viscosity at 30°C | End-effect |
|---|---|
| 0.017 poise | 11.5 cm |
| 0.058 | 2.94 |
| 0.145 | 1.94 |
| 0.265 | 1.28 |
| 1.166 | 0.60 |
| 1.48 | 0.65 |
| 6.124 | 0.52 |
| 9.2 | 0.60 |
| 11.3 | 0.59 |
| 27.5 | 0.56 |
| 153.9 | 0.49 |

Table VII shows the variation of the end-effect with viscosity observed with the combination of cup 1 and bob 1. Entirely similar data were obtained with other combinations. For viscosities above 1 poise the effect is nearly constant (about 0.6 cm in the example shown). As one goes to lower viscosities, however, the end-effect becomes progressively greater. The greater the clearance between cup and bob, the more rapidly the end-effect increases as viscosity decreases. These facts too can be explained by assuming that at low viscosities the rotating ends of the bob interfere with laminar motion of liquid between the cylindrical surfaces.

Even with these variations, if only those combinations of cup and bob are used for which the clearance is small (say, less than 0.8 cm), a value for the end-effect may be found which permits determination of viscosity in poises over a wide range. This is illustrated by the data in Table VIII. Viscosities were calculated from Eq. (4), with the best value for $h_0$ and hence for $h^*$ determined by the multiple-bob method described above. It should be noted that at no point in the determination of the viscosities in Table VIII have the certified or known values for the samples been used. Over this range the correction for end-effect may be applied to give viscosities with an accuracy within ±5 percent.

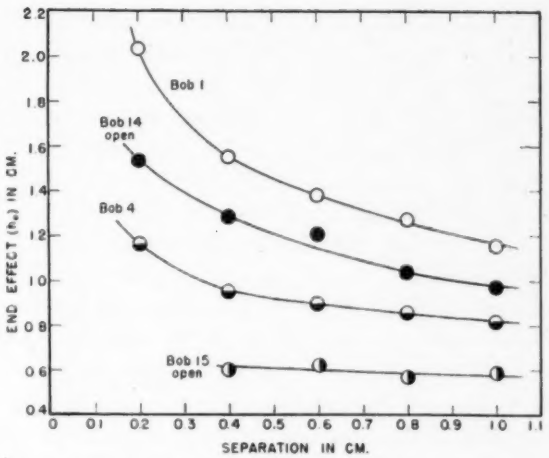


FIG. 5. Variation in end-effect for closed and open bobs.

## DISCUSSION

The advantages of the co-axial cylinder viscometer are so numerous that it deserves wider use for industrial measurements. As it is commonly used, however, the data obtained cannot be expressed in rational units and, as a consequence, the technical literature is cluttered with meaningless measurements. The unsatisfactory state of instrumentation in this field is in part responsible, but the mechanical changes necessary to convert a standard commercial Stormer viscometer are comparatively simple and can be made at relatively small cost. The modified instrument makes possible the measurement of viscosities based on accepted physical principles and yields data which are dimensionally consistent and experimentally reproducible. The precautions necessary for satisfactory operation —aside from such obvious matters as temperature control, centering of bob and cup, etc.— are to a large extent elucidated by the experimental data presented above.

In making cups and bobs for the Stormer viscometer, the important dimensions are the

TABLE VIII. Viscosities determined by correcting bob length for end-effect. $\eta = (K/r^2h^*) \times$ (Load/r.p.m.).

| Combination | | Cup 1—bob 1 | | Cup 2—bob 1 | | Cup 2—bob 4 | |
|---|---|---|---|---|---|---|---|
| $K/r^2$ | | 7.95 | | 22.4 | | 4.32 | |
| Clearance | | 0.18 | | 0.78 | | 0.24 | |
| Correction, $h_0$ | | 0.58 | | 1.00 | | 0.82 | |
| Effective length, $h^*$ | | 4.11 | | 4.53 | | 4.31 | |
| Sample | Viscosity, known | Viscosity, detmd. | Deviation (%) | Viscosity, detmd. | Deviation (%) | Viscosity, detmd. | Deviation (%) |
| NBS: M-11 | 1.166 | 1.16 | −0.5 | — | — | 1.15 | −1.4 |
| N-13 | 6.124 | 5.90 | −3.7 | 5.97 | −2.5 | 6.00 | −2.0 |
| OB-1 | 153.9 | 151. | −1.9 | — | — | 148. | −3.8 |
| Litho-varnishes | | | | | | | |
| No. 00000 | 1.5 | 1.49 | 0 | 1.52 | 0. | 1.45 | 0. |
| No. 1Trans. | 9.2 | 9.3 | +1.1 | 9.0 | −2.2 | 9.3 | +1.1 |
| No. 1 Reg. | 11.6 | 11.7 | +0.9 | 12.0 | +3.4 | 11.6 | 0.0 |
| No. 3 Reg. | 27.5 | 27.9 | +1.5 | 27.0 | −1.8 | 27.5 | 0.0 |

inside diameter of the cup and the diameter and length of the bob. Machining tolerances should be within 0.002 cm (0.001 in.). For most measurements two cups and bobs, making available three clearances, will be found enough; we have found cups 1 and 2 and bobs 1 and 4 most useful.

Because of the nature of the study we were making, the end-effects were determined without any reference to standard viscosity samples except for final confirmation. For this purpose the method of multiple bobs is recommended. For most applications and industrial uses, however, a simple calibration with standard samples is more convenient and entirely satisfactory. It is enough to determine $P$, the ratio of load to r.p.m., as described above, and substitute for it and the known value of $\eta$ in the equation $\eta = K_v \cdot P$ in order to determine the constant $K_v$. This constant combines the end-effect with all the various instrument constants, dimensions of cup and bob, etc.

Within the range from 1 to 150 poises (and probably considerably higher) calibration with a single standard sample will be found sufficiently accurate for most purposes. Below 1 poise, however, since the end-effect has been shown to become increasingly large, calibration should be made with a standard the viscosity of which is close to that of the material to be measured. If this is not possible, the multiple-bob method should be used.

A separation of at least 1 cm should be kept between the bottom of the bob and cup, and an overlay of about 5 mm of liquid above the top of the bob is desirable. In addition to constancy in end-effect, one advantage of the bob immersed well below the liquid level when measuring solutions or suspensions is that evaporation of all except the most volatile solvents introduces small or negligible effects during the course of measurement.


### ACKNOWLEDGMENT

The authors are indebted to Mrs. Dorothy P. Stubbs and Mr. Samuel E. Miller who made many of the experimental measurements.


## The Theory of Disk-Loaded Wave Guides


E. L. CHU* AND W. W. HANSEN

*Department of Physics, Stanford University, Stanford University, California*



(Received July 11, 1947)



The properties of circular wave guides loaded with apertured disks are discussed both qualitatively and quantitatively. Formulae and curves are given for various quantities including the wave and group velocities, the attenuation, and the power flow.


### INTRODUCTION

IN the normal circular wave guide shown in Fig. 1a, the running waves of field propagate with a phase velocity greater than that of light. By the introduction of apertured disks, as shown in Fig. 1b, which also defines some of our notation, this velocity can be reduced as much as desired. In addition to altering the phase velocity, the loading disks change the group velocity and, two parameters being available, the two velocities can be controlled independently. Finally, the periodic spacing of the disks introduces a high frequency cut-off, in addition to the low frequency one already present, so that the loaded structure has many of the characteristics of a band pass filter. We propose to report here certain calculations on the properties of such structures, which we call disk-loaded wave guides.

While the main formulae we use are of general interest, some special formulae and many of the numerical examples are developed to fit the special circumstances of an important possible use of disk-loaded guides—namely, that of accelerating electrons. Indeed, interest in this problem has been the primary motive for developing the theory that follows.

Before describing the details of the calcula-


* On leave from the Institute of Physics, Academia Sinica, Shanghai, China.

tions, it will be useful to consider several qualitative descriptions of the operation of such a structure.

One point of view regards the disk-loaded guide as derived from an infinite sequence of end-to-end cylindrical cavity resonators by opening up "coupling holes" between adjacent cavities. Then if we consider the behavior at various frequencies, as is done in Fig. 2, we start at zero frequency with Fig. 2a showing the electric-field lines terminating on the disks and decreasing rapidly in strength as we go from left to right. Here we are below the low frequency cut-off, the device acts as an attenuator, and curvature of electric-field functions toward the axis, when going in the $r$ direction, is canceled by curvature away from the axis in the $z$ direction to give the zero total curvature required at zero frequency. As we increase the frequency, the curvature away from the $z$ axis decreases until at the resonant frequency of the uncoupled resonators without holes ($\lambda = 2.61b$) the fields are in phase everywhere in the guide, there is no attenuation, and the field curvature is all in the $r$ direction, as shown in Fig. 2b. This field configuration may be regarded as obtained by removing disks of radius $a$ from the inter-resonator boundaries of a sequence of resonators all oscillating in phase, such removal not altering the fields since the currents on opposite sides of any removed disk are equal and opposite. As we further increase the frequency, so running the cavities off resonance, it becomes necessary to supply reactive power to each cavity. This comes through the coupling hole from the adjacent cavity which must then be of somewhat different phase. The resultant field pattern is sketched in Fig. 2c and it must now be remembered that this represents a running wave. As the frequency is further increased, the phase shift per section increases until it becomes 180° at which point the fields are as shown in Fig. 2d. As the frequency is further increased, more phase shift is impossible, attenuation again sets in and the fields are as in Fig. 2e. Thus we see that the two cut-off frequencies correspond to the two modes of cavity oscillation shown in Figs. 2f and 2g.

A second point of view regards the disk-loaded guide as derived from an ordinary guide by the introduction of loading disks which may at first be taken as having small radial extent. From this point of view the fields of Fig. 2a are obvious and Fig. 2b is nearly so; we merely have to remark that, at cut-off, the disks do not influence the electric field since they are at right angles thereto. As we enter the pass region, the disks do not suppress the propagation so long as the disks are closer together than half a loaded-guide wave-length, for in such a case the reflections from succeeding disks cannot add up but must, over a long distance, cancel. This ceases to be so when the guide wave-length decreases to the point that the disks are a half-wave apart, for then the reflections add and transmission is impossible. We then enter the attenuation region as in Fig. 2d.

The third point of view, and the one most closely connected with the mathematics here used to reduce qualitative ideas to quantitative, starts with the fields, and more particularly the fields near the axis, as given, and seeks a structure that fits the fields, as opposed to the above, and usual, procedure of starting with a structure and finding the fields.

Thus we start by requiring a field which, for $r<a$, is finite, axially symmetric, and represents a wave running in the $z$ direction with (real) wave number $k_3$. These conditions completely specify the wave functions—the only possible solution of Maxwell's equations is

$$\begin{aligned} E_z &= E_0 J_0(k_1 r) e^{-jk_3 z}, \\ E_r &= E_0 j(k_3/k_1) J_1(k_1 r) e^{-jk_3 z}, \\ B_\phi &= E_0 j(k/k_1) J_1(k_1 r) e^{-jk_3 z}, \end{aligned} \tag{1}$$

with all other components zero. Here $E_0$ is a constant, we use Gaussian units and a positive time factor, and

$$k_1^2 + k_3^2 = k^2 = 4\pi^2/\lambda^2.$$

It would appear that since $k_3$, which regulates the wave velocity, is unrestricted we can make waves which go with any velocity whatever. But we note that, the velocity being given by $v/c = k/k_3$, a velocity less than that of light implies a $k_3$ which is greater than $k$, and so an imaginary value of $k_1$. While the above are still solutions, their characteristics change when $k_1$ becomes imaginary, and we must investigate their properties for both real and imaginary $k_1$.

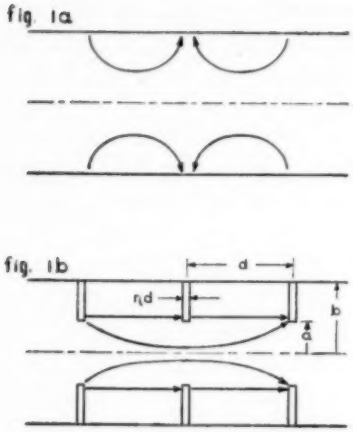


FIG. 1. The sketch of Fig. 1a shows the configuration of electric-field lines in an unloaded circular wave guide, while Fig. 1b shows the fields in a guide loaded by means of apertured disks, and also defines the notation used in describing the guide dimensions. The special case shown has the loads one-quarter wave apart—any other spacing is, of course, possible.

For real $k_1$ the Bessel function is oscillatory so that $E_z$ passes through zero for an infinite number of values of $r$. A qualitative field plot for this case is given in Fig. 3a. When $k_1$ is positive imaginary, however, $J_0$ and $J_1$ are monotonic increasing functions of $r$, so that the $E$ lines cannot reverse directions with the result that the field is qualitatively as shown in Fig. 3b.

Now, having specified the fields, we ask what metallic boundaries we can introduce to confine them to a finite region in space. In the case of fields like those of Fig. 3a one answer is well known: we can introduce a conducting tube in the position indicated by the dotted lines, in which case the electric field is everywhere perpendicular to the conductor and the currents carried by the conductor support the discontinuity in magnetic field. But this is impossible for the fields of Fig. 3b, for they never become perpendicular to the axis.

But another, and more general, possibility becomes apparent if we consider a special type of boundary. If we use a conducting sheet, the correct boundary conditions are $E_{\tan}=0$, $B_{\tan}\neq 0$, or $E/B=0$. But if we now add to the sheet a number of closely spaced conducting fins, each $\lambda/4$ long and perpendicular to the main sheet, we have a boundary which will sustain an electric field without a magnetic field since each pair of adjacent fins acts as a quarter-wave resonant line. The correct boundary conditions are then $E/B=\infty$. Moreover, it is easy to see that by choosing a fin depth between zero and $\lambda/2$, it is possible to obtain any desired value of $E/B$.

Thus, by using such a finned boundary we can contain any field and in particular the one assumed above. Thus we are led to the disk-loaded guide, and conclude that waves in such a structure can be made to run with any velocity desired.

In carrying out an analysis along the above lines it is plain that the results will approach exactness as the fins get closer and the phase shift per fin approaches zero. On the other hand, as the fin spacing is increased no qualitative changes occur until the phase change per fin becomes $\pi$, at which point the approach breaks down completely. This corresponds, of course, to the high frequency cut-off.

We can now conclude our introductory remarks by specifying the quantities given and to be computed and the approximations to be made.

The six quantities $a$, $b$, $d$, $\eta d$, the skin depth $\delta$ characterizing the guide material, and $\lambda$, may be regarded as given, and may obviously be reduced to five by measuring lengths in terms of $\lambda$. These five we take as $ka$, $kb$, $kd$, $\eta$, and $\lambda/\delta$. Usually $\lambda/\delta$ is large, in which case it may be

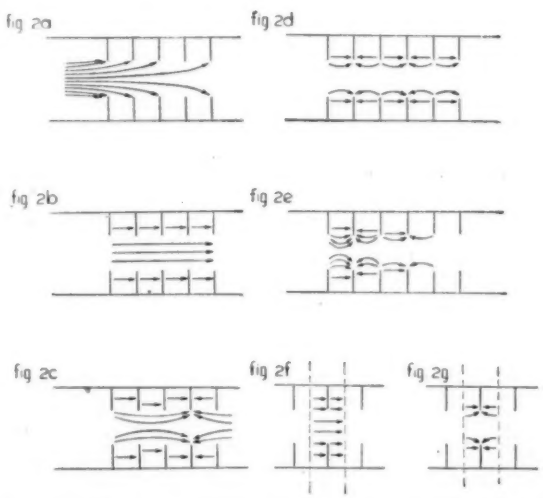


FIG. 2. Sketches a–e show the qualitative behavior of the $E$ lines in a loaded guide as the frequency is raised from zero to above the high frequency cut-off. Illustrations f and g show how a cavity can be constructed from a section of the guide by the addition of conducting planes, shown as dotted lines. The two indicated modes of oscillation of this cavity correspond to the low and high frequency edges of the pass band for the loaded guide.

disregarded in wave-length calculations and will appear only in loss calculations. Moreover, we will often assume that $kd$ is negligibly small, in which case there remain three quantities $ka$, $kb$, and $\eta$. Further, $\eta$ may sometimes be negligible also.

In principle there are only two quantities to compute, the wave number in the $z$ direction, which we call $k_3$ and which would be called the propagation constant in filter theory, and a characteristic impedance $Z_i$, to be defined more precisely later. As to $k_3$, a slightly more convenient quantity is $k_3/k=1/\beta$, where the wave velocity is $\beta_c$. We also note that $k_3$ is complex so that we must compute both real and imaginary parts, the latter being a measure of the attenuation.

Although $k_3$ and $Z_i$ contain all the information, it is useful to compute also certain related quantities. These will be defined as the occasion arises but we may mention that the group velocity and the axial field for a given power are important, and that it is useful to compute not only the attenuation but the $Q$.

As to the approximations involved, they depend on the calculational approach used. As indicated in the qualitative discussion, at least three procedures are possible. First, we can treat the structure as a series of resonators perturbed by the coupling through the center holes. For such a calculation we must have $a \ll b$, $a \ll d$. Second, we may consider the loading to be nearly continuous, in which case we must have $d \ll a$, $d \ll b-a$. Third, we may consider a cylindrical wave guide, perturbed by the addition of loading disks. For this calculation we take $b-a \ll d$, $b-a \ll b$. For the computation of $k_3$ we have used all three methods. For the attenuation, impedance, and other quantities which are less critical we have usually used approximations based on the second approach. Thus it happens that the numerical majority of our results depend on this second approach, which will now be explained in detail.

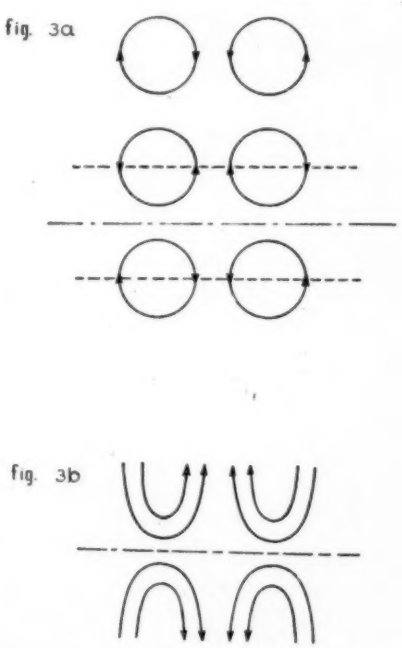


FIG. 3. Sketch a shows qualitatively the shape of $E$ lines given by Eq. (1) for real values of $k_1$, while b shows them for imaginary $k_1$. In the former case a cylindrical conducting boundary can be introduced at the radius indicated by the dashed lines.

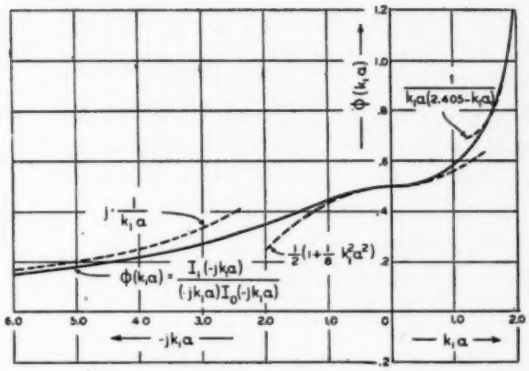


FIG. 4. This shows $\phi$ as a function of $k_1a$, real values of the argument being on the right-hand side, and imaginary values on the left. Various approximate formulae are shown in dotted lines.

## CALCULATIONS

### 1. Phase and Group Velocity

In (1) we have already given the fields to be used for $r<a$. For $a<r<b$ we take

$$E_z = CE_0Z_0(kr)e^{-jk_3(z)},$$
$$E_r = 0, \qquad (2)$$
$$B_\phi = CE_0jZ_1(kr)e^{-jk_3(z)},$$

with $C$ a constant and $Z_0$ a Bessel function that is zero at $r=b$,

$$Z_0 = J_0(kr)N_0(kb) - N_0(kr)J_0(kb), \qquad (3)$$

and

$$Z_1 = J_1(kr)N_0(kb) - N_1(kr)J_0(kb). \qquad (4)$$

Here $(z)$ is equal[1] to zero when $-d/2 < z < d/2$, to $d$ for $d/2 < z < 3d/2$, etc., with the loading disks at $z = d/2,\ 3d/2 \cdots$. Otherwise said, $(z)$ is equal to the value of $z$ midway between the two nearest loading disks. Also, the fields are to be zero in the space occupied by the disks.

Plainly these are solutions of Maxwell's equations, and they satisfy the boundary conditions on the cylinder $r = b$ and on the plane surfaces of the disks. To join this function to that for $r < a$, we (a) make the values of $B_\phi$ match at $r = a$, and (b) make $(1-\eta)E_z$ from (2) at $r = a$ equal $E_z$ from (1). To do this we must adjust the constant $C$ and also find a $k_1$ such that the equation

$$\phi(k_1 a) = \frac{1}{k_1 a}\frac{J_1(k_1 a)}{J_0(k_1 a)} = \frac{1}{(1-\eta)ka}\frac{J_1(ka)N_0(kb) - N_1(ka)J_0(kb)}{J_0(ka)N_0(kb) - N_0(ka)J_0(kb)} = \frac{1}{1-\eta}\alpha(ka, kb) \qquad (5)$$

is satisfied.

This makes $B_\phi$ continuous at $r = a$, $z = (z)$, and the average value of $E_z$ likewise, and this is the best that can be done with these approximate functions. Besides the fact that $E_z$ and $B_\phi$ are not continuous at $r = a$, for general values of $z$, we note $E_r$ is finite for $r < a$ and zero for $a < r$. This is also correct on the average, for charge accumulates on the edges of the loading disks because of the difference in current from section to section.

The above is easy to understand, and is certainly right in the limit $k_3 d \to 0$. If $k_3 d$ is finite, the correct procedure would be to take $E_z$ at $r = a$ to be of the form $\cos k_3 z f[z - (z)]$, where $f$ is some suitable function of the distance from the

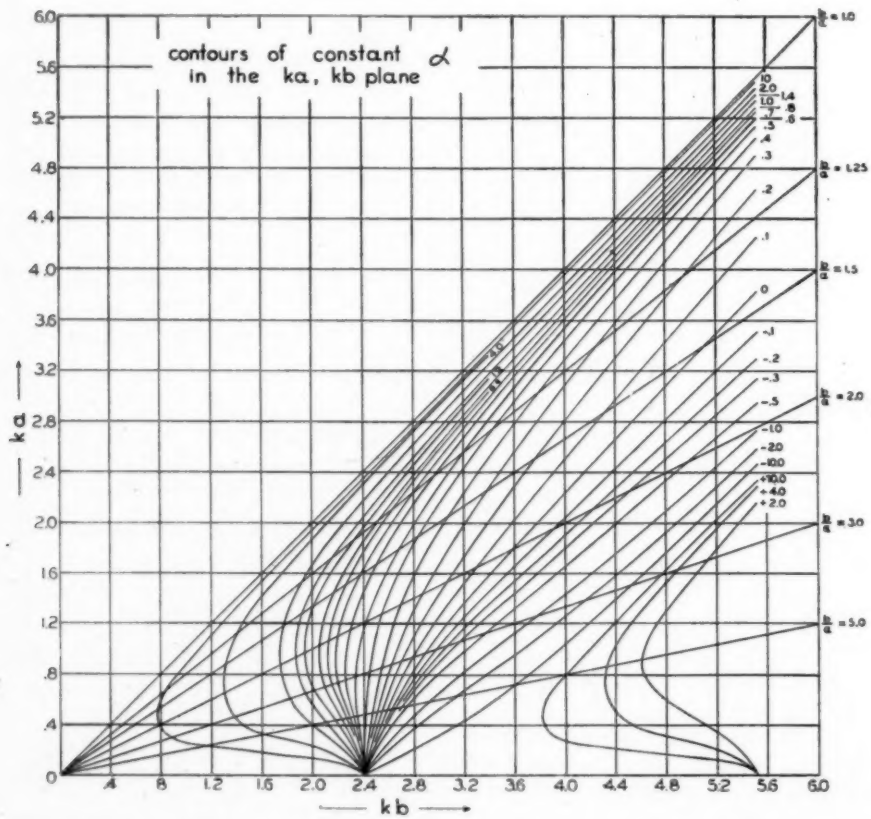


FIG. 5. Shows contours of constant $\alpha$ in the $ka$, $kb$ plane.

[1] This notation is similar in spirit, though not in detail, to the standard notation $(x)$ for "the integral part of $x$."

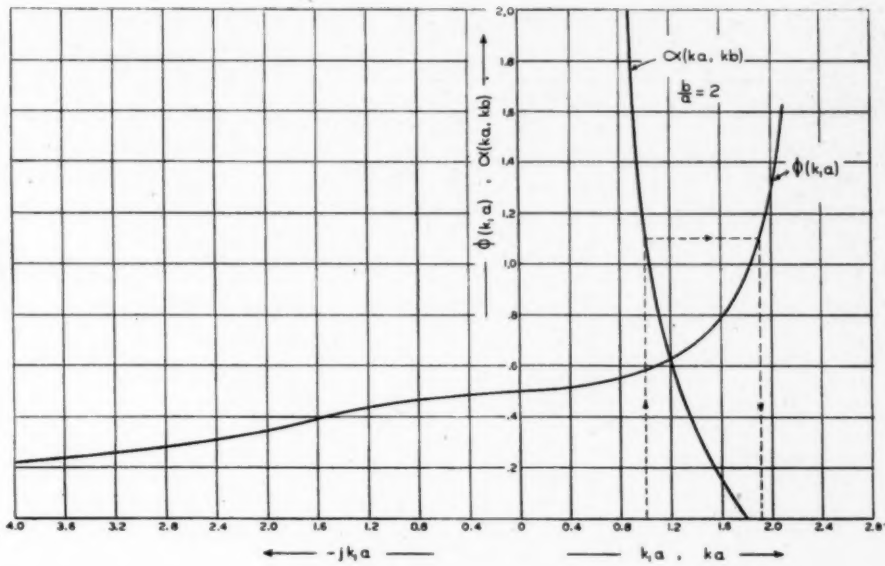


FIG. 6. The functions $\phi$ and $\alpha$ are plotted against $k_1a$ and $ka$ for $b/a=2$.

center of the cell in which $z$ lies.[2] This function would then be expanded as a Fourier integral for $r<a$ and as a Fourier series for $a<r$, whereupon if the assumed form of $E_z$ is correct, the computed values of $B_\phi$ will match everywhere on $r=a$. To carry such a calculation out in detail would be possible but not simple. In certain cases, however, some progress can be made. In particular, if $d\ll a$ and $d\ll b-a$, a good guess for $f$ will be $[1-(4z^2/d^2)]^{-\frac{1}{2}}$. If we take this form for $f$ without verification we need match only at one point, say at the center of a cell, and if we furthermore carry only one Fourier term in the magnetic-field series for both $r<a$ and $a<r$, we get a crude but tractable result, namely, that one merely multiplies the left-hand side of (5) by $J_0(k_3d/2)$ to get

$$J_0(k_3d/2)\cdot\phi(k,a)=\alpha(ka,kb)/1-\eta. \qquad (6)$$

This correction, while reaching a maximum value of $J_0(\pi/2)=0.571$ at $k_3d=\pi$, rises slowly and for small values of $k_3d$ is often negligible. In much of what follows, it will be omitted in the interests of simplicity.

To solve this equation, we need values of $\phi$ and $\alpha$. In Fig. 4 we give a plot of $\phi$ for both real and imaginary values of $k_1a$, together with various useful and easily derived approximate formulae. And in Fig. 5 we give a contour map of $\alpha$ in the $ka$, $kb$ plane.

In obtaining this map, and for various future purposes, the following easily derived approximate expressions are useful

$$\begin{aligned}
&\alpha\cong(1/k^2a^2)(1/\ln\xi),\quad \xi=b/a,\quad ka\ll1,\quad kb\ll1,\\
&\alpha\cong(1/k^2a^2)[1/\ln(2/\gamma ka)],\quad \gamma=1.781,\\
&\qquad\qquad ka\ll1,\quad J_0(kb)\neq0,\\
&kb\cong2.405+1.545(1/2-\alpha)k^2a^2,\\
&\qquad\qquad ka\ll1,\quad kb\cong2.405,\\
&\alpha=(1/ka)\cot(kb-ka),\quad 1\ll ka,\quad 1\ll kb.
\end{aligned} \qquad (7)$$

For given $b$ and $a$, and therefore fixed $b/a=\xi$, $\alpha$ is now a function of $k$ or of $ka$, which can be determined from Fig. 5. A typical curve of $\alpha$ *vs.* $ka$, for $kb/ka=2$ is plotted in Fig. 6. On this same graph, we have plotted $\phi$ as a function of $k_1a$.

To solve (5) for given $k$ and $\eta=0$, we enter the chart at $ka$ and follow the vertical dotted line to an intersection with the $\alpha$-curve, proceed horizontally to find an equal value of $\phi$, and then drop down to the axis to find the value of $k_1a$. Finally, we compute $(k_3/k)=(1-(k_1a/ka)^2)^{\frac{1}{2}}$ and so are able to construct a graph of $k_3/k$ *vs.* $ka$ or $kb$.

It is instructive to follow the results qualitatively as $ka$ increases from zero. For $ka$ small, $\alpha$ and so $\phi$ are large and we easily find $(k_3/k)\cong j(2.405/ka)(1-(ka/2.40)^2)^{\frac{1}{2}}$, i.e., the guide acts

[2] A justification of this statement would be simply a paraphrase of Floquet's theorem on the solutions of Hill's equation. See, for example, Whittaker and Watson, *Modern Analysis* (Cambridge University Press, New York, 1945), p. 412.

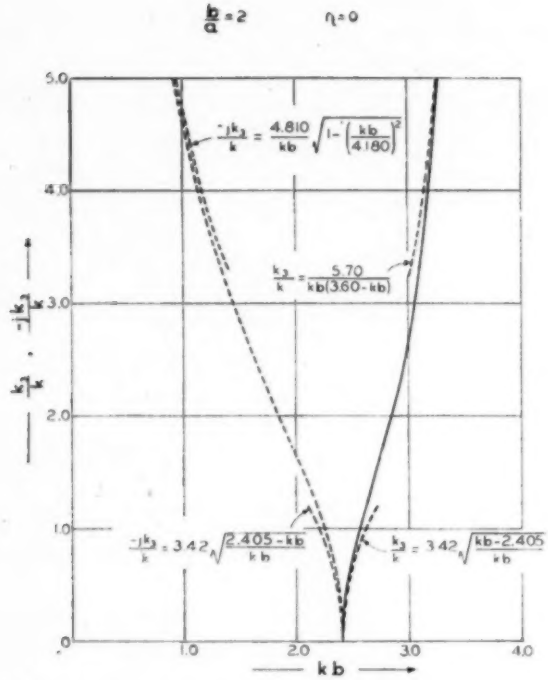


FIG. 7. Shows $k_3/k$ as a function of $kb$ for $b/a=2$, $\eta=0$, $kd\cong 0$. Also shown are a number of approximate formulae.

as an attenuator, and with the attenuation characteristic of a tube of radius $a$. The wave number $k_3$ first becomes real when $k_1a=ka$, i.e., at the intersection of the two curves, where $\alpha$ and $\phi$ are usually about 0.5. Moreover, at this low frequency cut-off, which occurs at $kb=2.405$, $k_1$ is a linear function of $k$ and so $k_3/k$ has the approximate form $(k_3/k)\cong(2(kb-2.405)/2.405)^{\frac{1}{2}}\cdot(-dk_1/dk)^{\frac{1}{2}}$, and so the curve has a vertical tangent at cut-off. As we further increase $ka$, $k_1a$ decreases and the next interesting point is at $k_1a=0$, where $k_1a$ changes from real to imaginary, and $k_3/k$ passes through unity. Nothing striking happens to $k_3/k$, it being easily verified that its derivative is given by

$$\frac{dk_3}{dk}=\frac{k}{k_3}-\frac{k_1}{k_3}\frac{d\alpha/dka}{d\phi/dk_1a}\frac{1}{1-\eta}, \quad k_1a\neq 0, \tag{8}$$

and

$$\frac{dk_3}{dk}=1-\frac{1}{1-\eta}\frac{8}{ka}\frac{d\alpha}{dka}, \quad k_1a\cong 0. \tag{9}$$

These formulae are of some importance, for they give the reciprocal of the group velocity, and this quantity is often of direct interest, especially in the special case $k_1=0$, $k_3=k$ where the wave velocity is $c$.

As $ka$ increases further, $\alpha$ and so $\phi$ approach zero, $k_1$ becomes large and imaginary, and $k_3$ large and real. An approximate formula, valid in

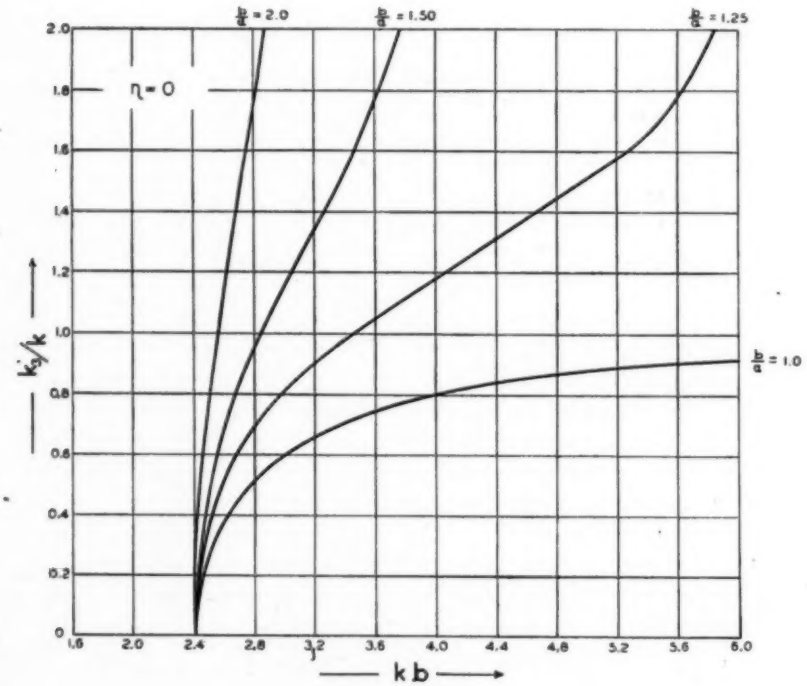


FIG. 8. Shows $k_3/k$ as a function of $kb$ for a variety of ratios $b/a$.

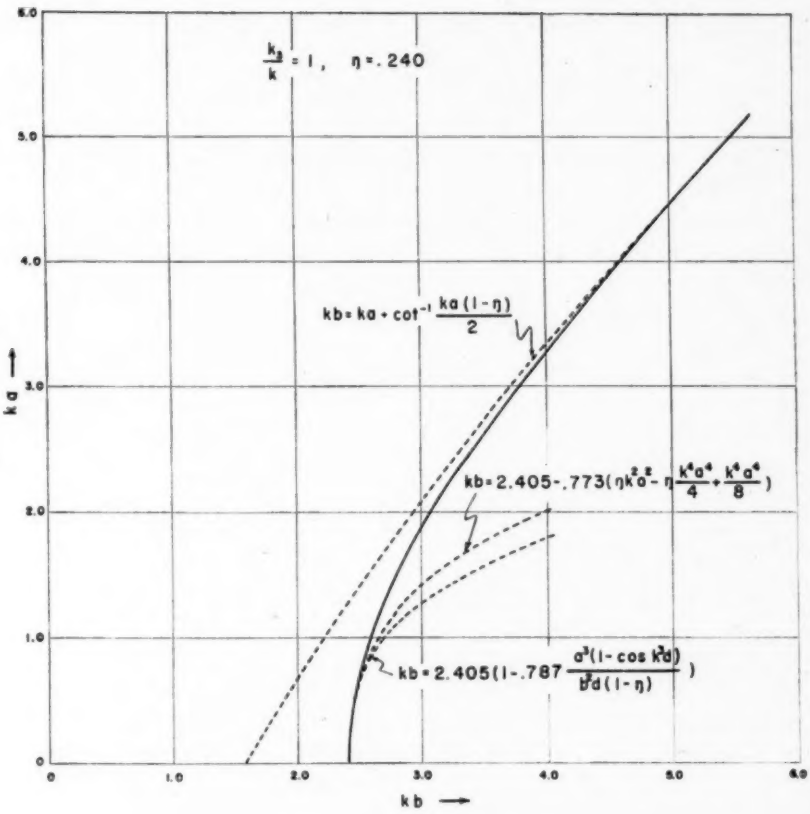


FIG. 9. The value of $ka$ that makes $k_3=k$ is plotted against $kb$. The full curve is based on the assumption that $d\ll a$, $d\ll b-a$, as are two of the dotted curves which give approximations to the solid curve. Also shown dotted is a result valid in the limit $a\ll d$, $a\ll b$.

this region, is

$$(k_3/k)=0.571((1-\eta)/ka(ka-k^+a))dka/d\alpha,$$

with $k^+a$ the value of $ka$ which makes $\alpha=0$.

As remarked before, the present theory is not good in this region, for when $k_3d=\pi$, the wave functions are not well approximated by single Fourier terms. Nevertheless, a good guess at the high frequency cut-off may be had by assuming it to occur at $k_3d=\pi$.

To illustrate the above quantitatively we have prepared Fig. 7 which shows $k_3/k$ as a function of $kb$ for $kb/ka=2$, $\eta=0$, together with a number of approximate formulae. In Fig. 8, $k_3/k$ is plotted as a function of $kb$ for several values of $kb/ka$. Both these figures assume that $k_3d$ is small.

Guides operated at $k$ and loading values such as to give $k_3/k=1$, i.e., phase velocity equal to that of light, have been of special interest to us, and in Fig. 9 we plot for various values of $kb$ the value of $ka$ that gives $k_3/k=1$. Two approximations are also shown, namely,

$$kb=2.405+0.772[\eta k^2a^2-\eta(k^4a^4/4)+(k^4a^4/8)], \quad ka\ll 1, \quad kd\ll 1, \quad (10)$$

$$kb=ka+\cot^{-1}(ka/2)(1-\eta), \quad 1\ll ka, \quad kd\ll 1/ka. \quad (11)$$

We may note that as $ka$ approaches zero it must inevitably become smaller than $kd$, in which case our analysis breaks down. Nevertheless, if $d\ll b$ there is a region in which (10) is useful.

We may now develop the theory for the case $a\ll d$. Here we proceed by considering the loaded tube as derived from a sequence of uncoupled cavities perturbed by the introduction of coupling holes. The problem is solved by variational methods, the behavior of the trial function near the coupling hole being approximated by finding a solution of the appropriate static problem. The result is

$$kb\cong 2.405\left[1+0.787\frac{a^3}{b^2d(1-\eta)}(1-\cos k_3d)\right], \quad \eta d\ll a\ll d, \quad a\ll\lambda, \quad (12)$$

and this result is also plotted in Fig. 9.

On the other end of the possible range of values of $a$ we may have $b-a\ll d$, and in this

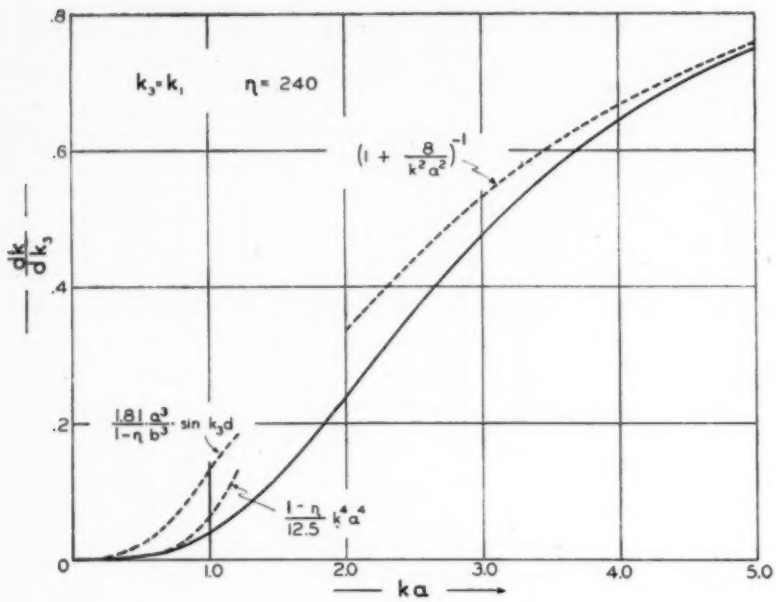


FIG. 10. The quantity $dk/dk_3$, which is the group velocity divided by $c$, is shown as a function of $ka$. The solid line is computed from a theory valid when $d \ll a$, $d \ll b-a$, as are two approximate results shown dotted. Also shown is the result of a theory valid when $a \ll d$, $a \ll b$.

case it is obviously best to take as the unperturbed problem an unloaded guide and introduce the loading disks as perturbations. There are then two cases, $(b-a) \ll \eta d$ and $\eta d \ll b-a \ll d$.

In the first case we may take as a perturbed field simply the unperturbed fields with the volume occupied by the loading rings removed. The results are most easily expressed by giving $k$ in terms of the various dimensions and $k_3$, thus

$$k = k_3[1+(2.405/k_3b)^2]^{\frac{1}{2}} \times [1+5.77(\eta k[b-a]/[kb]^2)], \quad (b-a) \ll \eta d. \quad (13)$$

In the other case, when $\eta d < b-a < d$, the loading disk may be considered as thin, and we use as a perturbed field the unperturbed one minus a potential function such that the boundary conditions on $E$ are satisfied over the ring while $E$ is undisturbed at large distances from the ring. This function is found by a solution of Laplace's equation, under the simplifying assumption that the cylindrical problem may be unrolled into a plane one, i.e., $b-a \ll b$. From this electric field a corresponding magnetic field is derived and the change in frequency computed in terms of the surface integral of $E_1 \times B_2$, with $E_1$ the original field and $B_2$ an addition due to the perturbation. The result is, then

$$k = k_3[1+(2.405/k_3b)^2]^{\frac{1}{2}} \times [1-\pi/2(k_3/k)^2([b-a]^2/bd)]. \quad (14)$$

The group velocity for guides loaded to give a phase velocity of $c$ has also been of interest, and in Fig. 10 we plot $dk/dk_3$ against $ka$ for $kb = 2.66$ together with various approximate formulae. One of these approximate formulae, good for $a \ll d$, is obtained simply by differentiating (12), the other two are derived on a basis best explained in a following section.

## 2. Impedance, Power Flow, and Energy Storage

As is usual in distributed constant problems, any number of definitions of characteristic impedance are possible: the one that is useful for connecting guides of different impedances is defined as equal to the ratio of the transverse voltage to the wall current. If we evaluate this in the midplane of a loading disk using the fields of (1) and (2) we find the impedance in e.m.u. to be

$$Z_i = c\frac{k_3}{k}\frac{2(1-J_0(k_1a))}{k_1aJ_1(k_1a)}. \quad (15)$$

For many purposes it is more useful to know the power flow, and this can be expressed either in terms of $E_0$, the peak axial field, or in terms of the integral of $E_r$, designated above as the transverse voltage. The power flow is easily evaluated from the Poynting vector, the result

being

$$P=(1/256\pi^2)k^3k_3a^4[8/(k_1a)^2]\times[J_1^2(k_1a)-J_0(k_1a)J_2(k_1a)](E_0\lambda)^2/c. \quad (16)$$

A plot of $8/(k_1a)^2$ times the bracketed Bessel functions is given in Fig. 11.

A special case of interest is that for which $k_3=k$, $k_1=0$, in which case we find

$$E_0\lambda=(4/\pi)(Pc)^{\frac{1}{2}}(\lambda/a)^2, \quad k_3=k. \quad (17)$$

If one wishes to use radial voltage, the conversion can be accomplished by using the formula connecting the peak value of $E_r$ and $E_0$,

$$(1/E_0\lambda)\int_0^a E_r dr=(kk_3/2\pi k_1^2)(1-J_0(k_1a)). \quad (18)$$

### 3. Energy Storage

The mean energy stored per unit length is of interest, not only in itself, but also in connection with $Q$ calculations to follow and for use in an alternative method of finding the group velocity. This latter use derives from the relation

$$(\text{Energy stored/cm})(\text{group velocity})=P, \quad (19)$$

and owes its usefulness to the facts that $P$ is easy to compute and that it is often not hard to approximate the energy storage, whereas approximations to $dk/dk_3$ have not been obvious.

We may note that when the group velocity is computed from (19) it comes out in terms of integrals of squares of Bessel functions, whereas when computed from $dk/dk_3$ it depends on derivatives of Bessel functions and it is, at first sight, hard to see in detail why the results are the same. We will not go into this matter, but remark that it is similar to the well-known theorem whereby the derivative of an impedance, with respect to frequency, can be found from the energy stored in the impedance.

We will not write down the exact formulae for energy storage, since the result is easy to obtain analytically and most tedious to use numerically.

Two approximations are useful, however. In

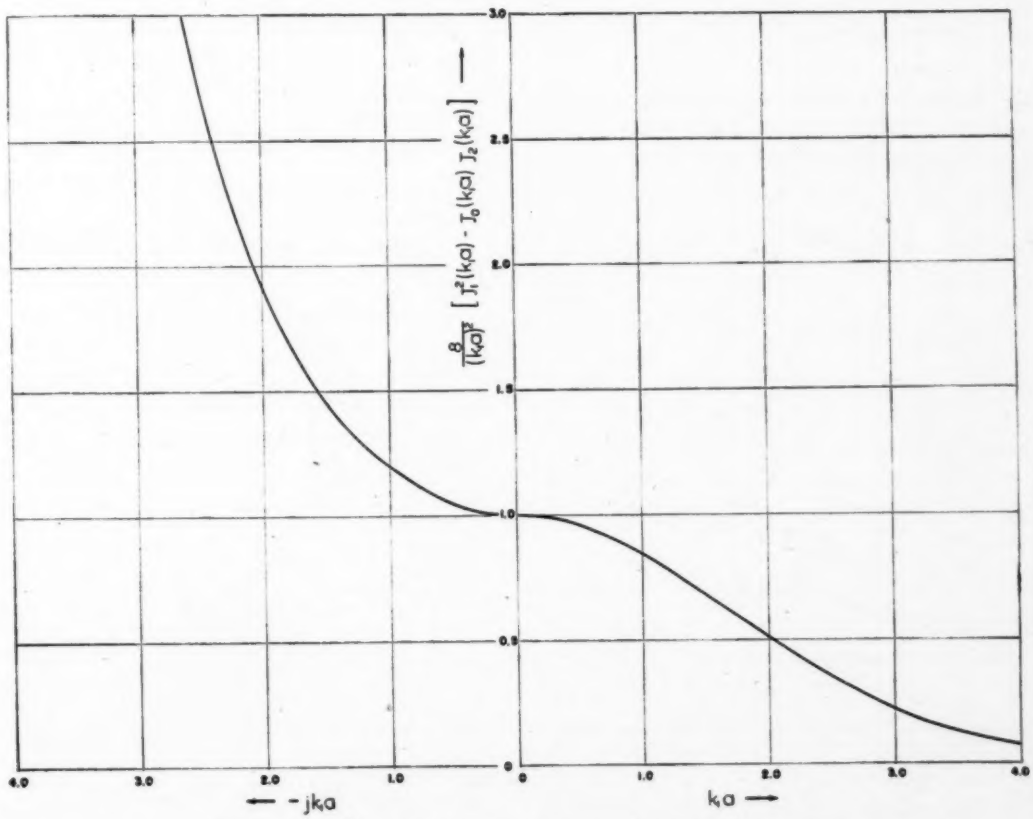


FIG. 11. Plot of a function useful in computing power flow in loaded wave guides.

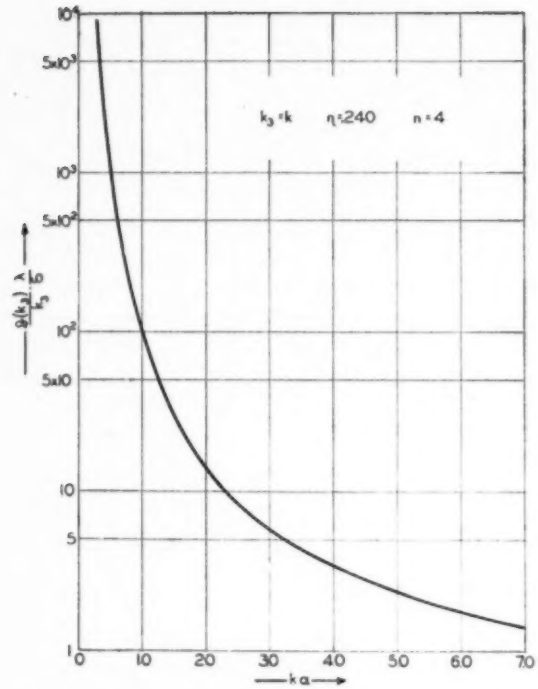


FIG. 12. The imaginary part of the propagation constant, multiplied by $\lambda/k_3\delta$ is plotted against $ka$. The radius $b$ is such as to give $k_3=k$, there are 4 loading disks per wavelength, and the fields of Eqs. (1) and (2) are used.

the first place, if $ka\to0$ we can approximate $B_\phi$ quite well as $[2.405E_0/(1-\eta)kb]J_1[2.405(r/b)]$ in which case the energy storage, as computed by doubling the magnetic energy, comes out as

$$\text{Mean energy/cm}\cong0.195E_0^2/(1-\eta)k^2, \qquad ka\ll1, \quad (20)$$

and combining this with the expression for power flow we get one of the approximations for $dk/dk_3$ used in Fig. 10.

Next, consider the special case $k_3=k$ and let $kb\to\infty$, so that $kb\cong ka+(2/(1-\eta)ka)$. Then we have $B_\phi=E_0kr/2$ for $r<a$, and we can take $B_\phi\cong(E_0/1-\eta)(1/(kb-ka))=$constant for $a<r<b$. This approximation is obviously good for large $ka$ and is surprisingly close for small $ka$, being only 1.55 times too small for $ka=0$. Using these fields, we find

$$\text{Mean energy/cm}\cong\frac{E_0^2}{8k^2}\left(\frac{k^4a^4}{8}+\frac{1}{1-\eta}\frac{kb+ka}{kb-ka}\right), \qquad k_3=k, \quad 1\ll ka, \quad (21)$$

and this may be further simplified by using (11) to relate $kb$ and $ka$. Doing so, we get the remaining approximate formula of Fig. 10.

### 4. Losses

If a power $P$ crosses some plane transverse to the guide, the power at some distance down the guide will be smaller because of losses, i.e., $dP/dz$ is finite. Before computing the losses, we must first consider how the results are to be expressed. At least three forms are useful. First, we may compute the voltage attenuation $I(k_3)=(1/2P)(dP/dz)$; second, we can find $Q=2\pi\nu$ (energy stored/cm)/$(dP/dz)$; and third, we can compute $(dP/dz)/(E_0\lambda)^2$.

The first two may be related by way of (19), thus

$$Q=(1/2)[k/I(k_3)](dk_3/dk). \qquad (22)$$

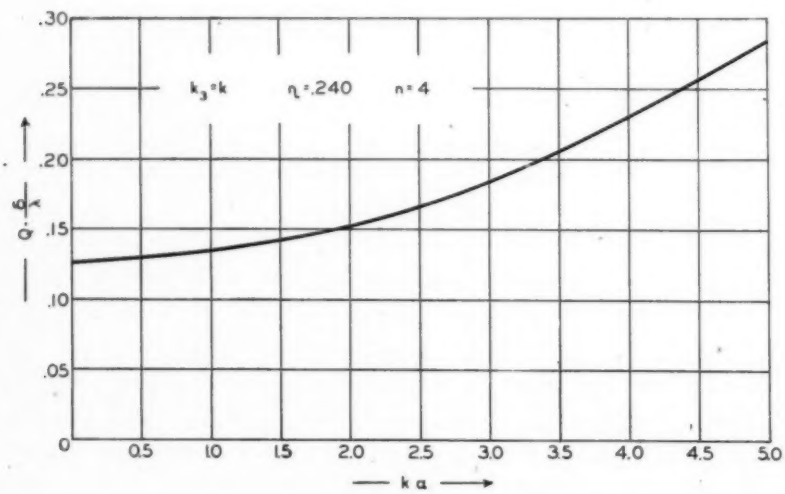


FIG. 13. The quantity $Q\delta/\lambda$ is plotted against $ka$ under the same assumptions as in Fig. 12.

The actual calculation is simple enough in principle, the losses being evaluated as $B^2\delta/8$ per cm$^2$ per cycle, with $\delta=(\rho/2\pi\omega)^{\frac{1}{2}}$ the skin depth. The detailed results will not be written down since the formulae, while easy to obtain, are too complex to allow one to determine their behavior by inspection.

The results of a typical calculation are given in Figs. 12, 13, and 14, which give $I(k_3)/k_3(\lambda/\delta)$, $Q(\delta/\lambda)$, and $(\lambda^2/\delta)(dP/dz)/(E_0\lambda)^2$ as functions of $ka$, when $kb$ is such that $k_3=k$ and there are four loading disks per wave-length.

While the general formulae are quite complex, some approximations will now be given which are usefully simple. All of these are for the special case $k_3=k$.

First, let $ka\ll 1$. Then we find, by using the same field as that used for (20),

$$\frac{I(k_3)}{k_3}=\frac{\delta}{\lambda}\frac{6.25}{k^4a^4(1-\eta)^2}[n+2.61(1-\eta)], \qquad ka\ll 1,\quad k_3=k, \tag{23}$$

$$Q=(\lambda/\delta)[1-\eta/n+2.61(1-\eta)], \tag{24}$$

$$[1/(E_0\lambda)^2](dP/dz)=0.0308(\delta/\lambda^2c)\times[1/(1-\eta)^2][n+2.61(1-\eta)], \tag{25}$$

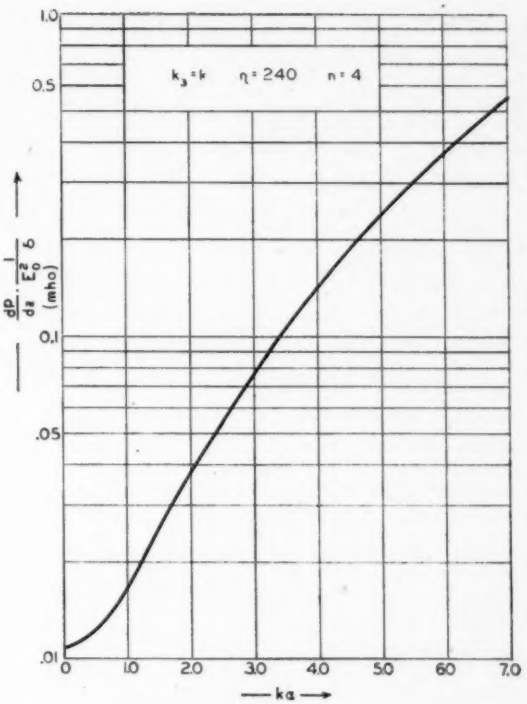


FIG. 14. The power loss per cm per volt/cm squared, divided by $\delta$, as measured in mho, is plotted against $ka$, the conditions being as described for Fig. 12.

with $n=2\pi/kd$, the number of loading disks per wave-length.

Next, let $1\ll ka$ and use the approximation of (21), when we find

$$\frac{I(k_3)}{k_3}\cong\frac{\delta}{\lambda}\frac{8\pi}{k^4a^4}\left[\frac{kb}{(1-\eta)(kb-ka)^2}+\frac{n}{2\pi(1-\eta)^2}\frac{kb+ka}{kb-ka}+\frac{n}{2\pi}\frac{\eta k^2ad}{(1-\eta)^2(kb-ka)^2}\right], \tag{26}$$

$$Q\cong\frac{\lambda}{\delta}\left[\frac{k^4a^4}{8}+\frac{1}{1-\eta}\frac{kb+ka}{kb-ka}\right]\Big/\left[\frac{2\pi kb}{(1-\eta)(kb-ka)^2}+\frac{n}{(1-\eta)^2}\frac{kb+ka}{kb-ka}+\frac{n\eta k^2ad}{(1-\eta)^2(kb-ka)^2}\right], \tag{27}$$

$$\frac{1}{(E_0\lambda)^2}\frac{dP}{dz}=\frac{\delta}{\lambda^2c}\frac{1}{8}\left[\frac{kb}{(1-\eta)(kb-ka)^2}+\frac{n}{2\pi(1-\eta)^2}\cdot\frac{kb+ka}{kb-ka}+\frac{n}{2\pi}\frac{\eta k^2ad}{(1-\eta)^2(kb-ka)^2}\right]. \tag{28}$$

When $ka$ is sufficiently large, these may be simplified by using the approximate relation (11), with results

$$I(k_3)/k_3\cong(\lambda/b)(\delta/\lambda), \tag{29}$$

$$Q\cong(b/2\lambda)(\lambda/\delta), \tag{30}$$

$$\frac{1}{(E_0\lambda)^2}\frac{dP}{dz}\cong\frac{1}{32}\frac{k^3b^3\delta}{\lambda^2c}. \tag{31}$$

A qualitative understanding of the above formulae is useful and simple. For $k_3=k$ we have $E_r=B_\phi=E_0kr/2$ for $r<a$, and we will not do too badly by continuing $B_\phi$ in a linear manner to $r=b$. Thus the power flow will be proportional to $k^4a^4$, the energy stored to $k^4b^4$ and the energy loss on the walls will vary like $k^3b^3$, all for constant axial field. Thus the group velocity, which depends on the ratio of power transmitted to energy stored, at first rises rapidly as $ka$ increases and

then levels off as $ka$ approaches $kb$. Likewise, the linear attenuation, which depends on the ratio of power loss to power transmission, starts by decreasing rapidly as $ka$ increases. When $ka$ is large, the decrease is slower, being simply due to greater cross-sectional area for the wave to carry power as compared to the perimeter bounding the wave and introducing losses. On the other hand, $Q$ which depends on the ratio of energy stored to energy loss, depends mainly on $kb$ which at first increases only slowly with rising $ka$. Thus $Q$ at first drops slowly, though finally varying like $1/ka$, for essentially the same reason as the attenuation.

## CONCLUSION

Many of the important properties of disk-loaded wave guides have been developed, both qualitatively and quantitatively, and have been described by formulae, both approximate and exact, and a number of curves, which will, it is hoped, illustrate the more important points. Special attention has been paid to the wave number $k_3$ which has been computed by three methods. On the other hand, the formulae for loss and power flow are, for the most part, based on an approximation valid when the disk spacing is small, i.e., the loading is nearly continuous.

In a problem with so many variables, it is impossible, in a finite article, to cover all the proportions and conditions that might be of interest and we therefore do not feel apologetic when we point out some of the gaps in the present treatment. First, more accurate methods of calculating $k_3$ are certainly possible; the virtue of our methods is that they give closed or nearly closed formulae and so can be used to explore a wide range of variables without undue labor. Second, we have hardly touched on the behavior in the vicinity of the high frequency cut-off. Third, the loss and power-transmission calculations have been restricted to one method. And fourth, many of the illustrative graphs have been for a single case. Despite these lacunae, we hope that our results will be of use to others.

Finally, it is a pleasure to record the assistance of Mr. E. T. Jaynes with many of the early calculations and to acknowledge the liberal help of the Navy under Contract N6-ori-106.

# Equations for the Inductances of Three-Phase Coaxial Busses Comprised of Square Tubular Conductors

THOMAS JAMES HIGGINS
*Illinois Institute of Technology, Chicago, Illinois*

AND

HENRY PETER MESSINGER
*University of Illinois, Urbana, Illinois*

(Received July 15, 1947)

Equations are derived for calculating the associated inductances of the conductors of three-phase coaxial busses comprised of square tubular conductors. It is assumed that the conductors are nonmagnetic, are of such lengths that end effects are negligible, are right-cornered, and carry currents uniformly distributed over their cross sections. The general equations are obtained through use of geometric mean distance theory. Approximate equations, the conductors being considered as indefinitely thin, are epitomized in a table which yields values sufficiently accurate for most design work. In turn, these approximate equations are reduced to simple equations which also yield values sufficiently accurate for much design work. These equations for inductance lead to corresponding equations for the reactive voltage drops. Use of these various equations and the relative accuracy to be expected of them is illustrated by calculating the inductances and reactive voltage drops of typical busses.

The changes in the inductances due to rounding the edges of the conductors and the changes produced in both the inductances and the resistances by skin and proximity effects are investigated. The changes in the inductances due to rounding the edges can be approximated by use of a known equation. The changes in the inductances due to power frequency skin and proximity effects prove to be negligible; the changes in the resistances can be calculated by use of known skin-effect factors and newly derived proximity-effect factors.

Calculation of the inductances of three-phase coaxial busses constructed of tubular conductors made up of two channels or angles placed flange to flange is discussed. Finally, attention is called to a relatively little known means of obtaining balanced three-phase operation of geometrically unbalanced three-phase busses.

BY virtue of its axial-symmetric geometry, the coaxial-tubular bus possesses certain very desirable electrical and mechanical characteristics. Low inductance contributes to good voltage regulation. Reduced skin and proximity effects minimize line losses and average temperature rise under load. Axial-symmetric distribution of skin and proximity effects reduces current density distortion and attendant hot-spot concentrations, hence enables a greater current rating for a specified maximum copper temperature. As electromagnetic forces between conductors are largely eliminated, mechanical bracing against short-circuit forces can be correspondingly reduced. The nested conductors require less space for installation and a smaller supporting structure than they would if arranged side by side.

Yet, despite these desirable characteristics, the paucity of published descriptions of actual installations[1–4] indicates that few coaxial busses have been constructed to date. However, until the last few years factory distribution loads at frequencies greater than 60 cycles were not common. Again, most 60-cycle loads were supplied over relatively short distances. As these conditions are such that satisfactory operation can be obtained with the more conventional, though less electrically effective, construction of conductors placed side by side, this limited use of coaxial busses is not surprising. Now, however, by virtue of manufacturing procedures and techniques developed during the war, the bus designer is faced with the necessity of designing heavy-distribution busses which are not only long but also are to operate at frequencies of several hundred cycles and higher. But, the electrical characteristics of the coaxial bus especially suit it to satisfactory operation under either or

[1] L. R. Bogardus, "Resistance welder feed has low resistance drop," Elec. World **110**, 702–704 (1938).

[2] W. Specht, "Concentric bus for resistance welders," Elec. World **114**, 558 (1940).

[3] W. Specht, "A concentric channel bus for resistance welders," Weld. Eng. **26**, June, 31–32 (1941).

[4] "Power supply for resistance welding machines," Trans. A.I.E.E. **59**, 306–320 (1940); **60**, 185–192 (1941).

both of these conditions. Hence, it is to be expected that in the near future coaxial busses will find greater use than they have hitherto.

At present coaxial busses are constructed of circular tubular conductor, of square tubular conductor, and of structural tubular conductor comprised of two slightly separated channels or angles placed flange to flange. To predetermine the operating characteristics of these busses requires knowledge of the a.c. resistance, the a.c. inductance, the copper temperature under load, and the mechanical forces exerted during short-circuit. Equations[5,6] for calculating all four of these quantities are available for single or three-phase busses constructed of circular-tubular conductor and for single-phase busses constructed of square or structural tubular conductor. But for three-phase busses constructed of square or structural tubular conductor, though equations are available for calculating the a.c. resistance,[7,8] the copper temperature,[8] and the short-circuit force,[9] equations for calculating the a.c. inductance, *usually the determining factor in the design of a bus*, are not available.

Such equations are derived in this paper, it being assumed that the conductors are non-magnetic, of such lengths that end effects are negligible, right-cornered, and carry currents distributed uniformly over their cross sections. Of these four conditions, the first two are satisfied in practice. The third, however, though essential to tractable analysis, is usually not true in practice. Square tubes, channels and angles, drawn, rolled, bent, or otherwise formed in one piece, have rounded edges. But the error introduced by neglecting the rounded edges is small. Commonly, the result obtained, though a bit low, is yet sufficiently accurate for the work in hand. In any case, the incremental inductance associated with the rounded edges can be approximated closely by a simple semi-empirical equation derived by Dwight and Wang.[10] Finally, though skin and proximity effects render the current density over the cross sections of the conductors slightly non-uniform, detailed analysis[6] indicates and experiment confirms[11] that at power frequencies the a.c. inductance is practically identical with the d.c. inductance.

These four postulates granted as consistent with practice, derivation of the desired equations, though lengthy, is not difficult. The conductor cross sections are considered as combinations of parallel-sided square areas. By virtue of geometric-mean-distance theory the inductance associated with a particular conductor is expressed in terms of the self and mutual geometric mean distances of these areas. These geometric mean distances can be calculated from known equations. Accordingly, determination of the inductance as a function of the parameters defining the geometry of the bus reduces, essentially, to specific determination of the geometric mean distances involved and substitution of them in the general equation for the inductance.

The general equation comprises 48 terms. A simpler approximate equation similarly derived, but on the assumption that the conductors can be considered as being indefinitely thin (hence have cross sections comprised of line segments), affords values sufficiently accurate for many design purposes. As a further convenience to numerical computation, this equation is expressed in terms of a parameter whose values are to be ascertained from a given table of values. Finally, over the range commonly encountered in practice this parameter proves to be substantially constant. For this case the approximate equation reduces to absurdly simple equations that yield the inductance with negligible computation. These various equations lead to corresponding equations for the reactive voltage drops.

The desired equations, having been obtained

[5] T. J. Higgins, "The design of bus-bar industrial distribution systems: an epitomization of available data," Trans. A.I.E.E. **64**, 385–400, 486–488 (1945).

[6] T. J. Higgins, "Formulas for the inductance of coaxial busses comprised of square tubular conductors," Trans. A.I.E.E. **65**, 328–336 (1946).

[7] A. H. M. Arnold, "The alternating-current resistance of hollow square conductors," J. Inst. Elec. Eng. **82**, 537–545 (1938).

[8] H. B. Dwight, G. W. Andrew, and H. W. Tileston, "Temperature rise of bus bars," Gen. Elec. Rev. **43**, 213–216 (1940).

[9] T. J. Higgins, "Formulas for calculating short-circuit forces between conductors of structural shape," Trans. A.I.E.E. **62**, 659–663 (1943).

[10] H. B. Dwight and T. K. Wang, "Reactance of square tubular bus bars," Trans. A.I.E.E. **57**, 762–765 (1938).

[11] H. P. Messinger, *Equations for the Inductance of Coaxial Busses Constructed of Square Tubular Conductor* (Thesis, Library, Illinois Institute of Technology, Chicago, Illinois).

and checked, are used as illustrated by calculation of the inductances of typical busses constructed of square tubular conductor. Changes in inductance and resistance resulting from rounded corners on the conductors and from skin and proximity effects are discussed in detail. Procedures for calculating the inductance of coaxial busses constructed of channels or angles are advanced. Finally, attention is directed to a relatively little known means of obtaining balanced three-phase operation of geometrically unbalanced three-phase busses.

## I. DERIVATION OF THE GENERAL EQUATION

Consider a three-phase bus comprised of three coaxial square tubular conductors (Fig. 1). From well-known theory[12, 13] the inductances associated with the conductors are

$$L_x=(-2/I_x)\sum_{i=x}^{z} I_i \log D_{xi}, \tag{1}$$

$$L_y=(-2/I_y)\sum_{i=x}^{z} I_i \log D_{yi}, \tag{2}$$

$$L_z=(-2/I_z)\sum_{i=x}^{z} I_i \log D_{zi}, \tag{3}$$

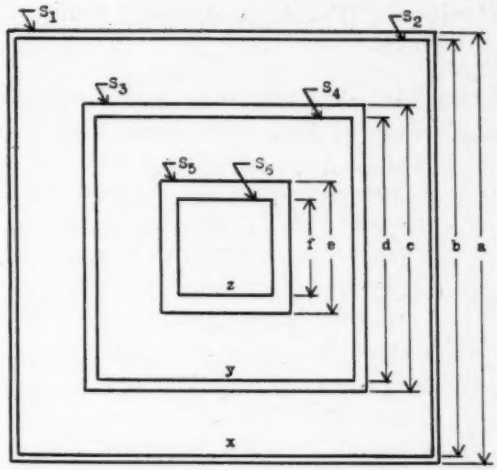


FIG. 1. Cross section of coaxial bus comprised of square tubular conductors.

where, typically, $L_x$ is the inductance associated with conductor $x$; $I_x$ is the current (expressed as a complex number) associated with conductor $x$; and $D_{xi}\equiv D_{ix}$ is the geometric-mean distance of the cross sections of conductors $x$ and $i$. The units of the various physical quantities are as discussed in Section V.

The geometric mean distances $D_{xx}$, $D_{xy}$ and $D_{xz}$ are (as derived in detail in Appendix I)

$$\log D_{xx}=[1/12(a^2-b^2)^2][12a^4\log a+12b^4\log b+(a^4-6a^2b^2+b^4)\log(a^2+b^2)-(a+b)^4\log(a+b)-(a-b)^4\log(a-b)+8ab(a^2-b^2)\tan^{-1}(a-b)/(a+b)+(a+b)(a-b)^3\pi+10(a^4+b^4)\log 2]-0.5\log 2+\pi/4-25/12, \tag{4}$$

$$\log D_{xy}=[-1/24(a^2-b^2)(c^2-d^2)][(a+d)^4\log(a+d)+(a-d)^4\log(a-d)-(a^4-6a^2d^2+d^4)\times\log(a^2+d^2)-(b+d)^4\log(b+d)-(b-d)^4\log(b-d)+(b^4-6b^2d^2+d^4)\log(b^2+d^2)-(a+c)^4\log(a+c)-(a-c)^4\log(a-c)+(a^4-6a^2c^2+c^4)\log(a^2+c^2)+(b+c)^4\log(b+c)+(b-c)^4\log(b-c)-(b^4-6b^2c^2+c^4)\log(b^2+c^2)-8ad(a^2-d^2)\tan^{-1}(a-d)/(a+d)+8bd(b^2-d^2)\tan^{-1}(b-d)/(b+d)+8ac(a^2-c^2)\tan^{-1}(a-c)/(a+c)-8bc(b^2-c^2)\times\tan^{-1}(b-c)/(b+c)-\{(a+d)(a-d)^3-(b+d)(b-d)^3-(a+c)(a-c)^3+(b+c)(b-c)^3\}\pi]-0.5\log 2+\pi/4-25/12, \tag{5}$$

$$\log D_{xz}=[-1/24(a^2-b^2)(e^2-f^2)][(a+f)^4\log(a+f)+(a-f)^4\log(a-f)^4-(a^4-6a^2f^2+f^4)\times\log(a^2+f^2)-(b+f)^4\log(b+f)-(b-f)^4\log(b-f)+(b^4-6b^2f^2+f^4)\log(b^2+f^2)-(a+e)^4\log(a+e)-(a-e)^4\log(a-e)+(a^4-6a^2e^2+e^4)\log(a^2+e^2)+(b+e)^4\log(b+e)+(b-e)^4\log(b-e)-(b^4-6b^2e^2+e^4)\log(b^2+e^2)-8af(a^2-f^2)\times\tan^{-1}(a-f)/(a+f)+8bf(b^2-f^2)\tan^{-1}(b-f)/(b+f)+8ae(a^2-e^2)\tan^{-1}(a-e)/(a+e)-8be(b^2-e^2)\tan^{-1}(b-e)/(b+e)-\{(a+f)(a-f)^3-(b+f)(b-f)^3-(a+e)(a-e)^3+(b+e)(b-e)^3\}\pi]-0.5\log 2+\pi/4-25/12. \tag{6}$$

[12] T. J. Higgins, "Formulas for the calculation of the inductance of linear conductors of structural shape," Trans. A.I.E.E. 62, 53–58 (1943).

[13] L. F. Woodruff, *Principles of Electric Power Transmission* (John Wiley and Sons, New York, 1939), edition 2, Chap. 2.

Substituting from Eqs. (4)–(6) in Eq. (1), collecting terms, and utilizing the relationship $I_x+I_y+I_z=0$ yields

$$
\begin{aligned}
L_x=&[-1/6(a^2-b^2)^2][12a^4\log a+12b^4\log b+(a^4-6a^2b^2+b^4)\log(a^2+b^2)-(a+b)^4\log(a+b)\\
&-(a-b)^4\log(a-b)+8ab(a^2-b^2)\tan^{-1}(a-b)/(a+b)+(a+b)(a-b)^3\pi+10(a^4+b^4)\log 2]\\
&+(I_y/I_x)[1/12(a^2-b^2)(c^2-d^2)][(a+d)^4\log(a+d)+(a-d)^4\log(a-d)\\
&-(a^4-6a^2d^2+d^4)\log(a^2+d^2)-(b+d)^4\log(b+d)-(b-d)^4\log(b-d)+(b^4-6b^2d^2+d^4)\\
&\times\log(b^2+d^2)-(a+c)^4\log(a+c)-(a-c)^4\log(a-c)+(a^4-6a^2c^2+c^4)\log(a^2+c^2)\\
&+(b+c)^4\log(b+c)+(b-c)^4\log(b-c)-(b^4-6b^2c^2+c^4)\log(b^2+c^2)-8ad(a^2-d^2)\\
&\times\tan^{-1}(a-d)/(a+d)+8bd(b^2-d^2)\tan^{-1}(b-d)/(b+d)+8ac(a^2-c^2)\tan^{-1}(a-c)/(a+c)\\
&-8bc(b^2-c^2)\tan^{-1}(b-c)/(b+c)-\{(a+d)(a-d)^3-(b+d)(b-d)^3-(a+c)(a-c)^3\\
&+(b+c)(b-c)^3\}\pi]+(I_z/I_x)[1/12(a^2-b^2)(e^2-f^2)][(a+f)^4\log(a+f)+(a-f)^4\\
&\times\log(a-f)^4-(a^4-6a^2f^2+f^4)\log(a^2+f^2)-(b+f)^4\log(b+f)-(b-f)^4\log(b-f)\\
&+(b^4-6b^2f^2+f^4)\log(b^2+f^2)-(a+e)^4\log(a+e)-(a-e)^4\log(a-e)+(a^4-6a^2e^2+e^4)\\
&\times\log(a^2+e^2)+(b+e)^4\log(b+e)+(b-e)^4\log(b-e)-(b^4-6b^2e^2+e^4)\log(b^2+e^2)\\
&-8af(a^2-f^2)\tan^{-1}(a-f)/(a+f)+8bf(b^2-f^2)\tan^{-1}(b-f)/(b+f)+8ae(a^2-e^2)\\
&\times\tan^{-1}(a-e)/(a+e)-8be(b^2-e^2)\tan^{-1}(b-e)/(b+e)-\{(a+f)(a-f)^3-(b+f)(b-f)^3\\
&-(a+e)(a-e)^3+(b+e)(b-e)^3\}\pi]. \qquad (7)
\end{aligned}
$$

This is the desired equation for the inductance associated with conductor $x$. Comparison of Eqs. (1) and (2) indicates that the corresponding equation for $L_y$ follows from Eq. 7 by interchanging $x$ with $y$, $a$ with $c$, and $b$ with $d$. Similarly, comparison of equations 1 and 3 indicates that the corresponding equation for $L_z$ follows from Eq. 7 by interchanging $x$ with $z$, $a$ with $e$, and $b$ with $f$.

## II. CORROBORATION OF THE GENERAL EQUATION

Consider a three-phase bus comprised of conductors $x$, $y$, $z$ carrying currents $I_x$, $I_y$ and $I_z$ which satisfy the relationship $I_x+I_y+I_z=0$. One conductor, say $x$, can be considered as carrying current $I_x$ and the two remaining conductors can be considered as connected in parallel and carrying the return current $(I_y+I_z)$. In effect, therefore, the bus is a single-phase bus with going conductor $x$ carrying current $I_x$ and subdivided return conductor comprised of parallel components $y$ and $z$ carrying current $(I_y+I_z)=-I_x$. The inductance of such a bus is

$$L=L_x+L_yL_z/(L_y+L_z). \qquad (8)$$

If now conductors $y$ and $z$ are considered as identical and superimposed (whence $y\equiv z$), the resulting single-phase bus is, effectively, comprised of two coaxial square tubular conductors. Accordingly, if Eq. 7 is correct, Eq. (8) should yield the known equation of such a bus. By virtue of $y\equiv z$, we have $e\equiv c$ and $f\equiv d$. Utilizing these identities in Eq. (7) for $L_x$ and in an analogous equation for $L_y\equiv L_z$, substituting the resulting expressions in Eq. (8), and collecting terms yields, corroboratively, the known solution (Eq. 9 of reference 6) for a single-phase bus comprised of two coaxial square tubular conductors.

## III. APPROXIMATIONS TO THE GENERAL EQUATION

The general equation for the inductance associated with a conductor comprises 48 terms: 29 logarithmic, 9 arctangentic, and 10 algebraic. But by use of the proper tools (an electric calculating machine and the 15-place Work Projects Administration[14,15] tables of natural logarithms and arctangents), the computation incident to the calculation of the associated inductances of a given bus can be effected without difficulty. The computation, however, will be lengthy (the computation incident to example 1 below required approximately 15 hours to perform on a 10-row electric calculating machine by one of the authors, experienced in such computation). For this reason it is most desirable to have approximate equations which enable rapid determination of values sufficiently accurate for much (in many

[14] *Tables of Natural Logarithms* (Columbia University Press, New York).
[15] *Tables of Arctangents* (Columbia University Press, New York).

instances, all) of the computation incident to the final design of a bus.

A means of deriving such equations stems from the writers' earlier investigation[6] of the inductance of a single-phase coaxial bus comprised of square tubular conductors. Therein, values of inductance calculated from the general equation were found to be in excellent agreement with values of inductance calculated from much simpler approximate equations. These equations are derived on the basis that the cross sections of the conductors are comprised of line segments of dimensions equal to the external dimensions of the actual conductors.

Consider, then, the cross section of each conductor as comprised of four line segments (Fig. 2). As previously, the associated inductances are given by Eqs. (1)–(3). Therein, however, the geometric mean distances are now those pertinent to the cross sections of Fig. 2. The geometric mean distances $D_{xx}$, $D_{xy}$ and $D_{xz}$ are (as derived in detail in Appendix II)

$$\log D_{xx}=\log a+(1/4)\log 2+\pi/4-3/2, \tag{9}$$

$$\begin{aligned}\log D_{xy}=(1/8ac)[&(a+c)^2\log(a+c)\\&-(a-c)^2\log(a-c)+2ac\log(a^2+c^2)\\&-2(a^2-c^2)\tan^{-1}(a-c)/(a+c)\\&+0.5(a^2-c^2)\pi]-0.5\log 2\\&+\pi/4-3/2,\end{aligned} \tag{10}$$

$$\begin{aligned}\log D_{xz}=(1/8ae)[&(a+e)^2\log(a+e)\\&-(a-e)^2\log(a-e)+2ae\log(a^2+e^2)\\&-2(a^2-e^2)\tan^{-1}(a-e)/(a+e)\\&+0.5(a^2-e^2)\pi]-0.5\log 2\\&+\pi/4-3/2,\end{aligned} \tag{11}$$

Substituting from Eqs. (9)–(11) in Eq. 1, collecting terms and utilizing the relationship $I_x+I_y+I_z=0$ yields

$$\begin{aligned}L_x=&-2\log a-(3/2)\log 2\\&-(I_y/I_x)(1/4ac)[(a+c)^2\log(a+c)\\&-(a-c)^2\log(a-c)+2ac\log(a^2+c^2)\\&-2(a^2-c^2)\tan^{-1}(a-c)/(a+c)\\&+0.5(a^2-e^2)\pi]-(I_z/I_x)(1/4ae)\\&\times[(a+e)^2\log(a+e)-(a-e)^2\log(a-e)\\&+2ac\log(a^2+e^2)-2(a^2-e^2)\\&+\tan^{-1}(a-e)/(a+e)+0.5(a^2-e^2)\pi].\end{aligned} \tag{12}$$

Correspondingly, equations for $L_y$ can be obtained from Eq. (12) by interchanging $x$ with $y$ and $a$ with $c$. Similarly, corresponding formulas for $L_z$ can be obtained in interchanging $x$ with $z$ and $a$ with $e$.

Simple algebraic manipulation of the expressions for the mutual geometric mean distances yields equations especially convenient to computation. Thus, designate $K(r)$ by

$$\begin{aligned}K(r)=(1/4)[&\log(1+A^2)-2\log(1-A^2)\\&-(1/2r)(1-r)^2\log A\\&+(r^{-1}-r)(\pi/4-\tan^{-1}A)+2\log r\\&+\log 2+\pi-6],\end{aligned} \tag{13}$$

where $A=(1-r)/(1+r)$ and $r=(1-A)/(1+A)$. A table of values of $A$, $r$ and $K(r)$ is given in Appendix III.

Then Eqs. (9)–(11) can be written in the form

$$\log D_{xx}=K(1)+\log a, \tag{14}$$

$$\log D_{xy}=K(c/a)+\log a, \tag{15}$$

and

$$\log D_{xz}=K(e/a)+\log a. \tag{16}$$

Similarly,

$$\log D_{yy}=K(1)+\log c, \tag{17}$$

$$\log D_{zz}=K(1)+\log e, \tag{18}$$

and

$$\log D_{yz}=K(e/c)+\log c. \tag{19}$$

Substituting as indicated in Eqs. (1)–(3), noting that $K(1)=-0.5413$, and utilizing the identity $I_x+I_y+I_z=0$ in appropriate fashion yields

$$\begin{aligned}L_x=-2\{&-0.5413-K(e/a)\\&+(I_y/I_x)[K(c/a)-K(e/a)]\},\end{aligned} \tag{20}$$

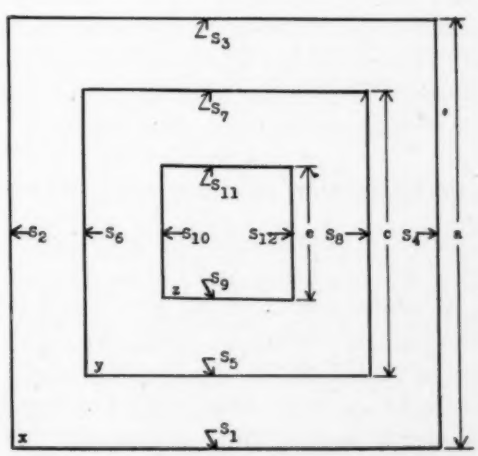


FIG. 2. Cross section of coaxial bus comprised of square tubular line-segment conductors.

$$L_y=-2\{-0.5413-K(e/c)+(I_x/I_y)\log a/c+(I_z/I_y)[K(c/a)-K(e/c)]\}, \quad (21)$$

$$L_z=-2\{-0.5413+\log e/c-K(e/c)+(I_x/I_z)\log a/c+(I_x/I_z)\times[K(e/a)-K(e/c)]\}. \quad (22)$$

Now Table I of Appendix III evidences that for $1\geq A\geq 0.1$, hence $0\leq r\leq 0.82$, $K(r)$ is substantially constant ranging from $-0.553\geq K\geq -0.561$. The values of $r$ found in practice approximate the upper limit. Accordingly, selecting $r=0.75$ as representative, whence

$$K(c/a)\cong K(e/a)\cong K(e/c)\cong -0.556,$$

Eqs. (20)–(22) reduce to the simple approximate equations

$$L_x=-0.030, \quad (23)$$

$$L_y=-0.030-2(I_x/I_y)\log a/c, \quad (24)$$

$$L_z=-0.030-2\log e/c-2(I_x/I_z)\log a/c, \quad (25)$$

valid for $c/a$, $e/a$, and $e/c$ not greater than approximately 0.8.

For purposes of computation, the approximate Eqs. (20)–(22) possess considerable advantage over the general Eq. (7). The latter comprises 48 terms, the former only a few. Moreover, these few terms involve the simplest of calculations. The logarithmic term can be read from a slide rule or from standard tables; the values of $K$ from Table I, calculated from Eq. (13). And even this table can be dispensed with in much work. Equations (23)–(25) afford sufficiently accurate values. Thus, in virtue of the fewness and simplicity of the terms comprising the approximate equations, they afford rapid computation.

## IV. EQUATIONS FOR REACTIVE VOLTAGE DROP

In practice, calculation of associated inductance and reactance is incidental to calculation of what is actually desired: namely, the reactive voltage drop on the conductor, equal to $j2\pi fI(\equiv jwI)$. Saving in time of computation results, however, from calculating the reactive voltage drop directly from appropriate equations, to be obtained by multiplying the previously derived equation for indictance by $jwI$. Thus from Eqs. (1)–(3) we have

$$E_x=(-2jw)\sum_{i=x}^{z} I_i\log D_{xi}, \quad (26)$$

$$E_y=(-2jw)\sum_{i=x}^{z} I_i\log D_{yi}, \quad (27)$$

$$E_z=(-2jw)\sum_{i=x}^{z} I_i\log D_{zi}. \quad (28)$$

Particularly useful approximate equations are to be obtained from Eqs. (23)–(25). Thus

$$E_x=-j0.03wI_x, \quad (29)$$

$$E_y=-2jw[0.015I_y+I_x\log a/c], \quad (30)$$

$$E_z=-2jw[I_z(0.015+\log e/c)+I_x\log a/c]. \quad (31)$$

In similar obvious fashion, corresponding equations can be obtained from Eqs. 7 and analogous equations, from Eq. 12 and analogous equations, and from Eqs. (20)–(22).

## V. UNITS TO BE EMPLOYED

Equations (1)–(3) are valid for the c.g.s. electromagnetic system of units. Hence, the various equations for inductance yield values expressed in abhenrys per centimeter of bus length. Inasmuch, however, as the coefficients and arguments of the various terms comprising these equations can be written in dimensionless form (as, for example, in Eqs. (20)–(25)) we note that in substituting in these equations the currents, and likewise the linear dimensions of the conductors, can be expressed in any like unit.

On the other hand, inasmuch as the voltage drop on a conductor equals $jwLI$, in Eqs. (26)–(31) and in analogous equations the currents must be expressed in abamperes (1 abampere = 10 amperes), though the linear dimensions can yet be expressed in any like unit. The voltage drop, of course, will be in abvolts per centimer of bus length.

For convenience in computation we note the following. Multiplying abhenrys per centimeter by $3.048\times10^{-5}$ yields millihenrys per foot of bus length; multiplying by $11.48\times10^{-6}$ yields 60-cycle reactance in ohms per foot of bus length. Multiplying abvolts per centimeter by $3.048\times10^{-7}$ yields volts per foot of bus length. If in

Eqs. (26)–(31) and in analogous equations the currents are expressed in amperes and the resulting values multiplied by $3.048\times10^{-8}$ the voltage drops obtained are in volts per foot of bus length. Finally, $\log u(\equiv\log_e u)=2.3026\log_{10}u$, where $u$ is an arbitrary number.

## VI. SOME ILLUSTRATIVE EXAMPLES

To illustrate the use of the general and approximate equations and to gain knowledge of the accuracy to be expected of values calculated with the approximate equations, we consider the following examples.

Example 1. The problem is to calculate the six geometric mean distances and the associated inductances of a bus having cross section as in Fig. 1 with dimensions: $a=6$ inches, $b=5.6$ inches, $c=4.5$ inches, $d=4$ inches, $e=3$ inches, $f=1.2$ inches. The bus carries balanced currents $I_x=-0.5-j0.866$, $I_y=-0.5+j0.866$, and $I_z=1$ abampere.

Substituting these values in Eqs. (4)–(6) and analogous equations, rearranging terms, obtaining values of the logarithmic and arctangentic terms from the Work Projects Administration Tables, and effecting all calculations on a 10-row electric calculating machine yields

$$\log D_{xx}=1.2261,\quad \log D_{xy}=1.2019,$$
$$\log D_{yy}=0.9222,\quad \log D_{xz}=1.2011,$$
$$\log D_{zz}=0.3576,\quad \log D_{yz}=0.8733.$$

Substituting in Eqs. (1)–(3) as indicated and collecting real and imaginary terms yields

$L_x=-0.0484$ abhenry per centimeter of bus length,
$L_y=0.2306-j0.572$ abhenry per centimeter of bus length,
$L_z=1.359+j0.572$ abhenry per centimeter of bus length.

In calculating these values all logarithmic and arctangentic terms were taken to nine decimal places; values stemming from consequent arithmetic manipulations were held to the same number of decimals. Inasmuch as each of these final values of inductance stems from algebraic addition of some 50 terms, the ratio of the largest to the smallest approximating $10^6$, it is essential that some such degree of preciseness be held. But, since the resulting values of $L$ is physically significant to only two or three decimal places, it is not unlikely that a study of the number of decimal places to be held in the various stages of computation would reveal that a smaller number than actually used still would be satisfactory. Inasmuch, however, as 15-place tables were employed and the calculation was performed on a 10-row electric calculating machine, the added labor is negligible, and there is no uncertainty as to the effect of cumulative errors on the accuracy of the first several digits of $L$.

Example 2. The problem is to calculate the geometric mean distances and the associated inductances of a bus having cross section as in Fig. 2 with dimensions and currents equal, respectively, to the external dimensions ($a=6$ inches, $c=4.5$ inches and $e=3$ inches) and currents of the bus of example 1.

Substituting these values in Eqs. (9)–(11) and analogous equations and performing the indicated arithmetic yields

$$\log D_{xx}=1.2504,\quad \log D_{xy}=1.237,$$
$$\log D_{yy}=0.9628,\quad \log D_{xz}=1.232,$$
$$\log D_{zz}=0.5573,\quad \log D_{yz}=0.946.$$

Utilizing these values in Eq. (12) and analogous equations yields

$L_x=-0.0328+j0.002$ abhenry per centimeter of bus length,
$L_y=0.2574-j0.502$ abhenry per centimeter of bus length,
$L_z=1.0634+j0.50$ abhenry per centimeter of bus length.

Confirmatively, to three decimal places the same values of geometric mean distance and of associated inductance are yielded by the values of Table I conjoined with Eqs. (14)–(22).

Finally, from Eqs. (23)–(25) we have

$L_x=-0.030$ abhenry per centimeter of bus length,
$L_y=0.257-j0.497$ abhenry per centimeter of bus length,
$L_z=1.069+j0.498$ abhenry per centimeter of bus length.

Example 3. The problem is to calculate the reactive voltage drops on the conductors of the busses for examples 1 and 2.

The voltage drops can be calculated from

Eqs. (26), (27) and (28) by substituting therein the values of logarithmic mean distances calculated in examples 1 and 2. Alternatively, they can be calculated by multiplying the associated inductances by appropriate values of $jwI$. Utilizing the latter procedure and using inductances calculated from Eq. (7) yields

$E_x = 2jw(0.0141 + j0.0209)$ abvolt per centimeter of bus length,
$E_y = 2jw(0.190 + j0.243)$ abvolt per centimeter of bus length,
$E_z = 2jw(0.6795 + j0.286)$ abvolt per centimeter of bus length.

Using inductances calculated from Eqs. (12) and analogous equations and from (20), (21) and (22) yields

$E_x = 2jw(0.0082 + j0.0142)$ abvolt per centimeter of bus length,
$E_y = 2jw(0.153 + j0.237)$ abvolt per centimeter of bus length,
$E_z = 2jw(0.532 + j0.250)$ abvolt per centimeter of bus length.

Using inductances calculated from Eq. (23)–(25) yields

$E_x = 2jw(0.0075 + j0.013)$ abvolt per centimeter of bus length,
$E_y = 2jw(0.151 + j0.236)$ abvolt per centimeter of bus length,
$E_z = 2jw(0.532 + j0.249)$ abvolt per centimeter of bus length.

Comparison of the values calculated from the approximate Eqs. (20)–(22) with those calculated from the simple approximate Eqs. (23)–(25) indicates that in general the simple approximate equations furnish sufficiently accurate values. Comparison of both sets with the values calculated from the general Eq. (7) reveals that the former are somewhat higher. Though these values would be sufficiently accurate for preliminary—and in most instances, final—design purposes, it is yet desirable to have means of calculating somewhat more accurate values without incurring the heavy labor incident to calculation with Eq. (7). Such a means of calculation is suggested by the writers' previous work[6] on single-phase coaxial square tubular busses. Therein it is shown that a bus comprised of coaxial circular tubular conductors has an inductance which differs little from that of a bus comprised of coaxial square tubular conductors having (1) the same thicknesses and (2) internal and external dimensions equal to the internal and external diameters of the corresponding circular conductors. Analogously, it is to be expected that the inductances of similarly dimensioned three-phase busses will be in close agreement. If so, it is to be conjectured that this agreement is better than that between corresponding values for the square tubular conductors calculated from the given geometry and from the approximate assumption of line-segment cross sections. That such is true is substantiated by the following illustrative examples.

Example 4. The problem is to calculate the inductances and reactive voltage drops of the conductors of a bus having cross section as in Fig. 3 with dimensions and currents identical with those of example 1.

Calculating the pertinent geometric mean distances as detailed in Appendix IV, substituting as indicated in Eqs. (1) and (3) and (26)–(28), and collecting terms yields the desired values:

$L_x = -0.023$ abhenry per centimeter of bus length,
$L_y = 0.271 - j0.537$ abhenry per centimeter of bus length,
$L_z = 1.384 + j0.537$ abhenry per centimeter of bus length,

and

$E_x = 2jw(0.006 + j0.010)$ abvolt per centimeter of bus length,
$E_y = 2jw(0.165 + j0.252)$ abvolt per centimeter of bus length,
$E_z = 2jw(0.692 + j0.269)$ abvolt per centimeter of bus length.

Example 5. The problem is to calculate the inductances and reactive voltage drops of the conductors of a bus having cross section as in Fig. 4 with dimensions and currents identical with those of example 2.

Calculating the pertinent geometric mean distances as detailed in Appendix IV, substituting as indicated in Eqs. (1)–(3) and (26)–(28), and collecting terms yields the desired values:

$L_x=0$ abhenry per centimeter of bus length,
$L_y=0.297-j0.498$ abhenry per centimeter of bus length,
$L_z=1.099+j0.498$ abhenry per centimeter of bus length,
and

$E_x=0$ abvolt per centimeter of bus length,
$E_y=2jw(0.144+j0.249)$ abvolt per centimeter of bus length,
$E_z=2jw(0.549+j0.249)$ abvolt per centimeter of bus length.

Comparison of the two sets of values calculated in examples 4 and 5 with the corresponding first two sets of example 3 reveals

(i) That—corroborative of expectation—corresponding values for square and for circular conductors are in good agreement;

(ii) That—corroborative of conjecture—the values of example 4 afford a somewhat better approximation to the first set of values in example 3 than do the second set of values of example 3, calculated on the assumption of line-segment cross section.

## VII. CORRECTIONS FOR ROUNDED EDGES

To eliminate excessive edge heating caused by skin effect, square tubular conductors of commercial manufacture have rounded edges. Thus square tubular conductors of the sizes specified in examples 1 and 3 have rounded edges of outer, inner and mean radius indicated as follows:[16] $a=6$ inches; $t=(a-b)/2=0.2$ inch; $r_0=0.75$ inch; $r_i=0.55$ inch; $r_m=0.65$ inch, $c=4.5$ inches; $t'=(c-d)/2=0.25$ inch; $r_0=0.625$ inch; $r_i=0.375$ inch; $r_m=0.5$ inch, $e=3$ inches; $t''=(e-f)/2=0.9$ inch; $r_0=1$ inch; $r_i=0.1$ inch; $r_m=0.55$ inch.

Dwight and Wang[10] have derived, semi-empirically, that the approximate increase in self geometric mean distance caused by rounding the edges of a conductor of square cross section is

$$\Delta \log D_s=-[k^2\log k^{-1}+0.716k^2+0.5k^3+\cdots] \text{ abhenrys per centimeter of conductor length,} \quad (32)$$

where $k=0.463r_m/s$, $r_m$ is the mean radius of the rounded edge, $s$ the mean side of the square cross section, and $r_m$ is small compared with $s$, the accuracy increasing as $r_m/s\to 0$.

From Eqs. (1)–(3) it follows that the approximate increase in associated inductance is

$$\Delta L=2[k^2\log k^{-1}+0.716k^2+0.5k^3+\cdots] \text{ abhenrys per centimeter of conductor length.} \quad (33)$$

For conductor $x$, $s=a-t=5.8$ inches and $r_m=0.65$ inch. Hence, $k=0.052$, $\Delta L_x=0.020$, and $\Delta E_x(=jwI_x\Delta L_x)=2jw(-0.0049-j0.0093)$.

For conductor $y$, $s=c-t'=4.25$ inches and $r_m=0.5$ inch. Hence, $k=0.0545$, $\Delta L_y=0.0216$, and $\Delta E_y=-2jw(-0.005+j0.009)$.

For conductor $z$, $s=e-t''=2.1$ inches and $r_m=0.55$ inch. Hence, $k=0.122$, $\Delta L_z=0.011$, and $\Delta E_z=2jw(0.006)$.

Adding these corrections to the first set of values of examples 1 and 3 yields

$L_x=-0.029$ abhenry per centimeter of bus length,
$L_y=0.252-j0.572$ abhenry per centimeter of bus length,
$L_z=1.370+j0.572$ abhenry per centimeter of bus length,
and

$E_z=2jw(0.009+j0.012)$ abvolt per centimeter of bus length,
$E_y=2jw(0.185+j0.252)$ abvolt per centimeter of bus length,
$E_z=2jw(0.686+j0.286)$ abvolt per centimeter of bus length.

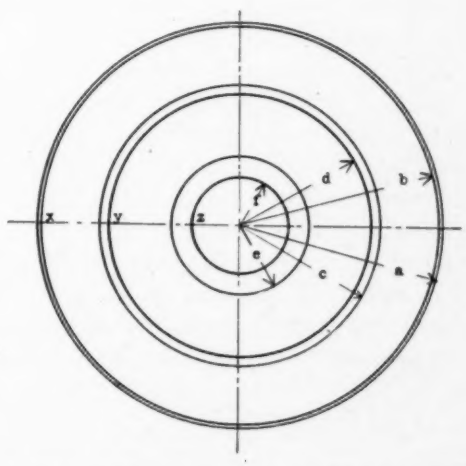


FIG. 3. Cross section of coaxial bus comprised of circular tubular conductors.

[16] *Chase Electrical Handbook* (Chase Brass and Copper Company, Inc., Waterbury, Connecticut, 1941), pp. 80–81.

The facts that rounding the corners of a conductor will result in a change of associated inductance and that the changes just calculated from Eq. (33) are of the correct order of magnitude are confirmed by comparing, in turn, the first set of values of example 1 (for the bus of Fig. 1), the values just listed (for a bus stemming from that of Fig. 1 through rounding the corners of the conductors), and the values of example 4 (for the bus of Fig. 3). Now a circular tubular conductor can be considered the limiting case of a rounded square tubular conductor, its internal and external sides being equal to the internal and external diameters of the circular conductor. Hence the values just listed should be—as they are—intermediate between the corresponding values for the square conductors of Fig. 1 and the circular conductors of Fig. 4.

## VIII. CORRECTIONS FOR SKIN AND PROXIMITY EFFECTS

As the frequency increases from zero to a specified value the currents in the conductors of the bus with cross section as in Fig. 3 tend to concentrate in thin surface strata on the adjacent surfaces of the conductors: the inner surface of conductor $x$ and the outer surface of conductor $y$, the inner surface of conductor $y$ and the outer surface of conductor $z$. This phenomenon results in a change of the associated inductance (and resistance) of each conductor. Detailed mathematical analysis[6, 11, 17] reveals that at 60-cycles the changes in the associated inductances of practically dimensioned busses such as those of example 4 are negligible.

In view of these negligible changes in the inductances of this coaxial circular tubular bus, the small differences between the inductances of this bus and those of the coaxial square tubular bus of example 1—especially, after applying corrections for the rounded edges, and the general geometric similarity between these two busses, we conclude that in practically dimensioned rounded square tubular busses in general 60-cycle skin and proximity effects are negligible insofar as the inductances of the bus are concerned. This conclusion is in accord with the results of analytic and experimental investigations of the inductances of single-phase coaxial[6, 11] and coplanar busses comprised of square tubular or rectangular conductors.

On the other hand, the reactive voltage drops will be somewhat, though slightly, changed by skin and proximity effects. This stems from the fact that the resistances of the conductors are changed by skin and proximity effects. Therefore the current distribution in the conductors, and thus the resistive and reactive voltage drops in the conductors, changes with frequency. At 60-cycles and for bus and conductor geometry commonly encountered in practice it commonly suffices to calculate the a.c. resistances of the square tubular conductors by multiplying their d.c. resistance $R_{d.c.}$ by the known[7, 8, 16] skin-effect factor $K_s$.

Accurate calculation of $R_{a.c.}$ requires that the values of $K_s R_{d.c.}$ thus obtained be multiplied, in turn, by appropriate proximity effect factors $K_p$. Because of the intractable mathematics involved, it has not been possible to calculate rigorously these factors for single-phase or three-phase coaxial square tubular conductors. On the other hand, the simpler—though yet mathematically difficult—corresponding problem for coaxial circular tubular conductors has been solved. In view of the above discussion and analysis of the corresponding inductances of these two busses, and in view of their general geometric similarity, it is to be expected that values of $K_p$ for a bus comprised of circular tubular conductors would be substantially the same as values of $K_p$ for a bus comprised of square tubular conductors having sides and thicknesses identical with the diameters and thicknesses of the corresponding circular conductors.

Now Dwight[17] has published equations ((22), (23), and (29) of Reference 17) for the ratio of $R_{a.c.}/R_{d.c.}(\equiv K_s K_p)$ for each of the three conductors of a three-phase coaxial circular tubular bus and curves (Fig. 2 of Reference 17) for the particular case of balanced currents. Accordingly, if a value obtained from Dwight's equations or curves is divided by $K_s$ for the same *circular tubular conductor*, there is obtained a value of $K_p$ which is a good approximation to the $K_p$ of the corresponding square tubular conductor. (It is to be noted that the required value

[17] H. B. Dwight, "Reactance and skin effect of concentric tubular conductors," Trans. A.I.E.E. **61**, 513–518, 976–977 (1942).

of $K_s$ can be obtained from Dwight's equations or curves: it is equal to the value of $K_sK_p \equiv K_s$ for the conductor when considered as the innermost conductor of a three-phase bus.) Commonly, however, the refinement stemming from use of the values of $K_p$ is not necessary in practice.

### IX. BUSSES COMPRISED OF STRUCTURAL TUBULAR CONDUCTOR

A conductor comprised of two slightly separated channels or angles, placed flange to flange, usually is not of a square cross section. If, however, the cross section does not differ too greatly from a square cross section, and commonly this is the case in practice, it is to be expected that a fairly good approximation to the actual inductance of the bus can be effected by judicious use of the equations for the square cross section. In an earlier paper[6] on single-phase coaxial busses the writers calculated that an equivalent square tubular bus with conductors having either the same external perimeters (rounded edges aside) or sides equal to the webs of the given structural conductors have inductances in good agreement with those of the structural tubular bus and showed that these analytic deductions were confirmed by experiment. It is to be inferred that selecting an equivalent three-phase bus on one or the other of the bases mentioned will yield approximate values of inductance within a few percent of the actual values, which is all that is required for most design purposes.

Skin-effect and proximity-effect factors for calculating the a.c. resistances of the conductors can be obtained in like manner.

### X. BALANCING CONDUCTOR CURRENTS IN THREE-PHASE COAXIAL BUSSES

Because of the unbalanced geometry of the three-phase coaxial bus the phase currents will, in general, not be balanced. In such case they must be calculated by the procedure detailed in chapter 2 of reference 13. For obvious reasons, however, balance is most desirable. Though a considerable degree of balance can be obtained by proper geometrical design (make, in so far as is feasible, the associated impedances identical), complete balance is not to be so obtained. The system can be balanced, however, by the use of

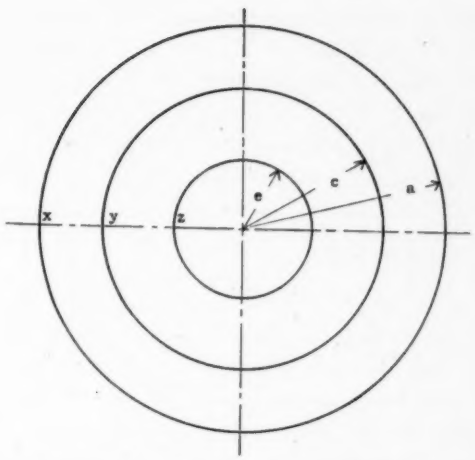


FIG. 4. Cross section of coaxial bus comprised of circular tubular line-segment conductors.

suitably designed and suitably placed metal sleeves fitted around the conductors. Though account of this scheme has long been published,[5, 18] and satisfactory results have been obtained in practice,[19] it would appear that comparatively little use of it has been made to date.

### APPENDIX I

The cross section $S_x \equiv S_1 - S_2$ of conductor $x$ of Fig. 1 can be considered as the symmetrical superposition of a positive square area $S_1$ of side $a$ and a negative square area $-S_1$ of side $b$. By well known theory[6, 12]

$$S_x^2 \log D_{xx} = S_1^2 \log D_{11} + S_2^2 \log D_{22} - 2S_1S_2 \log D_{12} \quad (34)$$

wherein as detailed in Appendix I of reference 6

$$S_1^2 \log D_{11} = -(25/12)S_1^2 - (1/6)[K(a, a) + K(0, 0) - 2K(a, 0)], \quad (35)$$

$$S_1S_2 \log D_{12} = -(25/12)S_1S_2 - (1/6)\{K[(a+b)/2, (a+b)/2] + K[(a-b)/2, (a-b)/2] - 2K[(a+b)/2, (a-b)/2]\} \quad (36)$$

and, generally,

$$K(A, B) = (A^4 - 6A^2B^2 + B^4) \log (A^2+B^2)^{\frac{1}{2}} - 4AB^3 \tan^{-1}(A/B) - 4A^3B \tan^{-1}B/A. \quad (37)$$

Substituting appropriately in Eq. 34, col-

[18] V. G. Egorov, "Equalizing currents in separate lines in complex bus bars," Elektrichestyo, 244–245 (1930).

[19] W. K. Boice, "Current-balancing reactors for turbine generators," Power Plant Eng. 48, October, 94, 120 (1944).

lecting corresponding terms, and solving for $\log D_{xx}$ yields Eq. (4).

In similar fashion, the cross section $S_y \equiv S_3 - S_4$ of conductor $y$ of Fig. 1 can be considered as the symmetrical superposition of a positive square area $S_3$ of side $c$ and a negative square area $-S_4$ of side $d$. By well-known theory

$$S_x S_y \log D_{xy} = S_1 S_3 \log D_{13} - S_1 S_4 \log D_{14} - S_2 S_3 \log D_{23} + S_2 S_4 \log D_{24}, \quad (38)$$

wherein the four terms on the right-hand side of Eq. 38 are analogous to those of Eq. (36).

Substituting appropriately in Eq. (38), collecting corresponding terms, and solving for $\log D_{xy}$ yields Eq. (5).

## APPENDIX II

The cross section $S_x$ of Fig. 2 is comprised of four identical line segments, $S_1$, $S_2$, $S_3$ and $S_4$. By well-known theory

$$S_x^2 \log D_{xx} = 4(S_{11}^2 \log D_{11} + 2S_1 S_2 \log D_{12} + S_1 S_3 \log D_{13}), \quad (39)$$

wherein as detailed in Appendix III of reference 6,

$$\log D_{11} = \log a - 3/2, \quad (40)$$

$$\log D_{12} = \log a + (1/2)\log 2 + \pi/4 - 3/2, \quad (41)$$

$$\log D_{13} = \log a + \pi/2 - 3/2. \quad (42)$$

Substituting appropriately in Eq. (39), collecting corresponding terms, and solving for $\log D_{xx}$ yields Eq. (9).

In similar fashion, the cross section $S_y$ of Fig. 2 is comprised of four identical line segments $S_5$, $S_6$, $S_7$, and $S_8$. By well known theory

$$S_x S_y \log D_{xy} = 4(S_1 S_5 \log D_{15} + 2S_1 S_6 \log D_{16} + S_1 S_7 \log D_{17}), \quad (43)$$

wherein as detailed in appendix III of reference 6,

$$\log D_{15} = (1/2)\{\log(a^2+c^2) + [(a^2-c^2)/ac] \times \tan^{-1}[(a+c)/(a-c)] - \pi(a-c)^2/4ac - \log 2 - 3\}, \quad (44)$$

$$\log D_{16} = (1/4)\{[(a+c)^2/ac]\log(a+c) - [(a-c)^2/ac]\log(a-c) - 2\log 2 + \pi - 6\}, \quad (45)$$

$$\log D_{17} = (1/2)\{\log(a^2+c^2) - [(a^2-c^2)/ac]\tan^{-1}[(a-c)/(a+c)] + \pi(a+c)^2/4ac - \log 2 - 3\}. \quad (46)$$

Substituting appropriately in Eq. 43, collecting corresponding terms and solving for $\log D_{xy}$ yields Eq. 10.

## APPENDIX III

The values of $K(r)$ in Table I are obtained by substituting the indicated values of $A$ and $r$ in Eq. (13), obtaining the values of the logarithmic and arctangentic terms from the Work Projects Administration Tables, and performing all computation on a 10-row electric calculating machine. To avoid cumulative errors all computation was effected to eight significant figures. For actual use, however, $K(r)$ need only to be known to the three or four significant figures given in Table I. For use in design, the designer may find it convenient to plot a curve of $K(r)$ *versus* $r$ from the values given.

TABLE I.

| $A$ | $r$ | $K(r)$ | $A$ | $r$ | $K(r)$ |
|---|---|---|---|---|---|
| 0 | 1 | −0.541 | 0.50 | 1/3 | −0.5611 |
| 0.10 | 9/11 | −0.553 | 0.55 | 7/31 | −0.5611 |
| 0.15 | 17/23 | −0.5560 | 0.60 | 1/4 | −0.5612 |
| 0.20 | 2/3 | −0.558 | 0.65 | 5/33 | −0.5612 |
| 0.25 | 3/5 | −0.5590 | 0.70 | 3/17 | −0.5612 |
| 0.30 | 7/13 | −0.5597 | 0.75 | 1/7 | −0.5612 |
| 0.35 | 13/27 | −0.5603 | 0.80 | 1/9 | −0.5612 |
| 0.40 | 3/7 | −0.5607 | 0.90 | 1/19 | −0.5612 |
| 0.45 | 11/29 | −0.5608 | 1.0 | 0 | −0.5612 |

## APPENDIX IV

The self geometric mean distance of a circular annulus is[13]

$$\log D_s = \log r_1 - [4(r_1^2 - r_2^2)^2]^{-1}[r_1^4 - 4r_1^2 r_2^2 + r_2^4(3 + 4\log r_1/r_2)], \quad (47)$$

wherein $r_1$ and $r_2$ are, respectively, the external and internal radii of the annulus.

The mutual geometric mean distance of a circular annulus and an area of arbitrary area within it is

$$\log D_m = (r_1^2 - r_2^2)^{-1}(r_1^2 \log r_1 - r_2^2 \log r_2) - 1/2. \quad (48)$$

Substituting appropriately in Eqs. (47) and (48) yields the self and mutual geometric mean distances of Fig. 3:

$$\log D_{xx} = 1.0764, \quad \log D_{xy} = 1.0649,$$
$$\log D_{yy} = 0.7739, \quad \log D_{xz} = 1.0649,$$
$$\log D_{zz} = 0.2174, \quad \log D_{yz} = 0.7543.$$

Substituting these values and those of the currents in Eqs. (1)–(3) and (26)–(28) yields the values of example 4. Confirmatively the values of reactive voltage drop on conductors $y$ and $z$ are in agreement with the values obtained by Dwight[17] who utilized the same bus to illustrate his paper. The value for $I_x$ is considerably smaller than Dwight's value. As, however, this small value stems from the algebraic summation of several large values, the difference in the two values is not surprising if (as the writers understand) Dwight's values were obtained by slide rule whereas the writers' were obtained by use of an electric calculating machine, all numerical values being held to eight decimal places during computation.

The self-geometric mean distance of a circle and the mutual geometric mean distance of the circle to any arbitrary area within it are identical:

$$\log D_s = \log D_m = \log r_1,$$

where $r_1$ is the radius of the circle.

Substituting appropriately in Eq. (49) yields the self- and mutual geometric mean distances of Fig. 4:

$$\log D_{xx} = 1.0986, \quad \log D_{xy} = 1.0986,$$
$$\log D_{yy} = 0.8109, \quad \log D_{xz} = 1.0986,$$
$$\log D_{zz} = 0.4055, \quad \log D_{yz} = 0.8109.$$

Substituting these values and those of the currents in Eqs. (1)–(3) and (26)–(28) yields the values of example 5.

---

## Calendar of Meetings

**November, 1947**

3–5 National Electronics Conference, Chicago, Illinois
3–7 American Institute of Electrical Engineers, Chicago, Illinois
6–7 Society of Automotive Engineers (Fuels and Lubricants Meeting), Tulsa, Oklahoma
7–8 Conference on X-Ray and Electron Diffraction, Mellon Institute of Industrial Research, Pittsburgh, Pennsylvania
9–12 American Institute of Chemical Engineers, Detroit, Michigan
17–19 Institute of Radio Engineers and the Radio Manufacturers Association, Engineering Department, Rochester, New York
28–29 American Physical Society, Houston, Texas

**December, 1947**

1–3 Society of Automotive Engineers (Air Transport Engineering Meeting), Kansas City, Missouri
1–5 American Society of Mechanical Engineers, New York, New York
26–31 American Association for the Advancement of Science, Chicago, Illinois
29–31 American Physical Society, Chicago, Illinois

**January, 1948**

2–3 American Physical Society, Los Angeles, California
21–23 American Society of Civil Engineers, New York, New York

# Mechanical Behavior of High Damping Metals*

CLARENCE ZENER
*Institute for the Study of Metals, The University of Chicago, Chicago, Illinois*
(Received July 16, 1947)

The relation between the various measures of internal friction are independent of the precise mechanism of the dissipation of energy when the internal friction is small, but not when it is large. In this paper the relation between the two measures most commonly used, logarithmic decrement and tangent of the angle with which strain lags behind stress, is deduced for all levels of internal friction in the important case in which the dissipation of energy is due to a relaxation process having a single time of relaxation. The conditions are further derived under which a specimen of such a metal will not vibrate, but returns aperiodically to its equilibrium configuration.

## I. INTRODUCTION

SEVERAL measures of internal friction are in common use. Engineers frequently report the specific damping capacity, $\Delta E/E$, defined as the ratio of the energy dissipated per cycle over the average energy of vibration. The measure generally used in physics varies according to the method used in its determination. When the method of free decay is employed, the logarithmic decrement $\delta$ is used. On the other hand, when the method of forced oscillation is employed, the angle $\alpha$ by which strain lags behind stress is usually measured, and the internal friction is reported in terms of $\tan\alpha$. At low values of internal friction all these various measures are related by simple conversion factors. Thus[1]

$$\Delta E/E = 2\delta = 2\pi \tan\alpha. \tag{1}$$

Recent measurements[2] in this laboratory have indicated that polycrystalline metals have, under appropriate conditions, a $\tan\alpha$ as large as 0.1. Under these conditions the term specific damping capacity becomes inappropriate since the very concept of energy of vibration is ambiguous. Under these conditions the relation between $\delta$ and $\tan\alpha$ in Eq. (1) begins to become inaccurate size in its derivation $\tan\alpha$ was assumed to be a small order quantity. The precise relation between $\delta$ and $\tan\alpha$ is dependent upon the mechanism of the dissipation of energy. One important mechanism of energy dissipation in metals arises from the relaxation of an internal parameter which is disturbed from its equilibrium value by a change in strain.[3–6] This parameter could refer, for example, to the stress induced difference in chemical potential of solute atoms in two types of interstitial positions. Frequently this internal parameter, which will be denoted by $A$, obeys a simple relaxation equation of the type

$$dA/dt = -\tau_\epsilon^{-1}A - \gamma\dot{x}, \tag{2}$$

where $x$ denotes the deformation and $\tau_\epsilon$ denotes the time of relaxation at constant strain. In such cases the relation between stress and strain is completely specified, and hence one may deduce, the precise relation between $\delta$ and $\tan\alpha$ obtained from free-oscillation and forced-oscillation experiments, respectively. This relation is obtained in section II. In section III the conditions are derived under which the material behaves in an aperiodic manner, that is, under which the material is self-overdamped.

## II. RELATION BETWEEN $\delta$ AND TAN$\alpha$

In the most appropriate method of investigating highly damping material one employs an auxiliary-inertia member so that the inertia of the specimen itself is of no consequence. One thereby avoids all uncertainty as to the precise manner in which strain is distributed throughout the specimen. The strain is everywhere specified

* This research has been supported by O. N. R., Contract No. N6ori-20-IV.
[1] C. Zener, Phys. Rev. **52**, 230 (1937).
[2] T'ing-Sui Kê, Phys. Rev. **71**, 533 (1947).
[3] C. Zener, W. Otis and R. Nuckolls, Phys. Rev. **53**, 100 (1938).
[4] R. H. Randall, F. C. Rose, and C. Zener, Phys. Rev. **56**, 343 (1939).
[5] J. Snoek, Physica **8**, 711 (1941); **9**, 862 (1942).
[6] C. Zener, Phys. Rev. **71**, 34 (1947).

by a single-deformation parameter $x$ which describes the overall deformation, e.g., angle of twist in a torsion experiment. We shall denote by $f$ the force conjugate to $x$, e.g., the torque acting upon specimen in a torsion experiment.

The deformation $x$ is a linear function of $f$ and the internal parameter $A$. Thus

$$x = M_R^{-1} f + \lambda A. \tag{3}$$

Here $M_R$ refers to the elastic modulus under conditions of complete relaxation, and is called the relaxed elastic modulus. We shall find it convenient to also introduce the unrelaxed modulus $M_U$, which refers to the elastic modulus measured under conditions in which no relaxation takes place. Upon using Eqs. (2) and (3) we see that

$$M_U/M_R = 1+\gamma\lambda. \tag{4}$$

We shall also find it convenient to introduce the time of relaxation of $A$ under conditions of constant stress, $\tau_\sigma$. Again comparing Eqs. (2) and (3) we find

$$\tau_\sigma/\tau_\epsilon = 1+\gamma\lambda. \tag{5}$$

Making use of these definitions we find that elimination of $A$ between Eqs. (2) and (3) leads to

$$dx/dt+\tau_\sigma^{-1}x = M_U^{-1}(df/dt+\tau_\epsilon^{-1}f). \tag{6}$$

The angle $\alpha$ by which strain lags behind stress in a forced oscillation experiment may now be found by substituting

$$f = f_0 e^{i\omega t}$$

into Eq. (6). We find

$$\tan\alpha = \frac{M_U - M_R}{(M_U \cdot M_R)^{\frac{1}{2}}} \cdot \frac{\omega(\tau_\epsilon\tau_\sigma)^{\frac{1}{2}}}{1+\omega^2\cdot\tau_\epsilon\tau_\sigma}. \tag{7}$$

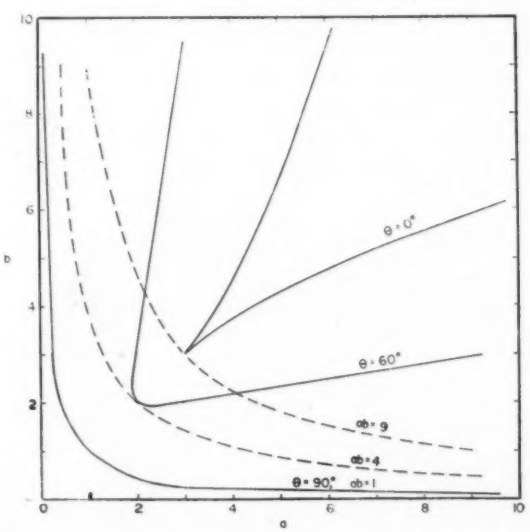


FIG. 1. Diagram for determination of conditions for $\delta_m$. Logarithmic decrement is constant along lines of constant $\theta$. Variation of frequency of vibration corresponds to motion along a line of constant $ab$.

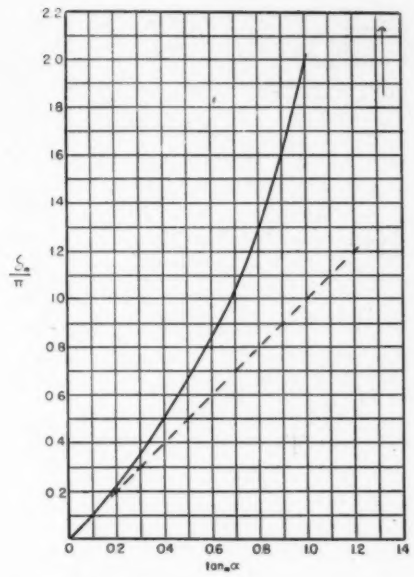


FIG. 2. Relation between maxima values of $\delta$ and of $\tan\alpha$ in a plot *vs.* frequency of vibration. Solid line gives exact relation. Dashed line gives extrapolation of relation valid at small values of internal friction.

In the case of a free oscillation experiment, the force $f$ in Eq. (6) is the negative of the force which acts upon the inertia member. Thus if we denote by $I$ the inertia,

$$Id^2x/dt^2 = -f. \tag{8}$$

An equation containing $x$ alone is now obtained by eliminating $f$ between Eqs. (6) and (8). We thus find

$$d^3x/dt^3+\tau_\epsilon^{-1}d^2x/dt^2+\omega_U^2(dx/dt+\tau_\sigma^{-1}x) = 0. \tag{9}$$

Here we have introduced the "unrelaxed" angular frequency

$$\omega_U = (M_U/I)^{\frac{1}{2}}. \tag{10}$$

We shall later find it convenient to introduce the "relaxed" angular frequency

$$\omega_R = (M_R/I)^{\frac{1}{2}}. \tag{11}$$

The logarithmic decrement is now found by sub-

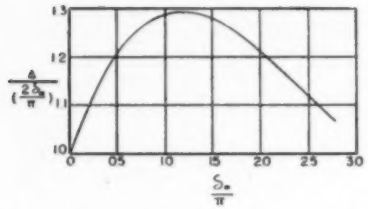


FIG. 3. Relation between relaxation strength and $\delta_m/\pi$.

stituting

$$x = x_0 e^{-\xi t} \tag{12}$$

into Eq. (9). According as $\xi$ is expressed as

$$\xi = \xi_0 e^{i\theta} \tag{13}$$

or as

$$\xi = \mu + i\eta \tag{14}$$

the logarithmic decrement is given by

$$\delta/\pi = 2\cot\theta \tag{15}$$

or

$$\delta/\pi = 2\mu/\eta. \tag{16}$$

Upon using the substitutions

$$E^3 = \omega_U{}^2\tau_\sigma{}^{-1}, \quad a = (\tau_\epsilon E)^{-1}, \quad b = \omega_U{}^2 E^{-2}, \quad U = E^{-1}\xi,$$

we transform this cubic equation into the standard form studied by Jahnke and Emde,[7] namely

$$U^3 - aU^2 + bU - 1 = 0. \tag{17}$$

As a clue as how to proceed to evaluate the logarithmic decrement from this cubic equation we note that

$$ab = M_U/M_R = 1 + \gamma\lambda, \tag{18}$$

and

$$b/a = (\omega_U\omega_R\tau_\epsilon\tau_\sigma)^{\frac{1}{2}}. \tag{19}$$

In experiments upon a given material at a given temperature, the product $ab$ therefore remains fixed. On the other hand the ratio $b/a$ varies as we vary the frequencies $\omega_U$, $\omega_R$, either by changes in dimensions of the specimen or through changes in the inertia $I$. Upon comparing the manner with which the angle $\theta$, and hence $\delta$, varies in $(a, b)$ space as shown in Fig. 1 taken from Jahnke and Emde,[7] with how the product $ab$ varies, we see that for a given product $ab$ the logarithmic decrement is a maximum when the ratio $b/a$ is unity. Our problem is therefore considerably simplified if we restrict ourselves to finding the maximum value $\delta_m$ of the logarithmic decrement in a plot of $\delta$ *vs.* frequency of oscillation. In practice this maximum value may also be obtained by a variation of temperature over a range so small that the ratio $M_U/M_R$ remains essentially constant, but sufficiently large so that $\tau_\sigma$ and $\tau_\epsilon$ vary by a large factor. This restriction allows us to replace $b$ by $a$ in Eq. (17). We now note that this simplified cubic equation may be factorized as follows,

$$(U-1)\{U^2 + (1-a)U + 1\} = 0. \tag{20}$$

The first root of Eq. (20) corresponds to an aperiodic motion. Upon solving for the two roots in the second factor, and upon noting the relations in Eqs. (14) and (16), we obtain

$$\delta_m/\pi = 2(a-1)\{4-(a-1)^2\}^{-\frac{1}{2}}. \tag{21}$$

We shall now compare $\delta_m$ with the maximum value of $\tan\alpha$, $\tan_m\alpha$, obtained in a plot of $\tan\alpha$ *vs.* $\omega$. Upon observing that the parameter $a$ in Eq. (21) is given by

$$a^2 = M_U/M_R, \tag{22}$$

we obtain from Eq. (7)

$$\tan_m\alpha = (1/2)(a - a^{-1}). \tag{23}$$

A plot may now be made of $\delta_m/\pi$ *vs.* $\tan_m\alpha$ through the two parametric equations (21) and (23). Such a plot is presented as Fig. 2. It is to be observed that $\delta_m$ becomes infinite when $a$ is 3, and hence when $\tan_m\alpha$ is 4/3, or when $\alpha$ is 53°. An analytic relation may be found between $\delta_m/\pi$ and $\tan_m\alpha$ when the internal friction is

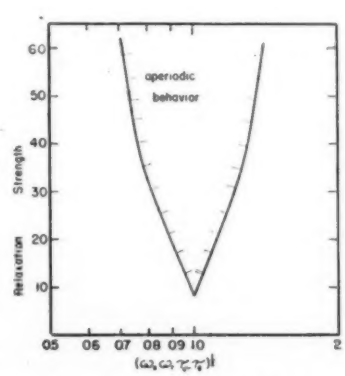


FIG. 4. Conditions for aperiodic behavior.

[7] E. Jahnke and F. Emde, *Funktionentafeln* (Teubner, Leipzig, 1938), second edition, addenda, pp. 20–23.

small. Towards this end we introduce the quantity

$$y=a-1,$$

and expand $\delta_m/\pi$ and $\tan_m\alpha$ in a power series in $y$. We obtain

$$\delta_m/\pi=y(1+y^2/8+\quad).$$
$$\tan_m\alpha=y(1-y/2+\quad)$$

and hence

$$\tan_m\alpha=(\delta_m/\pi)\{1-\delta_m/2\pi+\quad\}.$$

The quantity

$$\Delta=(M_U-M_R)/M_R$$

is known as the relaxation strength, and is of theoretical significance since it is directly related to the constants of the material. Thus from Eq. (4)

$$\Delta=\gamma\lambda.$$

In terms of the parameter $a$ the relaxation strength may be written as

$$\Delta=a^2-1. \qquad (24)$$

The parametric Eqs. (21) and (24) may now be used to obtain a plot of $\Delta$ *vs.* $\delta_m/\pi$. Such a plot is presented as Fig. 3. The analytic relation at small values of $\Delta$ is readily seen to be

$$\Delta=2(\delta_m/\pi)\{1+\delta_m/2\pi+\quad\}.$$

### III. CONDITIONS FOR APERIODIC BEHAVIOR

A specimen will not vibrate freely if all three roots of Eq. (17) are real. The boundary of the region in $(a,b)$ space for which all three roots are real may be found by the method outlined by Jahnke and Emde.[7] This boundary is labeled $\theta=0$ in Fig. 1. A more useful plot is obtained when this boundary is expressed in terms of the two variables

$$\Delta=ab-1$$

and

$$(\omega_U\omega_R\tau_\epsilon\tau_\sigma)^2=(b/a)^{\frac{1}{2}}.$$

Such a plot has been deduced by graphical methods from an enlarged plot of the aperiodic boundary in $(a,b)$ space, and is presented as Fig. 4.

---

# The Field of a Microwave Dipole Antenna in the Vicinity of the Horizon. II*

C. L. PEKERIS**
*Columbia University Mathematical Physics Group, Columbia University, New York, New York*
(Received July 20, 1947)

In this paper the results of a previous investigation are extended to include cases where the elevation of the transmitter $z_1$, or of the receiver $z$, is less than about 1 when expressed in natural units of height. When $z_1<1$ and $z>1$ the electromagnetic potential $\Psi$ in the vicinity of the horizon is given, in the case of strong absorption ($\beta\gg1$), by

$$|\Psi|=[(\tfrac{2}{3})^{\frac{1}{2}}/\pi(r\hat{r})^{\frac{1}{2}}]|(1+\beta z_1)G(p)/\beta|, \qquad (a)$$

where

$$\beta_v=i(k_0/q)^{\frac{1}{2}}(\epsilon_1-1)^{\frac{1}{2}}/\epsilon_1;\quad \beta_h=\beta_v\epsilon_1, \qquad (b)$$

and the notation of $I$ is used. Expression (a) equals expression $(B)$ or $(C)$ of $I$ multiplied by the factor $|(1+\beta z_1)|$.

When both $z_1$ and $z$ are less than about unity the potential is given by

$$|\Psi|=(L/r^3)|(1+\beta z_1)(1+\beta z)g(p')/\beta^2|, \qquad (c)$$

where $L$ is the natural unit of horizontal distance. Expression (c) is equal to the expression for the surface wave given in $(D)$ of $I$ multiplied by the factor $|(1+\beta z_1)(1+\beta z)|$.

IN I[1] closed expressions were obtained for the field in the vicinity of the horizon in the three cases: (1) $z_1>1$, $z>1$; (2) $z_1=0$, $z>1$; and (3) $z_1=0$, $z=0$. The purpose of this investigation is to extend the analysis to cover the cases (4) $z_1<1$, $z>1$ and (5) $z_1<1$, $z<1$. It was shown in Eqs. (16) and (17) of I that the Hertzian potential $\Psi$ of a dipole situated at elevation $z_1$ in an atmosphere of standard refraction is given by

$$\Psi_1=(-i\pi/3)e^{i\omega t}(qk_0^2)^{-\frac{1}{2}}\int_0^\infty J_0(kr)kdkN(u)$$
$$\times[M(u_1)+(B/A)N(u_1)],\quad z>z_1, \qquad (1)$$

* This paper is based on work done for the Naval Research Laboratory under contract N6ori-110, task order No. 3, with the Navy's Office of Research and Inventions. Publication assisted by the Ernest Kempton Adams Fund for Physical Research of Columbia University.
** On leave of absence from Massachusetts Institute of Technology.
[1] C. L. Pekeris, J. App. Phys. **18**, July, 1947. This paper will be referred to as I.

$$\Psi_2=(-i\pi/3)e^{i\omega t}(qk_0^2)^{-\frac{1}{3}}\int_0^\infty J_0(kr)kdkN(u_1)$$

$$\times[M(u)+(B/A)N(u)],\quad 0<z<z_1,\quad (2)$$

where

$$u(z)=u_0+z;\ u_0=(k_0^2-k^2)/II^2;\ k_0=2\pi/\lambda,\quad (3)$$

$$M(u)=u^{\frac{1}{2}}H_{1/3}^{(1)}[(2/3)u^{\frac{3}{2}}],$$

$$N(u)=u^{\frac{1}{2}}H_{1/3}^{(2)}[(2/3)u^{\frac{3}{2}}],\quad (4)$$

$$B/A=-[\beta M(u_0)-\dot{M}(u_0)]/Q(u_0);$$

$$Q(u_0)=\beta N(u_0)-\dot{N}(u_0).\quad (5)$$

In order to evaluate (1) for small values of $z_1$ we expand the integrand into a power series in $z_1$ as follows:

$$\begin{aligned}&Q(u_0)[M(u_1)+(B/A)N(u_1)]\\&=\beta[M(u_1)N(u_0)-N(u_1)M(u_0)]\\&\quad-[M(u_1)\dot{N}(u_0)-N(u_1)\dot{M}(u_0)]\\&=(6i/\pi)[(1+\beta z_1)-u_0z_1^2(\beta z_1+3)/6\\&\qquad-z_1^3(\beta z_1+2)/12+\cdots],\end{aligned}\quad (6)$$

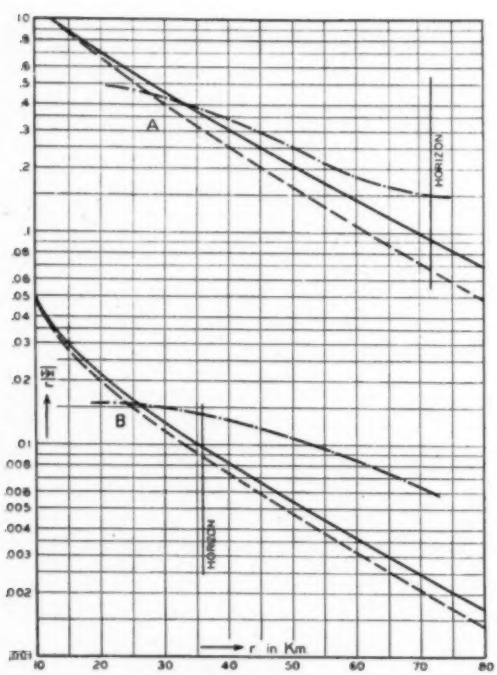


FIG. 1. Comparison of our results with those of B. van d. Pol and H. Bremmer.[2] $\lambda=700$ cm; A: $z_1=0.63$, $z=0.63$; B: $z_1=0$, $z=0.63$.

———— Exact values from normal-mode theory.
— — — — Eq. (20).
— · — · — Eqs. (A) and (B) of reference 1, valid when $z$ is large.

where use was made of the relations

$$N(x)\dot{M}(x)-M(x)\dot{N}(x)=(6i/\pi),$$

$$\frac{d^2N}{dx^2}+xN=0,\quad \frac{d^2M}{dx^2}+xM=0.\quad (7)$$

Since for the field in the vicinity of the horizon the principal contribution to the integrals in (1) and (2) arises from a small range of integration in the neighborhood of $k=k_0$, we may consider $\beta(=iv_0^{\frac{1}{2}}\epsilon_1^{-\frac{1}{2}})$ in (6) as a constant (to within $\beta_h^{-2}<10^{-5}$). Hence, on disregarding powers of $z_1$ above the first, we have

$$\Psi_1(z_1,z)\simeq(1+\beta z_1)\Psi(0,z),\quad (8)$$

$$\Psi(0,z)=2e^{i\omega t}(qk_0^2)^{-\frac{1}{3}}$$

$$\times\int_0^\infty J_0(kr)kdkN(u)/Q(u_0).\quad (9)$$

Expression (9), which is exact, has been evaluated in 1 for the case of strong absorption ($\beta\gg1$) and in the neighborhood of the horizon:

$$\Psi(0,z)\simeq[(3/2)^{\frac{1}{2}}/\pi(r\bar{r})^{\frac{1}{2}}]|G(p)/\beta|,$$

$$p=(3/2)^{\frac{1}{2}}(r-\bar{r})/L.\quad (10)$$

It can be shown that if the other terms in (6) are included, $G(p)$ in (10) must be replaced by

$$G(p)+i(3/2)^{\frac{3}{2}}z_1^2[(\beta z_1+3)/6(1+\beta z_1)]\frac{dG}{dp}$$

$$-z_1^3[(\beta z_1+2)/(1+\beta z_1)12]G(p)+\cdots.\quad (11)$$

Relation (8) agrees with a similar result arrived at by v. d. Pol and Bremmer[2] on the basis of the normal mode theory. Burrows and Gray[3] have also computed a function

$$F(L)=(3^{\frac{1}{2}}/2\pi)|G[(8/9)^{\frac{1}{2}}p]|,$$

using the normal-mode theory.

Turning now to the case where both $z_1$ and $z$ are small, we have to evaluate (9) for small $z$.

[2] B. v. d. Pol and H. Bremmer, Phil. Mag. **27**, Eq. (10), 265 (1939).
[3] C. R. Burrows and M. C. Gray, Proc. I.R.E. **29**, 14 (1941).

Hence we write

$$\frac{N(u)}{Q(u_0)}=\frac{N(u_0)}{Q(u_0)}\cdot\frac{N(u)}{N(u_0)}=[(qk_0^2)^{\frac{1}{2}}/T]$$
$$\times\{-i+[(u_0)^{\frac{1}{2}}N(u_0)-i\dot{N}(u_0)]/Q(u_0)\}$$
$$\cdot\left[1+\frac{z\dot{N}(u_0)}{N(u_0)}+\cdots\right], \quad (12)$$

$$T\equiv[(k_0^2-k^2)^{\frac{1}{2}}+\gamma(k_1^2-k^2)^{\frac{1}{2}}],$$

$$\Psi(0, z)=\phi+\psi+z\phi', \quad (13)$$

$$\phi=-2ie^{i\omega t}\int_0^\infty J_0(kr)kdk/T,$$

$$\psi=2e^{i\omega t}\int_0^\infty J_0(kr)kdk$$
$$\times[(u_0)^{\frac{1}{2}}N(u_0)-i\dot{N}(u_0)]/Q(u_0)T, \quad (14)$$

$$\phi'\simeq-2ie^{i\omega t}\int_0^\infty J_0(kr)kdk\dot{N}(u_0)/N(u_0)T. \quad (15)$$

In (15) we have not included the contribution from the second term in the braces of (12) because it is of the order of $1/\beta$ relative to the contribution from the first term. The integral in (15) is to be understood as the limit approached as $h\to 0$ when a factor $\exp[-ih(k_0^2-k^2)^{\frac{1}{2}}]$ is inserted in the integrand. Since for large $\beta$, $Q\simeq\beta N(u_0)$ we have

$$\psi=(\Lambda+\phi')/\beta,$$

$$\Lambda\equiv 2e^{i\omega t}\int_0^\infty J_0(kr)kdk(u_0)^{\frac{1}{2}}/T. \quad (16)$$

It can be shown that for large $\beta$

$$\Lambda\to -Le^{i\theta}/(\beta r^2)=-\beta\phi,$$

$$\theta=(\pi/2)+\omega t-k_0 r. \quad (17)$$

Hence

$$\phi'=\beta(\phi+\psi)=\beta\Psi(0, 0);$$
$$\Psi(0, z)=(1+\beta z)\Psi(0, 0), \quad (18)$$

where $\Psi(0, 0)$, the surface wave on a spherical earth, is given by

$$\Psi(0, 0)=(e^{i\theta}L/\beta^2r^2)g(p'). \quad (19)$$

Combining (18) with (8) we arrive at an expression for the field in terms of the surface wave when both $z_1$ and $z$ are small:

$$\Psi(z_1, z)=(1+\beta z_1)(1+\beta z)\Psi(0, 0). \quad (20)$$

In Fig. 1 a comparison is shown between the field obtained by van d. Pol and Bremmer[2] and values computed from Eqs. (20) and (19). Here $z_1$ or $z$ is not more than 0.63, so that Eqs. (A) and (B) of I, which are valid only for $z>1$, are inadequate.

# Letters to the Editor

## Grain Growth in Alpha-Brass

J. E. Burke
*Institute for the Study of Metals, University of Chicago, Chicago, Illinois*
June 30, 1947

An extensive series of data on isothermal grain growth in alpha-brass has recently been published by Walker.[1] Plotting from these data log$D$ (grain diameter in mm), *vs.* log time, one obtains a series of isothermal curves. An example for 42.4 percent deformation prior to recrystallization is shown in Fig. 1. One should like to know whether time and temperature for this process are related by a heat of activation $Q$. If so, times at temperature $T_1$ should be related to times at temperature $T_2$ by the equation:

$$\ln(t_1/t_2)=(Q/R)(T_2^{-1}-T_1^{-1}).$$

This equation can be solved to give values of $t_1/t_2$ to convert times at a given temperature to times at any

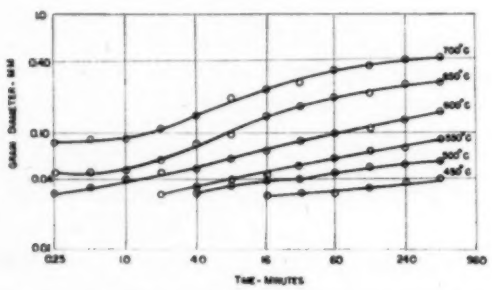


Fig. 1. Isothermal grain growth at various temperatures in alpha-brass.

reference temperature. By taking $Q$ as 60,000 cal. per mole it is found that the data taken at all temperatures can be plotted on a smooth curve at a single reference temperature, with only a reasonable experimental scatter. Figure 2 shows this for the curves of Fig. 1, at a reference temperature of 500°C. It thus seems proper to assign a heat of activation to the process. This curve is not a straight line.

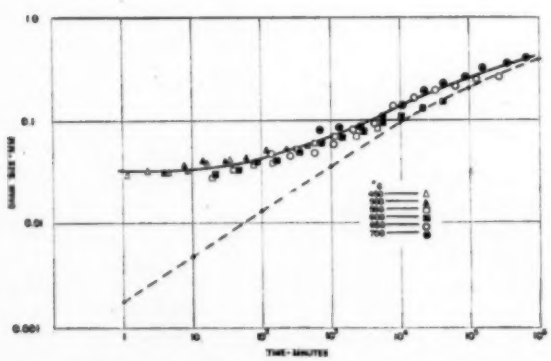


Fig. 2. Solid line: composite grain-growth curve at 500°C reference temperature; Dashed line: composite curve corrected by subtracting 0.03 mm.

Beck, Kremer, and Demer[2] report that their data for grain growth in high purity aluminum follows the relationship:

$$D=kt^n,$$

where $k$ is a constant and the exponent $n$ increases linearly with temperature. Obviously this relationship cannot hold for short times, for, at $t=0$, $D$ has a finite value, $D_0$.

The present data are expressed reasonably well by the relationship:

$$D-D_0=k_1t^n,$$

where $D_0$ is the grain size at the time of recrystallization, $k$ is a temperature-dependent constant, and the exponent $n$ has the value 0.425 until late in the growth process. The dotted line in Fig. 2 was obtained by subtracting the recrystallized grain size reported by Walker for this series (0.03 mm) from the solid curve through the experimental points. It can be seen that it is a straight line until the late stages of growth, but that the slope definitely falls off then. Similar results are obtained from other series of data in Walker's work.

This work was supported by the Office of Research and Inventions, U. S. N. (Contract No. N6ori-20-IV).

[1] Harold L. Walker, University of Illinois Eng. Exp. Sta. Bull. No. 359 (Nov. 1945).
[2] Paul A. Beck, Joseph C. Kremer, and L. Demer, Phys. Rev. **71**, 555 (1947).

## Comments on "Grain Growth in Alpha-Brass"

Paul A. Beck
*University of Notre Dame, Notre Dame, Indiana*
September 12, 1947

In the above note J. E. Burke calculated a heat of activation value from grain-growth data on brass obtained by H. L. Walker.[1] Considering the scatter of the data, his value of 60 kcal./g of atom is in reasonable agreement with the heat of activation value of 73.5 kcal./g atom previously calculated for brass by Beck, Kremer, and Demer,[2] by an essentially identical method, from other published grain-growth data. Thus, Burke's result tends to confirm Beck, Kremer, and Demer's conclusions with regard to the heat of activation value from grain-growth data on brass.

Burke states that the relationship,

$$D=k\cdot t^n, \qquad (1)$$

found by Beck, Kermer, and Demer for isothermal grain growth in high purity aluminum cannot hold for short times, for at $t=0$, $D$ has a finite value, $D_r$, the grain size as recrystallized. Obviously, Burke uses $t$ to denote the time for grain growth. The zero point of his time scale is at the moment when recrystallization is just complete. However, in the nomenclature used by Beck, Kremer, and Demer $t$ denotes the total time of annealing, which includes the time for recrystallization.* Clearly, Burke's objection is based on a misunderstanding of the nomenclature.

Since most of the annealing periods used by Beck, Kremer, and Demer are very long in comparison with the time for recrystallization, the error committed by using "grain-growth time" instead of "total time," as a result of the above misunderstanding, is negligible, except for the shortest annealing periods at the lowest annealing temperatures. Consequently, the whole matter would be lacking in significance were it not for another mistake in Burke's note. He uses the time data from Walker's paper as if these meant "time for grain growth" in the above sense. Actually, Walker, like Beck, Kremer, and Demer, uses the "total time" of annealing. As some of the times of recrystallization in Walker's work are relatively long (such as 16 min. at 450°C), the error resulting from this misinterpretation is significant.

The dotted line in Burke's Fig. 2 gives $\log(D-D_r)$ as a function of $\log t$, where $t$ is supposed to be the time for grain growth, but it is actually the total time of annealing of Walker's specimens, as explained above. Although the initial portion of this line was so selected across the "reasonable scatter" of the transposed experimental points that it is straight, Burke admits that deviation from the straight line definitely occurs at longer annealing periods. Nevertheless, he considers that the data are reasonably well expressed by the relationship:

$$D-D_r=k_1t^n. \tag{2}$$

A comparison of relationships (1) and (2), by using Beck, Kremer, and Demer's grain-growth data on high purity aluminum at 400°C, is given in Fig. 1. It is clear that the plot of $\log D$ *vs.* $\log t$ closely approximates a straight line. Plotting the same data as $D-D_r$ *vs.* $t_g$ ($t_g$ is used here to designate "grain-growth time" in order to avoid confusion) results in a curve which asymptotically approaches the above straight line at very large $t_g$ values. Similar curves are obtained for other annealing temperatures. Obviously, relation (2) does not fit the grain-growth data for high purity aluminum, but formula (1) does.

It can be easily shown that the initial portion of the curve in the figure approaches a slope of $n=1$. If $t_g$ approaches zero, $D/D_r$ approaches 1, that is $D/D_r=1+d$, where $d$ is a very small number, and

$$D-D_r=d\cdot D_r. \tag{3}$$

In Eq. (1) the constant $k$ can be eliminated if one puts $D=D_r$ for $t=R$, where $R$ is the time for just complete recrystallization. The following formula is then obtained:

$$D/D_r=(t/R)^n$$

or, substituting $t_g=t-R$,

$$D/D_r=(1+t_g/R)^n. \tag{4}$$

From (4), with the above relations,

$$1+d=(1+t_g/R)^n,$$

and from this, for a small value of $t_g$,

$$d=(n/R)t_g. \tag{5}$$

By substituting (5) into (3) one obtains

$$D-D_r=n(D_r/R)t_g. \tag{6}$$

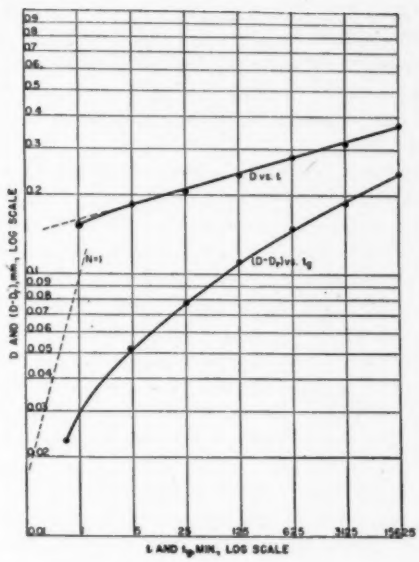


FIG. 1.

Formula (6) shows that for small values of $t_g$ the relationship between $D-D_r$ and $t_g$ is linear. This means that at very short times in the logarithmic plot the curves for all temperatures approach the slope of $n=1$. At long annealing times they approach the $D=k\cdot t^n$ straight lines, where the slope, $n$, increases with the temperature.*

* A fuller discussion of these questions is included in a detailed paper by Beck, Kremer, Demer, and Holzworth to be published in Metals Technology, September, 1947.

[1] Harold L. Walker, University of Illinois Eng. Exp. Sta. Bull. No. 359 (1945).

[2] Paul A. Beck, Joseph C. Kremer, and L. Demer, Phys. Rev. **71**, 555 (1947).

## Electron Microscope and Electron-Diffraction Study of Slip in Metal Crystals

R. D. HEIDENREICH AND W. SHOCKLEY
*Bell Telephone Laboratories, Inc., Murray Hill, New Jersey*
August 20, 1947

THE process of plastic deformation in metal crystals has been the subject of many investigations, both experimental and theoretical, over a long period of years. The new experimental results to be described briefly in this letter have been presented orally before two different groups* but have not appeared in print. A fuller account of the methods and results will appear in a British publication.

The current experiments concerning the structure of slip bands were carried out using 99.99 percent aluminum cast in the form of small single crystals (20×6×2 mm). The as-cast crystals were mechanically polished through 4/0 French emery to produce a flat, 6×20 mm surface and then electropolished to remove the heavily worked layer. The samples were then annealed 3–4 hours above 600°C,

electropolished again, and then etched and rinsed[1] to produce a clean, dry surface exhibiting etch pits indicating the orientation of the crystal. Electron-diffraction reflection patterns from the crystals prepared in this manner were Kikuchi line patterns: taken as a criterion for a reasonably perfect crystal.

The electron micrographs were obtained from anodic-oxide replicas of the crystals produced by anodizing in a 2.5 percent boric acid solution neutralized with ammonium hydroxide. These replicas are capable of a resolution of real structure down to at least 50A.

Plastic deformation was accomplished either by pulling the crystals in tension or by compression along the long axis of the crystal after the final surface was prepared. Examination of the surfaces with a light microscope at 50–100× indicated the orientation of the slip lines and their relative density and distribution for various amounts of plastic deformation.

The following conclusions were arrived at from combined electron microscope and electron-diffraction results on numerous aluminum crystals with various amounts of deformation.

(*A*) *Electron Microscope*—The electron micrographs clearly show that the slip bands observed in a light microscope are actually laminar regions (see Fig. 1). Observations of slip bands at various orientations to the prepared surface and their traces through etch pits indicate that the laminae are about 200A thick and of rather indefinite extent. From micrographs taken of crystals with various amounts of plastic deformation, the development of slip bands is proposed to be as shown in Fig. 2. The initial slip occurs in a single (111) plane (in the slip direction) until a displacement of about 2000A is experienced. This particular plane apparently then offers sufficient resistance to further motion that slip begins anew on another (111) plane about 200A removed from the original. The process repeats and results in a laminar slip region. In the case of two adjacent slip regions, the laminae finally merge at high deformations to produce a large field of laminae as shown in the final stage in Fig. 2.

(*B*) *Electron Diffraction*—As mentioned, electron-diffraction patterns from the newly prepared crystal are Kikuchi line patterns.

Patterns taken with the electron beam parallel to and normal to the slip traces observed on the prepared surface, at various deformations, indicated that the material between visible slip bands is relatively unaffected at small deformations. That is, the Kikuchi lines persist until the spacing of the slip bands is reduced to about 5$\mu$ or somewhat less (about 5 percent elongation). At about 5 percent elongation the Kikuchi lines disappear, leaving only a spot pattern, and at still higher deformations the spots begin to split up, indicating rotation of various parts of the crystal. Slip on a second set of planes is usually observed at elongations in excess of about 5 percent.

Patterns taken normal to the slip traces generally do not exhibit Kikuchi lines but show, instead, multiple Laue spots. As the deformation increases more spots appear, and their total angular spread increases to as much as 8–10° at 10 percent elongation.

The electron microscope and electron-diffraction results are consistent in the conclusion that practically all the distortion occurs in the slip bands and very little in the remainder of the crystal.** The laminae in a slip region experience not only a translation in the slip direction, but also slight rotation relative to one another as indicated by the electron-diffraction patterns taken normal to the traces. This rotation is probably a result of constraints imposed during deformation. It is suggested that the rotation of

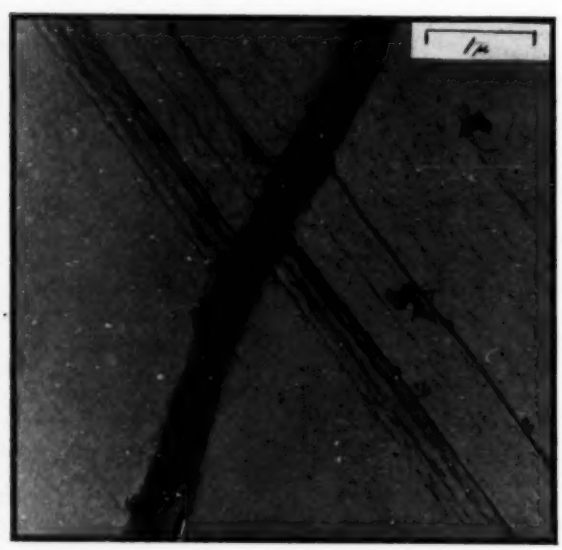


FIG. 1. Intersecting slip bands at surface of electropolished and etched aluminum crystal showing laminar nature of slip region.

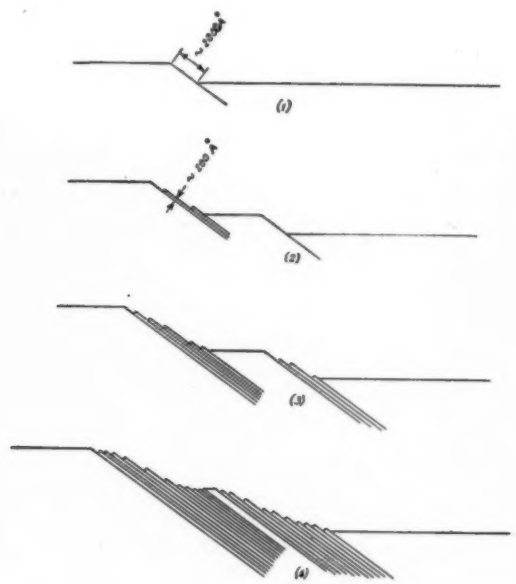


FIG. 2. Progressive formation of laminar slip region with increasing deformation. Adjacent slip regions merge to produce large field of laminae at high deformation.

the laminae is responsible for asterism in x-ray Laue photographs of deformed metals.

The laminar nature of the slip bands in aluminum suggests similar studies of other metals. First results show that nickel exhibits similar phenomena. In a private discussion, Mr. R. Maddin of Yale University has indicated that the results he has obtained with brass crystals are quite similar to those with aluminum.

* American Society for X-Ray and Electron Diffraction, Montreal, June 23–26, 1947; Bristol Conference on Theoretical Physics, Bristol, England, July 2–9, 1947.

[1] R. D. Heidenreich and L. Sturkey, J. App. Phys. **17**, 127 (1946).

** The conclusion is in general agreement with that of Guinier from studies of the x-ray background scattering produced by a deformed aluminum crystal. A. J. Guinier, Proc. Phys. Soc. (London) **57**, 310 (1945).

# New Books

## Helium

By W. H. Keesom. Pp. 494, Figs. 258, 25×17 cm. Elsevier Publishing Company, Inc., New York, 1942. Price $10.00.

Professor Keesom has used the war years in Holland to good advantage for the world of science by writing an excellent book about the helium atom in its gaseous, liquid, and solid states. There is, in addition, a review of work on the helium nucleus and on subjects related to the outer electrons. By compiling the experimental work on liquid helium and by inserting his keen criticism of the work, Professor Keesom has rendered in this section alone a valuable contribution to research workers in the field of low temperatures. From experience this reviewer has found that *Helium* is an active and authoritative text used by low temperature research laboratories.

The manuscript had been completed by Keesom in 1941, and for this reason the very important researches on liquid helium by P. Kapitza and by L. Landau got into the text through the supplementary notes at the end of the book. Since the publication of *Helium* in 1942, there have been published experimental and theoretical papers (again mostly by the Russians: Kapitza, Peshkov, Andronikashvilli, Lifshitz, and Landau) which would amply warrant another monograph on the subject of liquid helium by some recognized authority. Keesom has done a good job of summarizing F. London's theory about He *II* being a condensation in momentum space and the theoretical research by the Dutch workers Bijl, DeBeer, and Michels very properly receives attention. The experiments on flow of liquid helium in phase *II* are sometimes confusing, and the reader would do well to mentally sort out these as problems to be tackled by a theory after the first-order physical properties are understood. The x-ray evidence for spatial order in He *II* by Keesom and Taconis, and the subsequent theory involving holes in the lattice, is not too convincing.

Professor Keesom's book serves as an excellent source of information concerning the temperature scale, and sharply brings to attention the confusion which exists about the vapor pressure *vs.* temperature for liquid helium below 2°K. It would seem that the Leiden and Oxford laboratories have their respective viewpoints about the temperature scale below 2°K clearly stated in Keesom's book and that the eighth International Conference of Weights and Measures would render a service to the now numerous low temperature laboratories by asking its own Advisory Committee for Thermometry to use Keesom's book as a report and to recommend one temperature scale to be used by all laboratories until such time as another scale shall be warrented. The problem of an international temperature scale below −190°C will undoubtedly be taken up by the Advisory Committee for Thermometry, and in this respect Keesom's book gives prominence to the Leiden helium thermometer and the virial coefficients or gas-law correction terms used at Leiden. The Berlin helium thermometer and gas-law correction terms used by Henning have been presented by Keesom without criticism; the Berlin scale is not in precise accord with the Leiden scale.

Keesom's book is two things: (a) it is a complete source book for information about helium in its gaseous, liquid, and solid state, and (b) it is a monument to the lifetime research of Kamerlingh Onnes, of W. H. Keesom, and of their many collaborators. There are many excellent diagrams of apparatus, but space did not permit the book to reveal the intricate low temperature techniques which have made Leiden the great laboratory in this field of science.

Charles F. Squire
*The Rice Institute*

## Introduction to Aerodynamics of a Compressible Fluid

By Hans Wolfgang Liepmann and Allen E. Puckett. Pp. 262, 6×9¼ in. John Wiley and Sons, Inc., New York, and Chapman and Hall, Limited, London, 1947. Price $4.00.

This book is a compilation in a systematic manner of most non-classified material on this extremely important phase of aerodynamics. It has been presented by two well-known authorities in this field as an introduction to the subject rather than as a standard classroom textbook, no problems and few practical examples being presented.

The book, one of the Galcit Aeronautical Series, is divided into two phases. Part I furnishes the reader a background of fundamentals, including basic thermodynamics, one-dimensional equations of motion, isentropic channel flow and applications, shock waves, and optical methods of flow observation. The chapter on optical methods is extremely descriptive, being quite brief in its mathematical discussions, although the essential introductory material is presented. The lack of illustrated examples, illustrations of flow phenomena, and comparison

with experimental data, primarily caused by wartime restrictions, is a great handicap in the clarification of this section.

Part II is an introduction to the more mathematical literature on the subject and deals with two- and three-dimensional motions of a compressible fluid. This comprises an introduction to practically all present day methods of solution of compressibility problems, covering specifically the method of small perturbations, the method of development of the potential function into a power series in the thickness parameter or in the Mach number, the hodograph methods, the method of characteristics, and certain exact solutions. A very brief discussion of viscosity effects and experimental data is included, the latter being necessarily brief because of the small amount of unclassified material available in this field. Again much is lost in the lack of practical examples, comparison with experiment, and the lack of pictorial illustrations of flow phenomena. This is greatly offset by the clarity of mathematical presentation.

The book is primarily aimed for graduate consumption, requiring a good working knowledge of differential and integral calculus as well as a knowledge of advanced calculus.

A brief table of references is also included.

SYDNEY D. BLACK
*Case Institute of Technology*

## Antennae, an Introduction to Their Theory

BY J. AHARONI. Pp. 265, $6\frac{1}{4}\times9\frac{3}{4}$ in., Figs. 149. Oxford University Press, London, 1947. Price $8.50.

The study of antennae is peculiarly difficult both theoretically and experimentally. While much progress has been made during the past decade, many interesting and important problems remain unsolved. Accordingly, all who are engaged in research in this field, and especially those who teach courses in it in graduate schools, will welcome J. Aharoni's systematic and comprehensive introduction to its mathematical theory. Because of the advanced nature of the subject, the book is, in effect, an integrated presentation of a special branch of mathematical physics. It is carefully planned, well organized, and its principal contents are delineated in sufficient detail to permit analytical sequences to be followed readily by a reader adequately prepared in the methods of classical theoretical physics and in electromagnetic theory.

The book begins with an illuminating introduction which summarizes and describes briefly the three general methods which have been used by various investigators in the theoretical analysis of antennae. Appropriately, the author uses these methods as the subjects of his three chapters: I. "Antennae and Boundary-Value Problems" (86 pages); II. "Antennae and Integral Equations" (149 pages); III. "Antennae as Wave Guides" (29 pages). The presentation of antenna theory in this manner is an important feature of the book since it emphasizes a unity of subject and of purpose in a diversity of method.

In Chapter I the introduction is followed by an excellent, concise review of electromagnetic theory. The main part of the chapter discusses with exceptional clarity typical boundary-value problems involving planes, spheres, cylinders, and cones. A study of free and forced oscillations of spheres and spheroids following the work of Stratton and Chu and of Ryder concludes the chapter.

Chapter II opens with a derivation of ordinary electric-circuit theory from general electromagnetic principles beginning with the power equation expressed in terms of the scalar and vector potentials and the densities of charge and current. This is an important and well-written section. It serves to correlate in a fundamental manner the circuit aspects of antenna theory with conventional electric-circuit analysis. This correlation is effectively pursued and developed in subsequent analyses of the magnetic dipole (or small loop) and the electric dipole. From these, the argument continues logically to thin-wire antennae for which the integral equation is derived in quite general form. The study of the center-driven antenna and of the receiving antenna follows closely the original work of Hallén and its extension by King and Blake and King and Harrison. The chapter continues with the derivation of the electromagnetic field following the conventional procedure of assuming a sinusoidal current distribution; it concludes with a section on the effect of the earth on the field, and a section on direction finding.

Chapter III is devoted to a concise but clear presentation of the theory of the bi-conical antenna of small angle and to the relationship between antenna theory and transmission-line theory as developed by Schelkunoff.

Taken as a whole, *Antennae, an Introduction to their Theory* is an authoritative and valuable book which skillfully delineates and summarizes major phases of antenna theory as published up through the year 1945. It should prove to be an excellent text and reference book for advanced students and research workers in the field of antennae and applied electromagnetism.

RONOLD W. P. KING
*Harvard University*

## Technological and Physical Investigations on Natural and Synthetic Rubbers

BY A. J. WILDSCHUT. Pp. 173+xi, Figs. 72, Tables 17, 14.5×20.5 cm. Elsevier Publishing Company, Inc., New York, 1946. Price $3.00.

This monograph is one of a series describing research in Holland in the five years of German occupation (1939 to 1944), during which period regular journal publication

was interrupted. Although not intended as exhaustive, the investigations described provide a surprisingly comprehensive coverage of the field. The material is presented in the orderly manner associated with a compilatory book without neglecting those descriptions of experimental details expected in an original contribution. The monograph will be carefully studied by all scientific workers concerned with the properties of elastomers. They will find experimental results and concepts which are new, as well as those which are confirmatory of, or occasionally at variance with, material previously published elsewhere. As an example of the former, measurements of the tensile strength of unelongated and elongated rubbers at the temperature of liquid hydrogen are reported for the first time, to the reviewer's knowledge. The latter is illustrated by the results and conclusions of J. M. Goppel on the degree of crystallization as a function of elongation, measured by means of x-rays, which differ from those obtained in America by J. E. Field. It is regrettable that outside contemporary literature, particularly American and British, was for the most part unavailable during the period of preparation, precluding its integration with the work presented. However, the desirability of prompt publication, in the reviewer's judgment, outweighed any possible gain to be derived from the inspection of all published material.

Part I of the monograph is concerned primarily with technological investigations. In Chapter 1, a survey of the various rubbers and rubber-like materials investigated, their classification and formulation, is followed by data, with discussion, of a comprehensive list of mechanical properties. Then aging, electrical and standard physical properties, and resistance to chemicals are presented. Chapter 2 includes measurements on the plasticity of unvulcanized rubbers, a discussion of aging tests and the mechanism of aging, and mathematical interpretations of the stress-strain curve. Studies of the vulcanization process are given in Chapter 3, with emphasis on the use of synthetic resins as vulcanizing agents.

Part II is devoted to more fundamental physical studies. It is prefaced, in Chapter 4, by a discussion of physical methods in structural research. Plastic and elastic properties, with which Chapter 5 is concerned, are suggested as the most important. The thermodynamics of vulcanized rubbers, the plastic flow, the elasticity and permanent set, and the internal friction are each analyzed in considerable detail. Experimental techniques are described. The effects of very low (−253°C) and high temperatures and of swelling on the mechanical properties, particularly tensile tensile strength, are shown in Chapter 6. The x-ray investigations previously mentioned are set forth in Chapter 7. Several investigations on the electrical properties of rubber are treated briefly in Chapter 8. Finally, in Chapter 9, general conclusions of the entire work, emphasizing the uses and limitations of the various rubbers and the advances in knowledge of fundamental properties bearing on the theory of structure, are summarized.

I. B. Prettyman
*The Firestone Tire and Rubber Company*

# New Booklets

The Gaertner Scientific Corporation, 1201 Wrightwood Avenue, Chicago 14, Illinois, announces the publication of *Bulletin 151–74, Large Two-Lens Quartz Spectrograph.* 8 pages, free on request.

Leeds and Northrup Company, 4902 Stenton Avenue, Philadelphia 44, Pennsylvania, publishes a quarterly newspaper-style bulletin entitled *Modern Precision.* 8 pages, many photographs.

Burrell Technical Supply Company, 1936 Fifth Avenue, Pittsburgh 19, Pennsylvania, has published a 4-page bulletin describing its "unit-package" tube furnaces for temperatures up to 2650°F.

Dow Corning Corporation, Midland, Michigan, announces an issue of silicone notes entitled *DC 710 Silicone Oils.* 8 pages, free on request.

Sound Products Section of Radio Corporation of America has published a comprehensive new manual on the engineering and installation of sound systems. It is designed for use by architects, building engineers, and the construction industry generally, and covers all types of buildings. 288 pages, bound in simulated black leather, fully illustrated and indexed. Available at $5 from RCA sound systems distributors or direct from the RCA Sound Products Section, Camden, New Jersey.

# Here and There

### New Appointments

David A. Katcher has been appointed editor of a new semipopular magazine on physics to be published early next year by the American Institute of Physics. The new magazine is planned to fill some of the gap which now exists between specialized technical journals and popular science magazines. Katcher comes to the Institute from the Naval Ordnance Laboratory in Washington, D. C.

Isaac L. Auerbach, Albert Auerbach, Gerald Smoliar, and Joseph D. Chapline, Jr. were recently added to the staff of the Electronic Control Company, Philadelphia, Pennsylvania.

Cyril J. Staud has been named Director of Kodak Research Laboratory, and John A. Leermakers is the new Assistant Director and head of the Photographic Theory Department.

Walter Ramberg has been appointed Chief of the Mechanics Division of the National Bureau of Standards, succeeding Hugh L. Dryden, who is leaving the Bureau to become Director of Research for the National Advisory Committee for Aeronautics. The appointment of Grote Reber, radio physicist and engineer, to the staff of the Bureau was also announced recently.

R. C. Mason has been named Manager of the Electro-Physics Department of the Westinghouse Research Laboratories, succeeding Gaylord W. Penney, who was recently appointed Westinghouse Professor of Electrical Engineering at the Carnegie Institute of Technology.

### Princeton Professor Drowned

Assistant Professor Shuichi Kusaka, a member of the Department of Physics at Princeton University and an authority on cosmic-ray theoretical research, was drowned on August 31 while swimming at Beach Haven, New Jersey.

### RCA Fellowship Award

An RCA Fellowship was established in January 1947 for the purpose of encouraging RCA engineers to obtain advanced degrees and to help in the recruiting of young engineers for research and development. First RCA Victor employee to be awarded the fellowship was Harry J. Woll, engineer at the company's Camden plant. He will study for the Ph.D. degree at the University of Pennsylvania, and during this period will be on leave of absence from the company.

### Acta Crystallographica

A new journal of crystallography, Acta Crystallographica, sponsored by the recently formed International Union of Crystallography, will start publication in January 1948. (See Journal of Applied Physics, April 1947.) It will be published by the Cambridge University Press under the editorship of Professor P. P. Ewald, a former editor of the Zeitschrift für Kristallographie, and a panel of regional co-editors. The annual subscription will be $10 for six issues and, by courtesy of the American Institute of Physics, arrangements have been made for subscribers in the U.S.A., its possessions, and Canada to subscribe through that body. Subscribers in other countries should subscribe directly through the Cambridge University Press, Bentley House, Euston Road, London, N.W. 1, England. Articles for publication will be accepted in English, French, German, or Russian, and authors in the U.S.A. are invited to submit manuscripts to Professor I. Fankuchen, Brooklyn Polytechnic Institute, 85 Livington Street, Brooklyn 2, New York.

### Westinghouse Scientist Honored

Arpad L. Nadai, Consulting Engineer of the Westinghouse Research Laboratories, has been awarded the Worcester Reed Warner Medal by the American Society of Mechanical Engineers, honoring noteworthy contributions to the permanent literature of engineering. Earlier this year Dr. Nadai delivered the James Clayton Lecture before the British Institution of Mechanical Engineers in London and Manchester.

### British American Research, Limited

National Research Corporation, Cambridge, Massachusetts, announces the formation of British American Research, Limited, which has recently been incorporated in Scotland as a joint venture with Daniel Varney, Limited. The latter company was engaged during the war in the manufacture of scientific research instruments and laboratory apparatus. The new company will undertake the manufacture and sale of high vacuum equipment.